# HECTD1 promotes base excision repair in nucleosomes through chromatin remodelling

Thesis submitted in accordance with the requirements of the University of Liverpool for the degree of Doctor in Philosophy by

Eleanor Madders

April 2021

# Abstract

Base excision repair (BER) is the major cellular DNA repair pathway that recognises and excises damaged DNA bases to help maintain genome stability. Whilst the major enzymes and mechanisms co-ordinating BER are well known and established, the process of BER in chromatin where DNA is compacted with histones, remains unclear. Using reconstituted mononucleosomes containing a site-specific synthetic abasic site (tetrahydrofuran, THF), we have previously demonstrated that the DNA damage is less efficiently incised by recombinant AP endonuclease 1 (APE1) when the DNA backbone is facing the histone core (THF-IN) compared to that orientated away (THF-OUT). However, when utilising HeLa whole cell extracts, the difference in incision of THF-IN versus THF-OUT is less pronounced suggesting the presence of chromatin remodelling factors that stimulate THF accessibility to APE1. Therefore, adopting an unbiased purification scheme involving the separation of proteins in HeLa cell extracts by different ion-exchange and size exclusion chromatography columns, a chromatin remodelling activity was purified from HeLa cell extracts and was identified as the E3 ubiquitin ligase, HECTD1.

I have subsequently, cloned and purified a truncated form of HECTD1 and demonstrated in my established *in vitro* mononucleosome model that HECTD1 stimulates incision of THF-IN by APE1. Furthermore, I also provide evidence that HECTD1 ubiquitylates histones H2B/H3, which may stimulate chromatin remodelling. Additionally, I have elucidated that HECTD1 appears to play a broader role at multiple stages of the BER pathway via demonstration that a recombinant truncated form of HECTD1 can stimulate incision by the DNA glycosylase NTH1 of occluded thymine glycol sites within mononucleosome substrates (TG-IN) *in vitro.* Furthermore, utilising siRNA-mediated depletion of HECTD1 in alkaline comet assays and clonogenic survival assays, I observed deficiencies in DNA damage repair, and decreased cell survival following x-ray irradiation, hydrogen peroxide and methyl methanesulfonate treatment, particularly in normal fibroblasts versus non-targeting siRNA control-treated cells. However, in neutral comet assays, assessing double strand break repair, no difference in DNA damage repair between siRNA-mediated depleted HECTD1 versus non-targeting siRNA control-treated cells is observed. Thus, I have now identified HECTD1 as a novel and important factor in specifically promoting BER in chromatin.

# Acknowledgments

First and foremost, I would like to thank my supervisor, Dr Jason Parsons for giving me the opportunity to work on this PhD project. I am very grateful for his support, guidance, expertise and advice throughout my time in the laboratory and whilst writing this thesis.

I am very lucky to have been part of such a supportive research group and would like to thank all past and present members. In particular, I would like to thank Dr Katie Nickson, Dr Jonathan Hughes, Rachael Clifford and Hayley Fowler, for their help, encouragement and friendship over the course of my PhD. I also wish to thank North West Cancer Research for funding this PhD project.

Finally, I thank my family, my Dad, brother Rory and sister Gabby for their constant support, love and encouragement throughout my years of study and research. Achieving this PhD would not have been possible without them.

# Table of Contents

# List of Figures

**Figure 6.11** Analysing $H_2O_2$-induced DSB DNA damage repair kinetics following siRNA knockdown of HECTD1 in normal lung fibroblasts

# List of Tables

# Abbreviations

| | |
|---|---|
| **•OH** | Hydroxyl radicals |
| **$^1O_2$** | Singlet oxygen |
| **6-4PPs** | 6-4 pyrimidine-pyrimidone photoproducts |
| **7meG** | N7-methylguanine |
| **8-oxoG** | 8-oxoguanine |
| **A** | Adenine |
| **ACRs** | ATP-dependent chromatin remodelling complexes |
| **ALC1** | Amplified in Liver Cancer 1 |
| **AMP** | Adenosine monophosphate |
| **APC** | Adenomatous polyposis coli |
| **APC/C** | Anaphase-promoting complex/cyclosome |
| **APE1** | AP endonuclease 1 |
| **APS** | Ammonium persulphate |
| **AP sites** | Apurinic/apyrimidinic site |
| **ATP** | Adenosine triphosphate |
| **BER** | Base Excision Repair |
| **BRCA1** | Breast cancer gene 1 |
| **BRCA2** | Breast cancer gene 2 |
| **BSA** | Bovine serum albumin |
| **C** | Cytosine |
| **CDD** | Complex/Clustered DNA damage |
| **CETN2** | Centrin 2 |
| **CHD** | Chromodomain helicase DNA binding |
| **CPDs** | Cyclobutane pyrimidine dimers |
| **CRL** | Cullin-RING ubiquitin ligase |
| **CSA** | Cockayne syndrome proteins A |
| **CSB** | Cockayne syndrome proteins B |
| **CtIP** | Carboxy-terminal binding protein (CtBP)- interacting protein |
| **$Cu^{2+}$** | Copper ion |
| **CUL4a** | Cullin 4a |
| **DDB1** | DNA damage binding protein 1 |
| **DDB2** | DNA damage binding protein 2 |

| | |
|---|---|
| **DDR** | DNA damage response |
| **DMEM** | Dulbecco's modified eagle's medium |
| **DNA** | Deoxyribose nucleic acid |
| **DNA-PKcs** | DNA-dependent protein kinase catalytic subunit |
| **DSB** | Double strand break |
| **E1** | E1-activating enzyme |
| **E2** | E2-conjugating enzyme |
| **E3** | E3 ubiquitin ligases |
| **E. coli** | Escherichia coli |
| **EMT** | Epithelial-mesenchymal transition |
| **EndMT** | EndMT |
| **EXO1** | Exonuclease 1 |
| **$Fe^{2+}$** | Iron ion |
| **FACT** | Facilities chromatin transcription |
| **FBS** | Fetal bovine serum |
| **G** | Guanine |
| **G** | Glycine |
| **GG-NER** | Global genome NER |
| **H** | Helicase bundle |
| **$H_2O_2$** | Hydrogen Peroxide |
| **$H_3$** | Ozone |
| **HECT** | Homologous to E6-AP carboxy |
| **HECTD1** | HECT Domain E3 Ubiquitin Protein Ligase 1 |
| **H-E3** | HECT-type E3s |
| **HEPES** | Hydroxyethyl piperazineethanesulfonic acid |
| **HhH** | Helix-hairpin-helix |
| **HNPCC** | Hereditary non-polyposis colon cancer |
| **HP1** | Heterochromatin protein 1 |
| **HR** | Homologous Recombination |
| **HSA** | Helicase-SANT |
| **HSP90** | Heat shock protein 90 |
| **IBR** | In-*b*etween-*R*ING |
| **ICLs** | Interstrand crosslinks |
| **INO80** | Inositol requiring 80 |

| | |
|---|---|
| **IR** | Ionising radiation |
| **ISWI** | Imitation switch |
| **K** | Lysine |
| **LET** | Linear energy transfer |
| **LIC** | Ligation independent cloning |
| **Lig** | Ligase |
| **LMPA** | Low melting point agarose |
| **M** | Methionine |
| **MBD4** | Methyl-CpG binding domain protein 4 |
| **Mdm2** | Mouse double minute 2 homolog |
| **$Mg^{2+}$** | Magnesium ion |
| **MIB** | MIB/HERC2 domain |
| **MPG** | N-methylpurine DNA glycosylase |
| **MMR** | Mismatch Repair |
| **MMS** | Methanesulfonate |
| **MNU** | *N*-methyl-*N*-nitrosourea |
| **MRN** | MRE11-RAD50-NBS1 |
| **MSL2** | Male-specific lethal-2 |
| **Mule** | Mcl-1 ubiquitin ligase E3 |
| **MUTYH** | MutY homologue |
| **MWCO** | Molecular weight cut off |
| **NAD** | Nicotinamide adenine dinucleotide |
| **NAP-1** | Nucleosome assembly protein 1 |
| **NCPs** | Nucleosome core particles |
| **NEIL1** | Endonuclease VIII-like 1 |
| **NEIL2** | Endonuclease VIII-like 2 |
| **NEIL3** | Endonuclease VIII-like 3 |
| **NER** | Nucleotide Excision Repair |
| **NES** | Nuclear export signals |
| **NHEJ** | Nonhomologous end-joining |
| **NLS** | Nuclear localization sequences |
| **NMPA** | Normal melting point agarose |
| **NNK** | 4-(methylnitrosamino)-1-(3-pyridyl)-1-butanone |
| **NT** | Non-targeting |

| | |
|---|---|
| **NTH1** | Endonuclease III-like protein 1 |
| **O** | Oxygen |
| **$O_2^{\bullet-}$** | Superoxide |
| **O6meG** | O6-methylguanine |
| **OGG1** | 8-oxoguanine DNA glycosylase 1 |
| **$ONOO^-$** | Peroxynitrite |
| **PAGE** | Polyacrylamide gel electrophoresis |
| **PAR** | Poly ADP-ribose |
| **PARP** | Poly [ADP-ribose] polymerase 1 |
| **PBS** | Phosphate-buffered saline |
| **PCR** | Polymerase chain reaction |
| **PCNA** | Proliferating cell nuclear antigen |
| **PCV** | Packed cell volume |
| **PIPKIγ90** | Phosphatidylinositol 4-phosphate 5-kinase type I γ |
| **PMSF** | Phenylmethylsulfonyl fluoride |
| **PNKP** | Polynucleotide kinase 3'-phosphatase |
| **Pol** | Polymerase |
| **PRC1/2** | Polycomb repressive complex 1 and 2 |
| **PTMs** | Post translational modifications |
| **PVDF** | Immobilon-FL polyvinylidene diflouride |
| **RAD23B** | RAD23 homolog B |
| **RBR** | RING between RING |
| **R-E3** | RING-type E3s |
| **RFC** | Replication factor C |
| **RNF20/40** | Ring finger protein 20/40 |
| **ROC1** | Regualtor of cullins 1 |
| **ROS** | Reactive oxygen species |
| **RPA** | Replication protein A |
| **RSC** | Remodels structure of chromatin |
| **SAM** | S-adenosylmetionine |
| **SATB1** | Special AT-rich Sequence-binding Protein 1 |
| **SDM** | Site-directed mutagenesis |
| **SDS-PAGE** | Sulphate polyacrylamide gel electrophoresis |
| **SHL** | Superhelical locations |

| | |
|---|---|
| **siRNA** | Small interfering mRNA |
| **SMUG1** | Single-strand-selective monofunctional uracil DNA glycosylase |
| **SSB** | Single strand break |
| **SUN** | SAD1/UNC domain |
| **SW1/SNF** | Switching defective/sucrose nonfermenting |
| **T** | Thymine |
| **TAE** | Tris-acetate-EDTA |
| **TC-NER** | Transcription-coupled NER |
| **TDG** | Thymine DNA glycosylase |
| **TEMED** | *N*,*N*,*N*′,*N*′-Tetramethylethylenediamine |
| **TFIIH** | Transcription initiation factor IIH |
| **TG** | Thymine glycol |
| **TGS** | Tris-glycine SDS |
| **THF** | Tetrahydrofuran |
| **THF-IN** | THF with DNA backbone facing inwards |
| **THF-OUT** | THF with DNA backbone facing outwards |
| **TLS** | Translesion synthesis |
| **U** | Uracil |
| **Ub** | Ubiquitin |
| **UPP** | Ubiquitin proteasome pathway |
| **UNGs** | Uracil DNA glycosylase |
| **USP/UBP** | Ubiquitin specific protease |
| **USP7** | Ubiquitin specific protease 7 |
| **UV** | Ultraviolet light |
| **UV-DDB** | UV radiation-DNA damage-binding protein |
| **UVSSA** | UV stimulated scaffold protein A |
| **WCE** | Whole cell extract |
| **XP** | Xeroderma pigmentusum |
| **XRCC1** | X-ray repair cross-complementing protein 1 |
| **γ-H2AX** | Phosphorylated H2AX |

# Chapter 1: Introduction

## 1.1 Genome stability and instability

The cell comprises all living organisms, forming the basic biological, functional and structural building blocks of life. Animal cells, enclosed within a phospholipid bilayer membrane, consists of an aqueous cytosol called the cytoplasm, providing the environment for housing the cells membrane-bound organelles. There are a variety of organelles with a range of responsibilities from producing adenosine triphosphate (ATP), for the use and storage of energy, hormones and enzymes, all of which are vital for performing all the biological functions of that specific cell type. The majority of organisms are single cells, however, others including humans are composed of extensive multicellular systems made up of a myriad of specialised groups of cells that communicate through elaborate systems to form complex biological systems which preform specialised functions. The human body consists of more than $10^{13}$ cells, all of which originate from embryonic cells that house all of the organisms genetic material [1]. The resulting whole organism is maintained through the action of a cascade of countless cell divisions and differentiations.

Within the nucleus of all living cells the heritable genetic information is stored in the form of double stranded biological polymers called deoxyribose nucleic acid (DNA). In human cells, the genome is composed of identical copies of DNA that is distributed between 23 pairs of chromosomes. Double stranded DNA consists of two complementary linear unbranched polynucleotide chains made up of four types of nitrogenous monomers called nucleotides; adenine (A), cytosine (C), guanine (G) and thymine (T). These polynucleotide chains are held by hydrogen bonding between bases as well as the specific complementary base pairing displayed between A pairing with T and C pairing with G. The order in which nucleotides are arranged forms a long sequence encoding the cells genetic information. The machinery required to read this genetic information as well as successfully duplicate the DNA during DNA replication is all contained within the cell.

A gene is a functional unit of DNA, which encodes all the instructions required to create a protein. Humans have around 20-25,000 protein coding genes, which remarkably only accounts for 2 % of the human genome. Proteins are made up of long polypeptide chains which are built from 20 types of amino acids, the type and order of which is coded for by the specific DNA sequence. Within the amino acid sequence, known as the DNA triplet code,

three DNA bases (codon) encode for a specific amino acid. The amino acids are joined together by peptide bonds and resulting polypeptide chains are folded into three dimensional proteins. With the amino acids providing different properties, interactions and functional groups, the amino acid sequence and thus DNA sequence has a huge impact on the function of the protein, of which there are a vast array. These include proteins that stimulate generation of ATP, cell mobility and structure, inter/intra cellular signal transductions and DNA repair.

Maintaining genome stability is fundamental for cellular survival, function and propagation of life. However, genomic variation can be generated from DNA replication infidelity and aberrant chromosome segregation. In addition to this, DNA is constantly under attack from both endogenous sources, such as reactive oxygen species (ROS) generated through cellular oxidation, and exogenous genotoxic agents including, ultraviolet (UV) radiation and ionising radiation (IR). Such DNA damaging events can result in changes to the nucleotide sequence, called a mutation. In some instances, mutations can be silent and have no significant impact on the cell if it falls within a non-coding region of the DNA. However, a mutation within a gene can have significant implications leading to alterations in the amino acid sequence of a protein. This can cause alterations in the protein structure and therefore its function, regulation and/or activity which can have detrimental effects on the cell and ultimately the organism. To prevent an accumulation of DNA damage compromising genome integrity and having a negative effect on the whole organism, the cell has developed complex systems called DNA repair pathways, the number of which and the many different DNA repair enzymes involved highlights the importance of DNA repair within a cell. In the vast majority of cases, DNA damage is signalled and repaired by the DNA damage response (DDR). However, in cases where DNA damage persists, genome instability ensues and which has been implicated in many human diseases, including premature ageing, neurodegenerative diseases and multiple types of cancer. In fact, genome instability underlies the six definable hallmarks of cancer; sustaining proliferative signalling, evading growth suppressors, resisting cell death, enabling replicative immortality, inducing angiogenesis, and activating invasion and metastasis [2]. Furthermore, with 367,000 new cancer cases in the UK every year, leading to 165,000 cancer deaths per year (2015-2017) (Cancer Research UK), cancer and the DNA damage associated with the development of the disease is a major UK and worldwide issue. Additionally, the current gold standard of care is adjuvant chemo and/or radiotherapy, which works by inducing extensive DNA damage in cancer cells, thereby acting through DNA damage for effective treatment, overwhelming the ability of the cell to repair the DNA,

resulting in cell death. Therefore, it is imperative that research into the basic biology of DNA repair continues as DNA damage is not only a driver of disease but also vital for its treatment.

## 1.2 DNA

DNA is the predominant genetic material, fundamental for all living organisms. The three dimensional structure was discovered nearly 70 years ago, where complementary base pairing across two polymers emphasised the double-helical structure of DNA [3]. Watson and Crick's molecular explanation built upon the 'transforming principle' theory that DNA provided the vehicle for the transfer of genetic material [4] and supported the discovery of equal A and T and G and C bases in double stranded DNA [5]. Furthermore, the complementary nature of DNA proposed in the 1950's suggested that genetic information could be copied, forming the basis of our understanding of genetics and fundamental for the heritability of genetic material.

The structure of DNA comprises of repeating sugar-phosphate components making up the fixed backbone of DNA, with bases lying within the DNA helix. Each 2'-deoxyribose is joined to its neighbouring pentose sugar by phosphate groups via phosphodiester bonds on the 3'-hydroxyl residue of the 2'-deoxyribose. As this bonding only occurs in the 5' to 3' direction, the ends of the sugar-phosphate DNA backbone are easily discernible, a 5'-phosphate at one end with a 3'-hydroxyl at the other. The single units of DNA consist of one of the bases; A, T, G or C covalently linked to a deoxyribose sugar by a glycosidic bond (shown in red in Figure 1.1A). This 2'-deoxyribonucleoside is then attached via a phosphodiester bond at the 5'-position of the pentose sugar (shown in yellow in Figure 1.1A) to form a 2'deoxyribonucleotide. Of the four bases, two are bulky two ring bases, purines (A and G) which pair with the pyrimidines (T and C), which are single ring bases. This complementary base pairing by hydrogen bonds (shown by the dashed lines in Figure 1.1B), two between A and T and three shared between G and C, join the two DNA polymers, creating double stranded DNA. Due to this base pairing, by nature these two DNA polymers are complementary but antiparallel to each other. Furthermore, as the two strands possess opposite polarity they intertwine forming the double helix of DNA.

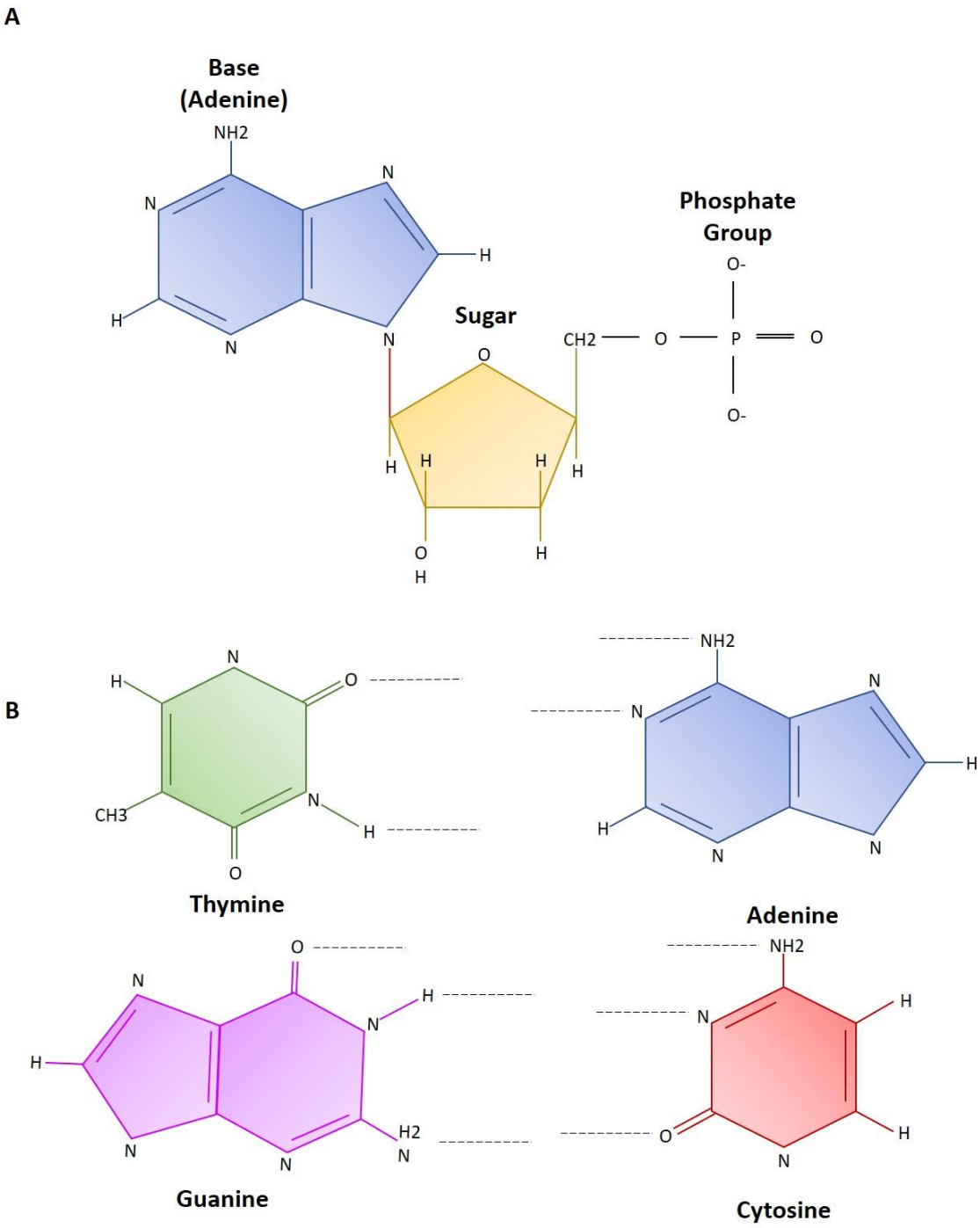


**Figure 1.1: The chemical structure of the four DNA bases and an example of nucleotide structure**

**A** Adenosine monophosphate (AMP) molecular structure, as an example of a nucleotide. The base, A, is covalently attached by a glycosidic bond (red bond) to a pentose deoxyribose sugar (yellow). This 2'-deoxyribonucleoside is linked via a phosphodiester bond (green bond) to a phosphate group to form the nucleotide. **B** The chemical structure of the four DNA

nitrogenous bases, T (green), A (blue), G (purple) and C (red). Hydrogen bonds indicated by black dashed lines for complementary base pairing between A and T and C and G.

The sheer number of hydrogen bonds, although much weaker than the covalent bonds which connect the structure of the individual nucleotides, provide sufficient stability to maintain the DNA double helix. Yet, hydrogen bonds are weak enough for allowing key biological processes, such as transcription and translation, essential for the cells survival. Further protection to the integrity of the DNA structure is achieved through stacking interactions. Firstly, through hydrophobic effects due to the arrangement of non-polar, hydrophobic bases in the interior of the helix and the hydrophilic polar DNA backbone. Through this hydrophobic effect, the nitrogenous bases are attracted to one another and spaced based upon their van der Waals distance. Although these single interactions are very weak, the net effect of several van de Waals forces provide considerable stability to DNA. However, the nature of the negatively charged phosphate residues within the DNA backbone can make DNA unstable. To remedy this, ionic interactions between positively charged, magnesium ions, arginine or lysine residues provide further strength and stability to DNA, protecting the genetic information and ultimately its heritability.

DNA must be tightly organised into small volumes so it can fit within the nucleus of the cell. Therefore, the compaction of genetic material into chromatin (see section 1.5) is essential for the organisation of DNA within the nucleus and involves co-ordinated levels of folding amongst histones and non-histone chromosomal proteins. Through reducing the surface area of DNA, this arrangement provides protection from endogenous and exogenous sources of DNA damage, but also limits free access to the DNA. Via multiple mechanisms, DNA within compacted regions is then made accessible to the complex machinery of essential biological processes including gene transcription, DNA replication and DNA repair.

## 1.3 DNA damage

DNA is under constant attack both endogenously, from normal cellular metabolism and from exogenous sources, such as IR. By design the double helix provides a degree of protection, but DNA is still susceptible to damage from spontaneous chemical reactions [6]. Endogenously DNA is threatened by spontaneous reactions, causing base loses (depurinations/depyrimidinations or apurinic/apyrimidinic (AP) site formation) and through cellular metabolism generating ROS, reactive nitrogen species and alkylating agents which

produce alkylated base damage (e.g. N7-methylguanine (7meG)), oxidised base damage (e.g. 8-oxoguanine (8-oxoG)), DNA single strand breaks (SSBs) and DNA double strand breaks (DSBs). This is exacerbated by damage induced by environmental stresses and toxins (e.g. IR and UV), leading to estimates of the total DNA damage as $10^5$ lesions per cell per day [7], [8]. If left unrepaired, accumulation of DNA damage can lead to mutations, blocked transcription and translation, incomplete DNA replication or segregation of chromosomes leading to chromosomal abnormalities and cell cycle delay, arrest or even apoptosis [6]. This resulting genomic instability is the hallmark of all forms of cancer [2] and has been implicated in the development of neurodegenerative diseases, including; Huntington's and Alzheimer's disease [9] as well as premature ageing [10].

### 1.3.1 Endogenous DNA damage

The majority of DNA damage within a cell is endogenous in origin, mainly due to oxygen and water in the cellular environment [11]. Endogenous DNA damage can arise from a range of events, including; hydrolysis, exposure to ROS and other reactive metabolites [12]. Hydrolysis is the simplest form of endogenous damage DNA is subject to, and occurs when the N-glycosidic bond between the DNA base and the 2'-deoxyribose sugar is labile in certain conditions, including; heating or the action of N-glycosylases, where, for example, cleavage of this glycosidic bond produces AP sites [13]. ROS, a by-product of normal cellular metabolism are also a major type of endogenous DNA damaging agents. For example, hydroxyl radicals (•OH) can result from a series of chain reactions, the consequence of electron leakage from the electron transport chain during mitochondrial respiration [14].

#### *1.3.1.1 Oxidation*

ROS are unavoidably produced through normal cellular physiology, including respiration, metabolism, the inflammatory response and phagocytosis. Similarly, ROS may also be generated by exogenous sources, such as UV radiation or IR [15], [16]. Types of ROS include superoxide ($O_2^{\bullet-}$), hydrogen peroxide ($H_2O_2$), ozone ($H_3$), singlet oxygen ($^1O_2$) and hydroxyl radicals (•OH) [12], [17]. Accumulation of ROS can lead to the development of oxidative stress, which occurs when the production of ROS exceeds the body's natural antioxidant defence mechanisms, resulting in damage to macromolecules such as DNA, proteins and lipids [18], [19]. Damage to DNA, including oxidised bases, SSBs and DSBs, is the most

frequently occurring damage by ROS, of which there is a huge potential for. In fact, each human cell metabolises $10^{12}$ molecules of oxygen per day, with an estimated 1-2 % of the oxygen metabolised converted into ROS [20], [21].

One such source of ROS generation is during mitochondrial respiration where 1-5 % of the oxygen undergoes single electron transfer, resulting in $O_2^{\bullet-}$ production [22]. Further sources of $O_2^{\bullet-}$ include, leakage of electrons from NADPH cytochrome P450 reductase in the endoplasmic reticulum, as well as being generated as a direct enzymatic by-product of xanthine oxidase, NADPH oxidase and cyclooxygenase [23]. $O_2^{\bullet-}$ itself has little reactivity but is reduced to $H_2O_2$ through a rapid dismutation reaction, either spontaneously or by superoxide dismutase. Additionally $H_2O_2$ is also a by-product of lipid metabolism in peroxisomes [24]. The majority of $H_2O_2$ is degraded to $H_2O$ by glutathione peroxidase and catalase. However, in the presence of transition metals such as iron ($Fe^{2+}$)and copper ($Cu^{2+}$), $H_2O_2$ can be reduced to highly reactive •OH via a Fenton reaction ($H_2O_2 + Fe^{2+} \rightarrow \bullet OH + OH^- + Fe^{3+}$) [12], [24]. The •OH have a very short half-life, only diffusing one or two molecular diameters before damaging local cellular structures [25], therefore it must be generated in close proximity to cause any damage. Thus, it is assumed that $H_2O_2$ acts as a latent form of the radical which can diffuse to the vicinity of the DNA molecule before reacting with the metal ion [26]. The inflammatory response is a further generator of ROS, with immune cells such as neutrophils, producing $O_2^{\bullet-}$and $H_2O_2$ to be used at sites of infection against the bacterial threat. These can subsequently interact to produce •OH via the Haber-Weiss reaction ($O_2^{\bullet-} + H_2O_2 \rightarrow O_2 + \bullet OH + OH^-$) [11].

Following exposure of DNA to ROS, multiple alterations can be induced, including SSBs, DSBs, abasic sites and a range of nucleotide modifications [27]. Guanine has the smallest oxidation potential (1.29 V), therefore is the most frequently modified base by ROS [28]. Its most abundant oxidatively modified base, formed by the hydroxylation in the C8 position of the guanine ring by a •OH. is 8-oxoG (Figure 1.2) [29]. Estimates of 8-oxoG steady-state levels are of $10^3$ lesions per cell/per day, and it is often used as a measurement of oxidative DNA damage [30]. This lesion is highly mutagenic, due to the incorrect incorporation of adenine by DNA polymerases during replication, leading to a GC to TA transversion mutations [31]. This in turn can give rise to diseases such as cancer [32], where up to $10^5$ 8-oxoG lesions per cell/per day has been reported [30]. It can also be further oxidised by various ROS to other, stable, and sometimes more mutagenic lesions, for example, 8-oxoG reacts with peroxynitrite ($ONOO^-$) to form spiroiminodihydantoin [33] and $^1O_2$ to form oxaluric acid [34].

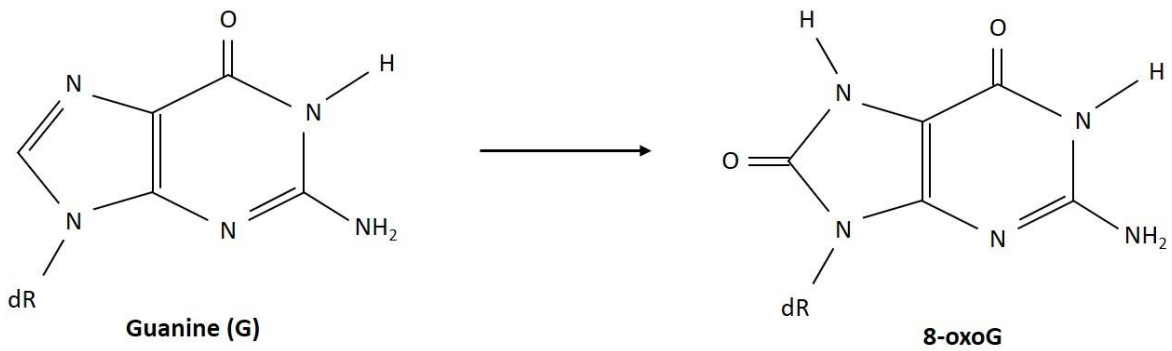


**Figure 1.2: Molecular structure of 8-Oxoguanine**

Schematic diagram of the formation of 8-oxoG from the oxidation of guanine in the C8 position of the ring by a •OH.

Whilst 8-oxoG is the most prevalent oxidative base damage, thymine glycol (Tg) is the most abundant form of an oxidised pyrimidine [35]. Tg is generated via a reaction of the 5,6-double bond of thymine with •OH, resulting in the addition of hydroxyl groups at the C5 and C6 positions (Figure 1.3) [36]. The biological implications of Tg sites include potential TA to GC transversions, although Tg generally pairs with adenine, it is weakly mutagenic resulting in T to C transitions [37]. More importantly, Tg is known to block DNA polymerases, stalling replication inferring lethality, but it can also be by-passed by translesion synthesis (TLS), leading to possible base misincorporations and again TA to GC transversions [38], [39]. Similarly to 8-oxoG, the presence of Tg sites in DNA has been used as a marker for oxidative stress [40], [41], with an estimate of 400 Tg formations per cell per day [40], [42].

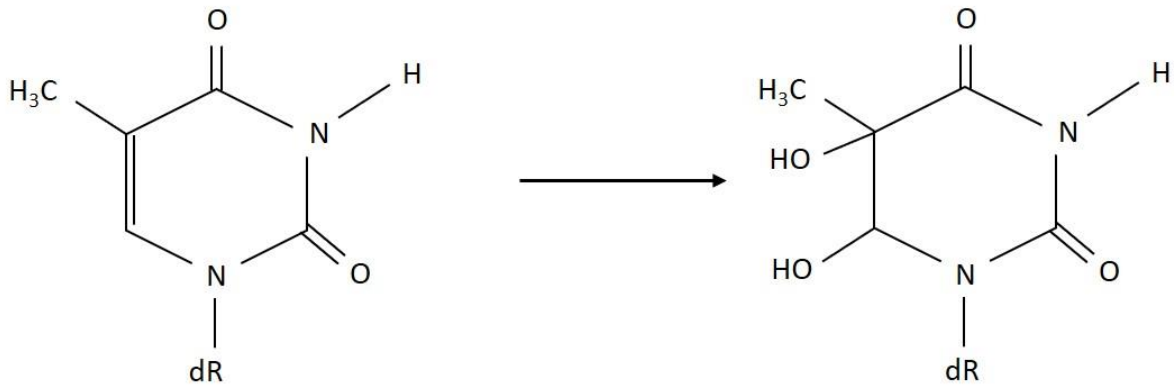


**Figure 1.3: Molecular structure of Thymine Glycol**

Schematic diagram of the formation of Tg, generated via a reaction of the 5,6 double bond of thymine with •OH and the addition of hydroxyl groups at the C5 and C6 positions.

### *1.3.1.2 Hydrolysis*

Within DNA the N-glycosidic bond between bases and the deoxyribose sugar is labile under certain conditions, including hydrolysis, heating, base alkylation, oxidation and the action of N-glycosylases during BER. This results in the separation of the nitrogenous base from the phosphodiester backbone, generating an AP site (Figure 1.4) [13], [43], [44]. These reactions are often referred to as depurinations, as in DNA purines are lost at a 20 times faster rate than pyrimidines [45]. AP sites are among the most frequent endogenous lesions found in DNA, with an estimated 10,000 lesions/per cell/per day [7], with 50,000-200,000 AP sites/genome found in many human and rodent tissues [46]. If these lesions are by-passed by TLS, they can be highly mutagenic as the DNA polymerase would preferentially incorporate adenine opposite the AP site, causing G to T or A to T transversions and frameshift mutations [11]. These single-base substitutions are found in many oncogenes [47], but can also be highly cytotoxic, due to stalled replication and transcription as well as to contribute to the formation of DNA strand breaks [48].

Another common lesion generated by hydrolysis is the hydrolytic deamination of cytosine to uridine or 5-methylcytidine to thymidine, which occurs at a rate of 100-500 events per cell/per day [7]. Although this is 1/500$^{th}$ the rate of depurination events, hydrolytic deamination do result in mutagenic nucleotide sequence changes [49]. Uracil generated from cytosine deamination is rapidly excised by uracil-DNA glycosylase, and the resulting AP

site easily repaired. However, the resulting thymidine from the deamination of 5-methylcytidine forms a GT base pair, which requires correction via the very slow mismatch repair system [7]. Consequentially, these transition sites account for a third of the single point mutations causing inherited diseases in humans [50], and is frequently present at CpG sites in a variety of cancer-associated genes, including the p53 tumour suppressor gene [51], [52].

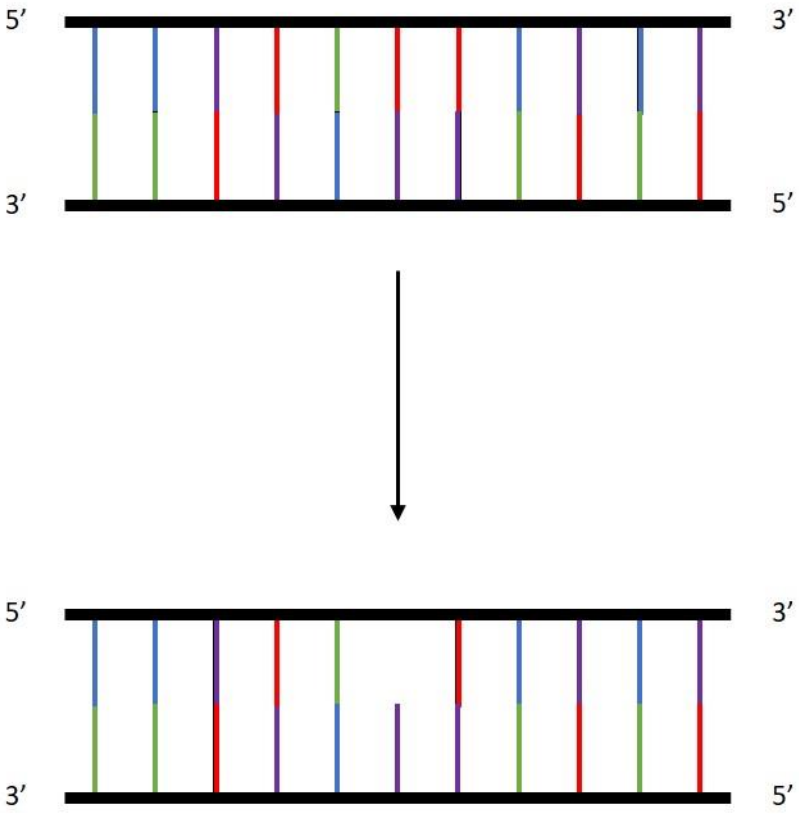


**Figure 1.4: Apurinic/apyrimidinic site in DNA**

Schematic diagram shows an AP site in DNA with the colours showing the bases and DNA backbone in black. The AP site is shown where there is no base due to separation of the nitrogenous base from the phosphodiester backbone.

### *1.3.1.3 Errors from DNA processing*

The importance of the fidelity of cellular DNA polymerases is evidenced by the mutator phenotype, resulting from mutations in these enzymes [53]. The error rate *in vitro* has been demonstrated to range from $2x10^{-4}$ for DNA polymerase β involved in base damage repair, to $1x10^{-7}$ for DNA polymerases δ and ε associated with DNA replication [54]–[56]. The vast

majority of mispaired bases overlooked by DNA polymerase proof-reading are repaired by the DNA mismatch repair system [57]. However, in some cases mutations do occur. Factors which contribute to increased mutation frequencies include, the sequence context of DNA with repetitive segments having the potential to form secondary DNA structures, and stalling replication leading to increased nucleotide misincorporation, as demonstrated with the d(CGG)n nucleotide repeats associated with fragile X syndrome [58]. Accuracy of base incorporation is also dependent on a balanced pool of nucleotides, with alterations in the relative concentrations being shown to increase spontaneous mutation rates in cells [11]. Errors can also arise during the DNA repair process, in particular the repair of DNA DSBs, which have a high mutagenic potential due do both complimentary strands being compromised. Non-homologous end joining in particular is known to be error prone, resulting in base changes proximal to the DSB, whereas homologous recombination which is thought to be error free, has been shown to highly mutagenic, particularly when DSBs are clustered [59] or large sections of DNA needs to be synthesised [60]. This inaccurate repair of DSBs gives rise to a vast array of genetic diversity found in cancers, such as chromosomal rearrangements and translocations, point mutations and copy number variations [61]–[63].

### 1.3.2 Exogenous DNA damage

Exogenous damage to DNA is a result of the action of environmental sources, which can be physical or chemical in nature. Exogenous agents include UV and IR, physical genotoxins which occur naturally from the sun and cosmic irradiation, as well as artificial sources, in the case of medical irradiation. Chemical sources, such as alkylating agents found in diesel pollutants also cause exogenous DNA damage, including SSBs (Figure 1.5A), DSBs (Figure 1.5B) and DNA adducts [10].

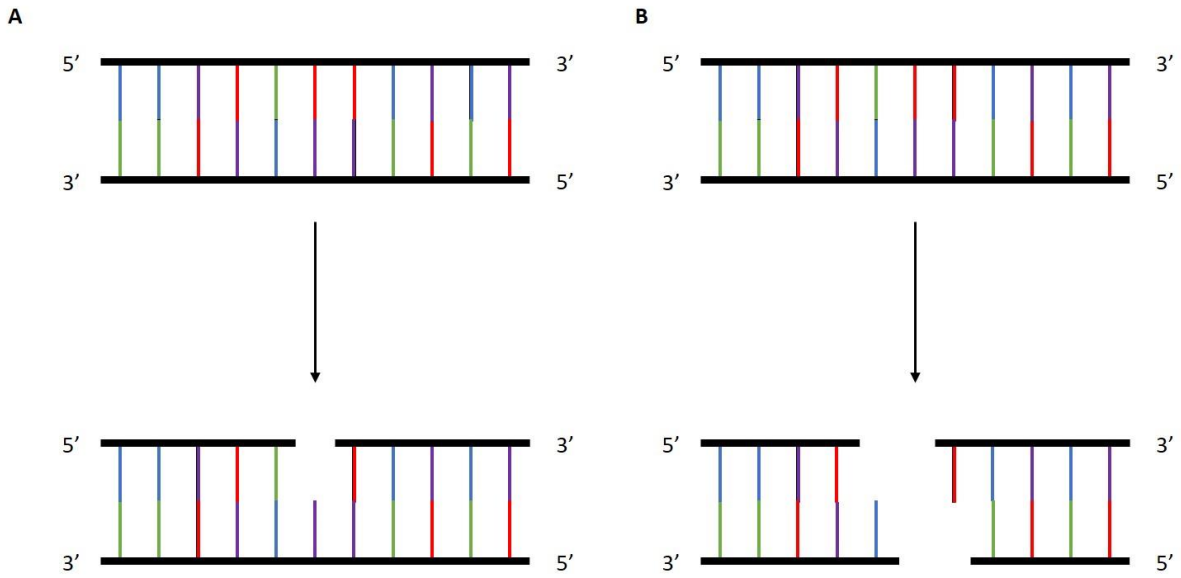


**Figure 1.5 DNA strand breaks**

Schematic diagram of the formation of DNA strand breaks with the colours showing the bases and DNA backbone in black. **A** DNA SSB is a break in one side of phosphodiester backbone **B** DNA DSB is a break in opposite sites of phosphodiester backbone.

### *1.3.2.1 Alkylation*

Alkylation is a process when alkylating agents transfer an alkyl group to the DNA, modifying the structure and therefore disrupting its function. Alkylating agents are ubiquitous, therefore human exposure is inevitable. They arise endogenously during metabolism, and exogenously in air, food, water, tobacco smoke and fuel pollutants. Furthermore, alkylating drugs are commonly used as a cancer treatment, thereby these patients are exposed to high doses of alkylating agents [44]. All the nitrogen sites within DNA bases (Figure 1.1) and the oxygen atoms in the base as well as the phosphodiester bonds are subject to alkylation. In general, the effects of base alkylation are genotoxic and cytotoxic, with O-alkylation being highly genotoxic and mutagenic and N-alkylation more cytotoxic [64]–[66]. Alkylating agents may be monofunctional (one chemical moiety) or bifunctional (two chemical moieties) and fall into two groups based upon their reactivity. $S_N1$-type (e.g. *N*-methyl-*N*-nitrosourea (MNU)) agents target both oxygens and nitrogens, whereas the $S_N2$ type (e.g. methyl methanesulfonate (MMS)) alkylate nitrogens [67], [68].

The types of DNA damage generated by alkylating agents can be primary products, methylations for example, or secondary damage through abasic sites, strand breaks and

interstrand crosslinks (ICLs) [44]. The most well defined endogenous source, S-adenosylmethionine (SAM), donates a methyl group in most enzymatic transmethylation reactions but can also non-enzymatically methylate DNA [7], [69], [70]. Primary products can also arise from exposure to exogenous agents, such as the highly carcinogenic, tobacco-specific nitrosamine 4-(methylnitrosamino)-1-(3-pyridyl)-1-butanone (NNK) [71]. These agents give rise to methylated bases including $N^7$-methylguanine (7meG) and $O^6$-methylguanine ($O^6$meG) (Figure 1.6) [44], [72]. 7meG is the most common methylated base (75 %) being produced at a rate of 4000 residues/human genome/day [68], [70], yet is not mutagenic due to maintained coding specificity. However, it is susceptible to depurination, forming mutagenic AP sites [73]. $O^6$meG lesions, although much less common (10-30 per cell per day), are prone to mismatch with thymine by MMR, resulting in mutagenic effects including cytotoxic DSBs [12], [44], [69]. This resulting cytotoxic effect is one reason monofunctional alkylating agents, such as MMS and temozolomide, are attractive options as anti-cancer drugs [74]. Additionally, bifunctional agents, chlorambucil or carmustine for example, are also commonly used in treating cancer, as these give rise to complex lesions, such as highly cytotoxic ICLs [44].

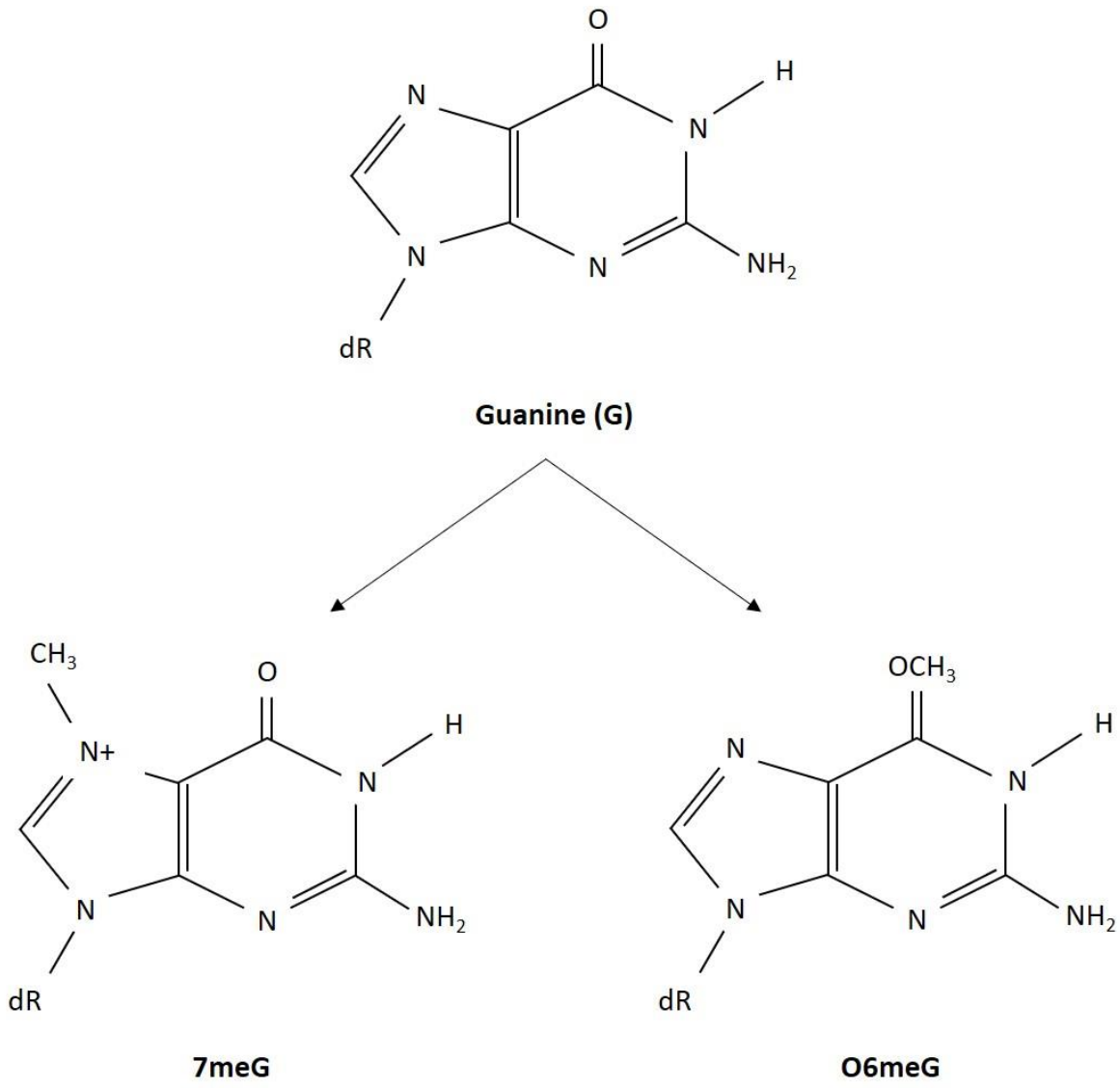


**Figure 1.6: Molecular structure of N7-methylguanine and O6-methylguanine**

Schematic diagram of the formation of the alkylated base 7meG and $O^6$meG from guanine due to the transfer of a methyl group.

### *1.3.2.2 Ionising Radiation*

IR is an exogenous source of DNA damage which has both natural (cosmic and gamma radiation) and artificial (medical X-ray/radiotherapy) origins. IR passes through material, such as cells, along a radiation track in which energy is deposited resulting in damage to biomolecules [8]. DNA is damaged in one of two ways, directly by 1-electron oxidation generating oxidative base lesions, of which 70 types of radiation-induced lesions have been characterised [75], or indirectly via water radiolysis radicals, resulting in the formation of

DNA base damage, abasic sites, DNA strand breaks and complex/clustered DNA damage (CDD) [8], [76], [77]. The most abundant lesions generated by IR are DNA base damage, abasic sites and DNA SSBs, with 1 Gy γ-radiation estimated to induce approximately 850 pyrimidine (e.g. Tg sites), 450 purine lesions (e.g. 8-oxoG) and 1000 DNA SSBs per cell. In contrast, only 20-40 DNA DSBs per cell are induced [78].

DNA DSBs, a break in both strands of the DNA phosphodiester backbone (Figure 1.5B), separated by 10 bp or less [79], are the most harmful lesion produced by IR, leading to apoptosis if not repaired. As well as being cytotoxic they are highly mutagenic if improperly repaired, leading to genomic instability via chromosomal rearrangements, insertions or deletions [77]. In addition to DSBs, CDD is also a major contributor to the cell killing effect of IR. Non-DSB CDD is defined as two or more lesions induced in close proximity (within 1 to 2 helical turns of the DNA), which arises due to the spatial deposition of energy along highly structured radiation tracks [80]. Furthermore the incidence complexity of non-DSB CDD increases with the radiation ionisation density, estimated from 30 % for low linear energy transfer (LET) IR up to 90 % for high-LET α-particles (α-IR) [81]–[84]. The base excision repair (BER) pathway is responsible for the majority of the repair of non-DSB CDD, but at a reduced efficiency [85], the extent of which is determined by the complexity, type, separation and orientation of the lesions [77]. This results in a reported persistence of CDD in cells and tissues several hours post-IR and an associated cell killing effect [80], [86], [87].

#### *1.3.2.3 Ultraviolet Radiation*

UV radiation, due to solar exposure, is an unavoidable source of exogenous DNA damage, with a day of sun exposure inducing up to $10^5$ UV photoproducts per exposed skin cell [6]. The UV spectrum is characterised according to wavelength, UVA (315-400 nm), UVB (280-315 nm) and UVC (100-280 nm). UVC is fortunately absorbed by the Earth's atmosphere, thereby is a negligible source of DNA damage [88]. However, UVA and UVB exposure, either from the sun or artificial sources (e.g. sun beds) are the most important etiological factor associated with the development of skin cancer [89], and the International Agency for the Research on Cancer has classified both UVA and UVB as a Class I carcinogen [90].

UV radiation induces DNA damage by providing the energy to modify the covalent bonds between pyrimidine residues. UVB induced mutations are well understood and can be accounted by two major DNA lesions, both with atypical covalent bonds between pyrimidines. Cyclobutane pyrimidine dimer (CPD), accounting for 75 % of UV photoproducts

and the pyrimidine-(6-4)-pyrimidone photoproduct (6-4 PP) the remaining 25 % [91]–[94]. These bulky DNA adducts distort the DNA helix by 7-9$^{o}$ for CPDs and 44$^{o}$ for 6-4 PP lesions, interfering with transcription and replication, therefore compromising genomic integrity [93], [95]. Furthermore, the mutagenic potential of these lesions is highlighted in the high incidence of C-T and CC-TT transition mutations at dipyrimidine sequences within unrepaired UVB lesions [91], referred to as 'UV-signature mutations' in skin cancer [96], [97].

In contrast, UVA is poorly absorbed by DNA, therefore damages DNA through indirect mechanisms of action [98], [99]. It is through absorption by chromophores that UVA exerts its DNA damaging effects, and these so-called photosensitizers are involved in photoreactions to generate ROS, such as, $O_2^{\bullet-}$, $H_2O_2$, $^1O_2$ and •OH. This can result in oxidative DNA damage, including base oxidation (8-oxoG and Tg), AP site and SSB formation [75], [98]. Furthermore, UVA is known to be a source of CPDs, in particular TT-CPDs, formed via a photosensitized triplet energy transfer mechanism [100].

## 1.4 DNA repair

Maintenance of genomic integrity and stability is integral for the survival of an organism, essential for ensuring proper cellular function, and for the successful replication and passage of genetic material to progeny. Conversely, the role of accumulated DNA damage, induced via endogenous and exogenous sources, compromises genomic integrity and has been well documented to be heavily implicated in human disease development, including cancer, neurodegenerative diseases and premature ageing [2], [9], [10]. Fortunately, cells possess a high fidelity system consisting of a complexity of damage sensors, DNA repair pathways, cell cycle checkpoints and damage tolerance mechanisms. This system, collectively known as the DNA damage response consists of ∼450 genes [101], encoding for a vast number of pathways and proteins, indicative of the range of DNA damaging genotoxic events the cell is subject too. The four major DNA repair pathways, double strand break (DSB) repair, nucleotide excision repair (NER), mismatch repair (MMR) and base excision repair (BER) have evolved to recognise and repair specific types of DNA damage and restore DNA to its undamaged state, ensuring continued genomic integrity.

### 1.4.1 Double Strand Break Repair

DSBs are considered the most cytotoxic form of DNA damage, arising from both endogenous (e.g. ROS) and exogenous (e.g. IR) sources. The repair of DSBs is imperative for cellular survival as they can result in cell death, or genomic rearrangements, such as insertions, deletions and chromosomal translocations, which are a primary initiation step in the development of many cancers [102]. Conversely, generation of DSBs are also key for certain biological processes, such as increasing genetic diversity during meiosis and in the diversification of the antigen receptors and immunoglobulins of immune cells via the breaks which occur during the process of V(D)J recombination and immunoglobulin heavy chain (IgH) class switch recombination [103], [104]. Whether detrimental or biologically vital, DSBs nevertheless require efficient processing and repair to avoid induction of major chromosomal aberrations. Two major types of DSB repair pathways have been identified, non-homologous end joining (NHEJ) and homologous recombination (HR).

#### *1.4.1.1 Non-Homologous End Joining*

NHEJ is the predominant method for the repair of DSBs throughout the cell cycle, repairing nearly all DSBs outside of the S and $G_2$ phase of the cell cycle and around 80 % of DSBs which are not proximal to a replication fork within these phases [105]. NHEJ is not restricted within the cell cycle, as it does not require a template for repair. However, this renders the pathway error prone due to the repair mechanism reattaching DNA with no regard for homology and modifying break sites with insertions/deletions (indels), linking NHEJ to mutations and chromosomal aberrations [102].

The process of classical NHEJ is divided into three main stages, firstly DSB recognition, followed by the processing of non-ligatable DNA ends and finally the joining of suitable DSBs (Figure 1.7). Additionally, and of note, NHEJ can directly religate broken DNA ends without the need for DNA end resection to initiate repair. Within NHEJ, repair is initiated by recognition and binding of the DSB by the Ku70/80 heterodimer, which encircles the DNA duplex, structurally supporting broken DNA ends. This also acts as a scaffold for the assembly of other NHEJ proteins and recruitment of the DNA-dependent protein kinase catalytic subunit (DNA-PKcs) forming the DNA-PK holoenzyme [106]. Activated DNA-PKcs acts as a major regulator within NHEJ [107], one such role is through activation of the endonuclease activity of Artemis at DNA ends, resulting in the endonucleolytic removal of 5’ and 3’ DNA overhangs, to facilitate ligation of the DNA ends by the XRCC4–DNA ligase IV complex [108],

[109]. Additional proteins such as, polynucleotide kinase/phosphatase (PNKP) [110] and MRE11-RAD50-NBS1 (MRN complex) [111] may also be recruited by DNA-PKcs to further process the DNA ends if they are not able to be directly ligated. Following DSB end processing, nucleotide addition can occur by the Pol X family polymerases, Pol μ and Pol λ, before ligation by DNA ligase IV in complex with XRCC4, XLF, and sometimes PAXX to resolve the strand break [112]. In addition to this pathway, a further mode of DSB repair is via alternative NHEJ, a poly(ADP-ribose) polymerase (PARP)-dependent sub pathway of NHEJ which involves MRN DNA end resection, followed by PARP-1 binding to DNA ends, and completion of repair by X-ray repair cross-complementing protein 1-DNA ligase IIIα (XRCC1-Lig IIIα) or DNA ligase I (Lig I) sealing the DSB [76].

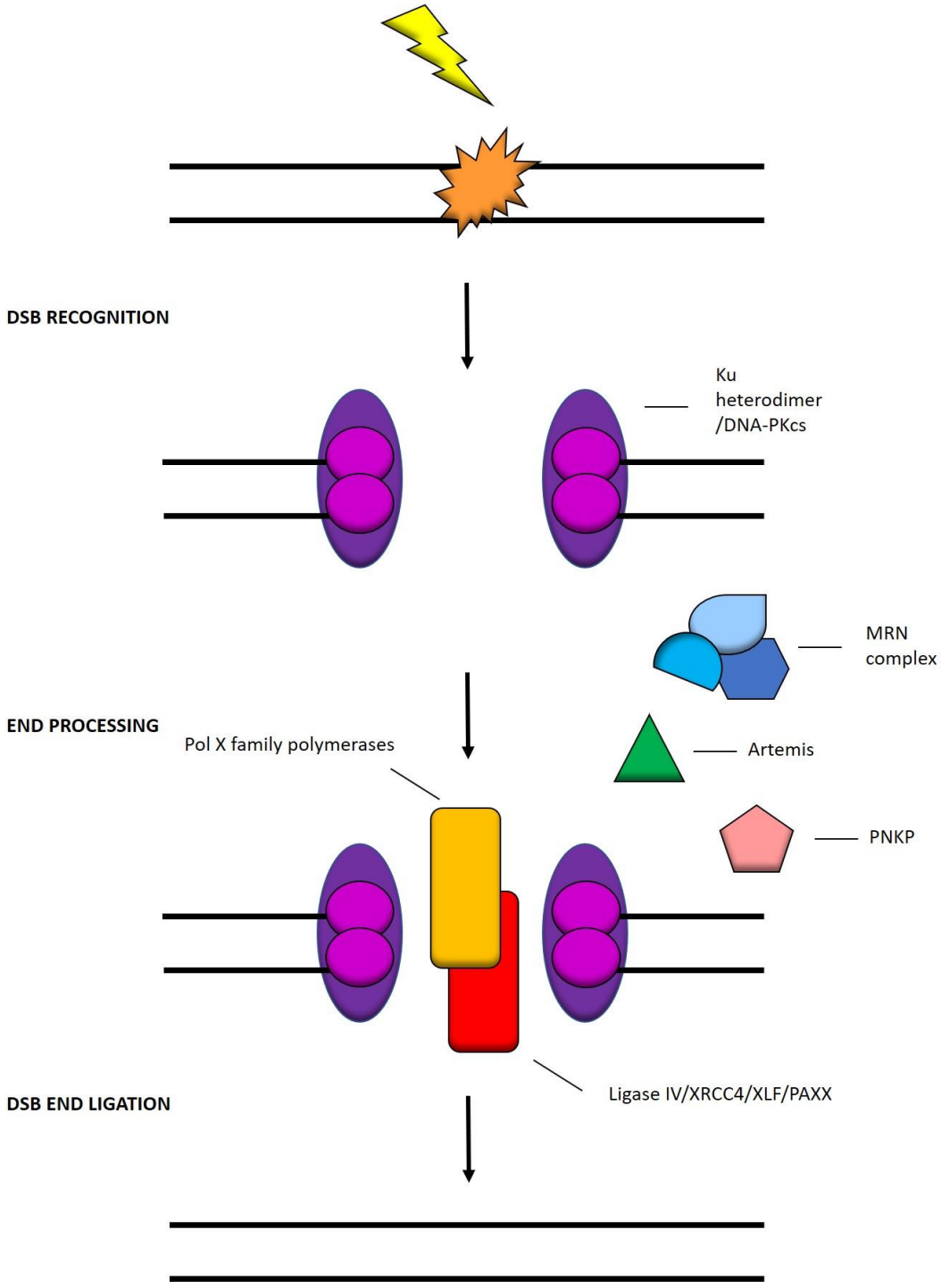


**Figure 1.7: Schematic of the non-homologous end joining pathway**

The DSB is recognised by the Ku 70/80 heterodimer encircling the DNA duplex as a scaffold. DNA-PKcs is recruited forming the DNA-PK holoenzyme, which acts as a major regulator in NHEJ. DNA ends are processed by Artemis, PNKP and the MRN complex. Nucleotide addition

can then occur by the Pol X family polymerases and the strand break resolved by ligase IV/XRCC4/XLF/PAXX. Adapted from [113], [114].

#### *1.4.1.2 Homologous Recombination*

In contrast to NHEJ, HR requires a homologous sequence, usually the sister chromatid as a template for repair [115]. This restricts HR to the S and $G_2$ phases of the cell cycle, where the sister chromatid is available, but which allows for the restoration of any missing genetic material, proximal to the DSB, resulting in a largely accurate repair system [116].

DNA end resection initiates HR (Figure 1.8) and is catalysed by the recruitment and binding of the MRE11-RAD50-NBS1 (MRN) complex to the DSB. The resection of the 5'-terminated end through the 3'-5'-exonuclease activity is achieved through the action of the MRE11 subunit in combination with CtIP (carboxy-terminal binding protein (CtBP)- interacting protein) and generates a 3'-ssDNA overhang [117], [118]. In some instances, long range resection enzymes such as exonuclease 1 (EXO1) or DNA2 are required to catalyze bidirectional resection in the 5'-3' direction, away from the DNA end, generating extended ssDNA overhangs [119], [120]. The 3' ssDNA overhang is initially coated by replication protein A (RPA), which functions protectively to prevent the self-annealing of ssDNA. RPA is then replaced by RAD51 to form a nucleoprotein filament or presynaptic filament. Formation of the nucleoprotein filament triggers homology search, template pairing and strand invasion [121]. All these steps are positively and negatively mediated by several recombination regulators (breast cancer gene 1 and 2 (BRCA1 and BRCA2) and RAD51 paralogs), which often promote recombination within the proper context via direct interaction with RAD51 [122]–[124]. Although the exact mechanism of homology searching is unknown, it is thought that the presynaptic filament locates homology by randomly probing the genome with multiple temporary contacts, and that when a region of 7 nucleotides of homology is located, strand invasion occurs [125], [126]. Following strand invasion, a displacement loop (D-loop) is generated due to the invasion of the presynaptic filament into the homologous donor template. The 3'-ssDNA strand within the D-loop is then used to prime DNA synthesis, using the invaded strand as a template, DNA synthesis occurs down the length of the paired duplex and thus repairs the broken DNA [127]. The majority of DNA synthesis during HR is catalysed by DNA polymerase δ and polymerase ε [128]–[130], although translesion polymerases have been implicated in this role [131], [132]. The repair process can then be completed by one of two recombination sub-pathways, synthesis-dependent strand annealing (SDSA) or DSB

repair (DSBR). In SDSA, the invading strand is separated from the undamaged template DNA and anneals to the end of the DNA break. Repair is completed by DNA synthesis and ligation, generating non-crossover intact DNA [115], [127]. During DSBR, both 3'-ssDNA overhangs are paired with the template DNA and the D-loop is processed into double Holliday junctions. These are then processed via cleavage and ligation into crossover or non-crossover restored DNA [115], [133].

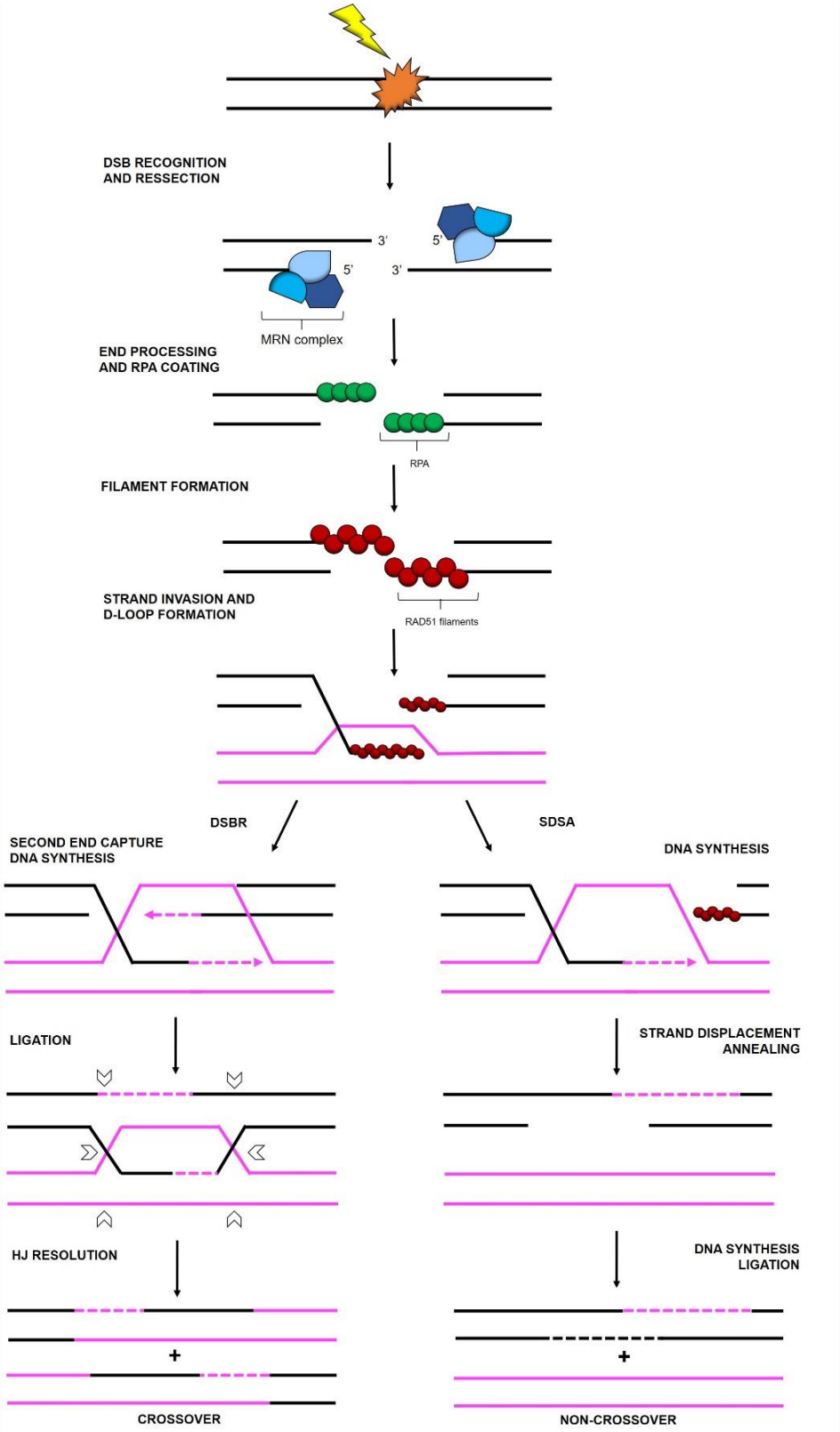


**Figure 1.8: Schematic of the Homologous Recombination pathway**

HR is initiated via the recruitment of the MRN complex to the DNA ends which catalyses DNA end resection, generating 3' ssDNA overhangs which are coated with RPA. RPA is then replaced by RAD51 to form a nucleoprotein filament, triggering homology search, template

pairing and strand invasion. Following strand invasion, a D-loop is generated and the 3'-ssDNA strand is used to prime DNA synthesis, using the invaded strand as a template. The repair process is then completed via the DSBR pathway (left arm) or the SDSA pathway (right arm). In SDSA, the invading strand is separated from the undamaged template DNA and anneals to the end of the DNA break. Repair is completed by DNA synthesis and ligation, generating non-crossover intact DNA. During DSBR, both 3'-ssDNA overhangs are paired with the template DNA and the D-loop is processed into double Holliday junctions. These are then processed via cleavage and ligation into crossover or non-crossover restored DNA. Adapted from [134], [135].

### 1.4.2 Nucleotide excision repair

NER has a wide ranging specificity, processing various helix-distorting DNA lesions. These include 6-4PPs and CPDs which form upon exposure to UV radiation, and many bulky DNA adducts induced by mutagenic environmental chemicals or cytotoxic drugs such as cisplatin [136]. In humans, hereditary defects in NER have been implicated in several diseases including xeroderma pigmentosum (XP) [137], where extreme sensitivity to sunlight is seen with a 1000-fold increase in the risk of developing skin cancer, and the UV sensitivity disorder Cockayne syndrome associated with premature ageing [138]. There are two distinct sub-pathways of DNA damage detection in NER, global genome NER (GG-NER) and transcription coupled NER (TC-NER). GG-NER, as the name suggests, detects and remove lesions throughout the genome, whereas TC-NER detects the blockage of transcription elongation, indirectly ensuring the rapid repair of lesions of transcribed genes [136].

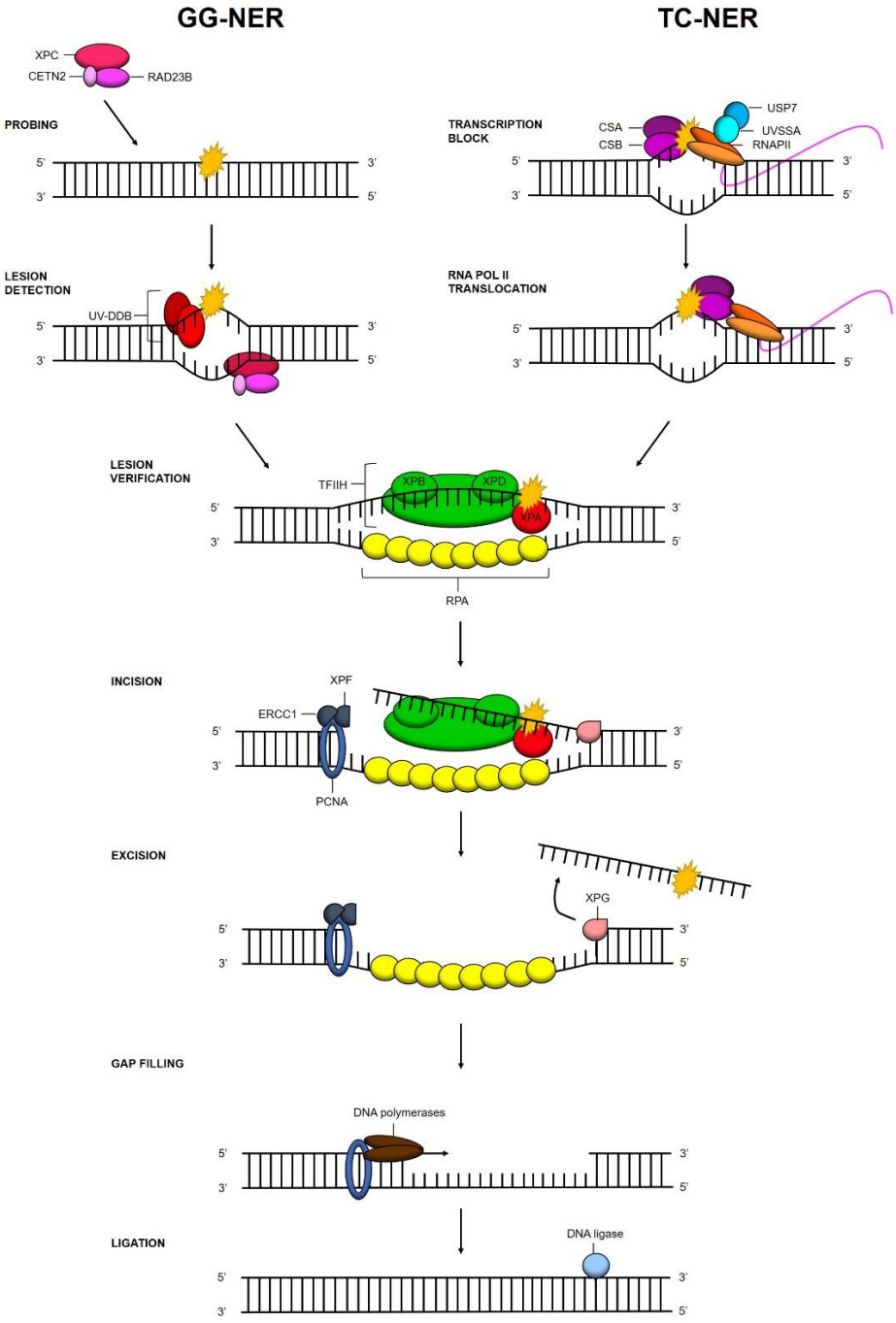


**Figure 1.9: Schematic of the NER pathway**

Shown is the two sub-pathways of NER; GG-NER (left arm) and TC-NER (right arm). GG-NER is initiated via lesion recognition and binding by the XPC-RAD23B-CETN2 and UV-DDB complex. TC-NER is initiated by translocation of stalled RNAPII by CSA and CSB. Following lesion recognition, TFIIH and the DNA helicases XPB and XPD unwind the DNA around the lesion. RPA then coats and protects the ssDNA, and XPF-ERCC1 and XPG incise the backbone removing the damaged DNA. PCNA is the loaded onto the DNA directing the recruitment of

replicative polymerases and DNA ligase to fill and seal the gap, completing repair. Adapted from [139].

#### *1.4.2.1 Global Genomic NER*

GG-NER (Figure 1.9, left arm) is initiated by DNA damage sensing by the GG-NER specific factor xeroderma pigmentosum complementation group C (XPC) in complex with UV excision repair protein RAD23 homolog B (RAD23B) and centrin 2 (CETN2), which provides stabilisation. This complex scans the DNA for helical distortions, binding to ssDNA which has developed due to thermodynamic destabilisation of the DNA by the lesion [140], [141]. Following this initial recognition, a lesion verification step follows where at the junction between the ssDNA and dsDNA (created by the lesion), the C-terminal double β-hairpin domain of XPC-RAD23B is inserted [142] and it is this non-specific binding which explains the broad range of damage targeted by GG-NEC [143]. In certain cases, as with UV-radiation-induced CPDs which only produce mild helical destabilisation, the XPC complex cannot initiate repair [144], [145]. Therefore, the UV radiation-DNA damage-binding protein (UV-DDB) complex is required. This comprises of the DNA damage-binding protein 1 (DDB1) and 2 (DDB2) which recruit and form a larger complex with the Cullin-RING ubiquitin ligase (CRL) containing cullin 4A (CUL4a) and regulator of cullins 1 (ROC1). DDB2 binds to the DNA damage, UV-DDB complex kinks the DNA and ROC1 ubiquitylates XPC facilitating its DNA binding [146]–[148]. Following recognition of the lesion by XPC, the ten protein subunit transcription initiation and repair factor, transcription initiation factor IIH (TFIIH), is recruited [149]. Within TFIIH the two DNA helicases, XPB and XPD, which have opposing polarities, unwind the DNA around the lesion [150]. The lesion is then excised by two endonucleases, XPF-ERCC1, 5’ to the lesion and XPG, 3’ to the lesion, resulting in a ∼30 nucleotide single strand gap. Facilitating this process is XPA which coordinates accurate incision, and RPA which coats and protects the ssDNA [151]. Finally, DNA gap filling synthesis and ligation is directed by the replication proteins proliferating cell nuclear antigen (PCNA), replication factor C (RFC), replicative polymerases DNA Pol δ, DNA Pol ε or DNA Pol κ, and DNA ligase I or X-ray repair cross-complementing 1-DNA ligase III (XRCC1-LigIII) complex [152], [153].

#### *1.4.2.2 Transcription coupled NER*

Despite the activity of UV-DDB within GG-NER, the processing of lesions, such as CPDs, is often of poor quality and can lead to replication stalling. To avoid negative outcomes associated with this, including generation of DSBs or triggering of cell death [154], the TC-NER pathway has evolved to selectively repair transcription blocking lesions [155]. TC-NER (Figure 1.9, right arm) is indirectly initiated due to lesion stalling of RNA polymerase II (RNAPII) during transcription elongation, which recruits Cockayne syndrome proteins A (CSA) and B (CSB), triggering translocation of RNAPII and further assembly of the TC-NER machinery [156]. This includes binding of specific TC-NER factors such as, UV stimulated scaffold protein A (UVSSA) and ubiquitin specific processing protease 7 (USP7) which act to stabilise CSB [157]. Following this recognition step, it is thought that the stalling of transcript elongation induces lesions recognised by the GG-NER sub-pathway and repair proceeds with the same steps as GG-NER, starting with the binding of TFIIH [139].

### 1.4.3 DNA Mismatch Repair

MMR processes nucleotide misincorporation during DNA synthesis or mismatches with the DNA helix, which risk becoming fixed as mutations following DNA replication [158]. The pathway also acts to prevent mutations arising due to the natural error rate of replicative polymerases [159] and errors associated with strand slippage or unusual secondary DNA structures within repetitive sequences [160], [161]. The biological implications of inactive MMR is a 1000-fold elevation in spontaneous mutation rate [162], which has been implicated in human cancer development, including being a known cause of hereditary non-polyposis colon cancer (HNPCC) [163], [164]. MMR has been most extensively characterised in Escherichia coli (E. coli), however the pathway is evolutionarily conserved from prokaryotes to eukaryotes and substantial information is now available on the yeast and human systems [165]. In eukaryotes, MMR is initiated by mismatch recognition by the heterodimers MutSα or MutSβ. MutSα repairs mismatched base pairs and short indel loops of 1-2 bp, whereas MutSβ repairs longer indels of 1-15 bp. Utilising ATP, MutSα and MutSβ act as sliding clamps to search for mismatches, once located and bound, MutLα is recruited. The endonuclease activity of MutLα, coupled with the activity of PCNA and EXO1, removes the mismatch containing stretch of DNA. RPA provides protection to the ssDNA whilst gap filling by replicative polymerases completes repair [166].

### 1.4.4 Base Excision Repair

Base excision repair (BER), a sophisticated cellular mechanism first reported in the 1970s by Thomas Lindahl, detects small, non-helical distorting lesions [167]. Sites of DNA damage processed by BER include SSBs, apurinic/apyrimidinic (AP) sites, alkylated and oxidised DNA bases, which are generated at a rate of over 10,000 DNA base lesions and SSB per cell per day. This is largely as a result of DNA hydrolysis, cellular oxidation and environmental factors, such as IR [7]. If left unrepaired, accumulation of these types of DNA damage compromises genomic integrity and have been implicated in human disease development, including premature ageing, neurodegenerative diseases and several cancers. The BER pathway is highly conserved from prokaryotes to eukaryotes, with functional homologs existing between bacteria, yeast and humans [168]. The pathway can be broadly divided into four distinct steps; DNA base damage excision, AP site incision, DNA end processing and DNA ligation. Following BER initiation, subsequent repair can follow one of two sub pathways, short patch repair (Figure 1.10, central branch), the dominant pathway where a single nucleotide gap is created and filled, or the lesser utilised long patch repair (Figure 1.10, right branch) which creates a 2-10 nucleotide gap [169].

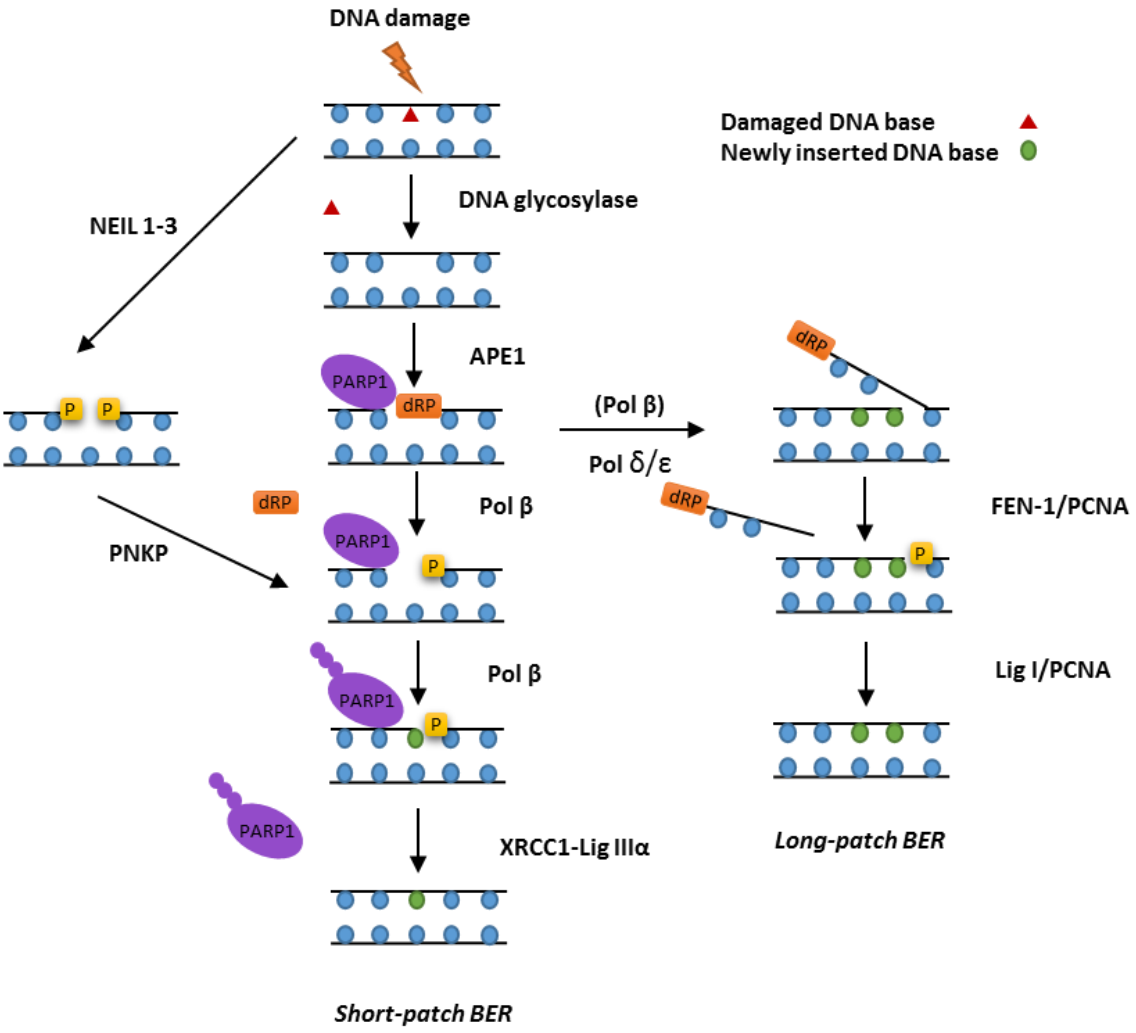


**Figure 1.10: Schematic of the BER pathway**

A damage-specific DNA glycosylase initially detects the lesion in the DNA and excises the damaged base through catalysing the cleavage of the N-glycosidic bond, leaving an AP site, which recruits both APE1 and PARP1. APE1 cleaves the AP site, yielding a 3'-hydroxyl group adjacent to a 5'-deoxyribosephosphate (dRP) which is removed by Pol β that simultaneously fills in the gap with a new nucleotide (central branch). Alternatively, if BER is initiated by the NEIL DNA glycosylases (left branch), a single nucleotide gap containing 3'- and 5'-phosphate ends is created via β,δ- elimination. The 3'-phosphate is subsequently removed by PNKP prior to the activity of Pol β that fills in the gap. In short-patch BER, the nick in the phosphodiester backbone enhances PARP1 poly (ADP-ribosyl)ation activity allowing for the recruitment of XRCC1-Lig IIIα, which seals the nick and completes repair. If there is resistance of the 5'-dRP moiety to Pol β dRP lyase activity, long-patch BER (right branch) is initiated in which there is a polymerase switch to Pol δ/ε which adds 2-8 more nucleotides into the single nucleotide

gap, creating a 5'-flap which is excised by FEN-1. The remaining nick is then repaired by Lig I in association with PCNA to complete the BER process. Taken from [170].

#### *1.4.4.1 DNA base damage excision*

The DNA base damage is recognised by a DNA glycosylase, of which 11 damage-specific enzymes (Table 1.1) exist that detect and excise the damaged base [171], [172]. These enzymes utilise a 'base flipping' mechanism whereby the damaged base is flipped 180 degrees from the sugar phosphate backbone, breaking the hydrogen bonds between the bases, and which then places the damaged base in the active site of the DNA glycosylase for excision. Yet, within the glycosylases there are two different types, monofunctional and bifunctional, that contrast in terms of their activities.

The monofunctional DNA glycosylases (uracil DNA glycosylase [UNG], single-strand-selective monofunctional uracil DNA glycosylase [SMUG1], thymine DNA glycosylase [TDG], N-methylpurine DNA glycosylase [MPG], methyl-CpG binding domain protein 4 [MBD4] and MutY homologue [MUTYH]) only possess DNA glycosylase activity and will therefore only remove the damaged base by severing the N-glycosidic bond. This yields an AP site which recruits AP endonuclease 1 (APE1) whose activity incises the DNA backbone, forming a 3'-hydroxyl group adjacent to a 5'-deoxyribosephosphate (dRP) moiety [173], [174].

Whereas the bifunctional DNA glycosylases (8-oxoguanine DNA glycosylase 1 [OGG1], endonuclease III-like protein 1 [NTH1] and endonuclease VIII-like proteins 1, 2 and 3 [NEIL1, NEIL2 and NEIL3]) in addition to their DNA base excision activity are also able to cleave the DNA backbone. The activity of the DNA glycosylases OGG1 and NTH1 form a resulting single nucleotide gap with flanking 5'-phosphate and 3'-α,β-unsaturated aldehyde (PUA) ends (β elimination). Similar to the monofunctional DNA glycosylases, this action is followed by cleavage of the 3'-aldehyde residue by APE1 generating the same 3'-hydroxyl end. However, due the cellular abundance of APE1 and relatively low activities of these bifunctional glycosylases, it is generally thought that APE1 circumvents this step and directly cleaves the AP site itself [175]. Alternatively, bifunctional DNA glycosylase action by the NEIL DNA glycosylases creates a single nucleotide gap with a flanking 5'-phosphate and 3'-phosphate ends (β,δ-elimination). The 3'-phosphate moiety requires removal by polynucleotide kinase phosphatase (PNKP), as the lesion is incompatible for DNA polymerase β (Pol β) activity (Figure 1.10, left branch) [176]. Irrespective of these different branches of the BER pathway,

a single nucleotide gap with a 3'-hydroxyl end, which acts as a substrate for a DNA polymerase is produced.

**Table 1.1: The human DNA glycosylases.** Adapted from [177].

| Name | Abbreviation | Classes | | Major type of DNA damage excised |
|---|---|---|---|---|
| 8-Oxoguanine DNA glycosylase 1 | OGG1 | HhH DNA glycosylases | Bifunctional (β-elimination) | 8-Oxoguanine formamidopyrimidines |
| Endonuclease III-like 1 | NTH1 | HhH DNA glycosylases | Bifunctional (β-elimination) | Oxidative damage to pyrimidines, including thymine glycol, 5-hydroxyuracil, 5-hydroxycytosine |
| Endonuclease VIII-like 1 | NEIL1 | Nei NEIL DNA glycosylases | Bifunctional (β, δ-elimination)) | Oxidative damage, with preference for pyrimidines |
| Endonuclease VIII-like 2 | NEIL2 | Nei NEIL DNA glycosylases | Bifunctional (β, δ-elimination)) | Oxidized cytosine derivatives |
| Endonuclease VIII-like 3 | NEIL3 | Nei NEIL DNA glycosylases | Bifunctional (β, δ-elimination)) | Hydantoins; prefers single-stranded DNA structures |
| Methyl-CpG binding domain protein 4 | MBD4 | UNGs | Monofunctional | Mismatches opposite guanine |
| MutY homologue | MYH | HhH DNA glycosylases | Monofunctional | Mispaired adenine |
| N-methylpurine DNA glycosylase | MPG | Methylpurine DNA glycosylase | Monofunctional | Alkylated bases |
| Single-strand-selective monofunctional uracil-DNA glycosylase | SMUG1 | UNGs | Monofunctional | Uracil and derivatives, preferably from single-stranded DNA |
| Thymine DNA glycosylase | TDG | UNGs | Monofunctional | Thymine or uracil from mispairs with guanine uracil derivatives |
| Uracil DNA glycosylase | UNG | UNGs | Monofunctional | Uracil residues |

#### *1.4.4.2 AP site incision*

In the initial step of BER, DNA glycosylase mediated reactions often generate an AP site, which is recognised and cleaved by APE1 on the 5'-side, producing a SSB with a 3'-hydroxyl

group and 5'-dRP termini [178]. Structurally, APE1 consists of a flexible N-terminal domain and a rigid globular C-terminal nuclease domain, the latter of which provides APE1 with its DNA binding and backbone cleavage activity [179], [180]. The nuclease domain binds APE1 to DNA and allows for AP site searching by sliding along the strand via interactions with the DNA phosphate backbone [181]. The AP site is identified via substrate specificity provided by the active site, APE1 kinks the DNA forcing the AP site into a 'flipped out' position within the active site [180], and cleaves the DNA phosphodiester bond through a catalysed acid-base reaction which is stabilised by magnesium ion ($Mg^{2+}$) binding [182]. The resulting SSB is then bound by PARP1 which becomes activated upon SSB binding, essential for its role in promoting resolution of the DNA damage in the end processing stages of BER [183]. In addition to its endonuclease activity, APE1 also possesses weak 3'-5'-exonuclease activity to remove 3'-end groups however, this role of APE1 remains inadequately understood [184]. Yet, the biological relevance has been demonstrated several times. This includes compromised exonuclease APE1 variants association with carcinogenesis [185], [186] indicating a vital proofreading role for APE1, removing ligation stalling DNA polymerase β mismatches [184], [187] and the removal of bi-functional glycosylase generated PUA groups [176].

#### *1.4.4.3 DNA end processing*

To fill the gap generated during BER, DNA polymerases are utilised that require a single nucleotide gap with a 3'-hydroxyl end and an undamaged template to act as a substrate. Four DNA polymerases are involved in BER, DNA Pol β, δ, ε and λ, with BER predominantly employing Pol β [188]–[190]. Pol β consists of two catalytic domains, an 8 kDa N-terminal DNA binding and dRP lyase domain and a 31 kDa C-terminal polymerase domain. There are three subdomains, the fingers, the thumb and the palm which facilitate catalysis [191], [192]. Pol β is recruited to DNA via interaction with APE1, PARP1 or the SSB. At the gap site, its C-terminal polymerase domain bends the ssDNA 90 degrees, whilst the dRP lyase activity of Pol β removes the 5'-dRP moieties and simultaneously inserts the correct undamaged nucleotide into the repair gap [190], [193]. Pol β also initiates long-patch BER (Figure 1.10, right branch) by adding the first nucleotide into the repair gap. In fact in certain circumstances, often due to resistance by the 5'-dRP moiety to Pol β dRP lyase activity, a polymerase switch to Pol δ/ε triggers long-patch BER. Pol δ/ε typically add 2-8 more nucleotides into the single nucleotide gap. This process creates a 5'-flap structure that is

excised by flap endonuclease-1 (FEN-1) which acts in a proliferating cell nuclear antigen (PCNA)-dependent process, with DNA ligase I (Lig I) finally completing repair [194], [195]. The fourth DNA polymerase in BER, Pol λ, with 32 % amino acid homology [196], has been suggested to be a back-up polymerase for Pol β. Although a less efficient alternative, Pol λ has been shown to catalyse background repair activity in Pol β-deficient mouse embryonic fibroblast extracts [189].

#### *1.4.4.4 DNA ligation*

Polymerase gap filling produces a resulting nick, this enhances PARP1's ADP-ribosylation activity, allowing for the auto-modification of PARP1 by the addition of negatively charged poly ADP-ribose (PAR) chains, which act as a scaffold to DNA repair proteins including the X-ray cross-complementing protein 1-DNA ligase IIIα (XRCC1-Lig IIIα) complex [197]. At which point the accumulation of sufficient negative charges allows for repulsion of PARP1 from the lesion allowing for ligation by the XRCC1-Lig IIIα complex. Ligases act by utilising ATP or nicotinamide adenine dinucleotide ($NAD^+$) to catalyse a phosphodiester bond between the 3'- hydroxyl and 5'-phosphate groups. This completes the predominant mode of BER, also known as short-patch BER (Figure 1.10, central branch) [198], [199]. The alternative pathway, long-patch BER (Figure 1.10, right branch) completes repair via Lig I mediated ligation [194], [195].

## 1.5 Chromatin

### 1.5.1 Chromatin structure

In eukaryotes, the vast majority of DNA within the cell is located within the nucleus. However, if all the DNA contained within the 46 chromosomes was laid out end to end, it would span 2 metres in length. Therefore, to fit in the 6 μm nucleus, cellular DNA must be folded and condensed into a highly organised structure. This is called chromatin and consists of a number of loops and coils, organised by histones and non-histone chromosomal proteins which bind to DNA and structure chromosomes. The first order of chromatin arrangement is the nucleosome, a histone-DNA complex, which link to form nucleosome arrays. These are further folded on top of one another to condense DNA to form chromatin fibres, which are

coiled and condensed to form chromosomes. This compaction into chromatin allows DNA to be packaged into small regions, but also serves to protect it from damage, control gene expression and strengthen DNA to allow for mitosis or meiosis when entering anaphase. Heterochromatin is the term for tightly packed chromatin, the structure of which turns off genes. Conversely, euchromatin is a relaxed area of chromatin and is typically the location of frequently expressed genes. Nevertheless, chromatin is dynamic, and can be arranged and regulated to accommodate for a range of biological processes, such as DNA transcription, replication, and repair.

#### *1.5.1.1 Chromatin organisation*

The compaction of chromosomes into chromatin is vital for DNA organisation within the nucleus and involves co-ordinated levels of folding amongst histones and non-histone chromosomal proteins. Conversely, the accessibility of DNA within compacted regions is modulated via multiple mechanisms to allow for essential biological processes including gene transcription, DNA replication and DNA repair. The nucleosome is the first order of DNA packaging [200], which consists of ~145-147 base pairs of DNA wrapped ~1.7 times around a histone octamer. The octamer consists of two copies of the four core histone proteins, H2A, H2B, H3 and H4, which are then separated by ~20-90 bp of linker DNA associated with the linker histones, H1 and H5 [201]. Initiation of nucleosome formation involves the wrapping of recently replicated or repaired DNA around the H3-H4 tetramer, followed by the addition of two H2A-H2B dimers [201]. Stability is provided to the nucleosome via 14 weak histone-DNA bonds, generated through interactions between the positively charged residues in the histone octamer and the DNA phosphate backbone in the minor groove [202]. Short sections of DNA, often associated with the linker histones (H1 and H5), also referred to as 'linker DNA', joins nucleosomes together to form nucleosomal arrays (10 nm beads-on-a-string like structures; Figure 1.11). These structures are packaged with neighbouring nucleosomes into 30 nm chromatin fibres, which following a high degree of compaction due to fibre-fibre interactions leads to the formation of a highly ordered tertiary structure observed in condensed chromatin [203].

Protruding out from the nucleosomes are the N-terminal tails of the histones that present lysine residues to be targeted for the addition, but also removal, of chemical moieties through histone post-translational modifications (PTMs). These PTMs, which include phosphorylation, ubiquitiylation, acetylation, methylation, SUMOylation and PARylation,

alter chromatin composition and function [204], [205]. In particular, these function to promote DNA accessibility either through direct destabilisation of the chromatin structure, or via stimulation of the recruitment of chromatin remodelling enzymes. Increasing evidence, at least acquired *in vitro*, suggests that histone PTMs and/or recruitment of chromatin remodelling factors may be integral in the processing of DNA damage through the BER pathway.

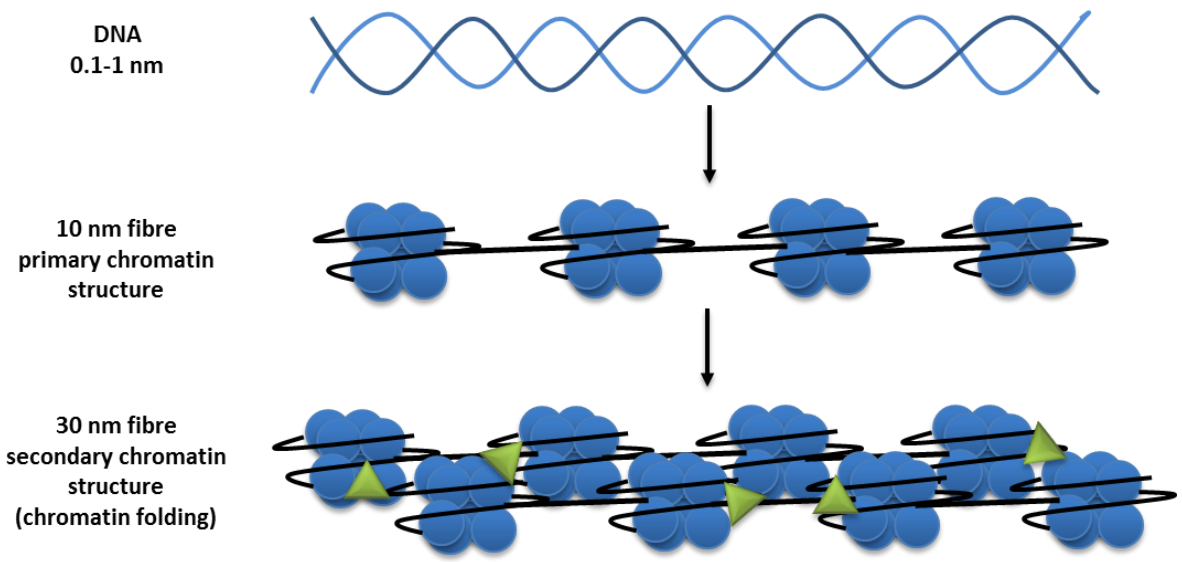


**Figure 1.11: The primary and secondary structures that form chromatin**

DNA is wrapped ~1.7 times around a histone octamer consisting of two copies each of histones H2A, H2B, H3 and H4 and linked to adjacent nucleosomes via linker DNA to form the primary structure of chromatin, the 10 nm fibre. These structures undergo packaging with neighbouring nucleosomal arrays and associate with architectural proteins (shown as green triangles) to form the 30 nm chromatin fibre, the secondary structure of chromatin. Taken from [170].

### *1.5.1.2 Nucleosome structure*

The crystal structure of the nucleosome, determined in 1997, gives our clearest depiction that 146 bp of human DNA wrapped 1.65 times in a left-handed superhelix around a central histone octamer (Figure 1.12) [201]. The nucleosome itself is symmetrical, with the dyad, centred on a single DNA base defining the axis of symmetry [206] and DNA locations represented by superhelical turns from the dyad, designated superhelical locations (SHL) -7

to SHL7. Two copies of each of the core canonical histone proteins (H2A, H2B, H3 and H4) make up the central histone octamer [207]. These core histones are positively charged and structurally constructed from three α helices, divided by two loops (α1-L1-α2-L2-α3). This histone fold motif is essential for heterodimerisation as each domain pairs with a complimentary histone fold (H2A pairs to H2B, and H3 pairs to H4) to form a handshake motif [201], [207], [208]. These heterodimers (two H2A/H2B and two H3/H4) come together to form a single structure, the four helix bundle. In histone H3, the α2 and α3 helices allow for two H3-H4 dimers to interact in a head on arrangement via a H3/H3 four helix bundle to form $(H3/H4)_2$ tetramers. Using a similar four helix bundle, the H2A/H2B dimers bind to the $(H3/H4)_2$ tetramer via the H4 and H2B histone folds to form the ordered histone octamer [209]. The architecture of the histone octamer also consists of several tail protrusions, including eight N-terminal tails, one from each of the histone proteins and two C -terminal tails protruding from histone H2A. These histones tails provide points of interaction with other nucleosomes and are the site of most PTMs [209]. The histone octamer forms a designated path for the nucleosomal DNA, with the octamer binding the central 121 bp of nucleosomal DNA. The histone-DNA interfaces are mediated by numerous protein, electrostatic interactions and direct and water-mediate hydrogen bonds to stabilise the nucleosome [201], [202], [210].

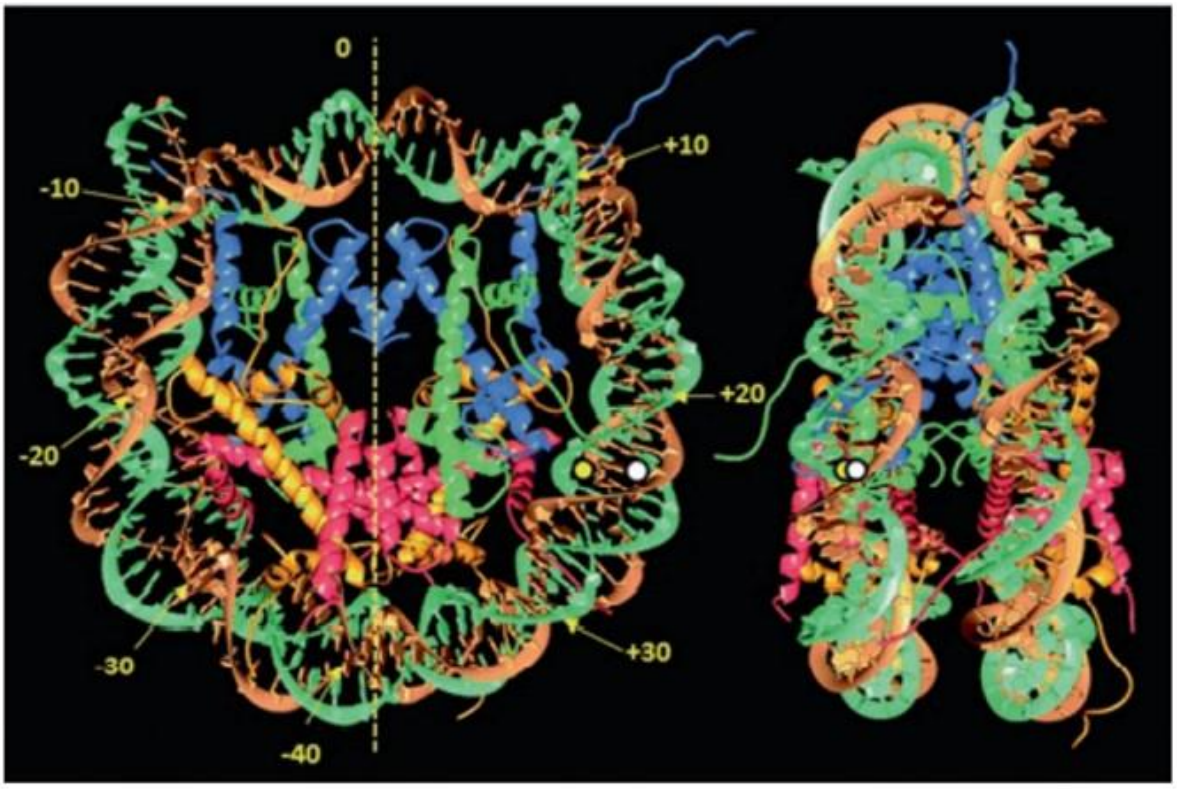


**Figure 1.12: Structural details of a nucleosome**

The structure of the nucleosome with detailed interactions of DNA and histones to near atomic level, with a view down the superhelical axis (left figure) and at a 90° angle (right figure). The ribbons in brown and green form the DNA backbone and the individual histones within the octamer are shown (H2A in orange, H2B in red, H3 in blue and H4 in green). The dyad axis shown as the dashed yellow line on the left, defined as the super helix site 0 is a 2-fold axis of symmetry and associated vertically with the DNA at the top of each image. Indicated on the DNA backbone are the numbering of bases relative to the dyad from the 5'-end (+) or the 3'-end (−), plus representative sites of DNA base damage facing inwards (yellow) and outwards (white) from the histone core. Image taken and adapted from [201].

### *1.5.1.3 Secondary structure*

Nucleosomes are joined together by 'linker DNA', which are short sections of DNA (15-20 bp) often associated with the linker histones (H1 and H5) to form nucleosomal arrays (10 nm beads-on-a-string like structures: Figure 1.11). Nucleosomal arrays are compacted to form the secondary structure of chromatin, a three-dimensional higher order structure, 30 nm chromatin fibres. The 30 nm fibre was first observed as early as 1980 [211], [212], however, the structure is still yet to be resolved with two possible models, the solenoid and zigzag. The

one start solenoid model consists of bent linker DNA joining neighbouring nucleosomes along a superhelical path [213]–[216]. The two start zig zag model involves two rows of nucleosomes connected by straight linker DNA in a radial or longitudinal arrangement [214], [217]–[219].

#### *1.5.1.4 Tertiary structure*

The model for higher order chromatin structures is primarily based upon the visualisation of extracted metaphase chromosomes, which reveal a radial-loop protein scaffold model basis for the tertiary structure to chromatin [220]. However, this view of an ordered hierarchical coiling of the 30 nm fibre, which is increasingly compacted to higher order structures, is only one model [221]. It has been demonstrated that this radial-loop model cannot be extrapolated to interphase chromosomes [222] and other models based upon a less ordered structure have been proposed. Such suggestions include, a molten globule or polymer melt physical arrangement of compacted and irregularly folded nucleosome arrays [203], [223], [224]. This, however, does not account for the rod-like structures seen at metaphase and other chromatin organising and compacting proteins, such as heterochromatin protein 1 (HP1) and polycomb repressive complex 1 and 2 (PRC1/2), are likely to coordinate these final levels of organisation [221].

### 1.5.2 Regulation of Chromatin structure

Chromatin, the highly ordered structure our DNA is compacted into, poses potentially major issues for the cell when undergoing DNA dependent activities. Therefore, regulation of the chromatin structure is vital to keep it dynamic, allowing the DNA to be accessible to enable the cell to undergo activities, including transcription, DNA replication, repair and recombination. Remodelling of chromatin is generally thought to occur by two major events, which are not necessarily mutually exclusive. The first is co-ordinated by histone PTMs and the second by ATP-dependent chromatin remodelling complexes (ACRs).

#### *1.5.2.1 Histone PTMs*

Histone PTMs are small chemical groups covalently added to the C or N-terminal tails of the histones, histone folds or globular domains (which mediate histone-histone or histone-DNA interactions) during or after protein synthesis [225]. There are over 100 histone PTMs reported, with the list growing each year, and the most up to date catalogue was published in 2015 [226]. However since then, histone acylations, hydroxylation, lipidation, monoaminylations and other nonenzymatic PTMs have been characterised [227]. The majority of histone PTMs occur on the N-terminal tails and the most well-known include, lysine acetylation, ubiquitylation and SUMOylation, lysine and arginine methylation, and serine, threonine and tyrosine phosphorylation [228]. These PTMs act as signals altering nucleosome stability and the local chromatin environment by changing chemical interactions either in or between nucleosomes [229]. PTMs therefore can enhance DNA damage accessibility in localised regions, and this process has been demonstrated to be particularly important in enhancing the efficiency of DNA DSB repair [230]. Histone PTMs can also act to stimulate the recruitment of ACRs.

#### *1.5.2.2 ATP-chromatin remodelling complexes*

ACRs utilise the energy of ATP hydrolysis to cause either the displacement or sliding of nucleosomes to expose DNA sequences, or even the ejection and subsequent replacement of histones. There are four families of ACRs (Figure 1.13). These are switching defective/sucrose non-fermenting (SW1/SNF), imitation switch (ISWI), chromodomain helicase DNA binding (CHD) and inositol requiring 80 (INO80). They all have a strong nucleosome affinity and share a conserved ATPase domain for remodelling and breaching histone DNA interfaces, histone PTM recognition domains, and domains to facilitate ATP hydrolysis to mediate histone-DNA contacts. Providing specificity for their respective families, the enzymes also possess flanking domains for family groupings [231]. SWI/SNF complexes are known to slide and evict nucleosomes from DNA and are classified by a C-terminal bromo domain which binds to acetylated lysines within N-terminal histone tails, and an N-terminally located helicase-SANT (HSA) domain, which interacts with actin related proteins. Within the ISWI family, multiple members catalyse nucleosome spacing and chromatin formation, and the distinguishing C-terminal SANT and SLIDE domains recognise nucleosomes and bind DNA and unmodified H4 tails. The CHD family are characterised by two tandem chromo domains, which bind methylated lysines within N-terminal histone tails.

Finally, the INO80 family is defined by their specialised split ATPase domain and whose functions include nucleosome sliding and histone eviction [231].

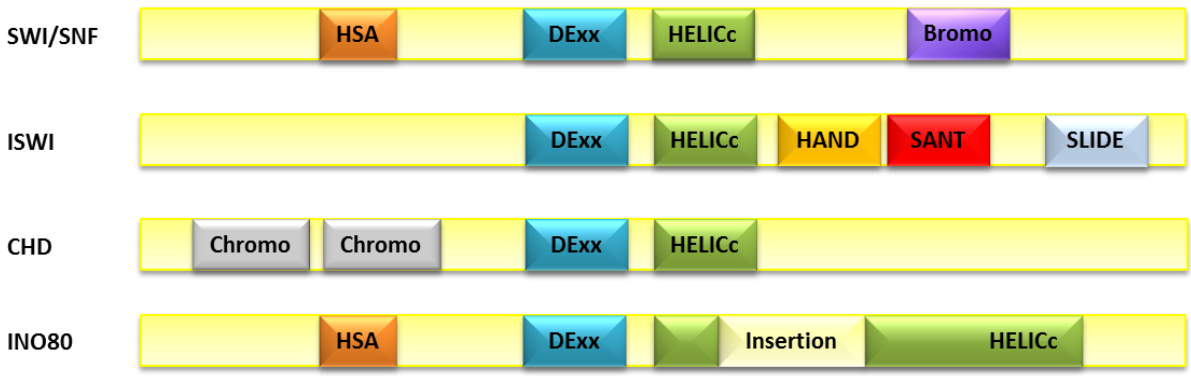


| Domain | Function |
|---|---|
| DExx/HELICc | Nucleic acid binding and ATP hydrolysis |
| HSA | Binds actin related proteins |
| Bromo | Recognises acetylated lysines in histone tails |
| Chromo | Binds methylated lysines in histone tails |
| HAND/SANT/SLIDE | Recognises nucleosomes and internucleosomal DNA |

**Figure 1.13: ATP-dependent chromatin remodelling complex families**

ACRs share the catalytic ATPase subunit comprised of the DExx (blue) and HELICc (green) domains. The flanking domains, HAS, Bromo, Chromo, HAND, SANT and SLIDE define the individual families. Taken from [170].

## 1.6 BER in chromatin

In the literature, the evidence for the functionality of chromatin remodelling events and histone modifications in facilitating the DNA damage response is ever increasing, however, studies have focused primarily on DSB repair and NER [232], [233]. This data highlights the importance for these events in tightly packed regions of chromatin and similarly, it can be assumed that BER requires complete, unobstructed access to DNA damage to promote efficient repair. Furthermore, as progression through BER creates increasingly mutagenic lesions, a seamless transition between each stage in a timely manner is essential to avoid extended repair times and cytotoxicity. Therefore, time, space and access to DNA damage is essential for the effective and efficient competition of BER in chromatin.

### 1.6.1 BER in chromatin models *in vitro*

#### *1.6.1.1 Mononucleosome investigations*

The current main focus for investigating chromatin remodelling events occurring in BER *in vitro* are nucleosomal studies. These investigations have utilised reconstituted nucleosome core particles (NCPs), in general using a single nucleosome (mononucleosome) as a representation of the chromatin environment. Construction of mononucleosome substrates generally uses either recombinant histone proteins or histones purified from chicken erythrocytes in combination with DNA containing 601 or 5S positioning sequences. These substrates can then be used within assays, monitoring the activity of purified recombinant BER proteins, relevant to each stage of the pathway, and examining the impact on lesion positioning. Such studies have provided strong evidence for altered BER efficiency in chromatin although this is very much dependent on the site of the DNA lesion within the mononucleosome and particularly whether the DNA backbone containing the damage is facing inwards or outwards from the histone core.

#### *1.6.1.2 DNA base damage excision in chromatin*

The first stage of BER is initiated by specific DNA glycosylase base recognition, via a dual unspecific 3D searching and 1D tracking along the DNA backbone [234], [235]. In general, this step is deemed efficient when the sugar phosphate backbone is outwardly facing away from the histone octamer (DNA base facing inwards), as the DNA glycosylase enzymes utilise the “base-flipping” mechanism. In contrast base recognition in impeded where the sugar phosphate backbone is inwardly facing (DNA base facing outwards). To provide sufficient DNA glycosylase access, the requirement for DNA dissociation from the histones, which is stimulated through chromatin remodelling enzymes, has been suggested.

Mononucleosome studies on the activities of the DNA glycosylases UNG2 and SMUG1 have reported a general impediment of enzyme activity associated with chicken erythrocyte histone octamer and *L. variegatus* 5S rRNA gene containing mononucleosomes. Here, a 3-fold (UNG2) and 9-fold (SMUG1) decrease in enzymatic activity against mononucleosome substrates compared to free DNA was observed irrespective of the rotational lesion positioning (positions 19, 22 and 51) [236]. Additional investigations, using chicken

erythrocyte histone octamers and *the X. borealis* 5S RNA gene to generate a range of different 154 bp uracil-containing mononucleosome substrates, corroborate this, and found that cleavage of uracil at position 22 (relative to the dyad) where the backbone was facing outwards, was at a 6-fold slower rate than cleavage of 42 bp free DNA. Furthermore, in contrast to an inwardly facing substrate (position 28), UNG2 activity against the uracil site was up to 3000 times slower when compared to the free DNA substrate. This study also details the importance of lesion positioning relative to the dyad, demonstarting that the DNA glycosylase activity of UDG2 was slower the further distance away from the dyad [237]. Multiple studies further develop these findings and have examined the activity of both UDG and APE1 on guanine-uracil mismatches. Utilising mononucleosomes generated from chicken erythrocyte histones and DNA containing the TG nucleosome positioning sequence, experiments have shown that efficiencies of uracil excision within mononucleosomes were 10-fold slower than of naked DNA. Furthermore, they also concluded that proficiency of uracil excision was dependent on rotational positioning, with an observed 2-3-fold increase in excision of the outwardly facing versus the inwardly facing mononucleosome substrate [238]. Supporting this are similar experiments using mononucleosomes containing the 601 DNA sequence, that demonstrated a 3-19-fold lower rate of excision of uracil in the outwardly orientated mononucleosome versus the free DNA, but also a 3-5-fold more effective excision of this substrate in comparison to inwardly facing mononucleosome substrates. Positioning relative to the dyad also resulted in differences in uracil cleavage, where the most efficiently excised inwardly facing substrate was the furthest away from the dyad (position 49). However, this trend was not observed when examining outwardly facing substrates [239]. Yet, as these studies use a combined assessment of the action of both UDG and APE1 enzymes, any conclusions on the effect of rotational positioning on DNA glycosylase enzyme action alone cannot be clearly drawn. To this effect, whilst the same observations were described above, where UDG preferentially excises uracil lesions within mononuleosomes where the DNA backbone is facing outwards versus inwards, APE1 was only able to stimulate UDG activity on the outwardly facing substrate by ~1.5-fold [240].

OGG1 DNA glycosylase/lyase activity has also been demonstrated to be impeded by chromatin. Using 227 bp 601 nucleosome positioning DNA containing 8-oxoG at position 108 (10 bp from the dyad) and recombinant *X. laevis* histone proteins, it was shown that cleavage of 8-oxoG within a mononucleosome subsrate was ∼90-fold slower and 4-fold less efficient than cleavage of naked DNA [241]. Extension of this study examined 8-oxoG processing within dinucleosomes, and reavealed that lesion excision within linker DNA was of a similar

rate to that of free DNA, but that the presence of histone H1 reduced the efficiency of OGG1 ∼10-fold [242]. Characterisation of NTH1-dependent lyase activity against mononucleosomes constructed using 171 bp *L. variegatus* 5S ribosomal DNA nucleosome positioning sequence DNA containing a thymine glycol (TG) site, found that the lesion within outwardly and inwardly facing TG mononucleosomes was processed at a ∼1.6-fold or ∼10-fold reduced rate than free DNA. Furthermore, cleavage of the inwardly facing TG substrate was at a ∼2-fold reduced rate in comparison to the outwardly facing TG substrate. Additionally, evidence of the negative impact of proximity of the lesion to the dyad axis on NTH1 activity was also presented, with the inward facing lesion at position 26 having an approximate 2-fold reduction in TG excision compared to the lesion at position 46. The effect of rotational positioning was still evident with proximity to the dyad, as the outwardly facing lesion at position 22 was excised with greater efficiency than the inwardly facing lesion. Again, this highlights the impact of lesion positioning on BER [243]. Corroborating this is further evidence in mononucleosomes generated with recombinant *X. laevis* histones reconstituted with 184 bp DNA containing TG sites and the *L. variegatus* 5S ribosomal DNA nucleosome positioning sequence. Here, a ∼2-fold reduction in NTH1 activity against inwardly facing TG mononucleosomes was seen comparatively to substrates where the backbone is outwardly facing [244]. Utilising similar substrates, a comparative study of NTH1 and NEIL1 activity in processing TG sites within mononucleosome substrates was performed. This was done under specific conditions, where the high non-specific binding activity of NEIL1 versus NTH1 was compensated for via a 50-fold difference in enzyme concentrations. Nevertheless, it was observed that both enzymes displayed a similar cleavage efficiency on the mononucleosomes with the DNA backbone facing outwards, ∼2-fold less than that of naked DNA. However, only 10 % of the inwardly facing TG sites from mononucleosomes were processed by NTH1 and NEIL1. Yet, with increasing NTH1 concentrations, enzyme efficiency against the substrate was significantly increased. Therefore, the study concluded that NTH1 possessed functionality on both accessible and occluded TG lesions. NEIL1's inability in processing TG sites within mononucleosomes was summarised to be due to its high non-specific DNA binding capacity and postulates a requirement of other proteins to suppress this DNA binding or recruit the enzyme to specific sites of oxidative damage. Alternatively, the promotion of TG processing by NEIL1 in chromatin could be mediated by chromatin remodelling enzymes [245]. Also of note, is the differing cellular roles of the enzymes, which may indicate that NEIL1 does not function in chromatin. Previous evidence suggests NEIL1 predominantly excises base damage from single stranded DNA generated during DNA

transcription and replication [246], in contrast to NTH1 that is a general DNA glycosylase for oxidative pyrimidines. Of interest though, these two enzymes are controlled by the same regulatory mechanism involving ubiquitylation-dependent degradation [247].

#### *1.6.1.3 AP site incision in chromatin*

With a similar approach to the assessment of DNA glycosylase activity, AP site detection by APE1 has also been found to be dependent on damage orientation within mononucleosomes. Evidence in mononucleosomes reconstituted using 147 bp 601 DNA or 150 bp TG motif containing DNA shows a 2-fold (TG sequence) and 3-fold (601 sequence) reduction in cleavage of a natural AP site or tetrahydrofluran (THF) by APE1 inwardly facing lesions, in comparison to outwardly facing sites. Furthermore, this reduced cleavage was investigated in gel shift mobility assays and demonstrated to be as a consequence of reduced APE1 binding to the inwardly facing substrate, rather than reduced activity [248]. Interestingly, following on from this study, it was revealed that two naturally occurring variants of APE1, R237C and G241R, have reduced activity on both inwardly and outwardly facing AP site containing 147 bp 601 DNA within mononucleosome substrates, but not on naked DNA. Yet, there was no evidence of differences in mononucleosome binding observed [249]. Also of note, is the *in vitro* evidence linking reduced APE1 activity on AP sites within mononucleosomes (15-fold reduction) with the mutation of five lysine residues (to arginines) in the amino tail region of histone H4. This highlights the potential importance of epigenetics in this stage of BER and predicting the involvement of histone tails and PTMs in DNA strand cleavage [250].

#### *1.6.1.4 DNA end processing in chromatin*

The impact of chromatin on the DNA synthesis stage of BER, co-ordinated by Pol β, seems to be dependent on a range of factors including the DNA substrate itself, translational positioning and rotational orientation of the single nucleotide gaps. Initial reports, from mononuclesomes constructed using 146 bp *L. variegatus* 5S rRNA gene containing DNA fragments and chicken erythrocyte histone octamers, demonstrated the ability of Pol β to extend a UDG and APE1 generated 3'-hydroxyl terminus (in position 22) by one nucleotide but at a lower efficiency when compared to free DNA. Additionally, the constraint of proximity to the dyad was observed, where at position 51 a greater reduction in the capacity

for extension was observed. Most probably, this is as a result of the increased energetic cost associated with introducing a 90 degree kink, a requirement for Pol β activity, into the DNA at these locations [236]. Following on from this, two studies concluded a complete inhibition of Pol β DNA synthesis activity as a result of histone octamer presence. These investigations observed no DNA synthesis in either outwardly or inwardly facing uracil mononucleosomes following cleavage by UDG and APE1 [238], and a strong inhibition of Pol β-dependent gap filling of a 227 bp 601 DNA sequence containing 8-oxoG mononucleosome, prepared via OGG1 and APE1 processing [241]. Thus, demonstrating irrespective of rotational setting, this stage of the pathway was a major restriction on BER in chromatin and indicating that nucleosome remodelling maybe an essential step for promoting Pol β activity.

Alternatively, single nucleotide gap containing substrates have been used to directly measure the impact of the mononucleosome structure on Pol β activity. In mononucleosomes constructed with recombinant *X. laevis* histone octamers and 184 bp *L. variegatus* 5S rDNA nucleosome positioning sequence DNA, Pol β was found to be ∼3-fold more active on a gap where the DNA backbone was outwardly facing versus inwardly facing [244]. This was thought to be a result of the natural bending of the outward substrate which facilitates the 90 degree kink required for Pol β activity. In contrast to this, studies with 147 bp 601 DNA sequence containing mononucleosomes, found inwardly facing gap substrate (position 10) were 2-fold more amenable to Pol β extension than there outwardly facing (position 4) counterpart. However, as both substrates were 2.5-3-fold less efficient substrates for Pol β than free DNA, the reported observations between inwardly and outwardly facing substrates on Pol β extension may be more indicative of the position of the GAP sites relative to the dyad [239]. Further evidence on the importance of translational positioning on gap filling activity is provided in a comparative study between outward facing substrates at position 10 and 35, and an inwardly facing substrate at position 49 which exhibited a 3- (position 35) and 4-fold (position 49) increase, respectively in Pol β extension activity [239]. A study similarly using 147 bp 601 DNA sequence based mononucleosomes has investigated the impact of the histone proteins on the individual steps co-ordinated by Pol β in the form of gap filling and 5'-dRP lyase activity. Interestingly, it was discovered that 5'-dRP residue removal by Pol β was strikingly enhanced by ∼16-fold in mononucleosomes (position 60) in comparison to free DNA, whereas 5'-dRP removal at positions 35 (outward facing) and 49 (inward facing) were cleaved with the same efficiency as free DNA. Regarding Pol β DNA synthesis activity, very strong inhibition (∼2600-fold) was observed when the gap was close to the dyad (position 10) in comparison to free DNA. Additionally, in comparison

to free DNA, at positions 49 and 35, the difference in kinetics was 277-fold and 4-fold. DNA synthesis proximal to the dyad (position 10) in outwardly facing GAP substrates, was again noticeably slower compared to the other sites (~6-fold and 360-fold versus positions 49 and 35, respectively) [251]. Therefore, it appears evident that of the two enzymatic steps that Pol β catalyses, the DNA synthesis stage is most greatly impacted by the presence of histone proteins within the mononucleosome.

#### *1.6.1.5 DNA ligation in chromatin*

End processing within BER, namely the ligation of the nick by XRCC1-LigIIIα, unlike the other stages of the pathway has been found to be unaffected by lesion orientation (in respect to the histone core). This is evidenced by studies within a 184 bp *L. variegatus* 5S ribosomal DNA nucleosome positioning sequence mononucleosome, where although initial investigations only demonstrated ∼40 % of the substrate appeared to be ligated, with a 10-fold increase in XRCC1-LigIIIα concentration, increases in ligation efficiency of both inward and outward facing nicks in 5S DNA was observed. Therefore, the theory that XRCC1-LigIIIα drove nucleosome disruption during BER to promote transient unwrapping of DNA from the histone octamer was developed. However, in full reconstitution reactions with the relevant enzymes in 601-based TG containing DNA sequences, very little ligation was observed. Therefore, the previously suggested model of XRCC1-LigIIIα-dependent unwrapping is counteracted by the lack of nucleosome disruption observed in these full reconstituted reactions, thus, providing little evidence to suggest that this mechanism of BER occurs in chromatin [244]. More recently though, evidence suggests spontaneous partial unwrapping of DNA from the histone octamer facilitates ligation by XRCC1-LigIIIα, which acts by encircling the DNA substrate. Comparison of nick ligation within 5S ribosomal DNA mononucleosomes positioned inwards towards the histone core showed a ∼3-fold reduction in ligation efficiency with the lesion 26 bp from the dyad axis compared to 46 bp away. This apparent reduced ligation efficiency of ligation was also confirmed in the more stable 601 DNA sequence by XRCC1-LigIIIα. Together, this suggests that ligation at sterically occluded sites within the mononucleosome only occurs when the nicked DNA is exposed by periodic, spontaneous partial unwrapping of DNA from the histone octamer [252].

### *1.6.2 BER in cell culture models*

Evidence from *in vitro* studies strongly suggest chromatin remodelling events are required *in vivo* to promote BER, particularly where DNA damage sites are inaccessible to BER enzymes. To enhance DNA damage accessibility, two not necessarily mutually exclusive major events are thought to mediate remodelling of chromatin. The first is co-ordinated by histone PTMs, and the second by ACRs. There are a large variety of histone PTMs which include the addition of small chemical groups to the N-terminal tails of the histones through acetylation, methylation and phosphorylation, and/or the addition of proteins such as ubiquitin (ubiquitylation) and small ubiquitin like modifier (SUMO) (SUMOylation). These PTMs act as signals altering nucleosome stability and the local chromatin environment by changing chemical interactions either in or between nucleosomes [229]. Utilising the energy of ATP hydrolysis, ACRs can cause either the displacement or sliding of nucleosomes to expose DNA sequences, or even the ejection and subsequent replacement of histones. There are four families of ACRs; SW1/SNF, ISWI, CHD and INO80 [231].

#### *1.6.2.1 Histone post-translational modifications*

Despite evidence of the large number of histone PTMs, the affect they can have on chromatin structure and evidence of substantial cross-talk between them, research into the epigenetic status of histone proteins within chromatin and its influence on BER is relatively limited. An initial study demonstrating the importance of histone ubiquitylation in chromatin remodelling in response to oxidative DNA damage, provided evidence of histone H2B lysine 120 ubiquitylation catalysed by the E3 ubiquitin ligase mouse double minute 2 homolog (Mdm2). Using siRNA mediated depletion of USP7 (a known regulator of Mdm2) in HeLa cells, it was demonstrated in alkaline comet assays that DNA damage induced by $H_2O_2$ resulted in a 2-fold delay of repair up to one hour post treatment, as a consequence of reduced cellular levels of Mdm2 and therefore histone H2B ubiquitylation. Thus, the model for a stabilising Mdm2/USP7 complex allowing for ubiquitylation of histone H2B by Mdm2 when DNA damage is detected, promoting open chromatin and therefore efficient BER, was proposed [253]. More recently, a study has investigated the response of oxidative DNA base damage and SSBs generation in HeLa cells via $H_2O_2$, $\gamma$-irradiation and high-linear energy transfer (LET) IR treatment and demonstrated that only the latter, which included $\alpha$-particle irradiation and low energy protons, was there elevated levels of histone H2B lysine 120 monoubiquitylation. Furthermore, histone H2B monoubiquitylation induction catalysed by

the E3 ubiquitin ligases ring finger protein 20/40 (RNF20/40) and male-specific lethal-2 homolog 1 (MSL2) was shown to be induced several hours after high-LET irradiation, correlating with the slow kinetics of repair indicative of CDD in the comet assay. It is well characterised that high-LET radiation generates CDD, defined by multiple types of DNA damage in close proximity. In fact, these sites are largely comprised of SSBs and/or alkali-labile sites and thus are likely dependent on the BER pathway for their repair. Therefore, this study provides supporting evidence for a key role for histone H2B lysine 120 ubiquitylation in enhancing efficiency of BER [80].

Histone acetylation has also been reported to have an impact on BER. Although the ambiguous nature of these reports, given that most have been performed *in vitro* using mononucleosome substrates, leaves some major conclusions lacking. One such example, in mononucleosomes prepared with 145 bp 601 8-oxoG containing DNA complexed with *X. laevis* histones, a ~1.5-2-fold increase in OGG1 activity on substrates where histone H2B had been acetylated, in comparison to mononucleosomes comprised of unmodified histone H2B, was seen. The neutralisation of lysine residues in histone H2B was hypothesised to result in relaxation of the mononucleosome and thus DNA unwrapping. Although there was no specific evidence for this, or even of further investigations into the impact of acetylation of specific lysine residues on stimulating OGG1 activity [254]. Interestingly, a more recent study has reported that site-specific acetylation on histone H3 within mononucleosomes decreases Pol β activity on single nucleotide gaps, conflicting the previously reported role of histone acetylation in BER. Of note, investigations using GAP mononucleosomes generated from UDG and APE1 treated 147 bp uracil containing DNA and *X. laevis* histone H3 acetylated at lysine 14 or 56, demonstrated inhibition of Pol β extension activity. This was only observed when substrates were outwardly orientated near the dyad (position 10). Also of interest, histone acetylation had no impact on UDG or APE1 activity on the excision of uracil outwardly or inwardly facing, so this appears specific to modulating Pol β during BER [255].

#### *1.6.2.2 Chromatin remodelling factors*

Identification of ACRs involved in BER has been a cumulative effort of both *in vitro* and *in vivo* studies. Early *in vitro* work with 601 DNA and *X. laevis* histone octamer mononucleosomes identified yeast SWI/SNF as a factor promoting OGG1 and APE1 excision of 8-oxoG by ~8-fold, improving efficiency to that of naked DNA. This study also discovered that OGG1 and APE1 generated GAP mononucleosomes were also processed at a ~7-fold improved rate by

Pol β in the presence of the SWI/SNF complex [241]. The authors also developed a dinucleosome model incorporating 8-oxoG into the linker DNA region, and discovered that the yeast ACR, remodels the structure of chromatin (RSC), a member of the SWI/SNF family, increased OGG1 activity against the 8-oxoG site by ~5-fold. Furthermore, they found that the histone chaperone nucleosome assembly protein 1 (NAP-1) enhanced 8-oxoG excision, mediating the removal of histone H1 from the linker DNA [242]. These studies are also supported by evidence from yeast, where RSC has been shown to promotes survival in response to MMS exposure, that generates DNA base alkylation and further endorsing efficient BER through making the chromatin more accessible [256], [257]. Additional evidence of RSC functioning within BER has been provided in studies using mononucleosomes comprised of 255 bp uracil containing 601 DNA with *X. laevis* histones. Here it was shown that the histone chaperone facilitates chromatin transcription (FACT), expressed and purified from HeLa cells, facilitates UDG1 excision of inwardly facing uracil sites via promotion of RSC's remodelling activity. It was also demonstrated that FACT and RSC collectively enhanced accessibility to the uracil lesion via nucleosome sliding, providing valuable insight into the mechanisms of chromatin remodelling involved in the first stage of BER [258].

Another study, utilising a less common but interesting approach, investigated the impact of the ACRs ISW1 and ISW2 on uracil oligonucleosome arrays, constructed with a sodium bisulfite treated tandem repeating DNA sequence of 12 copies of a 208 bp fragment of the *L. variegates* 5S ribosomal RNA gene, combined with histone octamers from chicken erythrocytes. GAP substrates were generated by treating the uracil lesions with UDG and APE1 and Pol β activity against these arrays was shown to be stimulated ~4-fold by yeast purified ISW1 and ~6-fold by ISW2. Although limited in scope, this study does suggest that at least the DNA polymerase step of BER is enhanced via these complexes [259]. Further suggestions of a role of ISWI complexes within BER is provided through more recent evidence that Special AT-rich Sequence-binding Protein 1 (SATB1), which has been previously demonstrated to direct ISWI to chromatin loop domains [260], has also been classified as an accessory factor in BER. SATB1 has been shown to directly interact with OGG1 to stimulate the activity of the enzyme on 8-oxoG containing DNA *in vitro* [261]. Although this does not provide direct evidence that SATB1 plays an important role in enhancing OGG1 activity on chromatin, it is suggestive of factors required to support chromatin remodelling during BER. Indeed, evidence that Amplified in Liver Cancer 1 (ALC1), a member of the SNF2 superfamily, is also a likely chromatin remodelling enzyme involved in SSB processing during BER. ALC1

was first reported to be recruited, in a poly(ADP-ribose)-dependent manner, to sites of laser-induced DNA damage in U2OS cells, and that shRNA-mediated depletion of ALC1 resulted in increased sensitivity of the cells to oxidative stress via $H_2O_2$ treatment [262]. In mononucleosomes ALC1 has also been shown to promote nucleosome sliding, which was enhanced by activated PARP-1. However, a specific role of ALC1 in BER is lacking justification, as this nucleosome sliding wasn't specifically shown to result in improved accessibility of the BER proteins to DNA base damage. Nevertheless, this study did provide supporting evidence that ALC1 promotes chromatin relaxation following laser micro-irradiation of U2OS cells [263]. Furthermore, ALC1 knockout in chicken DT40 cells resulting in an epistatic PARP-1 deletion displayed sensitivity to both $H_2O_2$ and MMS, and a deficiency in SSB repair following $H_2O_2$ treatment through comet assay analysis. Also, of note, ALC1 knockout in human TK6 cells displayed MMS sensitivity and slower repair kinetics of SSBs under MMS and $H_2O_2$ induced conditions. However, siRNA mediated-depletion of ALC1 in U2OS cells had no impact on the recruitment of XRCC1 or Pol β to laser induced DNA damage, suggesting a specific role for ALC1 in chromatin remodelling which promotes BER *in vivo* [264].

## 1.7 Ubiquitylation

Ubiquitin (Ub) is a small 76 amino acid, 8 kDa highly conserved and stable protein (Figure 1.14), which is generally covalently linked to lysine (K) residues of target proteins via ubiquitylation [265]. This occurs in a three step ATP-dependent process by an enzyme cascade involving an E1 activating enzyme, an E2 conjugating enzyme and an E3 ubiquitin ligase [266]. There are a range of Ub modifications with a myriad of outcomes. In its simplest form, ubiquitylation modifies proteins via the addition of single ubiquitin moieties, termed monoubiquitylation [267]. This can also occur at several K residues on the target protein, with the event being classed as mono or multi-ubiquitylation [268]. Furthermore, as Ub itself also contains K residues it can form ubiquitin chains, leading to polyubiquitylation at the residues K6, K11, K27, K29, K33, K48 or K63, with K48 and K63 chains being the most extensively characterised [269], [270]. Ubiquitylation and the ubiquitin proteasome pathway (UPP) has been demonstrated to mediate protein-protein interactions, play a regulatory role in protein localisation, conformation and activity as well as have an involvement in signalling networks and transcriptional regulation of a range of pathways including, DDR, the cell cycle and apoptosis [265].

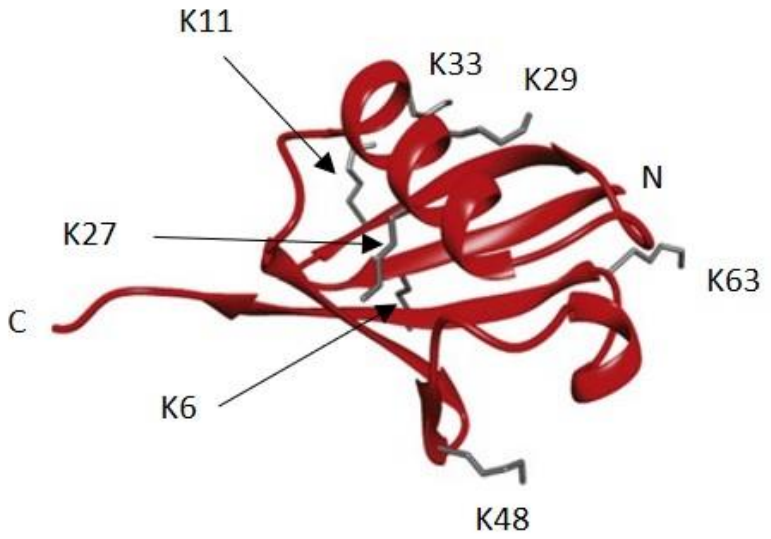


**Figure 1.14: The structure of ubiquitin**

Ub is a small 76 amino acid, 8 kDa protein which can be covalently linked through any of its lysine (K6, K11, K27, K29, K33, K48 and K63) residues or between the C-terminal glycine (G76) and N-terminal methionine (M1) residue of Ub moieties. Image taken from [271].

### 1.7.1 Ubiquitin Proteosome Pathway (UPP)

The UPP is an ATP-dependent three-step enzyme cascade (Figure 1.15). It is initiated via an E1 activating enzyme that mediates Ub activation in an ATP-dependent reaction, whereby the E1's cysteine active site and the C-terminus of Ub (glycine 76) bond form a high energy thiol ester E1-Ub intermediate. Next, the activated Ub is transferred from the E1 to a thiol group on the active site cysteine of an E2-conjugating enzyme. In the third step, the E3 ligase interacts with both the substrate protein and the Ub bound E2. This binding, facilitates the formation of an isopeptide bond between the C-terminus of the Ub moiety and the e-amino group of a K residue on the substrate protein [272]. The human genome encodes for 10 E1s, ~40 E2s and >600 E3s [273].

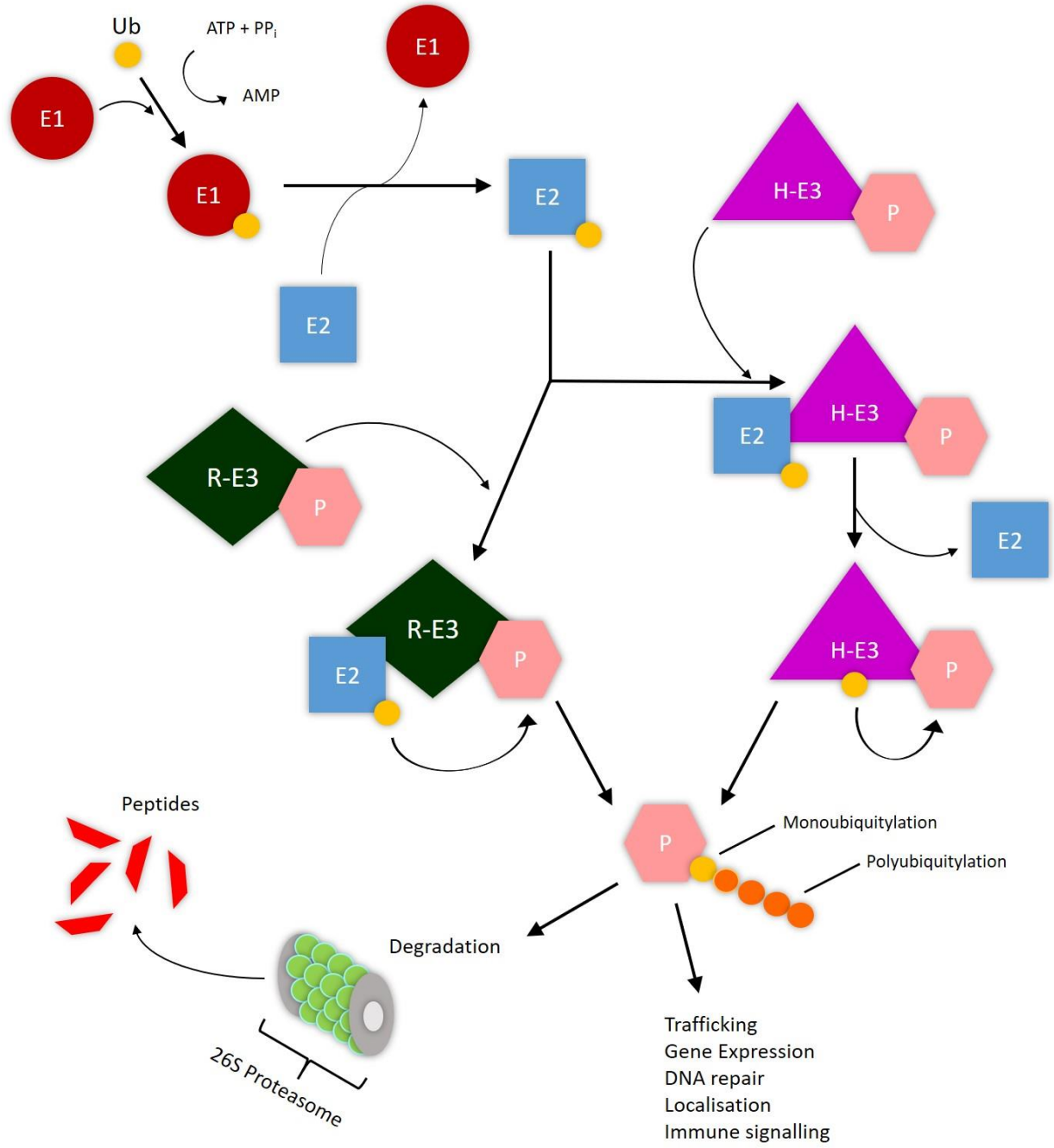


**Figure 1.15: The Ubiquitin Proteosome Pathway**

In an ATP-dependent reaction, Ub is activated and bound to an E1-activating enzyme (E1). Next, the ubiquitin is transferred from the E1 and conjugated to an E2-conjugating enzyme (E2). Finally, E3 ubiquitin ligases facilitate the transfer of ubiquitin from the E2 to lysine residues on the substrate protein (P). RING-type E3s (R-E3) mediate transfer of Ub to the protein. HECT-type E3s (H-E3) use a E3-Ub intermediate before transferring Ub moiety to the protein. Ub modifications include the addition of a single (monoubiquitylation) or multiple (polyubiquitylation) Ub moieties. Adapted from [271].

The E3 ligases, given that they consist of over 600 enzymes, provide the greatest variability and specificity to the UPP. The E3s can be divided into three subtypes, the really interesting new gene (RING)-type, which are the largest family comprising of 600 enzymes [271], the homologous to E6-AP carboxy terminus (HECT)-type of which there are 28 enzymes [274], and the RING between RING (RBR)-type family with 14 members [275]. RING-type E3s function through a mediation of the Ub transfer directly from the Ub bound E2 to the substrate protein. RING-type E3s are characterised by a zinc finger domain or a U-box domain, which is similar in structure but in lieu of zinc ion coordination, utilises charge and polar amino acid residues to provide a scaffold for E2 binding [276]. Therefore, the RING or U-box domains function as a scaffold to orientate the Ub bound E2 to mediate transfer of Ub to the target substrate protein. Another common feature of RING-types is dimerization, functioning as monomers or homo/heterodimers [271]. Additionally, some RING-type E3s have multiple subunits such as cullin-RING ligases (CRLs) and anaphase-promoting complex/cyclosome (APC/C) [277], [278]. HECT-type E3 ligases were the first family to be discovered through the identification of the E6AP protein [279], [280]. Within the HECT-type E3 family there are 28 members, the majority of which fall into two main subfamilies based upon similarities in the N-terminal domain. The NEDD4 subfamily, consisting of nine members which share WW and C2 domains and HERC E3 ligases, consisting of six proteins, which contain at least one regulator of chromatin condensation 1(RCC)-like domains (RLD). The remaining 13 HECT-type E3s are characterised as 'other' HECT E3's [274]. The HECT domain, positioned at the C-terminus of all HECT-type E3s, is a 40 kDa domain and provides the catalytic activity to these E3s and differentiates the HECT-type E3s from the RING-types. This catalytic mechanism involves the formation of an E3-Ub intermediate, where the Ub is firstly transferred to the cysteine active site of the HECT-type E3 via a transthiolation reaction, before the Ub moiety is conjugated to the target substrate protein [279], [281]. The RBR-type, like HECT-type E3s, contain an active site cysteine and conjugate Ub to the substrate via a E3-Ub thioester intermediate. However, they also possess a RING domain, resulting in their classification as RING-HECT hybrids [275]. Of the 14 RBR-type E3s identified, the most highly studied is Parkin, due to mutations in the PARK2 gene being associated with autosomal recessive juvenile Parkinson's disease [282], [283]. RBR-type E3s are complex multi-domain enzymes, however, they are defined based upon their RBE module which consists of an in-between-RING (IBR) domain sandwiched between two RING domains (RING1-IBR-RING2) [284], [285].

Further complexity is added to the UPP by the diverse types of Ub modifications (Figure 1.16). Monoubiquitylation typically is involved within signalling pathways and regulates the target protein in several ways including activity, localisation and interactions [267], [268]. Additionally, Ub itself contains several internal K residues (K6, K11, K27, K29, K33, K48 and K63) allowing for the formation of Ub polymer chains, termed polyubiquitylation. These chains can exist in a myriad of topologies, including homotypic chains (one linkage type), heterotypic chains (mixed linkage types) or branched chains (one ubiquitin is linked at multiple K residues) with K48 and K63 chains being most extensively characterised (Figure 1.16) [269], [270], [286], [287]. The outcomes of polyubiquitylation are numerous, however the most well-known outcome is the targeting of proteins for proteasomal degradation (Figure 1.15) [266]. This process is crucial for the cell to modulate steady-state and regulated protein levels, as well as to rapidly remove and degrade damaged proteins [288]. This is principally achieved through the addition of a four or more K48-linked homotypic polyubiquitin chains to target proteins for degradation via the 26S proteasome [289], although K11, K27 and K29-linked homotypic chains can also target proteins for degradation [290]. Furthermore, to note is the range of complexity which can be afforded by the differing types of Ub modifications, an example of which can be seen in the ubiquitylation of PCNA. This factor recruits DNA polymerases dependent on its ubiquitylation state, where monoubiquitylated PCNA on K164 triggers error-prone DNA repair, recruiting TLS polymerases [291]. In contrast, K63-linked polyubiquitylation of PCNA at the same site induces error-free DNA repair [292].

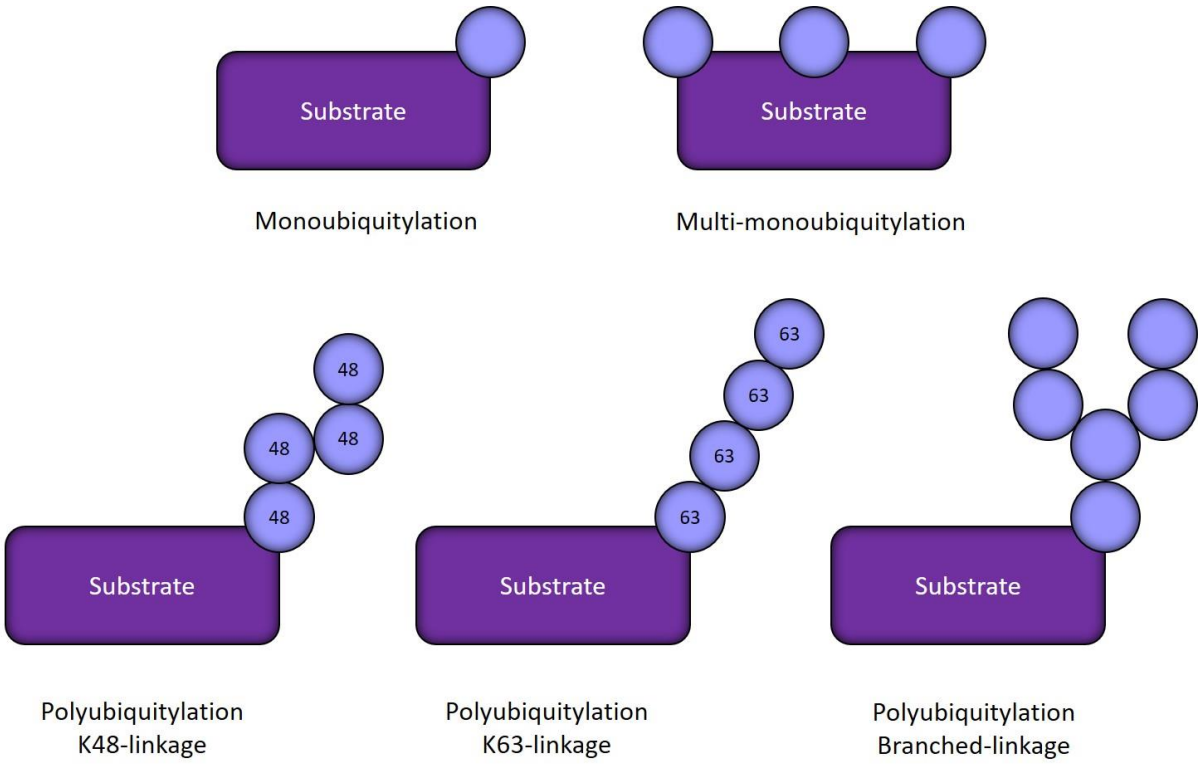


**Figure 1.16: Schematic representation of ubiquitin modifications**

In its simplest form, ubiquitylation modifies proteins via the addition of single ubiquitin moieties (monoubiquitylation) or at several K residues on the target protein (multi-monoubiquitylation). Additionally, Ub can be linked to itself via any of its seven internal K residues (K6, K11, K27, K29, K33, K48 and K63) allowing for the formation of Ub polymer chains, termed polyubiquitylation. These chains can exist in a myriad of topologies including, homotypic chains (one linkage type, K48 and K63 shown above), heterotypic chains (mixed linkage types) or branched chains (one ubiquitin is linked at multiple K residues). Adapted from [287].

## 1.8 Identifying the ACR promoting AP site repair

Within the Parson's laboratory, a previous PhD student utilised reconstituted mononucleosomes containing a site-specific synthetic abasic site (THF) (section 4.2-4.4), and demonstrated that the DNA damage is less efficiently incised by recombinant AP endonuclease 1 (APE1) when the DNA backbone is facing the histone core (THF-IN) compared to that orientated away (THF-OUT). However, when utilising HeLa whole cell extracts, the difference in incision of THF-IN versus THF-OUT was less pronounced suggesting the presence of chromatin remodelling factors that stimulate THF accessibility to APE1 (Figure

1.17). Of note, the previous PhD student also discovered, when examining individual PTMs, that the incision of the THF-IN mononucleosome substrate by WCE was significantly dependent on the presence of factors promoting ubiquitylation (Figure 1.18). Therefore, this led to the development of the hypothesis that incision of an AP site within a mononucleosome substrate that is inaccessible to recombinant APE1, is more efficiently incised by APE1 in WCE due to the presence of histone modifiers and/or chromatin remodelling factors.

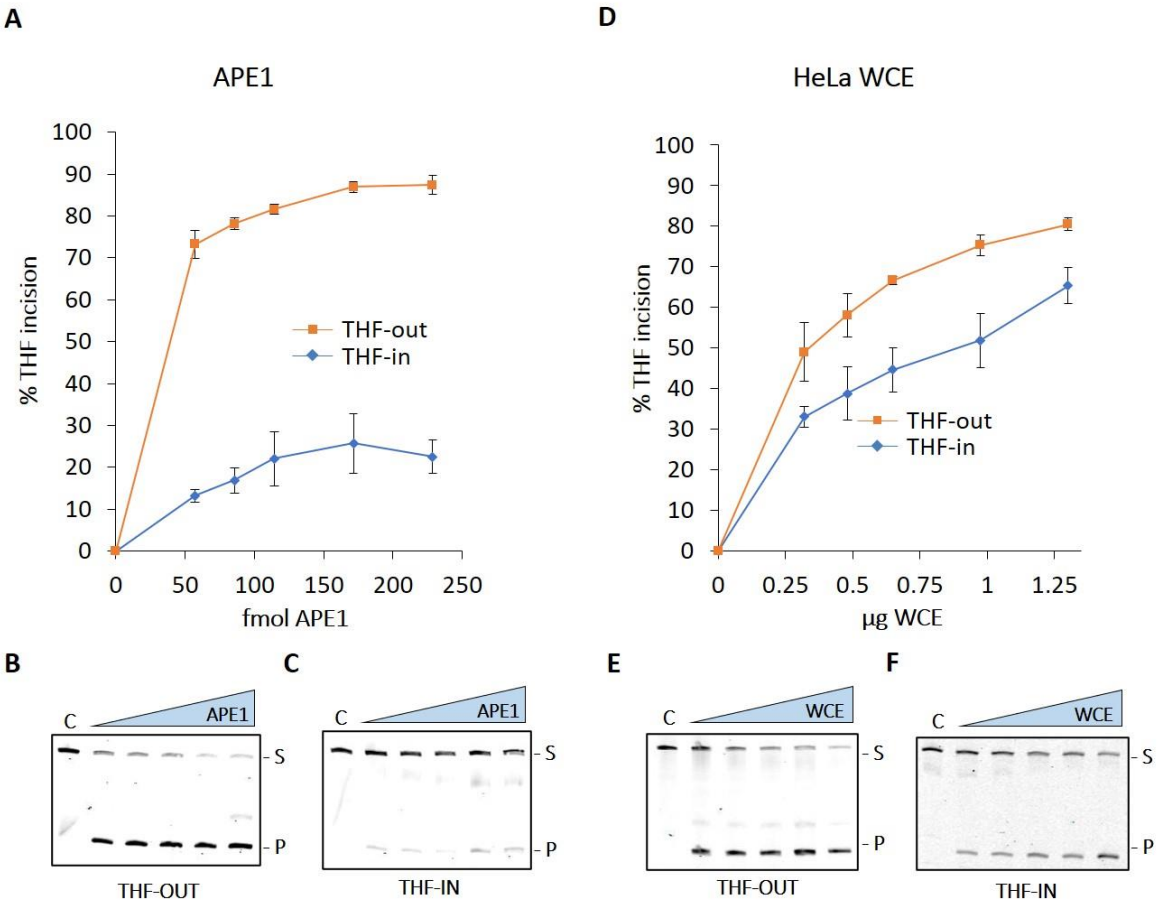


**Figure 1.17: HeLa whole cell extract more efficiently incises a THF-IN mononucleosome substrate than recombinant APE1**

Incision of THF-OUT and THF-IN mononucleosome substrates (50 fmol) by increasing amounts of **A-C**: recombinant APE1 and **D-F**: HeLa whole cell extract. Shown is the mean percent substrate incision ± S.D. from at least three independent experiments, and representative images from the respective gels. Adapted from [293], [294].

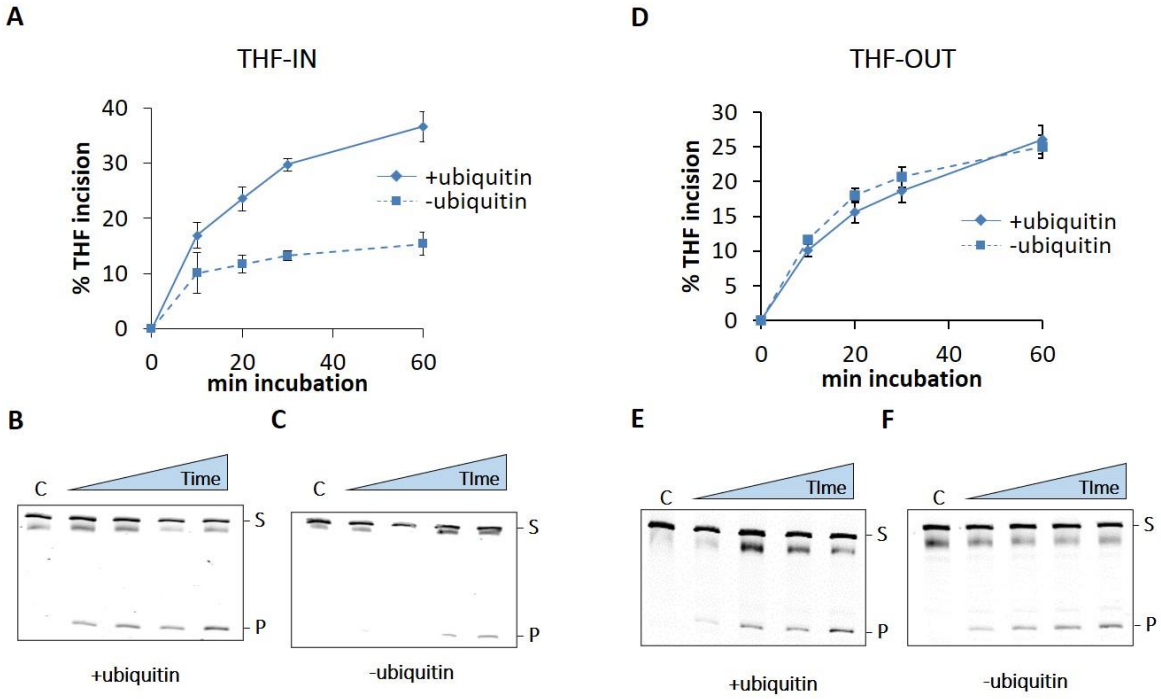


**Figure 1.18: Dependence of ubiquitylation on the effective incision of a THF-IN mononucleosome substrate by HeLa whole cell extract**

Incision of **A-C**: THF-IN and **D-F**: THF-IN mononucleosome substrates (50 fmol) with 1.3 µg and 0.04 µg HeLa WCE respectively, plus and minus 0.6nmol ubiquitin. Reactions were stopped after 10, 20, 30 and 60 minutes. Shown is the mean percent substrate incision ± S.D. from at least three independent experiments, and representative images from the respective gels. Adapted from [293], [294].

To identify this factor, an unbiased purification scheme involving the separation of proteins in HeLa cell extracts by different ion-exchange and size exclusion chromatography columns, purified a chromatin remodelling activity from HeLa cell extracts. Mass spectrometry analysis identified potential candidates, and further assessment of proteins specifically involved in ubiquitylation resulted in the identification of the E3 ubiquitin ligase, HECTD1 as a promising candidate, which was ideal to take forward for further characterisation.

### 1.8.1 HECTD1

HECTD1 is a 289 kDa member of the HECT E3 ubiquitin ligases. The HECT domain of HECTD1 is located at amino acid 2151-2610, with the active site at amino acid position 2579. In addition to its catalytic domain, HECTD1 possesses two armadillo repeat-containing (ARM) domains and an ankyrin (ANK) domain consisting of four repeats, both of which have been implicated in mediating protein-protein interactions [295]. The MIB/HERC2 (MIB) domain is thought to be a major interaction domain, also mediating protein interactions [296]. HECTD1 also consists of a SUN (SAD1/UNC) domain, thought to be involved in nuclear localisation [297], and a helicase bundle (H) (Figure 1.19) [298]. In regards to cellular localisation, HECTD1 is known to translocate between the nucleus and cytoplasm, possessing eight nuclear localization sequences (NLS) and four nuclear export signals (NES) [299]. In addition, HECTD1 has been observed to co-immunoprecipitate and pull-down with Importin α3/7, suggesting nuclear import by classical nuclear protein transport mechanisms [300].

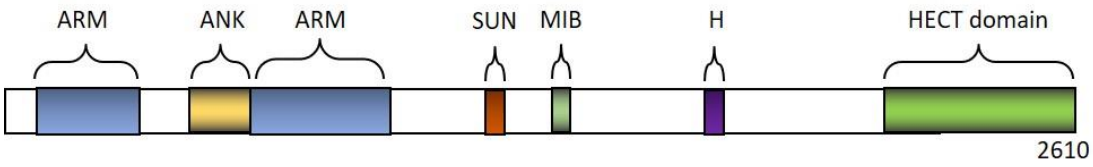


**Figure 1.19: Human HECTD1 domain architecture**

Human HECTD1 is 2610 aa in length consisting of two armadillo repeat-containing (ARM) domains, an ankyrin-repeat (ANK) domain, a SAD1/UNC (SUN) domain, a MIB/HERC2 (MIB) domain, a helical bungle (H) and a homologous to E6-AP carboxy terminus (HECT) domain. Adapted from [298].

#### *1.8.1.1 Cellular role of HECTD1*

*Hectd1*-homozygous mutant mouse embryos exhibit early lethality with several defects during their development, furthermore HECTD1 has been shown to target a range of distinct signalling pathways, implicating HECTD1 in several biological processes [301], [302]. HECTD1 was first characterised to target heat shock protein 90 (HSP90) for ubiquitylation and control the cellular localisation and secretion of the protein necessary for regulation of the behaviour of cranial mesenchyme cells [301], [303]. HECTD1 is also involved in cell migration, regulating focal adhesion formation via the ubiquitylation mediated degradation of

phosphatidylinositol 4-phosphate 5-kinase type I γ (PIPKIγ90), where HECTD1 ubiquitylation of PIPKIγ90 at K97 mediated cell migration [304]–[306]. In addition, observations in mouse embryonic fibroblasts isolated from *Hecdt1*-mutant mice demonstrated accelerated cell migration, which was associated with a HECTD1-mediated regulation of IQGAP1 protein levels effecting focal adhesion and focal complex dynamics [307]. Furthermore, HECTD1 functions as a negative regulator of Wnt/β-catenin signalling, by polyubiquitylating adenomatous polyposis coli (APC) with K-63 linked chains enhancing the interaction between APC and Axin, promoting β-catenin degradation [308]. Interestingly, HECTD1 was identified as a tankyrase druggable target, of interest as a potential cancer treatment [309], [310]. As an antagonist of the Wnt/β-catenin signaling pathway, a tankyrase-mediated degradation of HECTD1 can lead to the degradation of Axin, stabilising β-catenin and promoting growth [311]. HECTD1 has also been well characterised to have a role within epithelial-mesenchymal transition (EMT) and endothelial-mesenchymal transition (EndMT), implicated in the mediation of a range of target proteins. Through a ubiquitylation triggered degradation of the EMT transcription factor SNAIL, HECTD1 has been implicated in EMT. Furthermore, the observation of poor patient survival associated with low HECTD1 expression levels in cervical cancer specimens indicate that the protein is key for regulating cell migration. Investigations of hypoxia-triggered degradation of HECTD1 by microRNA and EGF mediated nuclear export of HECTD1 suggest that HECTD1 may regulate EMT through these signalling pathways in cervical cancer [299]. Also to note, HECTD1 has been shown to promote ubiquitylation-dependent degradation of ACF7, and HECTD1 depletion in T47D breast cancer cells via increased ACF7 protein levels enhanced EMT, promoting tumour growth, survival and metastasis [312]. Together these findings suggest HECTD1 may play a general role within EMT through targeting multiple mechanisms.

#### *1.8.1.2 Implications of HECTD1 in human health*

Of interest is the recent attention on circular RNA HECTD1 (circHECT1), in particular the circHECTD1/HECTD1 pathway. CircHECTD1 is thought to be transcriptional regulator of HECTD1, regulating the levels via competition with its pre-mRNA. Most extensively this pathway has been implicated in silicosis, an occupational lung disease caused by the inhalation of crystalline silica dust, where HECTD1 was shown to be upregulated in macrophages from silicosis patients [313]. It has been suggested that upon exposure to silicon dioxide, the pre-mRNA competition mechanism of circHECTD1 is disrupted and decreased circHECTD1 levels resulting in increased HECTD1 protein levels triggers excessive

cell proliferation and migrations via EMT and EndMT. Ultimately resulting in the hallmark of the disease, silicosis pulmonary fibrosis which is currently untreatable, these new discoveries have provided a potential novel target, circRNAs, in the treatment of silicosis [313], [314].

Additional implications of an important role for HECTD1 in human health, include its mapping to chromosome 14q12, the region associated with severe mental retard and Rett-like syndrome when duplicated or deleted [315]. Furthermore, via regulation of its known target proteins, HECTD1 has been implicated in cancer development. In fact, it has been demonstrated that the apidocyte-derived cytokine leptin upregulates HECTD1 expression [306], exacerbating the HECTD1-mediated ubiquitylation of PIPKIγ90 which is essential for ER-α-negative breast cancer cell invasion [304]. Interestingly, studies in MCF-7 breast cancer cells have implicated HECTD1 in the dysregulation of interphase loading of condensins, proteins which play an important role in the organisation of higher-order chromatin architecture. The architectural regulators condensin I and condensin II modulate estrogen-regulated enhancer activation, in part by the recruitment of HECTD1 which in turn via a control of enhancer-associated coactivators/corepressors (p300 and RIP140) binding, results in gene transcription. However, it has been suggested that aberrant gene expression, triggered by elevation in HECTD1 expression, possibly underlies human cancer development [316]. HECTD1 expression was also shown to be upregulated in cancer associated fibroblasts obtained from the bone marrow of breast cancer patients, in comparison to the primary sites, again implicating HECTD1 in fibroblast migration/proliferation [317]. A HECTD1 overexpression has been reported in LN-229 and LN-428 glioblastoma cells, associated with a USP15 stabilisation of HECTD1 causing a downregulation of Wnt pathway activity [318]. However, as previously stated, low HECTD1 expression levels has been associated with shorter disease-free survival in cervical cancer patients [299], and disease progression, including metastasis in breast cancer patients [312]. Reports have additionally demonstrated using multiple gene expression datasets a correlation of low HECTD1 protein expression and shorter disease-free survival in breast cancer patients and low mRNA levels of *hectd1* with reduced survival in multiple cancer types, including breast, lung and brain [312], [319]–[321]. This may be reflective of the apparent broad functionality of HECTD1, but also suggests further, more extensive studies on the role of HECTD1 in cancer development needs to be undertaken.

# Chapter 2: Aims

The major enzymes and mechanisms co-ordinating BER are well known and established, however, the process of BER in chromatin where DNA is compacted with histones, remains unclear. There is ever increasing evidence for changes to chromatin via remodelling events and histone PTMs which are necessary to facilitate the DDR, particularly in DSB repair and NER, where a number of chromatin remodelling events and histone modifications have been reported. This has, in particular, highlighted the importance of chromatin remodelling events within tightly packed regions of chromatin and similarly BER requires complete, unobstructed access to DNA base damage to promote efficient repair. Furthermore, progression through the BER pathway creates increasingly cytotoxic and mutagenic lesions, therefore, a seamless transition between each stage is essential, and repair must be completed in timely manner once BER in initiated. Thus time, space and access to DNA base damage is essential for the effective and efficient completion of BER in chromatin. Currently, the field is dominated by mononucleosome studies, which conclude that DNA lesion orientation and translational positioning impact the efficiency of BER enzyme activity. However, studies identifying chromatin remodelling enzymes or specific PTMs which are required to promote BER are limited.

Therefore, the study presented in this thesis aimed to characterise HECTD1 as an enzyme functioning as a BER chromatin remodeller, identify the mechanism via which HECTD1 is acting, and determine the requirement for HECTD1 in a cellular context. In order to achieve this, the research project presented had three aims:

I. Establishment of *in vitro* BER assays using mononucleosomal DNA containing occluded DNA damage sites to assess the ability of HECTD1 to promote multiple stages of BER
II. Establishment of ubiquitylation assays to identify HECTD1 substrates for ubiquitylation
III. Determine the requirement of HECTD1 in cell survival and DNA repair in response to genotoxins

# Chapter 3: Materials and Methods

## 3.1 Materials

### 3.1.1 601 nucleosome positioning sequence

The Widom 601 strong nucleosome positioning sequence was used for mononuclesome experiments [322]. The positioning of the THF and TG site was previously determined from the crystal structure and sequence [239]. The pGEM-3Z-601 ampicillin resistant plasmid was kindly provided by Prof Peter O'Neil (CRUK/MRC Oxford Institute for Radiation Oncology, University of Oxford, UK).

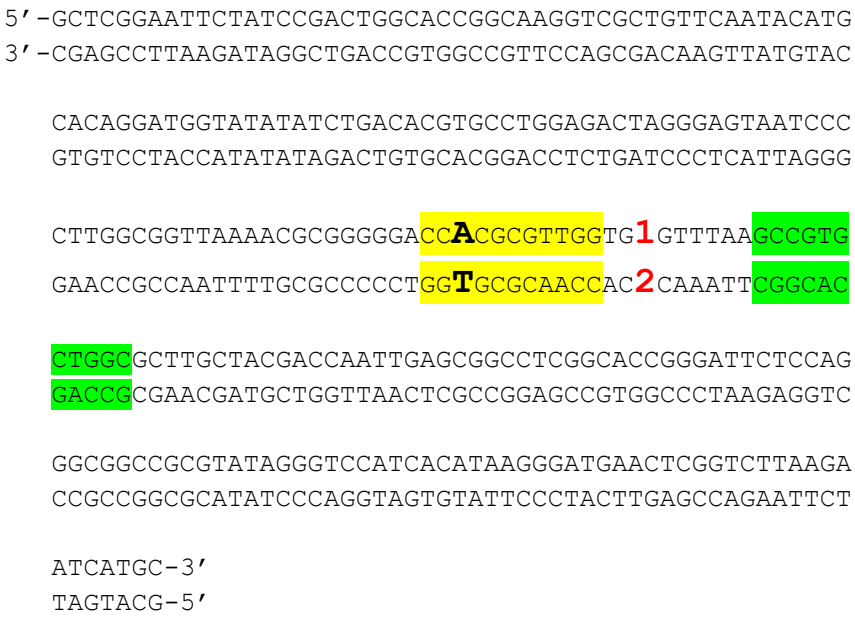


**Figure 3.1: Double stranded 256bp 601 nucleosome positioning DNA sequence**

Nucleotide sequence for the Widom 601 nucleosome positioning sequence. Nucleotides highlighted in yellow are a restriction digest site for Van91I and in green BglI. The nucleosome dyad is indicated to in black bold. The red 1 indicates a C base for THF 256bp DNA and an A base for TG 256bp DNA. The position of the THF or TG site is indicated by a red 2. DNA damage sites on the lower strand produced inwards facing THF or TG sites when reconstituted in the histone octamer.

### 3.1.2 Oligonucleotides

#### *3.1.2.1 Oligonucleotides for the preparation of damage containing oligos*

Fluorescently tagged primers (Table 3.1) were used to amplify the 601 nucleosome positioning sequence from the pGEM3Z-601 cloning vector. Unlabelled primers (Table 3.1) were also used to amplify the 601 nucleosome positioning sequence for use in nucleosome reconstitutions as a carrier DNA to largely inhibit exonuclease activity of extracts in the BER *in vitro* assay. Short (17 bp) oligonucleotide sequences (Table 3.2) were annealed together and used to introduce a THF or TG (labelled 1) to the 601 nucleosome DNA sequence. Fluorescently tagged primers and THF/TG oligonucleotides were obtained from Integrated DNA Technologies (Leuvan, Belgium). Unlabelled primers obtained from Eurogentec (Seraing, Belgium).

**Table 3.1: Primers for DNA damage site DNA preparation**

Primers for producing 601 nucleosome positioning sequence. Shown is the forward and reverse primer sequence.

| | Primer sequence |
|---|---|
| Inwards nucleosome facing sequence | Forward<br>5'-IRDYE800-GCTCGGAATTCTATCCGACTGGCACCGGCAAG-3'<br>Reverse<br>5'-IRDYE700-GCATGATTCTTAAGACCGAGTTCATCCCTTATGTG-3' |
| Unlabelled 601 DNA sequence | Forward<br>5'-GCTCGGAATTCTATCCGACTGGCACCGGCAAG-3'<br>Reverse<br>5'-GCATGATTCTTAAGACCGAGTTCATCCCTTATGTG-3' |

**Table 3.2: Oligonucleotide sequence containing an inwardly facing THF (1) or TG (2) site following nucleosome reconstitution**

Primer sequences to generate a 17bp oligonucleotide with a 3' 3 base overhang, with a THF (1) or TG (2) site positioned on the lower strand. Shown is the forward and reverse primer sequence.

| | Oligonucleotide sequence |
|---|---|
| THF-IN | 5'-phosTTGGTGCGTTTAAGCCGTGC-3'<br>5'-phosCGGCTTAAAC1CACCAACGC-3' |
| TG-IN | 5'-phosTTGGTGAGTTTAAGCCGTGC-3'<br>5'-phosCGGCTTAAAC2CACCAACGC-3' |

### *3.1.2.2 Oligonucleotides for ligation independent cloning*

LIC primers (Table 3.3) were utilised in order to clone the C-terminal cDNA sequence of murine *hectd1* (amino acids 1762-2612) containing the active E3 ligase HECT domain from the pCMV-HA-HECTD1 mammalian expression vector into the pET28a bacterial expression vector. All custom oligonucleotide LIC primers were obtained from Eurogentec (Southampton, UK).

**Table 3.3: Custom oligonucleotide LIC primers**

Primer sequences used to reclone murine HECTD1 in the pET28a bacterial expression vector. Shown is the forward and reverse primer sequence and target DNA template amplified using PCR by the LIC primers.

| DNA target | Oligonucleotide sequence |
|---|---|
| pET28a | Forward<br>5'-AGTAAAGGTGGATACCCCGAATTCGAGCTCCGTCGAC-3'<br>Reverse<br>5'-ATGGATTGGAAGTACCCGCTGCTGCCCATGGTATATCTCC-3' |
| pCMV-HA-HECTD1 | Forward<br>5'-TACTTCCAATCCATGGATGACGACTATGTGCTAAAGCGC-3'<br>Reverse<br>5'-TATCCACCTTTACTGGATTGAGATGAAAGCCTTTCTCCATTGTAGC-3' |

#### *3.1.2.3 Oligonucleotides for site-directed mutagenesis*

Site-directed mutagenesis primers (Table 3.4) were utilised in order to generate a single cysteine (C) to glycine (G) point mutation in the active site of the truncated form of HECTD1 (ΔN-HECTD1) using the pET28a-HECTD1-1761 plasmid. All custom oligonucleotide SDM primers were obtained from Eurogentec (Southampton, UK).

**Table 3.4: Custom oligonucleotide SDM primers**

Primer sequences used for the SDM of ΔN-HECTD1. Shown is the forward and reverse primer sequence for the C to G single mutant. Mutated C to G codons are highlighted in red.

| Mutant | Oligonucleotide sequence |
|---|---|
| C2579G | Forward<br>5'- TCGGTCAACACCGGTGTCCACTATCTTAAG -3'<br>Reverse<br>5'- CTTAAGATAGTGGACACCGGTGTTGACCGA -3' |

### 3.1.3 Plasmids

The pGEM-3Z-601 plasmid was kindly provided by Prof Peter O'Neil (CRUK/MRC Oxford Institute for Radiation Oncology, University of Oxford, UK). *Xenopus laevis* histone (H2A, H2B, H3 and H4) bacterial expression plasmids by Prof Karolin Luger (University of Colorado Boulder, Boulder, USA). The bacterial expression pET14b APE1 plasmid by Prof Dianov (CRUK/MRC Oxford Institute for Radiation Oncology University of Oxford, UK) and the mammalian expression plasmid for full length murine HECTD1 (pCMV-HA-HECTD1) was kindly provided by Prof Irene Zohn (Center for Neuroscience Research, Children's Research Institute, Washington, DC, USA). The C-terminal cDNA sequence of murine *hectd1* (amino acids 1762-2612) containing the active E3 ligase HECT domain was recloned into pET28a (pET28a-HECTD1-1761) by ligation-independent cloning (LIC). An E3 inactive mutant version of pET28a-HECTD1-1761 (pET28a-mutHECTD1-1761) was generated using a site-directed mutagenesis (SDM) technique. The bacterial expression plasmids for the E1 (UBE1) and 9x E2 (UbE2H, Cdc34a, UbE2D1, UbE2D2, UbE2D3, UbE1E1, UbE2L3, UbE2L6, and UbE2C) enzymes were from Addgene (Teddington, UK).

### 3.1.4 siRNA sequences

Small interfering RNA (siRNA) sequences were used to interfere and knockdown the expression of specific genes as listed in Table 3.5. For knockdown of HECTD1 expression a pool of 4 siRNA sequences was used to increase knockdown efficiency.

**Table 3.5: siRNA pool sequences for knockdowns.**

HECTD1 siRNA pool obtained from Dharmacon (Lafayette, Colorado USA) and Qiagen AllStars non-targeting control from Qiagen (Southampton, UK). siRNA pool contains 4 individual oligonucleotides. Sequences were obtained as 5 nmol lyophilised pellets and were diluted to 10 µM with RNase-free water in a Tissue culture hood with laminar flow, mixed on an orbital shaker for 30 minutes at room temperature and aliquoted.

| siRNA | Target sequence |
|---|---|
| Qiagen AllStars non-targeting control | NA |
| HECTD1 | 5'-GAACUGGACUUCUUUGUAU-3'<br>5'-GAAGAAAUCUACCUUAUGG-3'<br>5'-GGACUUACCUAUUUCUAAA-3'<br>5'-GUUAAUAGCUGUACUAGAA-3' |

### 3.1.5 Antibodies

Antibodies were used to probe for specific proteins of interest during immunoblot analysis. Antibodies were diluted in Odyssey blocking buffer (LI-COR Biosciences, Cambridge, UK) and 1x phosphate buffered saline (PBS, Fisher scientific UK, Loughborough, UK) 1:1 with 1 % tween-20 (Sigma Aldrich, St. Louis, Missouri, USA) and applied to Immobilon-FL polyvinylidene diflouride (PVDF) membranes (Sigma Aldrich, St. Louis, Missouri, USA). The primary antibodies used are summarised in Table 3.6 and the secondary antibodies in Table 3.7.

**Table 3.6: Primary Antibodies**

Reactivity, concentration, dilution, molecular weight, source and code shown where applicable for each antibody. Antibodies were obtained from Abcam, (Cambridge, UK), Bethyl Labs, (Montgomery, Texas, USA), Cell Signalling (Danvers, Massachusetts, USA), Prof Dianov (CRUK/MRC Oxford Institute for Radiation Oncology University of Oxford, UK), Novagen (Pledran, France), Sigma-Aldrich (St. Louis, Missouri, USA).

| Antibody | Reactivity | Concentration (mg/ml) | Dilution | Molecular weight (kDa) | Source | Code |
|---|---|---|---|---|---|---|
| APE1 | Rabbit polyclonal | NA | 1:10000 | 34 | Grigory Dianov | NA |
| HECTD1 | Rabbit polyclonal | 1 | 1:1000 | 290 | Bethyl Labs | A302-908a-m |
| His-tag | Mouse monoclonal | 0.2 | 1:1000 | NA | Novagen | 70796-3 |
| Histone H2A | Rabbit polyclonal | 0.1 | 1:100 | 14 | Abcam | ab18255 |
| Histone H2B | Rabbit polyclonal | 0.5 | 1:5000 | 17 | Abcam | ab1790 |
| Histone H3 | Mouse monoclonal | 0.1 | 1:1000 | 17 | Cell signalling | 3638S |
| Histone H4 | Rabbit polyclonal | 0.3 | 1:300 | 11 | Abcam | ab10158 |
| Tubulin | Mouse monoclonal | 1 | 1:10000 | 50 | Sigma-Aldrich | T6199 |
| Ubiquitin | Mouse monoclonal | 5 | 1:5000 | 8.5 | Abcam | ab7254 |

**Table 3.7: Secondary Antibodies**

Host organism, dilution, source and code shown for each antibody. Fluorescently tagged secondary antibodies were selected so secondary antibody could bind to primary antibody. Secondary antibodies were obtained from Invitrogen (Waltham, Massachusetts, USA) or Li-cor biosciences (Lincoln, Nebraska, USA).

| Antibody | Host organism | Dilution | Source | Code |
|---|---|---|---|---|
| Alexa Fluor 680 anti-mouse IgG | Goat | 1:10000 | Invitrogen | A21057 |
| Alexa Fluor 680 anti-rabbit IgG | Goat | 1:10000 | Invitrogen | A21076 |
| IR Dye 800 anti-rabbit IgG | Goat | 1:10000 | Li-Cor | 926-32211 |
| IR Dye 800 anti-mouse IgG | Goat | 1:10000 | Li-Cor | 926032210 |

### 3.1.6 General laboratory reagents

General laboratory reagents were obtained from Sigma-Aldrich (St Louis, USA), Bio-Rad (Hemel, Hempstead, UK), or Fisher Scientific (Loughborough, UK). Chromatography columns were from GE Healthcare (Little Chalfont, UK). Ubiquitin was from Boston Biochemicals (Cambridge, MA, USA). Overexpression of recombinant proteins was performed using Rosetta2 (DE3) pLysS bacterial cells (Merck-Millipore, Watford, United Kingdom) and purified via HisTrap HP affinity chromatography column (GE Healthcare, Little Chalfont, UK).

### 3.1.7 Tissue culture reagents

AG06173, AG16409 and WI-38 lung fibroblasts were obtained from Prof Dianov, (CRUK/MRC Oxford Institute for Radiation Oncology, University of Oxford, UK). All tissue culture reagents were obtained from Sigma Aldrich (St. Louis, Missouri, USA) including; Dulbecco's phosphate-buffered saline (PBS), trypsin-EDTA solution 0.25 % (2.5 g porcine trypsin and 0.2 g EDTA. 4 Na/L of Hank balanced salt solution with phenol red) and Dulbecco's Modified Eagle's Medium (DMEM) with hydroxyethyl piperazineethanesulfonic acid (HEPES) modification, 4500 mg/l, 25 mM HEPES and sodium bicarbonate, sterile filtered was

supplemented with 10 % fetal bovine serum (FBS, non-USA origin, sterile filtered) 2 mM L-glutamine, 100 U penicillin, 0.1 mg streptomycin and 1 % MEM Non-essential amino acid solution.

## 3.2 Sodium dodecyl sulphate-polyacrylamide gel electrophoresis (SDS-PAGE)

SDS-PAGE was utilised in order to separate the proteins based on their molecular weight. Gels were prepared by initially making the separating gel (377 mM Tris-HCl pH 8.8, 0.1 % SDS, 2 mM EDTA and the appropriate concentration of acrylamide/bis solution 30:0.8 (Bio-Rad, Hemel, Hempstead, UK)), 1 % ammonium persulphate (APS) and 0.1 % tetramethylethylenediamine (TEMED) were added to initiate polymerisation and the gel poured into a 1.5 mm empty gel cassette until three quarters full and the gel allowed to set following overlay with 100 % ethanol. The percentage gel used was dependent on the size of protein being analysed. Once set the 5 % stacking gel (125 mM Tris-HCl pH 6.8, 0.1 % SDS, 2 mM EDTA, 5 % acrylamide/bis solution (30:0.8; Bio-Rad, Hemel, Hempstead, UK), 1 % APS, and 0.1 % TEMED) was then added to the remaining quarter of the gel cassette, following removal of the ethanol, and either a 10-well or 15-well 1.5 mm comb added and the gel allowed to set. Protein extracts (typically 40 µg), *in vitro* ubiquitylation reaction samples or chromatography protein fraction samples were prepared in SDS-PAGE sample buffer (25 mM Tris-HCl pH 6.8, 2.5 % mercaptoethanol, 1 % SDS, 10 % glycerol, 0.05 mg/ml bromophenol blue, and 1 mM EDTA) and heated for 5 min at 95°C prior to loading on the polyacrylamide gel. Electrophoresis was performed in 1x Tris-glycine SDS (TGS) running buffer, (25 mM Tris-HCl, 0.192 M glycine and 0.1 % SDS, pH 8.5 (Fisher Scientific UK, Loughborough, UK) for 110 minutes at 125 V in a SDS-PAGE Mini Gel Tank (Fisher Scientific, Loughborough, UK). The Precision Plus Protein All Blue Prestained Protein Standards (10-250 kDa; Bio-Rad, Hemel, Hempstead, UK) were used as standard protein markers. Protein levels following electrophoretic separation via SDS-PAGE were analysed by either gel protein staining (section 3.3) or immunoblotting (section 3.4).

## 3.3 SDS-PAGE gel protein staining

The SDS-PAGE gel following electrophoresis (section 3.2) was then rinsed in dH2O before incubation in InstantBlue protein stain (Expedeon, San Diego, California, USA) for 1 hour at room temperature on a rotating platform. The gel was then washed in 1x PBS for 1 hour at

room temperature on a rotating platform. The gel was imaged using the Li-Cor Odyssey Infrared Imaging Analysis System (LI-COR Biosciences, Cambridge,UK).

## 3.4 Immunoblotting

Following separation of proteins by SDS-PAGE (section 3.2), proteins were transferred onto an Immobilon-FL polyvinylidene difluoride (PVDF) membrane (Millipore, Watford, UK) by electrophoresis at 20 V for 1 hour in transfer buffer (1x Tris-glycine (TG; 25 mM Tris-HCl pH 8.3, 192 mM glycine; Fisher Scientific, Loughborough, UK), 20 % methanol) using the Mini Blot Module (Fisher Scientific, Loughborough, UK). The PVDF membrane was blocked in Odyssey blocking buffer, diluted 1:1 in 1x PBS for 1 hour at room temperature on a rotating platform. The blocking buffer was then removed, and the membrane probed with the appropriate primary antibody diluted to the relevant concentration (Table 3.6) in Odyssey blocking buffer and 1x PBS (1:1), 0.1 % tween-20 and incubated overnight at 4°C on a rotating platform. The membrane was then washed three times for 5 minutes with 1x PBS containing 0.1 % tween-20 and the relevant secondary added diluted to the suggested ratio (Table 3.7) in Odyssey blocking buffer and 1x PBS (1:1) with 0.1 % tween-20 for 1 hour at room temperature. The membrane was washed as before and an additional final wash was performed with 1x PBS prior to imaging using the Li-Cor Odyssey Infrared Imaging Analysis System.

## 3.5 WCE preparation

Following the harvesting of cells (section 3.23.4), the cell pellet was frozen at -80°C for 1 hour. The pellet was thawed on ice and resuspended in once packed cell volume (PCV) of buffer I (10 mM Tris-HCl pH 7.8, 200 mM KCl, 1 µg/ml of each protease inhibitor; aprototin, chymostatin, leupeptin and pepstatin, 100 µM Phenylmethylsulfonyl fluoride (PMSF) and 1 mM DTT). Following resuspension two PCV of buffer II (10 mM Tris-HCl pH 7.8, 600 mM KCl, 40 % glycerol, 2 mM EDTA, 0.2 % NP-40, 1 µg/ml of each protease inhibitor; aprototin, chymostatin, leupeptin and pepstatin and 1 mM DTT) was added and the suspension thoroughly mixed before being mixed via rotation at 4°C for 30 minutes. The cell lysate suspension was centrifuged at 40,000 x g for 20 minutes at 4°C, the supernatant collected and stored at -80°C.

### 3.5.1 Protein concentration

Protein concentration was measured using the Bradford protein assay using the protein assay dye reagent (Biorad Laboratories Ltd, Hercules, California, USA) to measure absorbance at an optical density (OD) of 595 nm (A595) using a UV spectrophotometer, following zeroing of the spectrophotometer with a blank sample. A 0.2 mg/ml BSA protein standard was used as a reference to convert the A595 into mg/ml using the calculation:

**Sample concentration (mg/ml): = (0.2/A595$_{BSA}$) x 40 x A595$_{SAMPLE}$**

## 3.6 Acid extraction of histones

Following the harvesting of cells (section 3.23.4), the cell pellet was frozen at -80°C for 1 hour. The pellet was thawed on ice, resuspended in 100 µl hypotonic buffer (10 mM Tris-HCl (pH 8.0), 1 mM KCl, 1.5 mM $MgCl_2$, 1 µg/ml of each protease inhibitor: aprototin, chymostatin, leupeptin and pepstatin, and 100 µM PMSF) and the suspension thoroughly mixed before being mixed via rotation at 4°C for 30 minutes. The intact nuclei were then pelleted by centrifugation at 10,000 × g for 10 minutes at 4°C and following removal of the supernatant (cytoplasmic fraction), the nuclei resuspended in 80 µl 0.4 M sulfuric acid and incubated overnight at 4°C with rotation. Samples were then centrifuged at 16,000 × g for 10 minutes at 4°C, the supernatant containing histones removed into fresh eppendorf's and 40 µl trichloroacetic acid added dropwise with mixing. The histones were then pelleted by centrifugation at 16,000 × g for 10 minutes at 4°C, the supernatant removed, and the pellet washed with 100 µl ice cold acetone, centrifuged at 16,000 × g for 10 minute at 4°C, twice. The histone pellet was then air-dried for 5-10 minutes at room temperature, before being dissolved in 50 µl dd$H_2O$ and the protein concentration measured by the Nanodrop ND-1000 spectrometer.

## 3.7 Agarose gel electrophoresis

Agarose gel electrophoresis was used to separate DNA molecules based on their size in kilobases (kb). Agarose gels (1.5 %, 1 % or 0.7 %) were prepared by dissolving agarose (broad separation range) in 1x or 0.2x Tris-acetate-EDTA (TAE) buffer (Fisher Scientific, Loughborough, UK) and heated until the agarose had dissolved, 5 nM SYBR Safe DNA gel stain (Fisher Scientific, Loughborough, UK) was added to the solution (except when DNA was

fluorescently labelled) and poured into the gel tray of a Mini-Sub Cell GT electrophoresis tank (Bio-Rad, Hemel, Hempstead, UK) and left to set for 30 minutes. Once set DNA samples, prepared in 1x DNA loading dye (Fisher Scientific, Loughborough, UK) were loaded onto the submerged gel. The GeneRuler 1 kb DNA ladder (Fisher Scientific, Loughborough, UK) was used as a reference for DNA size. Electrophoresis was performed at 100 V for 1 hour in 1x TAE or at 75 V for 1.5 hours in 0.2x TAE and the gel was imaged using the Li-Cor Odyssey Infrared Imaging Analysis System.

## 3.8 Polyacrylamide gel electrophoresis (PAGE)

PAGE was utilised for the analysis of native DNA samples. Polyacrylamide gels (8 %) were prepared using acrylamide/bis-acrylamide solution 19:1 40 % (w/v) (National Diagnostics, Nottingham, UK) diluted in 0.5x TBE (44.5 mM Tris, 44.5 mM boric acid and 1 mM EDTA (Sigma Aldrich, St. Louis, Missouri, USA)) with 1.25 % APS and 0.25 % TEMED to initiate polymerisation. DNA samples were prepared in 5x EMSA loading buffer (30 % glycerol, 0.25 % xylene cyanol and 0.25 % bromophenol blue (Fisher Scientific UK, Loughborough, UK)) and electrophoresed for 3 hours at 175 V, 20 W using the Hoefer$^{TM}$ SE400 vertical electrophoresis unit (Fisher Scientific UK, Loughborough, UK) with the unit covered for light protection of the florescent tags. The gel was imaged using the Li-Cor Odyssey Infrared Imaging Analysis System.

## 3.9 Denaturing PAGE

Denaturing PAGE was utilised for the analysis of denatured DNA samples. Polyacrylamide denaturing (7 M urea) gels (8 %) were prepared using acrylamide/bis-acrylamide solution 19:1 40 % (w/v) diluted in 1x TBE (90 mM Tris, 90 mM Boric acid, 2 mM EDTA) and the solution sterile filtered (0.45 µm and 0.2 µm syringe filters) prior to polymerisation initiation with 1.25 % APS and 0.25 % TEMED. Once polymerised, the gel was pre-run to warm the gel to around 40°C by electrophoresis for 30 minutes at 300 V prior to sample loading. Samples were mixed 1:1 with formamide loading dye (formamide 0.025 % (w/v) (9.5 % (w/v) Sigma Aldrich St. Louis, Missouri, USA) 0.25 % bromophenol blue), heated at 95°C for 5 minutes prior to loading onto the 8 % polyacrylamide denaturing gel and being electrophoresed for 1.75 hours at 300 V, 20 W in 0.5 TBE. The gel was imaged using the Li-Cor Odyssey Infrared Imaging Analysis System.

## 3.10 Transformation of competent cells

Library efficient DH5α competent bacterial cells (Invitrogen, Fisher Scientific, Loughborough, UK) were used for the cloning and amplification of plasmid constructs for subsequent plasmid DNA purification (section 3.11). On ice, 50 µl DH5α cells were thawed and mixed with 1-10 ng of plasmid DNA (or the full 2 µl LIC reaction, or 1 µl Dpn1-treated SDM reaction) via gentle mixing. This mix was then incubated on ice for 30 minutes, before being transformed via heat shock at 42°C for 45 seconds and placed on ice for a further 2 minutes. To the DH5α cells, 950-1950 µl of pre-warmed (37°C) 5 ml lysogeny broth (LB; 2.5 % w/v LB granules (10 g/L Tryptone, 5 g/L yeast extract and 10 g/L sodium chloride; Fisher Scientific, Loughborough, UK), 0.5 % NaOH, pH 7.2) was added and the DH5α cells incubated at 37°C for 1 hour with shaking at 225 rpm. LB agar plates (2.5 % w/v LB granules, 1.5 % w/v agarose, 0.5 % NaOH, pH 7.2) were prepared with appropriate selective antibiotic (30 µg/ml of kanamycin or 50 µg/ml of ampicillin) and 50-2000 µl of transformed DH5α cells plated. Plates were left overnight to incubate at 37°C. Single colonies were selected and inoculated into 5 ml LB containing relevant selective antibiotic using a sterile inoculation loop and incubated at 37°C overnight with 225 rpm shaking.

Rosetta2(DE3)pLysS and Rosetta2(DE3) bacterial cells (Merck-Millipore, Watford, United Kingdom) were used for the overexpression of recombinant His-tagged proteins. On ice, 20 µl Rosetta2 cells were thawed and mixed with 5 ng of plasmid DNA via gentle mixing. This mix was then incubated on ice for 30 minutes, before being transformed via heat shock at 42°C for 30 seconds and placed on ice for a further 2 minutes. To the Rosetta2 cells, 500 µl of pre-warmed (37°C) 5 ml LB was added and the Rosetta2 cells incubated at 37°C for 1 hour with shaking at 225 rpm. LB agar plates were prepared with selective antibiotics and 50-200 µl of transformed Rosetta2 cells plated. Plates were left overnight to incubate at 37°C. Single colonies were selected and inoculated into 5 ml LB containing 30 µg/ml kanamycin and 34 µg/ml chloramphenicol selective antibiotics using a sterile inoculation loop and incubated at 37°C overnight with 225 rpm shaking.

## 3.11 Plasmid DNA purification from bacterial cultures

Following the amplification of plasmid DNA in 5 ml overnight cultures grown following the transformation of competent bacterial cells (section 3.10), the plasmid DNA was purified from bacterial contaminants using the QIAprep Spin Miniprep Kit (Qiagen, Southampton,

UK). The 5 ml overnight culture was centrifuged at 5000 rpm for 5 minutes to pellet the bacteria. The supernatant was removed, and the plasmid DNA purified from the bacterial pellet as per the QIAprep Spin Miniprep Kit manufacturer's instructions. DNA concentration was measured using Nanodrop ND-1000 spectrometer at a wavelength of OD 260nm. Confirmation of DNA sequence was achieved by DNA sequencing from the Sanger Sequencing Service (provided by Source Bioscience Sequencing, Nottingham, UK).

## 3.12 Ligation independent cloning

In order to generate the bacterial recombinant protein expression vector pET28a-HECTD1-1761 expressing truncated HECTD1 protein (ΔN-HECTD1), a LIC cloning strategy was employed [323]. The empty pET28a vector (Merck, Darmstadt, Germany) was amplified by PCR using custom oligonucleotide primers flanked by LIC sequences (Table 3.3). Similarly, gene inserts for a mammalian vector of murine *HECTD1* were amplified by PCR using custom oligonucleotide primers flanked by LIC sequences (Table 3.3). PCR reactions consisted of 5 ng of the relevant DNA component with 1x HF Phusion buffer (containing 1.5 mM $MgCl_2$ (Fisher Scientific, Loughborough, UK)) or 1x GC Phusion buffer (containing 1.5 mM $MgCl_2$ (Fisher Scientific, Loughborough, UK)), 200 µM of each dNTP (dATP, dGTP, dTTP and dCTP), 0.02 U/µl Phusion High-Fidelity DNA Polymerase (Fisher Scientific, Loughborough, UK) and 0.3 µM of relevant forward and reverse custom LIC primers (Eurogentec, Southampton, UK (Table 3.3)). PCR was performed in the Techne Prime Thermal Cycler PCR machine (Techne, Staffordshire, UK) where they were incubated for 2 minutes at 98°C, followed by 30 cycles of 98°C (30 seconds per kb), 57°C (30 seconds per kb), and 72°C (30 seconds per kb). Final extension was performed at 72°C for 5 minutes and reaction mixtures were stored at 4°C. PCR products were analysed via agarose gel electrophoresis (section 3.7) on a 1 % agarose gel in 1x TAE running buffer at 100 V for 1 hour. Gels were analysed using the LI-COR Odyssey Infrared Imaging System. Reactions were incubated with 0.02 U/µl DpnI for 90 minutes at 37°C in a Techne Prime Thermal Cycler PCR machine to digest methylated DNA. PCR DNA products were purified using the QIAquick PCR Purification Kit (Qiagen, Southampton, UK) as per the manufacturer's instructions. DNA concentration was measured using Nanodrop ND-1000 spectrometer at a wavelength of OD 260nm. Following this, complimentary LIC overhangs were generated. 10 µl reaction mixtures were prepared consisting of 5 µl purified PCR DNA product, 1x T4 DNA Polymerase buffer (165 mM Tris acetate pH 7.9, 330 mM sodium acetate, 50 mM magnesium acetate, and 5 mM DTT (Fisher Scientific, Loughborough,

UK)), 2.5 mM dCTP (for insert DNA) or dGTP (for vector DNA), 5 mM DTT, 0.5 mg/ml bovine serum albumin (BSA), and 0.5 U/µl T4 DNA polymerase (Fisher Scientific, Loughborough, UK)). Reactions were incubated at 22°C for 30 minutes followed by 80°C for 30 minutes in a Techne Prime Thermal Cycler PCR machine. LIC (vector:insert) reactions were incubated at ratios of 1:0.5, 1:1 and 1:3 at 22°C for 10 minutes to anneal insert into the bacterial expression vector. LIC reactions were transformed into library efficient DH5α competent bacterial cells (Invitrogen, Fisher Scientific, Loughborough, UK) via heat shock and the plasmids amplified and purified via the previously described methods (sections 3.10 and 3.11).

## 3.13 Site-directed mutagenesis

Site-directed mutagenesis was used to generate an E3 ligase inactive mutant of ΔN-HECTD1 (pET28a-mutHECTD1-1761) via a single cysteine (C) to glycine (G) point mutation in the active site. PCR reactions consisted of 250 pg/µl of the plasmid of interest (pET28a-HECTD1-1761), 0.3 µM of relevant forward and reverse custom SDM primers (Eurogentec, Southampton, UK (Table 3.4)), 1x HF Phusion buffer (containing 1.5 mM $MgCl_2$ (Fisher Scientific, Loughborough, UK)), 200 µM of each dNTP (dATP, dGTP, dTTP and dCTP) and 0.02 U/µl Phusion High-Fidelity DNA Polymerase (Fisher Scientific, Loughborough, UK). Samples were incubated in the Techne Prime Thermal Cycler PCR machine (Techne, Staffordshire, UK) for 2 minutes at 98°C, followed by 18 cycles of 98°C for 30 seconds, 55°C for 1 minute per kb and 72°C for 8 minutes. Final extension was performed at 72°C for 20 minutes before storage at 4°C. PCR products were analysed via agarose gel electrophoresis (section 3.7) on a 1 % agarose gel in 1x TAE running buffer at 90 V for 1 hour. Gels were analysed using the LI-COR Odyssey Infrared Imaging System (LI-COR Biosciences, Cambridge, UK). Reactions were incubated with 0.02 U/µl DpnI for 90 minutes at 37°C in a Techne Prime Thermal Cycler PCR machine to digest methylated DNA. SDM reactions were transformed into library efficient DH5α competent bacterial cells (Invitrogen, Fisher Scientific, Loughborough, UK) via heat shock and the plasmids amplified and purified via the previously described methods (sections 3.10 and 3.11).

## 3.14 Preparation of His-tagged proteins

### 3.14.1 Overexpression of recombinant His-tagged proteins

His-tagged pET28a-HECTD1-1761 or pET28a-mutHECTD1-1761 plasmid was transformed via heat shock into Rosetta2(DE3)pLysS bacterial cells and the plasmid DNA amplified in 5 ml overnight cultures (section 3.10). Following this, 400 µl of the 5 ml overnight Rosetta2 bacterial culture was used to feed three 40 ml LB cultures (containing 30 mg/ml kanamycin and 0.1 % glucose) and grown until an $OD_{600nm}$ of 0.6-0.8 at 37°C with 225 rpm shaking. The entire 40 ml cultures were expanded to 400 ml LB cultures (containing 30 mg/ml kanamycin and 0.1 % glucose) and grown until an $OD_{600nm}$ of 0.6-0.8 at 37°C with 225 rpm shaking. Protein expression was induced via the addition of 1 mM IPTG and incubated at 30°C with 225 rpm shaking for 3 hours. The cultures were centrifuged at 8000 rpm for 20 minutes, the supernatant aspirated and pellets stored at -80°C.

### 3.14.2 Bacterial cell lysis

The bacterial cell pellet previously acquired (section 3.14.1) was thawed and resuspended in bacterial lysis buffer (25 mM Tris-HCl, pH8, 0.5 M NaCl, 5 % glycerol, 5 mM imidazole, 100 mM PMSF and 1 µg/ml of each protease inhibitor; leupeptin, chemostatin, pepstatin and aprototin). 0.1 mg/ml lysozyme was added and the cells were incubated on ice for 15 minutes. Cells were lysed by sonication for 3x15 second bursts with 30 seconds intervals on ice. Cell lysates were transferred to Oakridge tubes and centrifuged at 25000 rpm for 20 minutes at 4°C. The supernatant was collected and filtered through a 1 µM syringe prefilters followed by a 0.45 µM syringe filter.

### 3.14.3 His-trap chromatography purification of recombinant His-tagged proteins

The bacterially overexpressed His-tagged recombinant proteins were purified from the bacterial cell lysate via 1 ml HisTrap HP affinity chromatography columns (GE Healthcare, Little Chalfont, UK) attached to the AKTA-prime FPLC. The column was equilibrated at 4°C using 2-3 column volumes of HisTrap buffer A (25 mM Tris-HCl pH 8.0, 0.5 M NaCl, 5 % glycerol, 5 mM imidazole, and 100 µM PMSF). The lysate was loaded onto the column which

was washed with HisTrap buffer A, eluting unbound proteins until UV signal stabilisation. Bound proteins were collected via a linear gradient of 5-250 mM imidazole with 20 ml HisTrap buffer A and HisTrap buffer B (25 mM Tris-HCl pH 8.0, 0.5 M NaCl, 5 % glycerol, 250 mM imidazole, and 100 µM PMSF) collecting 0.5 ml fractions. Fractions were analysed by SDS-PAGE (section 3.2), gel protein staining (section 3.3) and immunoblotting (section 3.4) using anti-His antibodies to select fractions. Fractions containing the purified recombinant protein of interest were pooled, concentrated and buffer exchanged into JPDB buffer (50 mM Tris-HCl pH 8, 50 mm KCl, 1 mM EDTA, 5 % glycerol) using 15 ml, 10 MWCO Amicon Ultra centrifugal filters (Millipore, Watford, UK) to 500 µl at 5000 rpm and 4°C before storage at -80°C.

## 3.15 Preparation of site specific DNA damage containing DNA

### 3.15.1 Amplification of 601 nucleosome positioning sequence

The 601 nucleosome positioning sequence was amplified from the pGEM3Z-601 plasmid using fluorescently tagged primers (Table 3.1). PCR reactions consisted of 200 µM dNTPS (Sigma Aldrich, St. Louis, Missouri, USA), 1x Phusion HF buffer, 2 mM $MgCl_2$, 0.02 U/µl Phusion Hot Start II DNA polymerase (Fisher Scientific UK, Loughborough, UK), 0.3 µM of each forward and reverse primers and 25 pg/µl P-GEM3Z-601 plasmid. PCR was performed in the Techne Prime Thermal Cycler PCR machine (Techne, Staffordshire, UK) where the 15 reactions were incubated for 1 minute at 98°C, followed by 40 cycles of 98°C for 20 seconds, 57°C for 45 seconds, and 72°C for 45 seconds. Final extension was performed at 72°C for 10 minutes and reaction mixtures were stored at 4°C. The 256 bp nucleosome positioning sequence was analysed via agarose gel electrophoresis (section 3.7) on a 1.5 % agarose gel in 1x TAE running buffer at 100 V for 1 hour. Gels were analysed using the LI-COR Odyssey Infrared Imaging System. The PCR reactions were pooled and purified using the QIAquick PCR purification kit as per the manufacturer's instructions, split across three columns and eluted in EB buffer. DNA concentration was measured using Nanodrop ND-1000 spectrometer at a wavelength of OD 260nm.

### 3.15.2 Restriction digests of the 601 nucleosome positioning sequence

The central 17 bp region with 3 base overhang of the 256 bp nucleosome positioning sequence was removed via restriction digest using 20 U BgII and 50 U Van91I restriction enzymes with 1 x Buffer R (Fisher Scientific UK, Loughborough, UK) and incubated overnight at 37°C at 800 rpm. To check the efficiency of the restriction digests the 127 bp and 106 bp digest products was analysed via agarose gel electrophoresis (section 3.7) on a 1.5 % agarose gel in 1x TAE running buffer at 100 V for 1 hour. Gels were analysed using the LI-COR Odyssey Infrared Imaging System. After efficient restriction digest, the entire sample was loaded onto an 8 % PAGE gel and the digest products separated in 0.5x TBE at 175 V, 20 W for 3 hours. The gel was imaged using the LI-COR Odyssey Infrared Imaging System. The digested products (127 bp and 106 bp) were excised from the gel and sliced into small pieces and placed into separate 1.5 ml amber tube and stored at -80°C for a minimum of 20 minutes in accordance with the freeze/squeeze method of DNA extraction [324].

### 3.15.3 DNA purification from gel pieces

DNA (127 bp and 106 bp) in gel pieces following freezing were incubated in TE buffer (10 mM Tris, pH 8 and 1 mM EDTA) at 37°C for 3 hours at 800 rpm. Following incubation, the TE buffer was removed and filtered through Spin-X columns by centrifugation at 13,000 x g for 1 minute. The flow through was collected and transferred to amber 1.5 ml tubes. Gel pieces were re-incubated in fresh TE buffer for 1 hour at 37°C and 800 rpm and the TE buffer filtered as before. The gel pieces were then added to the Spin-X columns and centrifuged at 13,000 x g for 5 minutes to remove any residual TE buffer. The filtrates were then concentrated using Amicon Ultra 0.5 ml devices (10 kDa MWCO (EMD Millipore, Darmstadt, Germany)) to approximately 50 µl. DNA concentration was measured using Nanodrop ND-1000 spectrometer at a wavelength of OD 260nm. The purification of the two digest products was checked and analysed using PAGE (section 3.8) on an 8 % polyacrylamide gel.

### 3.15.4 Preparation of duplex oligonucleotide

The duplex oligonucleotide was prepared for ligation by creating a reaction mix containing either the two 20 bp single strand DNA sequences for THF-IN or TG-IN (Table 3.2) at 10 pmol with 200 mM NaCl in TE buffer. The oligonucleotides were then heated at 95°C for 5 minutes in a metal heat block which was then removed from the heater to allow the samples to slow

cool to room temperature for approximately 2 hours, allowing strand annealing. After annealing they formed a 17 bp oligonucleotide with a 3'- 3-base overhang (17 bp duplex oligonucleotide).

### 3.15.5 Sequential ligation of restriction digest products

The DNA digest product with the highest DNA concentration was ligated to the 17bp duplex oligonucleotide, which was in 3 times excess of the DNA (127 bp or 106 bp) with 5 U T4 DNA ligase and 1x T4 DNA ligase buffer (Thermo Scientific, Massachusetts, USA) and incubated overnight at 4°C. Ligation efficiency was checked to ensure >90 % efficiency by analysis against an unligated DNA control using 8 % PAGE (section 3.8) and the 147 or 126 bp IR700 or AF680 tagged ligated DNA visualised. If ligation was unsuccessful, more duplex oligonucleotide DNA and T4 ligase was added and overnight ligation repeated. Once successful ligation was obtained the samples were heated at 65°C for 10 minutes to inactivate T4 DNA ligase and denature any duplex oligonucleotide DNA. The DNA was then purified by using the MinElute reaction clean-up kit following the manufacturer's instructions (Qiagen, Hilden, Germany). DNA was eluted by two sequential 10 µl elutions with buffer EB into a 1.5 ml amber tube.

Following this a second ligation of the ligated DNA and the remaining 106 bp or 126 bp DNA fragment was prepared together with 5 U T4 DNA ligase and 1x T4 DNA ligase buffer and incubated overnight at 4°C. Ligation efficiency was checked to ensure >90 % efficiency by analysis against the first ligation as a control using 8 % PAGE (section 3.8) and the fully ligated 256 bp DNA gel purified, extracted from gel pieces, concentrated and the purity checked as stated previously (section 3.15.3). The concentration of the final 256 bp DNA containing a THF or TG site was measured using Nanodrop ND-1000 spectrometer at a wavelength of OD 260nm and stored at -20°C until required.

## 3.16 Preparation of unlabelled 601 DNA

Unlabelled 601 nucleosomal DNA sequence, as carrier DNA, was prepared in the same manner as THF and TG containing DNA (section 3.15.1), amplified using the same PCR reactions and cycles but using non fluorescent primers (Table 3.1).

## 3.17 Expression and purification of recombinant histones

The protocol, which is detailed below, was followed from Luger *et al* [325] and the *Xenopus Laevis* histones (H2A, H2B, H3 and H4) expression vectors were obtained from Professor Karolin Luger (University of Colorado Boulder, Boulder, USA).

### 3.17.1 Recombinant histone expression

Rossetta2(DE3)pLysS cells were transformed with 2.5 ng pET-expression vector for H2A, H2B and H3, whereas the pET-expression vector for H4 was transformed into Rosetta2(DE3) cells (Merck-Millipore, Watford, UK) (section 3.10). For recombinant histone expression, 200 µl 2x TY media (1 % (w/v) bacto tryptone, 1 % (w/v) yeast extract, 0.5 % (w/v) NaCl, pH 7 (Sigma Aldrich, St.Louis, Missouri, USA)) was added to the cell/plasmid mix and incubated at 37°C for 1 hour with shaking at 225 rpm. TYE agar plates (1 % bacto tryptone, 0.5 % yeast extract, 0.8 % NaCl, 1.5 % (w/v) agar, (Fisher Scientific UK, Loughborough, UK)) were prepared with 50 µg/ml ampicillin and 34 µg/ml chloramphenicol selective antibiotics and 75 µl of transformed Rosetta2 cells plated. Plates were left overnight to incubate at 37°C. Single colonies were selected and inoculated in four separate universal tubes 2 ml 2xTY media containing 50 µg/ml ampicillin, 34 µg/ml chloramphenicol and 0.1 % glucose incubated at 37°C with shaking until an $OD_{600nm}$ of 0.4. 0.5 ml was removed from each culture and added to 10 ml 2xTY containing 50 µg/ml ampicillin, 34 µg/ml chloramphenicol and 0.1 % glucose and incubated at 37°C with shaking until an $OD_{600nm}$ of 0.4. 8 ml of each culture was then added to 500 ml 2xTY containing 50 µg/ml ampicillin, 34 µg/ml chloramphenicol and 0.1 % glucose and incubated at 37°C with shaking until an $OD_{600nm}$ of 0.4. Histone expression was induced by adding 0.2 mM IPTG (Fisher Scientific UK, Loughborough, UK) to each culture and incubated at 30°C with shaking for 2 hours. Cells were harvested and centrifuged at 5000 rpm for 10 minutes at room temperature and the supernatant removed. Each cell pellet was re-suspended in 10 ml wash buffer (50 mM Tris pH 7.5, 100 mM NaCl, 1 mM EDTA, 5 mM β-mercaptoethanol, 0.3 mM PMSF (Sigma Aldrich, St. Louis, Missouri, USA) and stored at -80°C.

### 3.17.2 Inclusion body preparation

The histone proteins are expressed in an insoluble form, thus must be isolated from inclusion bodies following cell lysis. Therefore, the bacterial cells in wash buffer were thawed at 37°C, 1 mg/ml lysozyme added and incubated on ice for 30 minutes. Cells were lysed by sonication

for 2x30 second bursts with 30 seconds intervals on ice. Cell lysates were transferred to Oakridge tubes and centrifuged at 25,000 rpm for 20 minutes at 4°C. The supernatant was removed and 10 ml wash buffer added (as used previously with added 1% Triton X-100, (Fisher Scientific UK, Loughborough, UK)). Lysates were further sonicated and centrifuged an additional three times as described before, on the final resuspension 10 ml wash buffer was added without Triton. In exception, H4 was only sonicated, centrifuged and re-suspended in wash buffer the once as it is prone to lysis. After this final wash step, all histones were centrifuged for a final time, the supernatant poured off and the histone pellets stored at -20°C.

### 3.17.3 Recombinant histone purification by gel filtration chromatography

Histone purification involved a two-step purification procedure and each histone protein was purified separately. The first step involved gel filtration using an AKTA fast protein liquid chromatography (FPLC, GE Healthcare, Little Chalfont, UK) under denaturing conditions. A 320ml Sephacryl S-200 gel filtration column, (GE Healthcare, Little Chalfont, UK) was attached to an AKTA FPLC purifier and equilibrated with gel filtration buffer (20 mM sodium acetate pH 5.2, 1 M NaCl, 7 M urea, 1 mM EDTA and 5 mM β-mercaptoethanol) for 1.5 column volumes at 1.5 ml/min. The histone pellets were individually incubated in 200 µl Dimethyl sulfoxide (DMSO (Sigma Aldrich, St. Louis, Missouri, USA)) for 30 minutes at room temperature then minced in 10 ml 1x unfolding buffer (7 M guanidinium HCl (Fisher scientific UK, Loughborough, UK), 20 mM Tris pH 7.5, 10 mM DTT) which was added dropwise. The pellets were stirred for 1 hour at room temperature. This was then centrifuged at 23,000 x g for 20 min at 20°C, the supernatant removed and filtered through 1 µm syringe filters. Using a 10 ml superloop (GE healthcare, Little Chalfont, UK) the sample was loaded onto the S-200 column at 1.5 ml/min. After approximately 85 ml, the protein started to elute and 4 ml fractions were collected until the UV signal reduced and stabilised so no more protein was being eluted. The peak fractions were analysed by 16 % SDS-PAGE (section 3.2) and gel staining (section 3.3) to identify peaks containing the relevant histones.

### 3.17.4 Recombinant histone purification by FPLC ion-exchange chromatography

Fractions from gel filtration chromatography (section 3.17.3) containing histones were dialysed in snakeskin dialysis tubing (35 mm Dry ID, 7 kDa MWCO (Thermo Fisher Scientific, Massachusetts, USA)) in 2 L of distilled water containing 2 mM β-mercaptoethanol at 4°C for

2 hours. The histone fractions were then dialysed in fresh distilled water containing 2 mM β-mercaptoethanol at 4°C overnight. The dialysed fractions were concentrated in Amicon Ultra centrifugal concentrators (3 kDa MWCO (Merck-Millipore, Watford, UK)) to approximately 1-2 ml. A 1 ml HiLoad 16/10 sepharose high performance MonoS column (GE Healthcare, Little Chalfont, UK), was attached to the AKTA FPLC and the column equilibrated with cold low salt buffer (20 mM NaAc pH 5.2, 0.1 M NaCl, 7 M urea, 1 mM EDTA, 5 mM β-mercaptoethanol) for 3 column volumes at 1 ml/min. The dialysed histone sample was then loaded onto the column which was washed until no more protein eluted. Histone proteins were gradient eluted with 20 ml low salt buffer to high salt buffer (20 mM NaAc pH 5.2, 1 M NaCl, 7 M urea, 1 mM EDTA, 5 mM β-mercaptoethanol) at 1 ml/min collecting 0.5 ml fractions. The peak fractions were analysed by 16 % SDS-PAGE and gel staining as above (section 3.17.3). Fractions containing histones were pooled and dialysed in snakeskin dialysis tubing (35 mm Dry ID, 7 kDa MWCO) in 2 L water with 5 mM β-mercaptoethanol at 4°C overnight. This was dialysed for a further 4 hours at 4°C with fresh water and 5 mM β-mercaptoethanol. The dialysed fractions were concentrated in Amicon Ultra centrifugal concentrators (3 kDa MWCO) to 0.5 ml. The concentration of the histones was measured Nanodrop ND-1000 spectrometer at a wavelength of OD 280 nm using molecular weights and extinction coefficients (ε) (Table 3.8). Histones were aliquoted in the following equimolar amounts in preparation for octamer refolding (2mg H2A, 2mg H2B, 2.25mg H3 and 1.17mg H4) and stored at -80°C.

**Table 3.8: Histone molecular weights and extinction coefficients (ε)**

Molecular weight and ε used to calculate the concentration of the histone proteins using the Nanodrop ND-1000 spectrometer at a wavelength of OD 280 nm

| Histone | Molecular weight (KDa) | ε (cm/M) x $10^3$ |
|---|---|---|
| H2A | 13.96 | 4.05 |
| H2B | 13.77 | 6.07 |
| H3 | 15.27 | 4.04 |
| H4 | 11.24 | 5.40 |

### 3.17.5 Refolding of the histone octamer

The histone aliquots were individually dissolved to a concentration of 2 mg/ml using 1.25x unfolding buffer (25 mM Tris-HCL pH 7.5, 8.75 M guanidinium HCL, 12.5 mM DTT) and incubated on ice for 2 hours to allow the proteins to unfold. All the histones were then mixed with an equal volume of 1x unfolding buffer to create a 1 mg/ml histone solution. Histones were then dialysed in snakeskin dialysis tubing (35 mm Dry ID, 7 kDa MWCO) in 600 ml refolding buffer (10 mM Tris-HCl pH7.5, 2 M NaCl, 1 mM EDTA, 5 mM β-mercaptoethanol) for 6 hours at 4°C and further dialysed overnight in fresh refolding buffer at 4°C. The histones were then dialysed for a final 4 hours in fresh refolding buffer at 4°C. The dialysed histone octamer was centrifuged at 14,000 rpm for 20 minutes at 4°C, the supernatant collected and concentrated using Amicon Ultra centrifugal concentrators (10 kDa MWCO) to 400 µl. This was then loaded in two 200 µl samples onto a 24 ml Superdex 200 10/300GL gel filtration column (GE Healthcare, Little Chalfont, UK), attached to a FPLC (equilibrated with refolding buffer for 1.5 hours at 0.5 ml/min) and 0.5 ml fractions collected until the UV signal reduced and stabilised. The peak fractions were analysed by 16 % SDS-PAGE and gel staining as above (section 3.17.3). Fractions containing the histone octamer in the correct equimolar ratios were pooled and concentrated to 0.5 ml using Amicon Ultra centrifugal concentrators (10 kDa MWCO). The concentration of the histones was measured Nanodrop ND-1000 spectrometer at a wavelength of OD 280nm and 40 % glycerol and 5 M NaCl was added to produce a 5 mg/ml histone octamer stock which was stored at -20°C.

## 3.18 Nucleosome Reconstitution

The nucleosome reconstitution mix was prepared by mixing 5 pmol fluorescently labelled 256 bp THF or TG DNA, 75 pmol unlabelled 601 nucleosomal DNA, 50 µg BSA molecular biology grade (New England Biolabs Ltd, Luton, UK), 0.01 % NP-40, 2 M NaCl, 80 pmol Histone Octamer in a final volume of 280 µl distilled water. This was incubated for 10 minutes at room temperature before being transferred to pre-washed (with distilled water and 0.1 mg/ml BSA) 6.4 mm diameter dialysis tubing 8 kDa MWCO (Fisher Scientific UK, Loughborough, UK). The mix was dialysed in 500 ml of decreasing concentrations of NaCl (1.6 M, 1.2 M, 0.8 M, 0.6 M, 0.2 M and 0.075 M NaCl, with 10 mM Tris HCl pH 7.4, 1 mM EDTA and 5 mM β-mercaptoethanol) for 1.5 hours each at 4°C and the final dialysis left overnight (0.075 M NaCl). The efficiency of the nucleosome reconstitution was analysed using a 0.7 % agarose gel in 0.2x TAE buffer (section 3.7). 50 fmol of the nucleosome

reconstitution and unlabelled 601 nucleosomal free DNA in 5x loading buffer with a 100 bp DNA ladder were loaded onto the agarose gel and electrophoresed at 75 V for 1.5 hours. The gel was imaged using the Li-Cor Odyssey Infrared Imaging Analysis System (LI-COR Biosciences, Cambridge,UK). Comparison to the free DNA was used to quantify successful nucleosome reconstitution whereby a shift to a high molecular weight species (approximately 700 bp) was observed when the nucleosome was formed. If >90 % successful, the mononucleosome substrate was stored at 4°C.

## 3.19 *In vitro* BER assay and DNA extraction

Reactions, prepared on ice, contained 50 fmol DNA containing the site-specific THF or TG site, 0.7 pmol GST-E1 activating enzyme, 2.5 pmol E2 conjugating enzyme (combination of 9 different E2s (UbE2H, Cdc34, UbE2D1, UbE2D2, UbE2D3, UbE2E1, UbE2L3, UbE2L6 and UbE2C)), 0.6 nmol ubiquitin (Boston Biochemicals, Cambridge, USA) and 1 µg acetylated BSA in buffer (25 mM Tris-HCl (pH 8.0), 50 mM KCl, 2 mM ATP, 8.5 mM $MgCl_2$, 0.5 mM EDTA, 8.5 % glycerol and 1 mM DTT), 50 fmol APE1 or 1.45 pmol NTH1 and ΔN-HECTD1 or ΔN-mutHECTD1 (0-15 pmol titration). Reactions were incubated in 1.5 ml amber eppendorfs for 1 hour at 30°C with 800 rpm. Reactions were stopped by the addition of 20 mM EDTA and 0.4 % SDS. DNA was extracted using phenol:chloroform:isoamyl alcohol (25:24:1) (Sigma Aldrich St. Louis, Missouri, USA) and then once with chloroform:isoamyl alcohol (24:1) (Sigma Aldrich St. Louis, Missouri, USA) where at each step the sample was vortexed and centrifuged at 15,000 x g for 1 minute and the upper aqueous (DNA containing) layer removed. Following this, reactions were cleaned up in Bio-Spin P-30 Gel Columns (Bio-Rad, Watford, UK), prepared with 3x washes in TE buffer centrifuged at 15,000 x g for 1 minute and 1 final wash at 15,000 x g for 2 minutes. Samples were added to the columns and centrifuged at 15,000 x g for 4 minutes before being analysed by 8 % denaturing PAGE (section 3.9).

## 3.20 *In vitro* ubiquitylation assay

To assess the *in vitro* ubiquitylation of APE1 and the core histone proteins (H2A, H2B, H3 and H4), reaction mixtures were prepared in LoBind reaction tubes (Eppendorf, Stevenage, UK). Reaction mixtures consisted of 5.88 pmol APE1 or 1.85 pmol histone octamer, 1x ubiquitin buffer (25 mM Tris-HCl pH 8.0, 5 mM $MgCl_2$, 200 µM $CaCl_2$, 1 mM DTT, and 10 µM MG-132),

40 mM ATP, 0.7 pmol glutathione S-transferase (GST)-E1 activating enzyme, 2.5 pmol E2-conjugating enzyme (a combination of nine different E2s, unless otherwise stated), and 0.6 pmol ubiquitin. The source of E3 ligase activity was provided by the addition of ΔN-HECTD1 (APE1 reactions; 2.76 pmol, 5.52 pmol and 13.8 pmol, histone octamer reactions; 5.1 pmol, 10.2 pmol and 20.41 pmol). Reactions were incubated at 30°C for 1 hour with 800 rpm shaking. The reactions were stopped by the addition of 3x SDS-PAGE sample buffer (25 mM Tris-HCl pH 6.8, 2.5 % β-mercaptoethanol, 1 % SDS, 10 % glycerol, 1 mM EDTA, 0.05 mg/ml bromophenol blue), heated at 95°C for 5 minutes, and analysed via 10 % SDS-PAGE (section 3.2) and immunoblotting (section 3.4).

## 3.21 *In vivo* ubiquitylation assay

To assess the *in vivo* ubiquitylation of the histone H2B and H3 proteins, WI-38 cells were seeded into 10 cm dishes, grown until 30-50 % confluent before being transfected with HECTD1 siRNA or non-targeting siRNA for 48 hours (section 3.24). Following this, cells were incubated on ice for 5 minutes to supress DNA repair activity and, except for in control conditions, irradiated with 10 Gy IR. Following induction of DNA damage (section 3.25), the media was aspirated, cells were washed in 5 ml PBS, media replaced, and cells incubated at 37°C and 5 % $CO_2$ in a humidified cell culture incubator for a set period (15 minutes, 30 minutes or 1 hour). Cells were then harvested (section 3.23.4), histone extracts prepared (section 3.6) before samples were analysed via 16 % SDS-PAGE (section 3.2) and immunoblotting (section 3.4).

## 3.22 DNase footprinting

### 3.22.1 DNase footprinting free DNA dose titration

Reactions, prepared on ice, contained 50 fmol DNA containing the site-specific THF site, DNase I (0-0.5 units) and 1x DNase I reaction buffer (10 mM Tris-HCl, 2.5 mM $MgCl_2$, 0.5 mM $CaCl_2$, pH 7.6) (New England Biolabs Ltd, Luton, UK). Reactions were incubated in 1.5 ml amber eppendorfs for 2 minutes at room temperature. Reactions were stopped by mixing 1:1 with formamide loading dye (formamide 0.025 % (w/v) (9.5 % (w/v) Sigma Aldrich St. Louis, Missouri, USA) 0.25 % bromophenol blue), heated at 95°C for 5 minutes prior to

electrophoresis analysis by 8 % denaturing PAGE (section 3.9) sequencing gel, electrophoresed for 80 minutes at 1800 V, 42 W in 0.5x TBE using the Thermo Scientific™ Owl™ Aluminium-Backed Sequencers (Fisher Scientific UK, Loughborough, UK) with the unit covered for light protection of the fluorescently-labelled DNA. The gel was imaged using the Li-Cor Odyssey Infrared Imaging Analysis System.

### 3.22.2 DNase footprinting mononucleosome dose titration

#### *3.22.2.1 Phenol:chloroform:isoamyl alcohol DNA extraction*

Reactions, prepared on ice, contained 100 fmol THF-IN mononucleosome substrate, DNase I (0-2 units) and 1x DNase I reaction buffer (10 mM Tris-HCl, 2.5 mM $MgCl_2$, 0.5 mM $CaCl_2$, pH 7.6) (New England Biolabs Ltd, Luton, UK). Reactions were incubated in 1.5 ml amber eppendorfs for 2 minutes at room temperature. Reactions were stopped by the addition of 20 mM EDTA and 0.4 % SDS. DNA was extracted using phenol:chloroform:isoamyl alcohol (25:24:1) (Sigma Aldrich St. Louis, Missouri, USA) and then once with chloroform:isoamyl alcohol (24:1) (Sigma Aldrich St. Louis, Missouri, USA) where at each step the sample was vortexed and centrifuged at 15,000 x g for 1 minute and the upper aqueous (DNA containing) layer removed. Following this, reactions were cleaned up in Bio-Spin P-30 Gel Columns (Bio-Rad, Watford, UK), prepared with 3x washes in TE buffer centrifuged at 15,000 x g for 1 minute and 1 final wash at 15,000 x g for 2 minutes. Samples were added to the columns and centrifuged at 15,000 x g for 4 minutes before being mixed 1:1 with formamide loading dye (formamide 0.025 % (w/v) (9.5 % (w/v) Sigma Aldrich St. Louis, Missouri, USA) 0.25 % bromophenol blue), heated at 95°C for 5 minutes prior to electrophoresis analysis by 8 % denaturing PAGE (section 3.9) sequencing gel, electrophoresed for 80 minutes at 1800 V, 42 W in 0.5x TBE using the Thermo Scientific™ Owl™ Aluminium-Backed Sequencers (Fisher Scientific UK, Loughborough, UK) with the unit covered for light protection of the fluorescently-labelled DNA. The gel was imaged using the Li-Cor Odyssey Infrared Imaging Analysis System.

#### *3.22.2.2 Ethanol precipitation DNA extraction*

Reactions, prepared on ice, contained 100 fmol THF-IN mononucleosome substrate, DNase I (0-2 units) and 1x DNase I reaction buffer (10 mM Tris-HCl, 2.5 mM $MgCl_2$, 0.5 mM $CaCl_2$, pH 7.6) (New England Biolabs Ltd, Luton, UK). Reactions were incubated in 1.5 ml amber eppendorfs for 2 minutes at room temperature. Reactions were stopped by the addition of 20 mM EDTA and 0.4 % SDS. DNA was extracted using phenol:chloroform:isoamyl alcohol (25:24:1) (Sigma Aldrich St. Louis, Missouri, USA) and then once with chloroform:isoamyl alcohol (24:1) (Sigma Aldrich St. Louis, Missouri, USA) where at each step the sample was vortexed and centrifuged at 15,000 x g for 1 minute and the upper aqueous (DNA containing) layer removed. Following this, the aqueous layer was mixed with 10 µg glycogen, 1/10 volume of 3 M NaAc pH 5.2 and 2.5 volumes of cold 100 % ethanol. Samples were mixed 3-5 times by inversion and incubated at -80°C for >1 hour. Samples were centrifuged at 16,000 x g for 30 minutes and the supernatant aspirated, 3 volumes of cold 70 % ethanol added and centrifuged for a further 10 minutes and the supernatant aspirated. Pellets were left to air dry for 5 minutes and 10 µl TE buffer added and pellets thoroughly resuspended. Samples were mixed 1:1 with formamide loading dye (formamide 0.025 % (w/v) (9.5 % (w/v) Sigma Aldrich St. Louis, Missouri, USA) 0.25 % bromophenol blue), heated at 95°C for 5 minutes prior to electrophoresis analysis by 8 % denaturing PAGE (section 3.9) sequencing gel, electrophoresed for 80 minutes at 1800 V, 42 W in 0.5x TBE using the Thermo Scientific™ Owl™ Aluminium-Backed Sequencers (Fisher Scientific UK, Loughborough, UK) with the unit covered for light protection of the fluorescently-labelled DNA. The gel was imaged using the Li-Cor Odyssey Infrared Imaging Analysis System.

### 3.22.3 DNase footprinting with the *in vitro* BER assay

Reactions, prepared on ice, contained 100 fmol THF-IN mononucleosome substrate, either 0 pmol or 10 pmol ΔN-HECTD1, 0.7 pmol GST-E1 activating enzyme, 2.5 pmol E2 conjugating enzyme (combination of 9 different E2s), 0.6 nmol ubiquitin (Boston Biochemicals, Cambridge, USA), 1 µg acetylated BSA in buffer (25 mM Tris-HCl (pH 8.0), 50 mM KCl, 2 mM ATP, 8.5 mM $MgCl_2$, 0.5 mM EDTA, 8.5 % glycerol and 1 mM DTT) and 50 fmol APE1. Reactions were incubated in 1.5 ml amber eppendorfs for 1 hour at 30°C with 800 rpm. Reactions were stopped by the addition of 20 mM EDTA and 0.4 % SDS. DNA was extracted using phenol:chloroform:isoamyl alcohol (25:24:1) (Sigma Aldrich St. Louis, Missouri, USA) and then once with chloroform:isoamyl alcohol (24:1) (Sigma Aldrich St. Louis, Missouri, USA)

where at each step the sample was vortexed and centrifuged at 15,000 x g for 1 minute and the upper aqueous (DNA containing) layer removed. Following this, the aqueous layer was mixed with 10 µg glycogen, 1/10 volume of 3 M NaAc pH 5.2 and 2.5 volumes of cold 100 % ethanol. Samples were mixed 3-5 times by inversion and incubated at -80°C for >1 hour. Samples were centrifuged at 16,000 x g for 30 minutes and the supernatant aspirated, 3 volumes of cold 70 % ethanol added and centrifuged for a further 10 minutes and the supernatant aspirated. Pellets were left to air dry for 5 minutes and 10 µl TE buffer added and pellets thoroughly resuspended. The samples were then incubated with 1 unit DNase I in 1x DNase I reaction buffer (10 mM Tris-HCl, 2.5 mM $MgCl_2$, 0.5 mM $CaCl_2$, pH 7.6) (New England Biolabs Ltd, Luton, UK). Reactions were incubated in 1.5 ml amber eppendorfs for 2 minutes at room temperature. Reactions were stopped by mixing 1:1 with formamide loading dye (formamide 0.025 % (w/v) (9.5 % (w/v) Sigma Aldrich St. Louis, Missouri, USA) 0.25 % bromophenol blue), heated at 95°C for 5 minutes prior to electrophoresis analysis by 8 % denaturing PAGE (section 3.9) sequencing gel, electrophoresed for 80 minutes at 1800 V, 42 W in 0.5x TBE using the Thermo Scientific™ Owl™ Aluminium-Backed Sequencers (Fisher Scientific UK, Loughborough, UK) with the unit covered for light protection of the fluorescently-labelled DNA. The gel was imaged using the Li-Cor Odyssey Infrared Imaging Analysis System.

## 3.23 Tissue culture

Tissue culture work was carried out using an aseptic technique and performed in a class II hood with laminar flow (Esco Global, Barnsley, UK) that was cleaned with 70 % ethanol thoroughly before and after use. Trypsin, PBS and complete DMEM media (containing 10 % FBS, 2 mM glutamine and 1 % pen-strep) were warmed in a water bath at 37°C prior to use. All plastics were tissue culture grade and cells were grown in a humidified cell culture incubator in 5 % $CO_2$ at 37°C.

### 3.23.1 Thawing cells

Cryovials containing cells frozen in DMEM and 10 % DMSO were removed from liquid nitrogen storage and rapidly defrosted for 1 minute in a 37°C water bath. 1 ml complete DMEM was added to the cells and gently mixed via pipetting. The cell suspension was centrifuged at 1500 rpm for 3 minutes and the DMSO containing supernatant removed. The

cell pellet was resuspended and diluted in complete DMEM media to 12 ml and transferred to a T75 flask and incubated at 37°C and 5 % $CO_2$ in a humidified cell culture incubator. Once cells were approximately 80-90 % confluent the cells were sub-cultured.

### 3.23.2 Sub culturing

Once cells were approximately 80-90 % confluent, cells were sub-cultured by aspirating DMEM media from the T75 flask and washing the monolayer of cells with 10 ml PBS. The PBS was aspirated, and the cells were incubated with 1 ml 0.25 % trypsin-EDTA for 1-5 minutes at 37°C and 5 % $CO_2$ in a humidified cell culture incubator. Once the adherent cells had detached the trypsin was neutralised using 9 ml media and the cells mixed to create a single-cell suspension. WI-38 cells were split 1:8 and AG06173 and AG16409 cells split 1:4 into a new T75 flask. Cells were stored incubated at 37°C and 5 % $CO_2$ in a humidified cell culture incubator.

### 3.23.3 Long-term storage of cells

Cells were collected (section 3.23.2) in order to bring them into a single-celled suspension. The cell suspension was centrifuged at 1500 rpm for 3 minutes. The resulting cell pellet was resuspended in 1 ml freezing medium (FBS with 10 % DMSO) and transferred to a cryovial. The cryovials were placed in a Corning™ CoolCell™ LX Cell Freezing Vial Container (Fisher Scientific, Loughborough, UK) and placed into a -80°C freezer for 24 hours before being transferred to long-term storage in liquid nitrogen.

### 3.23.4 Harvesting cells

Tissue culture dishes containing cells that were approximately 80-90 % confluent were removed from the tissue culture incubator, the media aspirated and the dishes washed with cold PBS before being aspirated. A second volume of cold PBS was added, adhered cells were carefully collected using a cell scraper and transferred to a pre-cooled 15 ml tube, this process was repeated a second time. The 15 ml tube was centrifuged at 1500 rpm for 5 minutes at 4°C, the supernatant removed, and the pellet resuspended in 1 ml of cold PBS before being transferred to a pre-cooled 1.5 ml eppendorf. The 1.5 ml microcentrifuge tube

was then centrifuged at 1500 rpm for 5 minutes at 4°C, the supernatant removed and the pellet frozen at -80°C.

### 3.23.5 Seeding cells

Cells were seeded prior to various experiments and assays and were collected (section 3.23.2) in order to bring them into a single-cell suspension. Cells were counted using a haemocytometer. In general, $5x10^6$ cells were seeded in 5 ml complete DMEM for a 10 cm dish and $1x10^5$ cells in 1 ml complete DMEM for a 3.5 cm dish.

## 3.24 RNA interference

Depletion of endogenous protein levels was achieved via siRNA-mediated mRNA depletion. Cells were seeded into either 3 cm or 10 cm dishes and grown until 30-50 % confluent in complete DMEM at 37°C and 5 % $CO_2$ in a humidified cell culture incubator. Per 10 cm dish, 10 µl Lipofectamine RNAiMax (Life Technologies, Paisley, UK) was added to 500 µl supplement-free DMEM and separately, 40 nM of siRNA (Table 3.5) added to 500 µl supplement-free DMEM. The supplement free DMEM/Lipofectamine RNAiMax mix was added to the supplement free DMEM/siRNA mix, mixed thoroughly and incubated for 10 minutes at room temperature. This 1 ml solution was then added dropwise to the 10 cm cell culture dish containing cells containing 5 ml complete media, and evenly distributed by gentle agitation of the dishes. Cells were incubated for 48 hours at 37°C and 5 % $CO_2$ in a humidified cell culture incubator. For 3 cm dishes, 2.5 µl Lipofectamine RNAiMAX and 40 nM siRNA was added to cells in 250 µl supplement free DMEM using the same method.

## 3.25 Induction of DNA damage

AG06173, AG16409 or WI-38 cells were seeded into tissue culture dishes, grown until 30-50 % confluent before being transfected with HECTD1 siRNA or non-targeting siRNA for 48 hours (section 3.24). DNA damage was induced through treatment with ionising radiation (IR) using the CellRad X-Ray irradiator (Faxitron, Tuscan, USA) at 3 Gy/minute, hydrogen peroxide ($H_2O_2$) or Methyl methanesulfonate (MMS).

## 3.26 Clonogenic assay

AG06173, AG16409 or WI-38 cells were seeded into 3.5 cm dishes, grown until 30-50 % confluent before being transfected with HECTD1 siRNA or non-targeting siRNA for 48 hours (section 3.24). Following this, cells were either incubated on ice for 5 minutes to supress DNA repair activity and irradiated with increasing doses of IR (0-4 Gy) or incubated with increasing does of $H_2O_2$ (0-300 µM) or MMS (0-1.5 mM) at 37°C and 5 % $CO_2$ in a humidified cell culture incubator. Following induction of DNA damage, the media was aspirated, cells were washed in 1 ml PBS, 200 µl 0.25 % trypsin-EDTA added to the cells which were incubated at 37°C and 5 % $CO_2$ in a humidified cell culture incubator until cells lifted off the tissue culture dishes. Trypsin was neutralised in 800 µl media and cells counted using a haemocytometer. A defined number of cells were seeded in 2 ml complete DMEM media at two different cell densities in triplet for each treatment in 6-well plates (Table 3.9). The plates were incubated at 37°C and 5 % $CO_2$ in a humidified cell culture incubator for 7-10 days until colonies were clearly visible (>50 cells/colony). Cells were fixed and stained by removing media, washing the cells in PBS, and adding 0.5 % crystal violet in 6 % glutaraldehyde (Fisher Scientific UK, Loughborough, UK) for 1 hour, washed and left to air dry. Colonies were counted using the GelCount colony counter (Oxford Optronix, Oxford, UK). Relative colony forming units (surviving fraction) were expressed as colonies per treatment relative to colonies observed in the untreated control for each treatment, calculated using the calculation shown below. Average surviving fractions were calculated, and values plotted on a log scale against treatment doses. Statistical analysis was performed by the CFAssay for R package [326].

$$\text{Plating efficiency} = \frac{\text{Number of colonies for untreated control}}{\text{seeding density of untreated control}}$$

$$\text{Surviving fraction} = \frac{\text{Number of colonies for selected condition}}{\text{(seeding density of for selected condition x average plating efficiency)}}$$

**Table 3.9: Clonogenic assay seeding densities relative to treatment**

Numbers shown are the two seeding densities used in triplicate per 6-well plate for HECTD1 and non-targeting siRNA treatments at each dose of IR, $H_2O_2$ or MMS.

| | Seeding density |
|---|---|
| IR (Gy) dose | |
| 0 Gy | 250/500 |
| 1 Gy | 500/1000 |
| 2 Gy | 1000/2000 |
| 4 Gy | 2000/4000 |
| $H_2O_2$ (µM) dose | |
| 0 µM | 250/500 |
| 50 µM | 500/1000 |
| 100 µM | 1000/2000 |
| 200 µM | 2000/4000 |
| 300 µM | 4000/8000 |
| MMS (mM) dose | |
| 0 mM | 250/500 |
| 0.25 mM | 500/1000 |
| 0.5 mM | 500/1000 |
| 0.75 mM | 1000/2000 |
| 1 mM | 1000/2000 |
| 1.25 mM | 2000/4000 |
| 1.5 mM | 2000/4000 |

## 3.27 COMET assay

The comet assay was used to study repair kinetics following induction of DNA damage [327]. WI-38, AG06173 or AG16409 lung fibroblasts were transfected with siRNA targeting either HECTD1 or the Qiagen AllStars non-targeting control sequence (section 3.24). To induce DNA damage, cells in suspension were treated with 1.5 Gy IR using the CellRad X-ray irradiator at 3 Gy/min or with 10 µM $H_2O_2$ for 5 minutes on ice in the alkaline comet assay and 4 Gy IR or 30 µM $H_2O_2$ in the same manner for the neutral comet assay. DNA damage was also induced

for the alkaline comet assay to cells in a monolayer via 0.5 mM MMS treatment in complete DMEM at 37°C and 5 % $CO_2$ in a humidified cell culture incubator for 1 hour.

### 3.27.1 Alkaline COMET assay

WI-38, AG06173 or AG16409 that had been transfected with siRNA for either HECTD1 or the Qiagen AllStars non-targeting control were trypsinised, diluted to $1x10^5$ cells/ml and 250 µl cell suspension placed into a 24 well plate prior to DNA damage induction for IR and $H_2O_2$ treatment or following DNA damage induction via MMS. Following this, on ice, cells were mixed with 800 µl 1 % low melting point agarose (LMPA (Fisher Scientific UK, Loughborough, UK)) in PBS loaded onto to a pre-coated microscope slides (1 ml 1 % normal melting point agarose (NMPA (Fisher Scientific UK, Loughborough, UK)) in distilled water). Once the agarose had set, slides were placed in a 37°C humidified incubator for a selected length of time to allow for DNA repair. Following incubation, slides were lysed in coplin jars containing cold lysis buffer (2.5 M NaCl, 100 mM EDTA, 10 mM Tris base, pH 10.5, 10 % DMSO and 1 % tween-20) for >1 hour at 4°C. Slides were placed in a comet assay tank (Appleton Woods Ltc, Birmingham, UK) and DNA was allowed to unwind for 30 minutes in cold electrophoresis buffer (300 mM NaOH, 1 mM EDTA, 1 % DMSO, pH>13), before electrophoresis was performed 25 V, 300 mA for 25 minutes. The slides were then washed 3 times with 1 ml cold neutralisation buffer (500 mM Tris-HCl pH 8) for 5 minutes and air dried overnight. Slides were rehydrated with distilled water (pH 8.0) for 30 minutes and the DNA stained with 1 ml SYBR Gold (1:20,000 in distilled water, pH8.0 (Fisher Scientific UK, Loughborough, UK) for 30 minutes and air dried again overnight (light protected). Slides were imaged using the BX61 Olympus microscope and 10x magnification (Olympus, Shinjuku, Japan), taking 10 images per slide, containing at least 5 cells per image, with 2 slides per time point. Images were analysed using Komet 6.0 software (Andor Technology, Belfast) in order to calculate % tail DNA values.

### 3.27.2 Neutral COMET assay

WI-38, AG06173 or AG16409 that had been transfected with siRNA for either HECTD1 or the Qiagen AllStars non-targeting control were trypsinised, diluted to $1x10^5$ cells/ml and 250 µl cell suspension placed into a 24 well plate prior to DNA damage induction for IR and $H_2O_2$ treatment. Following this, on ice, cells were mixed with 800 µl 1 % low melting point agarose (LMPA (Fisher Scientific UK, Loughborough, UK)) in PBS loaded onto to a pre-coated

microscope slides (1 ml 1 % normal melting point agarose (NMPA (Fisher Scientific UK, Loughborough, UK)) in distilled water). Once the agarose had set, slides were placed in a 37°C humidified incubator for a selected length of time to allow for DNA repair. Following incubation, slides were lysed in coplin jars containing cold lysis buffer (2.5 M NaCl, 100 mM EDTA, 10 mM Tris base, 1 % N-lauroylsarcosine, pH 9.5, 10 % DMSO and 1 % tween-20), for >1 hour at 4°C. Following lysis, slides were washed 3x with 1 ml cold electrophoresis buffer (1x TBE (18 mM Tris-borate, 0.4 mM EDTA, pH 8.3) for 5 minutes, before slides were placed and DNA was allowed to unwind in a comet assay tanks, for 30 minutes in cold electrophoresis buffer. Electrophoresis was performed 25 V, 20 mA for 25 minutes. The slides were then washed 3 times with 1 ml cold PBS for 5 minutes and air dried overnight. Slides were then stained, imaged and analysed in the same manner as outlined above in the alkaline assay.

# CHAPTER 4: RESULTS I

## *In vitro* investigation of HECTD1 as a chromatin remodelling enzyme enhancing APE1 activity

### 4.1 Introduction

The compaction of genetic material into chromatin is essential for the organisation of DNA within the nucleus and involves co-ordinated levels of folding amongst histones and non-histone chromosomal proteins. Via multiple mechanisms, DNA within compacted regions is then made accessible to the complex machinery of essential biological processes including gene transcription, DNA replication and DNA repair. Therefore, an increasing research focus has been the changes to chromatin via remodelling events and histone PTMs which are necessary to facilitate the DNA damage response. In particular, evidence has been reported during DSB repair and NER [232], [233]. This is specifically important for tightly packed regions of chromatin and similarly, it can assumed, that BER requires complete, unobstructed access to DNA base damage to promote efficient repair. Furthermore, as the pathway creates increasingly cytotoxic and mutagenic lesions as it progresses, it is essential that there is a seamless transition between each stage, and that repair is completed in a timely manner once BER in initiated. Therefore time, space and access to DNA base damage is essential for the effective and efficient completion of BER in chromatin.

Despite this, the molecular mechanisms through which this is co-ordinated and the specific enzymes that promote chromatin remodelling required for BER remain elusive. Recently, and as summarised in section 1.6, we have summarised the multitude of *in vitro* studies utilising mononucleosome substrates containing site specific DNA base damage that demonstrate the requirement for chromatin remodelling to facilitate BER, particularly in occluded regions. We also highlighted preliminary evidence to date for the identity of ACRs, their mechanisms and the role of histone PTMs in modulating the cellular capacity for BER [170].

A previous PhD student in our group, developed two mononucleosome substrates with site-specific THF sites in two orientations, rotationally positioned so the DNA backbone was facing outwards (THF-OUT) so accessible to APE1, or facing inwards (THF-IN) towards the histone octamer and therefore sterically occluded to APE1. Here it was discovered that the incision of a THF site within a mononucleosome substrate that is inaccessible to recombinant APE1 (THF-IN), is more efficiently incised by APE1 in WCE due to the presence of histone

modifiers and/or chromatin remodelling factors. This stimulatory activity within the WCE was isolated by adopting a sequential chromatography approach and mass spectrometry analysis identified the E3 ubiquitin ligase HECTD1 as a strong candidate required to facilitate BER through histone ubiquitylation and/or chromatin remodelling.

My aim was to establish a role for HECTD1 in enhancing the repair of DNA base damage within occluded sites within chromatin. In this chapter, I will describe use of previously established techniques within Dr Parsons' laboratory to generate THF-IN mononucleosome substrates. Additionally, I will describe LIC cloning as a technique used to clone the murine HECTD1 gene truncated at amino acid 1761 from the mammalian expression vector and into the pET28a bacterial expression vector, to allow the protein to be expressed and purified from *E coli* cells. Using these substrates, I aimed to establish conditions to examine the processing of these inaccessible THF-IN sites by APE1 via *in vitro* BER assays and investigate whether HECTD1 can enhance *in vitro* the activity of APE1 on THF-IN mononucleosome substrates.

## 4.2 Preparation of THF-IN site containing DNA

In order to analyse the ability of HECTD1 to stimulate APE1 incision of sterically occluded THF sites, it was important in the first instance to produce a THF-IN containing DNA segment with nucleosome interacting properties, positioned 10 bp from the dyad (Figure 4.1). This DNA substrate was generated containing a site specific THF site on the lower strand in the central area of the DNA sequence, with proximal restriction sites (section 3.1.1, Figure 3.1). The Widom 601 nucleosome positioning sequence was amplified from the pGEM-3Z-601 plasmid using PCR and the central 17 bp removed using Van91I and BglI restriction enzymes to produce, once purified, two DNA sequence fragments. These were sequentially ligated to a pre-prepared 17 bp duplex oligonucleotide containing a THF site on the lower strand, resulting in the production of a site specific THF-IN DNA substrate, which when complexed with a histone octamer, generated a mononucleosome substrate where the DNA backbone of the THF site faced inwards towards the histone octamer and was therefore occluded from APE1 (Figure 4.2).

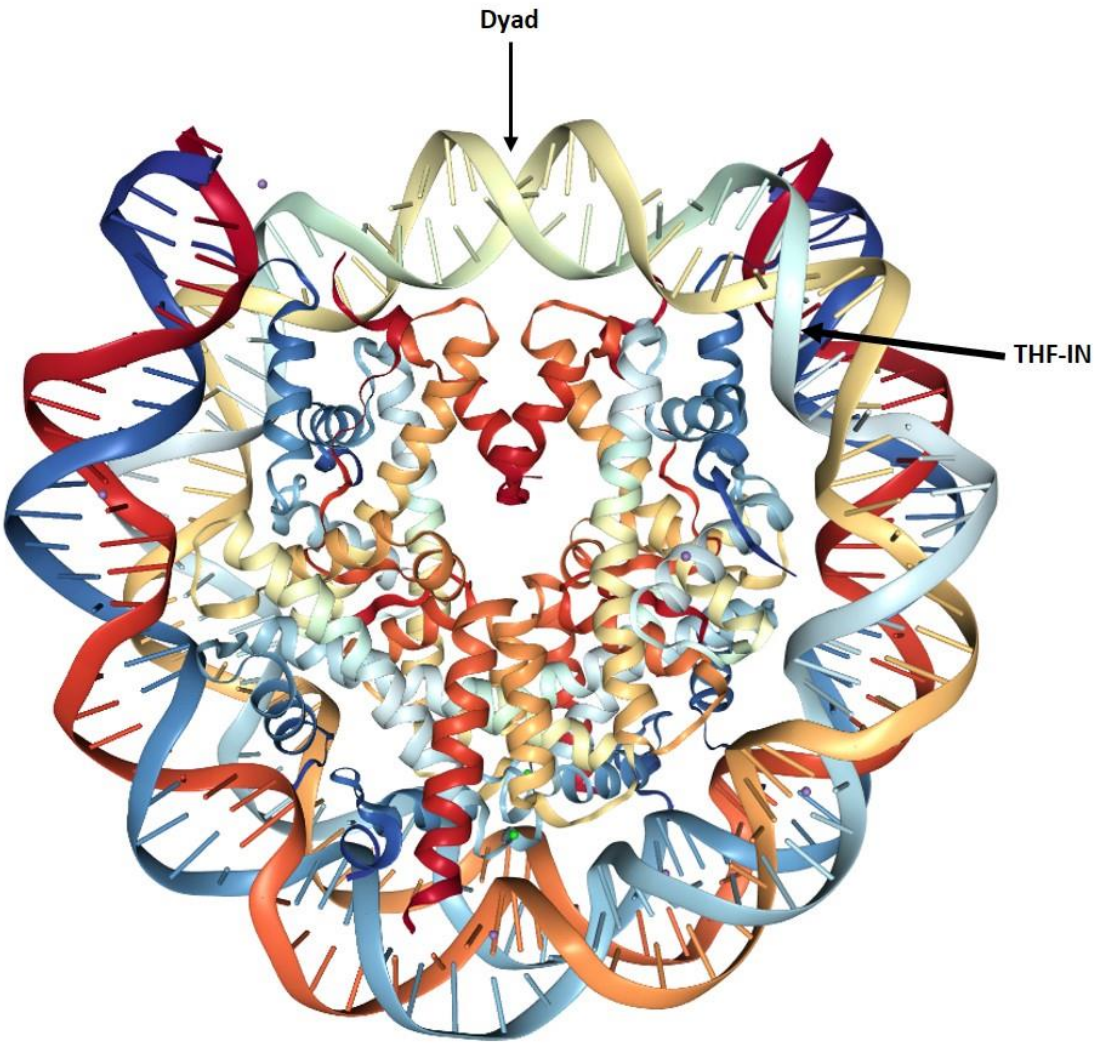


**Figure 4.1: Structure of the nucleosome core particle composed of the 601 DNA sequence**

Image was acquired from Protein Data Bank structure 3LZ0 (orientation 1) and indicated are the positions of the dyad and 10 bp from the dyad the THF-IN site, with the DNA backbone facing inward toward the histone core.

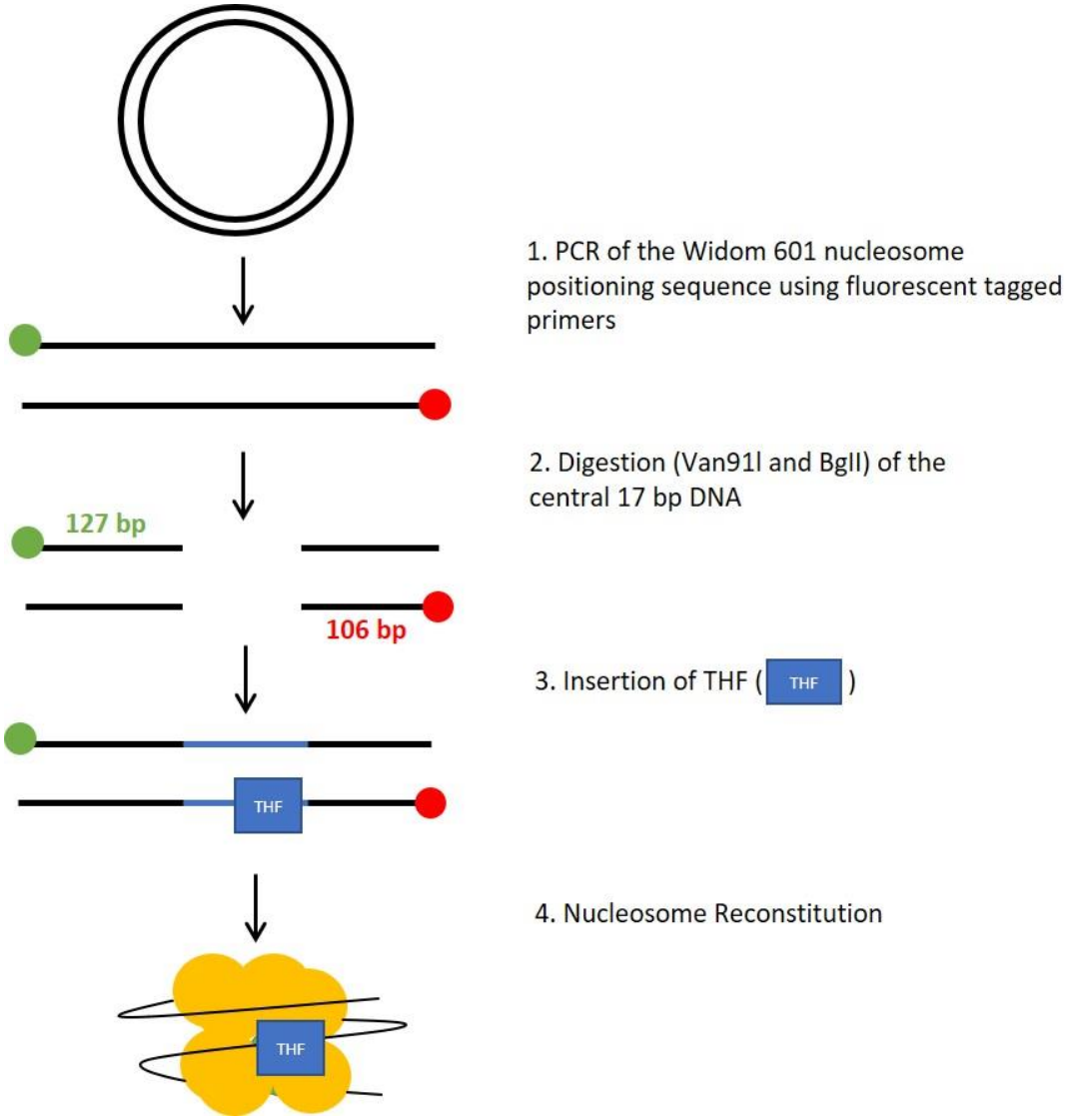


**Figure 4.2: Schematic diagram of the formation of the THF-IN containing DNA and nucleosome**

1. The 256 bp Widom 601 nucleosome positioning sequence was amplified from the pGEM-3Z-601 plasmid using PCR with fluorescently tagged primers (shown as red and green circles). 2.The central 17 bp was then removed using a Van91I and BglI double restriction digest to generate a green labelled (green circle) 127 bp digest product and red labelled (red circle) 106 bp digest product. 3. A 17 bp duplex oligonucleotide (shown in blue) containing a THF-IN (blue rectangle) was then sequentially ligated to the 127 bp (green) and 106 bp (red) DNA fragments, producing the final 256 bp DNA which was then 4. reconstituted with the histone octamer to form the THF-IN mononucleosome.

### 4.2.1 Amplification of the 601 nucleosome positioning sequence

The Widom 601 wild-type strong nucleosome positioning sequence was amplified from the pGEM-3Z-601 plasmid using PCR with 5'-fluroescent labelled primers (Figure 4.2, stage 1). For production of THF-IN DNA the forward primer was tagged with IRDye800 (green label) and the reverse with IRDye700 (red label), due to the increased signal intensity of the IRDye700 tag so THF incision could be more strongly visualised using the Odyssey Image Analysis system. As the DNA marker was not visible due to the use of fluorescently tagged primers negating the use of a SYTO60 dye, successful generation of the 256 bp 601 nucleosome positioning sequence PCR product was visualised as yellow, as the product contained both IRDye700 and IRDye800 5' labelled ends and the fluorescent primers were also clearly visible underneath each of the PCR products (Figure 4.3). The verified 256 bp DNA was subsequently purified using a PCR purification kit and the yield was found to be approximately ~135 µg for 15 pooled PCR reactions.

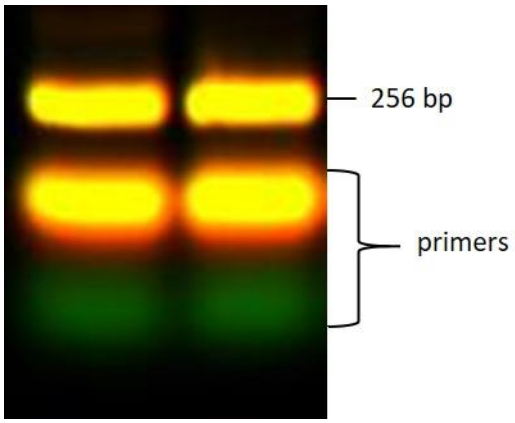


**Figure 4.3: Amplification of the 256 bp 601 nucleosome positioning sequence**
PCR product of the 601 wild-type strong nucleosome positioning sequence containing both the IRDye800 and IRDye700 florescent tags and the IRDye800 forward primer IRDye700 reverse primer separated by electrophoresis on a 1.5 % agarose gel at 100 V for 1 hour, imaged using the Li-Cor Odyssey Infrared Imaging Analysis System.

### 4.2.2 Double restriction digest of the 601 nucleosome positioning sequence

Following purification of the 256 bp 601 nucleosome positioning sequence, the central 17 bp region was removed using Van91I and BglI restriction enzymes (region shown in section 3.1.1, Figure 3.1). These enzymes produced a IRDye800 tagged 127 bp DNA fragment and a IRDye700 tagged 106 bp DNA fragment, both with sticky ends to facilitate subsequent

ligation (Figure 4.2, stage 2). Completion of the restriction digest was confirmed by comparison to the original purified 256 bp PCR product (Figure 4.4A, lane 1), where the Van91I and BglI digestion product (Figure 4.4A, lane 2) is absent of the 256 bp PCR product and only the 127bp and 106 bp DNA fragments are present. The 127bp and 106 bp DNA fragments were then purified from each other using PAGE separation and gel extraction. To assure 100 % efficiency in the production and purification of these digest products, the 127 bp (Figure 4.4B, lane 2) and 106 bp (Figure 4.4B, lane 3) DNA products were compared to the original PCR product (Figure 4.4B, lane 1). Again, as the DNA is fluorescently labelled use of a DNA marker was not applicable here.

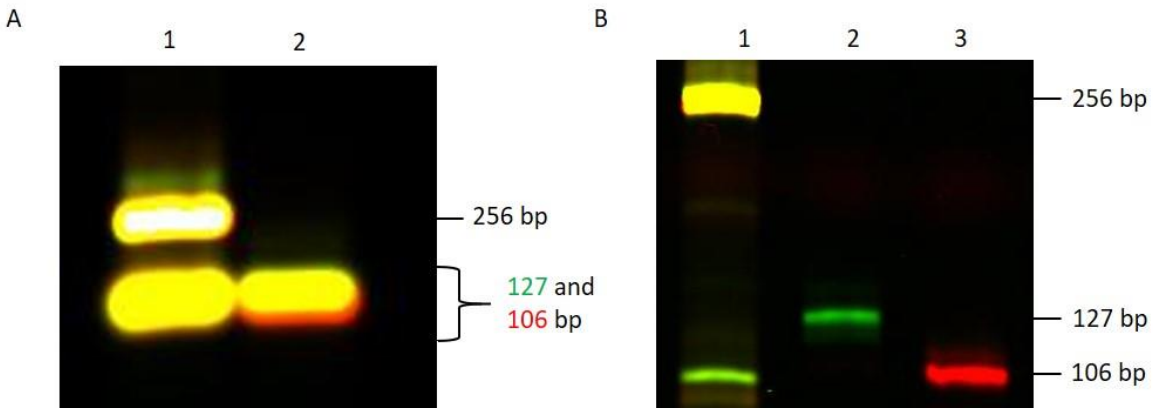


**Figure 4.4: 127bp and 106 bp Van91I/Bg11 restriction digest products**

**A.** Original 256 bp PCR product (lane 1) against the Van91I and BglI digestion product (lane 2) following separation by electrophoresis on a 1.5 % agarose gel at 100 V for 1 hour. **B.** Original 256 bp PCR product (lane 1) against the IRDye800 tagged 127 bp DNA digest product (lane 2) and IRDye700 tagged 106 bp DNA digest product (lane 3) following PAGE separation on an 8 % polyacrylamide gel in 0.5x TBE run at 175 V, 20 W for 3 hours, gel extraction and DNA purification. Gels were imaged using the Li-Cor Odyssey Infrared Imaging Analysis System.

### 4.2.3 Sequential ligations to incorporate the THF-IN site

To maximise ligation efficiency, the 127 bp and 106 bp DNA digest products were ligated sequentially to a 17 bp THF-IN containing duplex oligonucleotide with complimentary sticky ends (section 3.1.2.1, Table 3.2) (Figure 4.2, stage 3). In the first instance, the 127 bp segment was ligated to the THF-IN containing duplex oligonucleotide. This was successfully observed as a ligated 147 bp DNA ligation product (Figure 4.5A, lane 3) in comparison to the original 5'-IRDye800 labelled 127 bp DNA (Figure 4.5A, lane 2). This was gel purified using the

MinElute reaction clean up kit and then ligated to the 106 bp DNA digest product. Successful ligation was evidenced by the formation of the full 256 bp substrate DNA (Figure 4.4B, lane 3), in comparison to the unligated second ligation mix (Figure 4.5B, lane 2). This was purified using PAGE separation and gel extraction, and the successful purification of the final 256 bp substrate containing a site specific THF-IN site (Figure 4.5C, lane 2) was confirmed via comparison to the original purified PCR product (Figure 4.5C, lane 1). As before, the use of a DNA marker was not applicable here, due to the DNA being fluorescently labelled. This 256 bp substrate containing a site specific THF-IN site now could be used in the nucleosome reconstitution with the prepared histone octamer. This demonstrates that I had successfully developed a technique to generate a DNA substrate containing a site specific THF-IN site, which I could use to examine the effect of HECTD1 on APE1 incision activity rates at occluded THF sites in mononucleosomes. For ease of quantification, the DNA substrates were labelled so the IRDye700, the most intense signal when imaging with the Li-Cor Odyssey Infrared Imaging Analysis System, was on the DNA lesion-containing strand, which would be incised by APE1, therefore the incision rate by APE1 could be better visualised and accurately quantified.

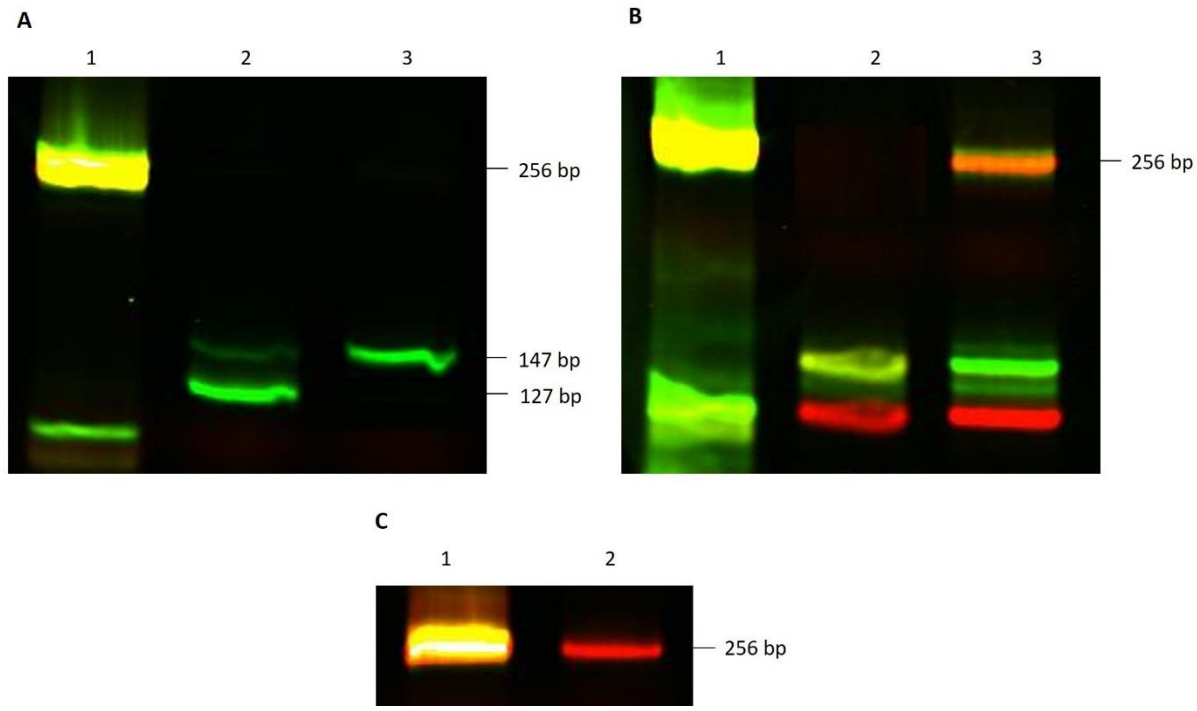


**Figure 4.5: Sequential Ligations to generate a 256 bp DNA substrate containing a THF-IN site**

**A**. Ligation Reaction 1. Original 256 bp PCR product (lane 1), before (lane 2) and after ligation (lane 3) of the IRDye800 tagged 127 bp DNA with the 17 bp duplex oligonucleotide. **B**. Ligation Reaction 2. Original 256 bp PCR product (lane 1), before (lane 2) and after the second ligation (lane 3) using the IRDye800 tagged 147 bp and IRDye700 tagged 106 bp DNA, producing a 256 bp product containing a THF-IN site. **C.** Original 256 bp PCR product (lane 1), final 256 bp substrate containing a site specific THF-IN site following purification by PAGE separation and gel extraction (lane 2). All PAGE gels contained 8 % polyacrylamide and 0.5x TBE, and were run at 175 V, 20 W for 3 hours, gels were imaged using the Li-Cor Odyssey Infrared Imaging Analysis System.

## 4.3 Histone octamer preparation

*E.coli* were individually transformed with pET-expression vectors for *Xenopus Laevis* histones (H2A, H2B, H3 and H4) and the recombinant histone overexpressed via IPTG induction. The bacteria were harvested, cells lysed and the proteins purified from inclusion bodies by gel filtration and ion-exchange chromatography under denaturing conditions (7 M urea), using an FPLC. The histones were then unfolded, combined in equimolar ratios and refolded to

form the octamer. The histone octamer was subsequently purified in high salt containing buffer (2 M NaCl) using size exclusion chromatography and an AKTA FPLC (Figure 4.6).

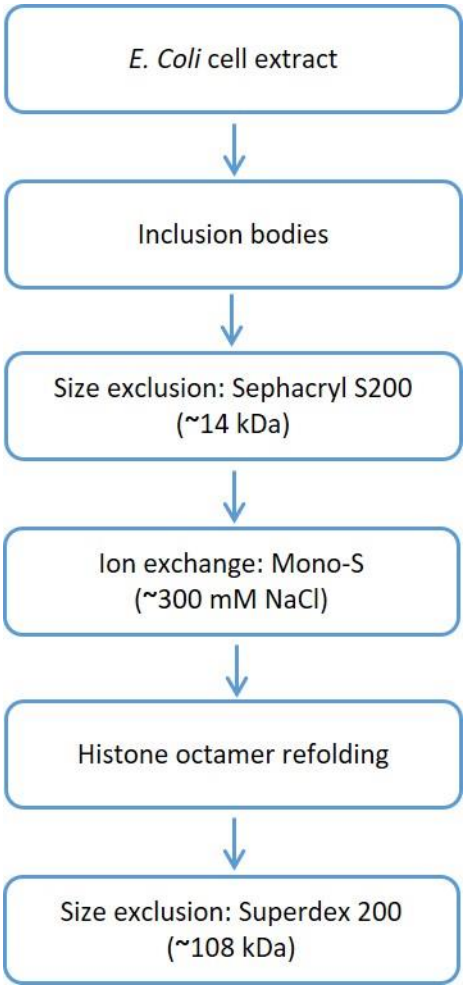


**Figure 4.6: Strategy for the histone purification process**

*E.coli* were individually transformed with each histone expression plasmid (for H2A, H2B, H3 and H4), and following IPTG induction to overexpress the proteins, the bacteria cells were harvested and lysed. Each histone was then individually purified from inclusion bodies. Firstly, using a Sephacryl S200 column (size exclusion chromatography) eluting at approximately 14 kDa followed by a Mono-S column (ion exchange chromatography) eluting at approximately 300 mM NaCl. Both chromatography steps used an AKTA FPLC and were under denaturing conditions (7 M urea). The presence of histones in fractions was analysed by SDS-PAGE and Instant Blue protein staining. Once identified, the histones were unfolded, combined in equimolar ratios and allowed to refold to form the histone octamer. The octamer was purified using a Superdex 200 column (size exclusion chromatography) and AKTA FPLC with a high salt buffer (2 M NaCl), with proteins eluting at approximately 108 kDa. Purity and stoichiometry of the histone octamer was analysed by SDS-PAGE and Instant Blue protein staining and the histone octamer containing fractions pooled.

### 4.3.1 Recombinant histone purification: gel filtration chromatography

Following lysis and purification of individual histones from inclusion bodies of *E.coli* overexpressing recombinant histones, the proteins were initially purified by size exclusion chromatography using a Sephacryl S200 column and a AKTA FPLC under denaturing conditions (7 M urea). The UV trace and fraction numbers collected when protein started to elute from AKTA FPLC correlates to the amount of protein being eluted and is shown for each of the four histones; H2A (Figure 4.7A), H2B (Figure 4.8A) H3 (Figure 4.9A) and H4 (Figure 4.10A). These traces show two major peaks, the first relating to bacterial DNA contaminants and the second, latter peak to the histone of interest. The proteins within these fractions were separated by SDS-PAGE and Instant Blue protein stained (H2A (Figure 4.7B), H2B (Figure 4.8B) H3 (Figure 4.9B) and H4 (Figure 4.10B)). Full length histone H2A (13.96 kDa) was shown to elute in fractions 10-15 (Figure 4.7), H2B (13.77 kDa) was shown to elute in fractions 10-14 (Figure 4.8), H3 (15.27 kDa) was shown to elute in fractions 9-18 (Figure 4.9) and H4 (11.24 kDa) was shown to elute in fractions 14-19 (Figure 4.10). Of note, the upper band correspond to the full-length histones and the lower band are slightly degraded histones. Fractions containing the histones were pooled together for further protein purification by ion-exchange chromatography.

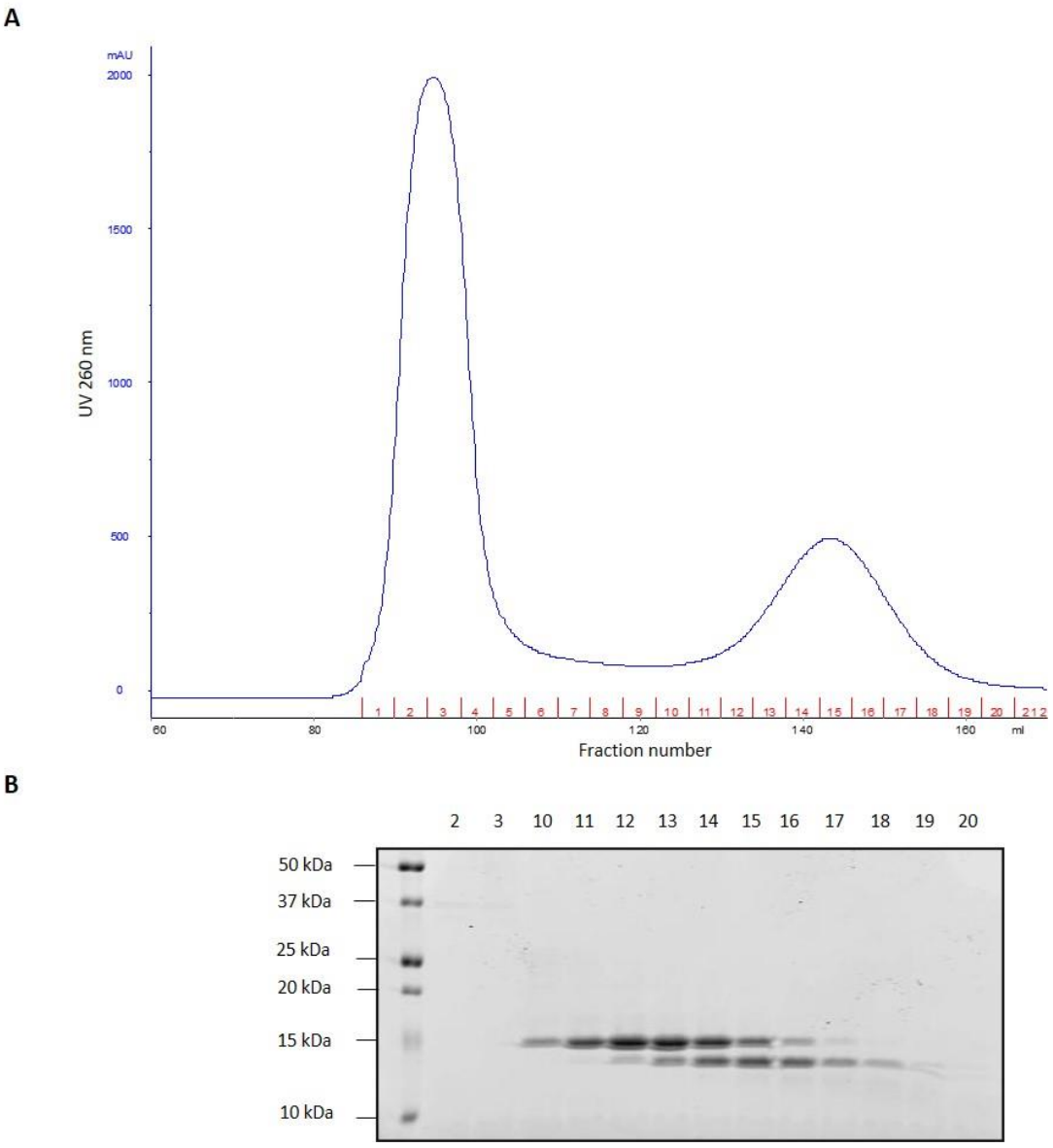


**Figure 4.7: Purification of recombinant histones H2A gel filtration chromatography**

Following protein overexpression in *E-coli*, histone H2A was initially purified by size exclusion chromatography using a gel filtration, Sephacryl S200 column and an AKTA FPLC under denaturing conditions (7 M urea). **A**. H2A UV trace (blue) from the FPLC are shown with the fraction number below in red. **B**. Shown below the chromatogram is the corresponding 16 % SDS-PAGE gel stained with Instant blue protein stain, fraction number indicated and with protein marker for 10-50 kDa. Gel was electrophoresed at 175 V for 110 minutes and imaged using the Li-Cor Odyssey Infrared Imaging Analysis System.

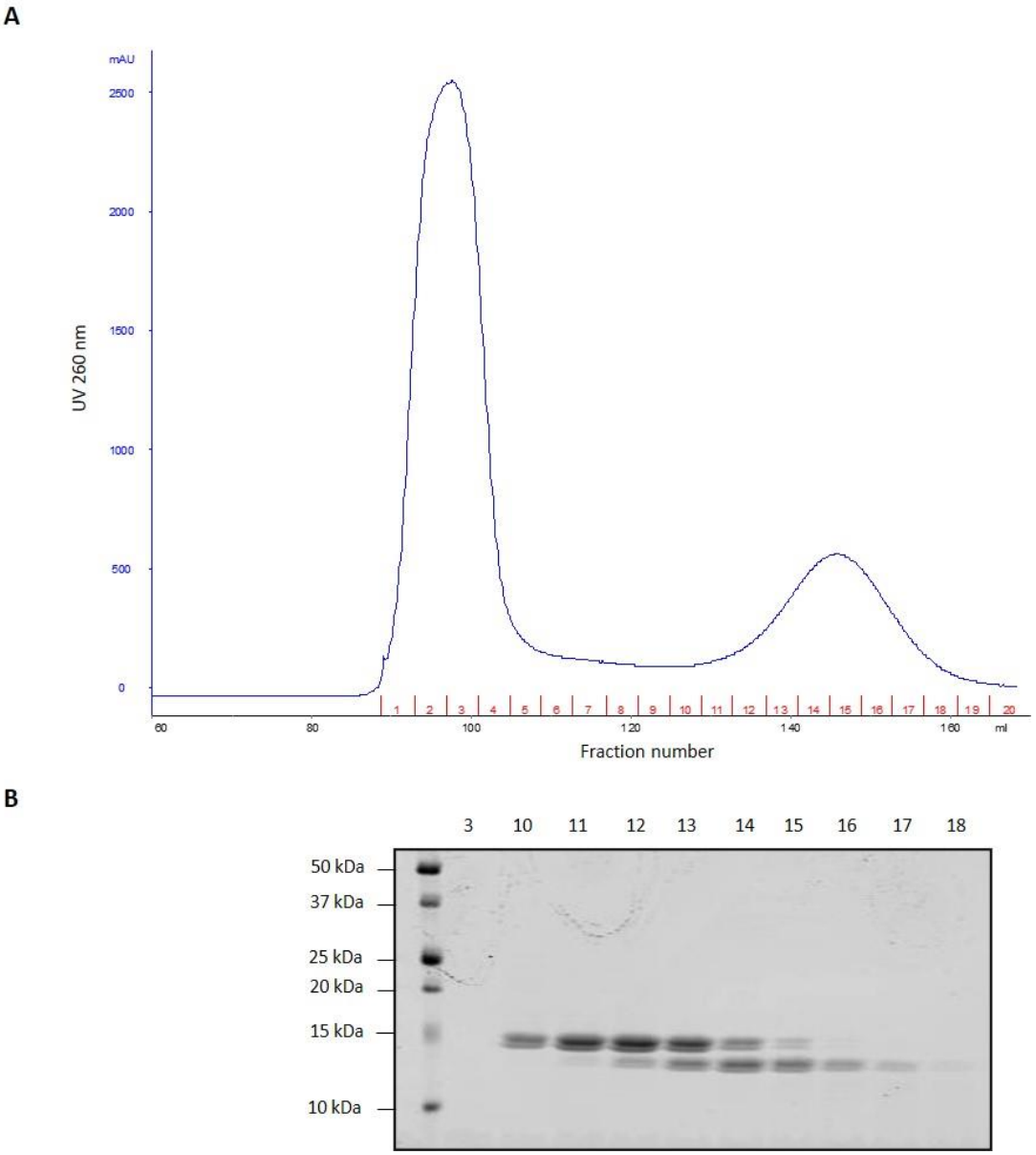


**Figure 4.8: Purification of recombinant histones H2B gel filtration chromatography**

Following protein overexpression in *E-coli*, histone H2B was initially purified by size exclusion chromatography using a gel filtration, Sephacryl S200 column and an AKTA FPLC under denaturing conditions (7 M urea). **A**. H2B UV trace (blue) from the FPLC are shown with the fraction number below in red. **B**. Shown below the chromatogram is the corresponding 16 % SDS-PAGE gel stained with Instant blue protein stain, fraction number indicated and with protein marker for 10-50 kDa. Gel was electrophoresed at 175 V for 110 minutes and imaged using the Li-Cor Odyssey Infrared Imaging Analysis System.

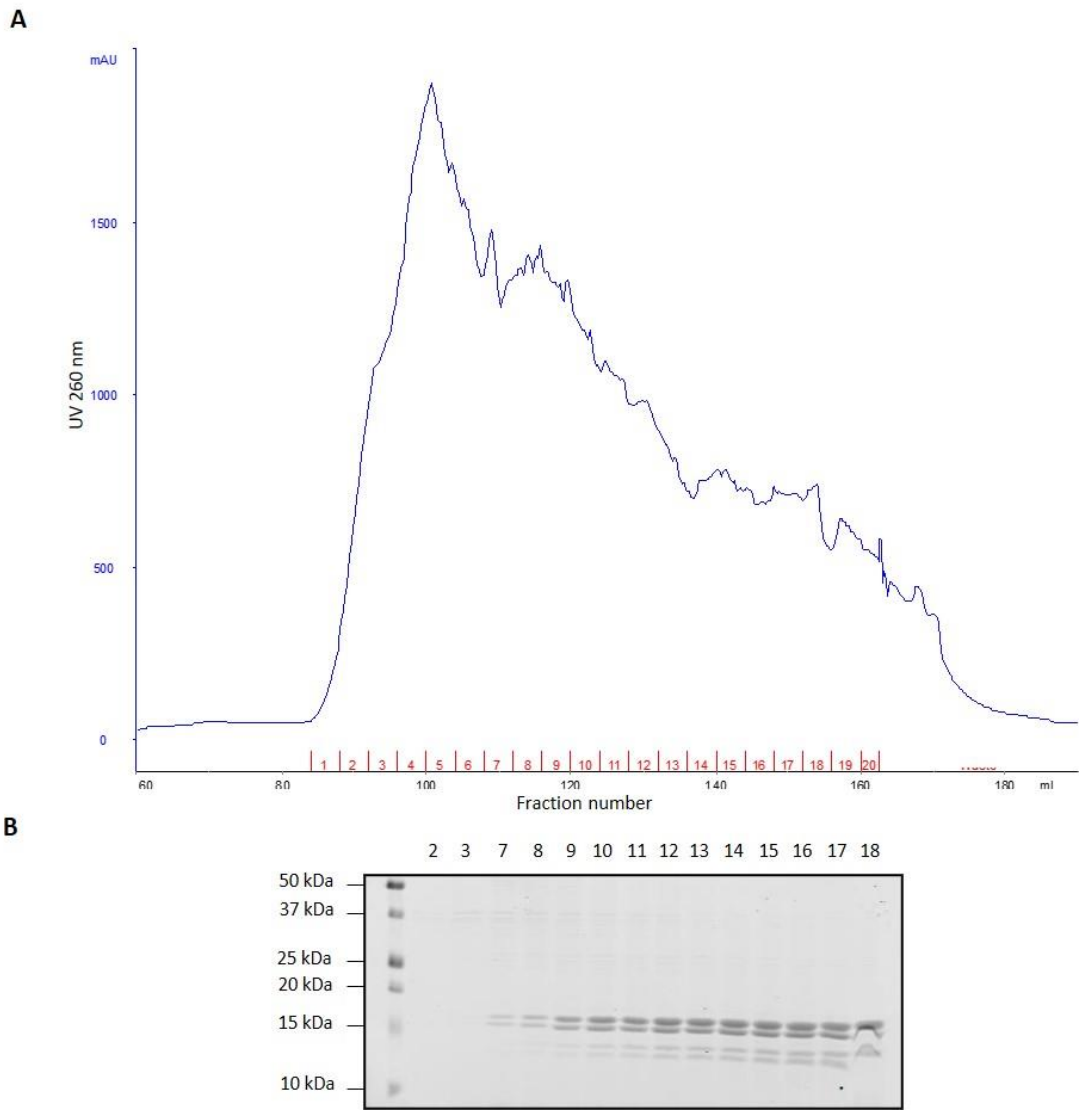


**Figure 4.9: Purification of recombinant histones H3 gel filtration chromatography**

Following protein overexpression in *E-coli*, histone H3 was initially purified by size exclusion chromatography using a gel filtration, Sephacryl S200 column and an AKTA FPLC under denaturing conditions (7 M urea). **A**. H3 UV trace (blue) from the FPLC are shown with the fraction number below in red. **B**. Shown below the chromatogram is the corresponding 16 % SDS-PAGE gel stained with Instant blue protein stain, fraction number indicated and with protein marker for 10-50 kDa. Gel was electrophoresed at 175 V for 110 minutes and imaged using the Li-Cor Odyssey Infrared Imaging Analysis System.

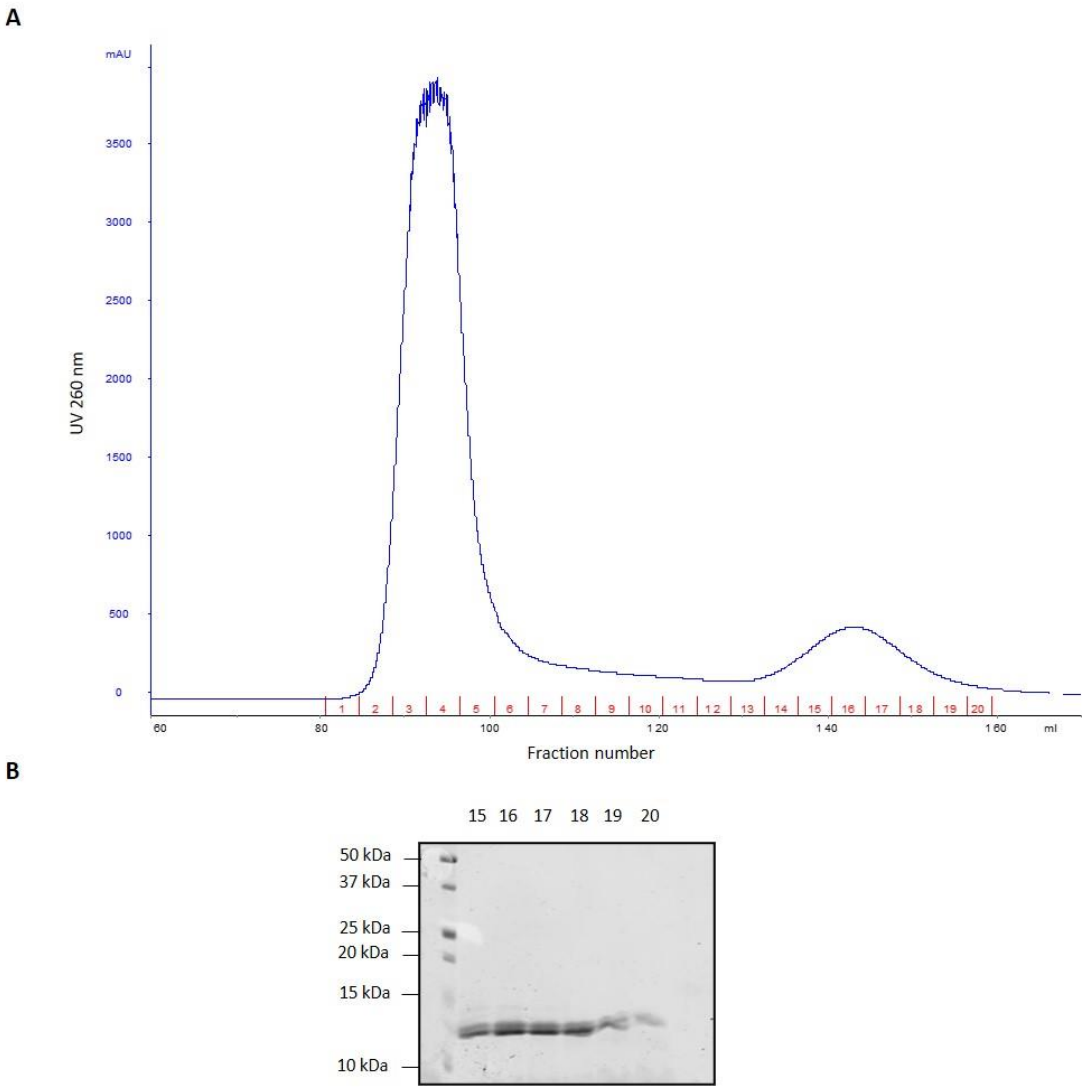


**Figure 4.10: Purification of recombinant histones H4 gel filtration chromatography**

Following protein overexpression in *E-coli*, histone H4 was initially purified by size exclusion chromatography using a gel filtration, Sephacryl S200 column and an AKTA FPLC under denaturing conditions (7 M urea). **A**. H4 UV trace (blue) from the FPLC are shown with the fraction number below in red. **B**. Shown below the chromatogram is the corresponding 16 % SDS-PAGE gel stained with Instant blue protein stain, fraction number indicated and with protein marker for 10-50 kDa. Gel was electrophoresed at 175 V for 110 minutes and imaged using the Li-Cor Odyssey Infrared Imaging Analysis System.

### 4.3.2 Recombinant histone purification: ion exchange chromatography

Pooled fractions from the initial size exclusion chromatography step were dialysed in distilled water containing 2 mM β-mercaptoethanol, before purification by ion exchange

chromatography using a Mono-S column and a AKTA FPLC under denaturing conditions (7 M urea). Fractions were collected following a salt gradient elution and the UV trace with fraction numbers is shown for each of the four histones; H2A (Figure 4.11A), H2B (Figure 4.12A) H3 (Figure 4.13A) and H4 (Figure 4.14A). The proteins within these fractions were separated by SDS-PAGE and Instant Blue protein stained. Full length histone H2A (Figure 4.11B) was shown to elute in fractions 13-19, H2B in fractions 12-18 (Figure 4.12B), H3 in fractions 12-20 (Figure 4.13B) and H4 in fractions 14-22 (Figure 4.14B). Of note, the upper band correspond to the full-length histones and the lower band, in the preceding fractions are slightly degraded histones. Fractions containing the individual histones were pooled, dialysed in distilled water containing 2 mM β-mercaptoethanol and concentrated using 3 kDa MWCO Amicon Ultra centrifugal concentrators to 15-30 mg/ml. The protein concentration of the histones were measured using a Nanodrop ND-1000 spectrometer at a wavelength of OD 280 nm with molecular weights and extinction coefficients (ε) and per 2 L bacterial culture yielded; H2A 26 mg, H2B 8 mg, H3 22.5 mg and H4 10.5 mg.

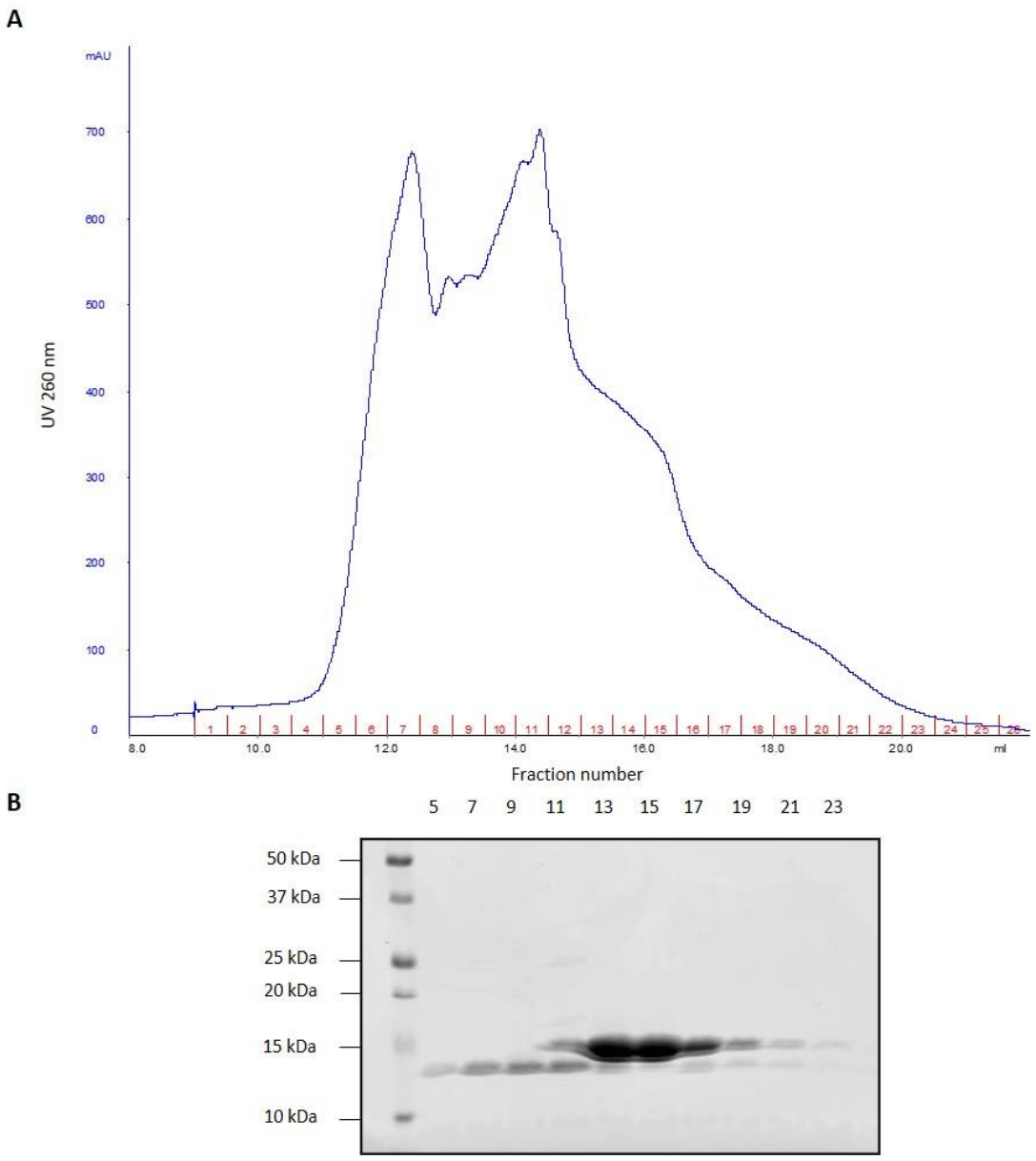


**Figure 4.11: Purification of recombinant histone H2A by ion exchange chromatography**

Pooled histone H2A containing fractions from the initial size exclusion chromatography step were further purified using a Mono-S column and a AKTA FPLC under denaturing conditions (7 M urea) and eluted under a salt gradient. **A**. H2A UV trace (blue) from the FPLC are shown with the fraction number below in red. **B**. Shown below the chromatogram is the corresponding 16 % SDS-PAGE gel stained with Instant Blue protein stain, fraction number indicated and with protein marker for 10-50 kDa. Gel was electrophoresed at 175 V for 110 minutes and imaged using the Li-Cor Odyssey Infrared Imaging Analysis System.

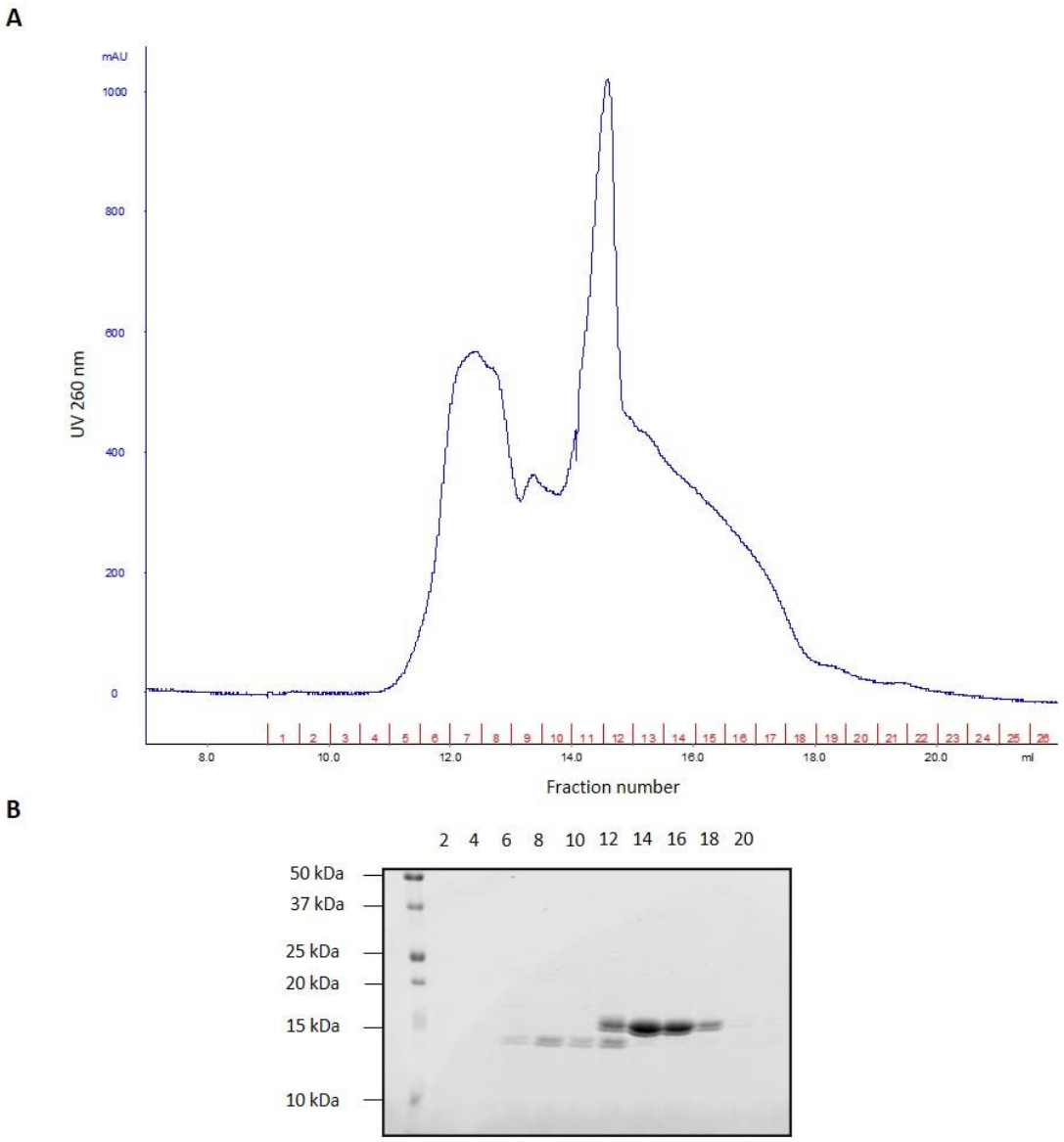


**Figure 4.12: Purification of recombinant histone H2B by ion exchange chromatography**

Pooled histone H2B containing fractions from the initial size exclusion chromatography step were further purified using a Mono-S column and a AKTA FPLC under denaturing conditions (7 M urea) and eluted under a salt gradient. **A**. H2B UV trace (blue) from the FPLC are shown with the fraction number below in red. **B**. Shown below the chromatogram is the corresponding 16 % SDS-PAGE gel stained with Instant Blue protein stain, fraction number indicated and with protein marker for 10-50 kDa. Gel was electrophoresed at 175 V for 110 minutes and imaged using the Li-Cor Odyssey Infrared Imaging Analysis System.

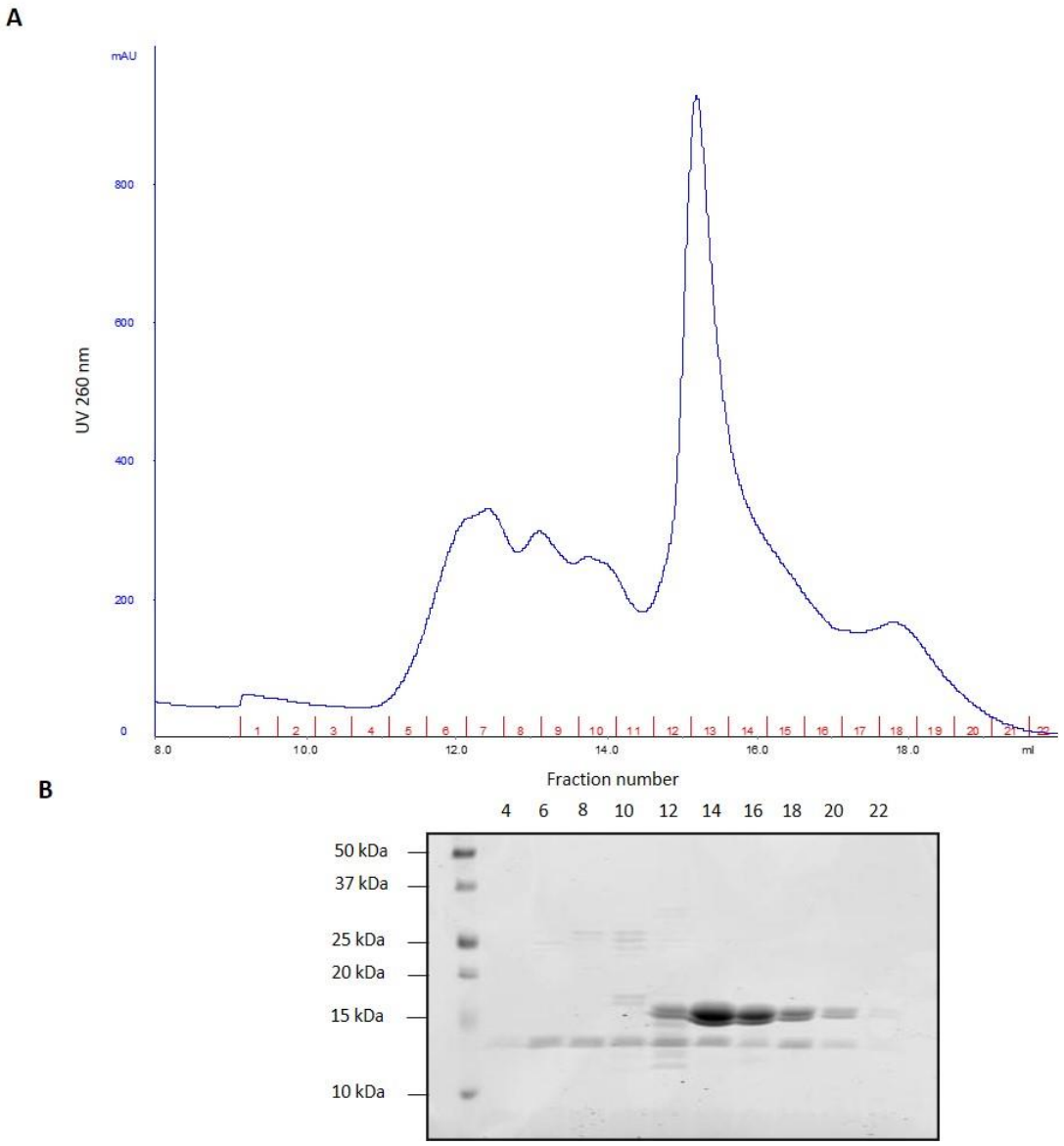


**Figure 4.13: Purification of recombinant histone H3 by ion exchange chromatography**

Pooled histone H3 containing fractions from the initial size exclusion chromatography step were further purified using a Mono-S column and a AKTA FPLC under denaturing conditions (7 M urea) and eluted under a salt gradient. **A**. H3 UV trace (blue) from the FPLC are shown with the fraction number below in red. **B**. Shown below the chromatogram is the corresponding 16 % SDS-PAGE gel stained with Instant Blue protein stain, fraction number indicated and with protein marker for 10-50 kDa. Gel was electrophoresed at 175 V for 110 minutes and imaged using the Li-Cor Odyssey Infrared Imaging Analysis System.

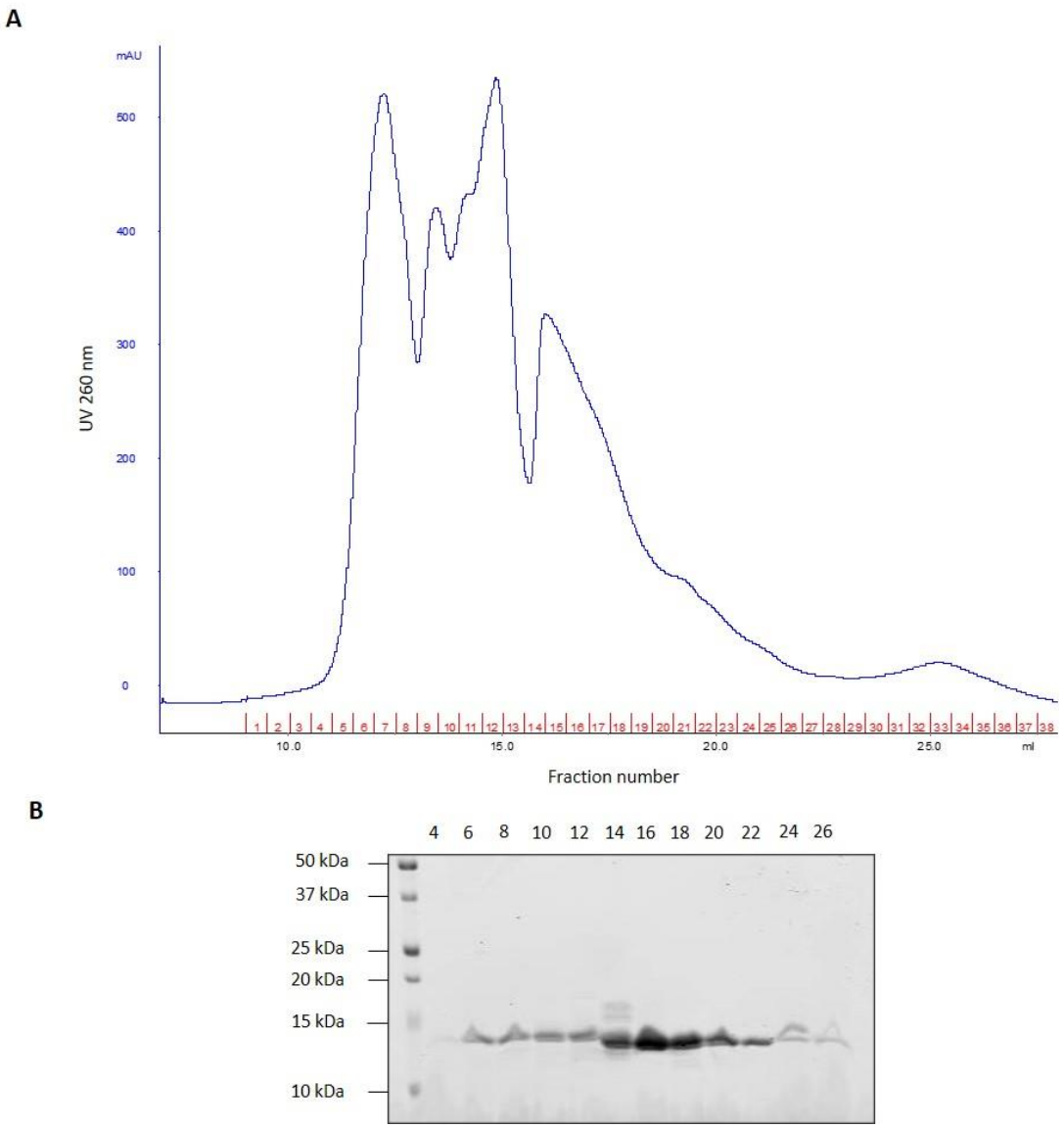


**Figure 4.14: Purification of recombinant histone H4 by ion exchange chromatography**

Pooled histone H4 containing fractions from the initial size exclusion chromatography step were further purified using a Mono-S column and a AKTA FPLC under denaturing conditions (7 M urea) and eluted under a salt gradient. **A**. H4 UV trace (blue) from the FPLC are shown with the fraction number below in red. **B**. Shown below the chromatogram is the corresponding 16 % SDS-PAGE gel stained with Instant Blue protein stain, fraction number indicated and with protein marker for 10-50 kDa. Gel was electrophoresed at 175 V for 110 minutes and imaged using the Li-Cor Odyssey Infrared Imaging Analysis System.

### 4.3.3 Refolding of the histone octamer

The histone octamer, formed by combining purified histones in equimolar ratios and dialysis in refolding buffer, was purified by gel filtration chromatography using a Superdex 200 column and an AKTA FPLC. Collected fractions and the UV trace obtained from the FPLC are shown (Figure 4.15A) in addition to the separation of proteins by SDS-PAGE and analysis by Instant Blue protein staining (Figure 4.15B). Fractions 25-27, indicated by the red asterisk, show histone octamer formation at the expected molecular weight (108 kDa; between 66-150 kDa), determined from calibration of the Superdex 200 column with protein molecular weight standards, as shown above the representative gel image. Note, fractions 28-34 contain H2A/H2B dimers which have failed to fully form the octamer with H3 and H4. Fractions containing the histone octamer were pooled, concentrated and stored in glycerol (for protein stabilization). This preparation acted as a histone octamer source for use in the nucleosome reconstitution with the site specific THF-IN DNA to generate the mononucleosome substrate for BER assays.

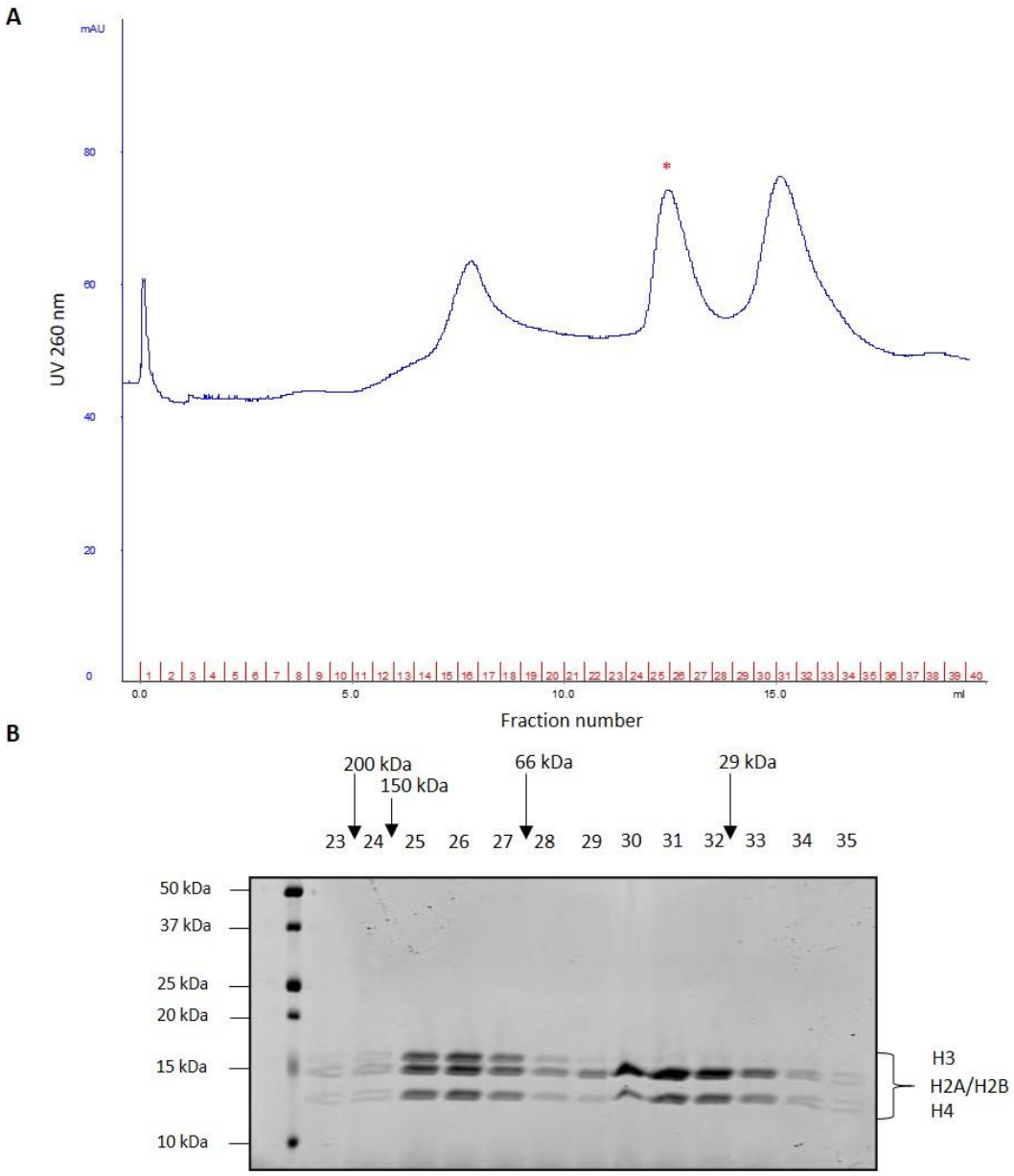


**Figure 4.15: Purification of the histone octamer by gel filtration chromatography**

The histone octamer, generated by combining purified histones in equimolar ratios and dialysis in refolding buffer, was purified by size exclusion chromatography using a Superdex 200 column and an AKTA FPLC. **A**. The UV trace (blue) from the FPLC with the red asterisk indicating the histone octamer peak is shown with the fraction number shown below in red. **B**. Below the chromatogram is the corresponding 16 % SDS-PAGE gel stained with Instant Blue protein stain, fraction number indicated, and calibrated with protein marker weight standards at 10-50 kDa. The gel was electrophoresed at 175 V for 110 minutes and imaged using the Li-Cor Odyssey Infrared Imaging Analysis System.

## 4.4 Generation of the site specific THF-IN mononucleosome substrate

Mononucleosomes were reconstituted by incubation of the purified histone octamer with the site specific THF-IN DNA substrate, in an optimised ratio in a high salt (2 M NaCl) containing buffer. The reconstitution was then dialysed using a salt gradient to promote mononucleosome formation (Figure 4.2, stage 4). This was confirmed by agarose gel electrophoresis, where a shift from the lower molecular weight of 256 bp free DNA to a higher molecular weight of approximately 750 kDa was observed, indicating successful nucleosome formation. A reconstitution efficiency of 95 % was deemed acceptable for use of the mononucleosome substrate in *in vitro* BER repair assays to measure APE1 activity.

### 4.4.1 Optimisation of nucleosome reconstitution

In the first instance, the optimal THF-IN substrate DNA:histone octamer ratio was investigated. A total of four ratios, 1:0.25, 1:0.5, 1:1 and 1:5 (THF-IN substrate DNA:histone octamer) were examined to determine which provided the most complete nucleosome reconstitution, whilst minimising any substantial aggregate formation. In all reconstitutions the THF-IN substrate DNA, histone octamer mix was incubated in a high salt (2 M NaCl) containing buffer and then dialysed using a salt gradient to promote mononucleosome formation. The DNA was then separated using agarose gel electrophoresis, where a shift from the lower molecular weight of 256 bp free DNA to a higher molecular weight of approximately 750 kDa was used to determine successful nucleosome formation. At ratios of 1:0.25 (Figure 4.16A, lane 3) and 1:0.5 (Figure 4.16A, lane 4) some nucleosome reconstitution was observed, although this was nowhere near the acceptable reconstitution efficiency of 95 %, therefore these ratios were not deemed appropriate for generating the mononucleosome substrate for use in the *in vitro* BER repair assay. Next, the ratios 1:5 (Figure 4.16B, lane 3) and 1:1 (Figure 4.16B, lane 4) were investigated for optimal nucleosome reconstitution. Observation of both the 1:5 (Figure 4.16B, lane 3) and 1:1 (Figure 4.16B, lane 4) ratios demonstrated near full nucleosome reconstitutions, reaching the acceptable 95 % nucleosome efficiency. However, at the 1:5 (Figure 4.16B, lane 3) ratio, a degree of smearing was seen, indicative of aggregate formation. As a 1:1 THF-IN substrate DNA:histone octamer ratio generated efficient nucleosome reconstitution, to avoid wastage of the histone octamer, the optimal THF-IN substrate DNA:histone octamer ratio was determined to be 1:1.

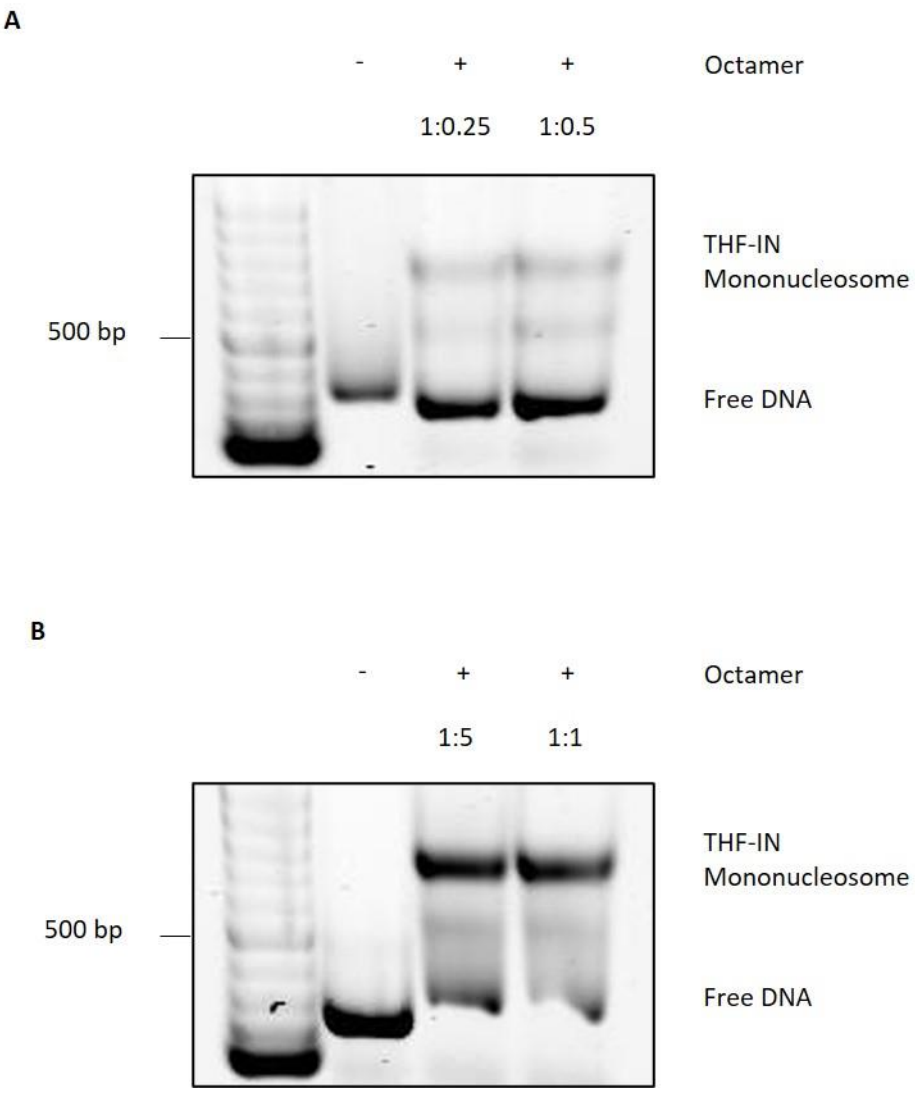


**Figure 4.16: Optimisation of THF-IN mononucleosome reconstitution**

Nucleosome reconstitution was compared using four ratio's **A** 1:0.25 (lane 3) and 1:0.5 (lane 4) THF-IN substrate DNA:histone octamer and **B** 1:5 (lane 3) and 1:1 (lane 4) THF-IN substrate DNA:histone octamer. All reconstitution were compare to free DNA (lane 2), whereby a shift from the 256 bp free DNA control, to a high molecular weight species (lane 3), approximately 700 bp, was observed if the THF-IN mononucleosome was successfully formed. DNA was separated using a 0.7 % agarose gel and electrophoresed in 0.2x TAE at 75 V for 1.5 hours. A 100 bp GeneRuler DNA ladder (lane 1) was utilised to identify the size of the DNA**.**

### 4.4.2 Generation of the THF-IN mononucleosome substrate

Mononucleosomes were reconstituted by incubation of the purified histone octamer with the site specific THF-IN DNA substrate, in a 1:1 ratio in a high salt (2 M NaCl) containing

buffer. The reconstitution was then dialysed using a salt gradient to promote mononucleosome formation (Figure 4.2, stage 4). This was confirmed by agarose gel electrophoresis, where a shift from the lower molecular weight of 256 bp free DNA to a higher molecular weight of approximately 750 kDa was observed (Figure 4.17), indicating successful nucleosome formation. Near full nucleosome reconstitution was observed (Figure 4.17, lane 3), with a reconstitution efficiency of 95 % which was deemed acceptable for use of the mononucleosome substrate in *in vitro* BER repair assays to measure APE1 activity.

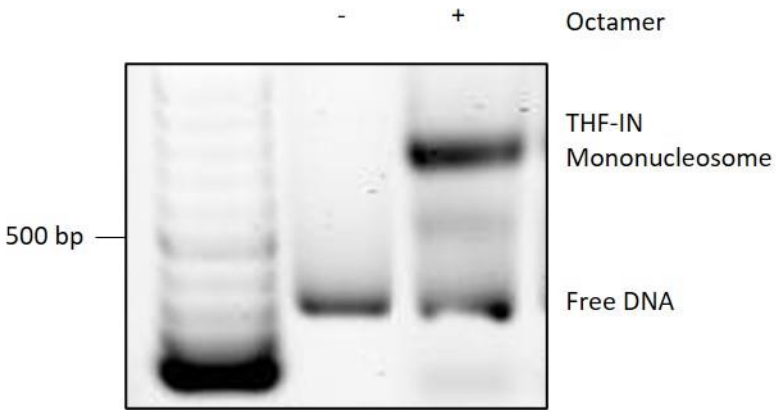


**Figure 4.17: Generation of a THF-IN Mononucleosome**

Nucleosome reconstitution was compared to free DNA (lane 2), whereby a shift from the 256 bp free DNA control, to a high molecular weight species (lane 3), approximately 700 bp, was observed when the THF-IN nucleosome was successfully formed. A 1:1 DNA: histone octamer ratio was used. DNA was separated using a 0.7 % agarose gel and electrophoresed in 0.2x TAE at 75 V for 1.5 hours. A 100 bp GeneRuler DNA ladder (lane 1) was utilised to identify the size of the DNA**.**

## 4.5 Cloning and purification of recombinant HECTD1

### 4.5.1 Ligation independent cloning (LIC) of HECTD1

LIC cloning was employed to clone the murine HECTD1 gene truncated at amino acid 1761 from the mammalian expression vector and into the pET28a bacterial expression vector (Figure 4.18). The protein was truncated, as full length murine HECTD1 consists of 2612 amino acids and is 289 kDa in size, making it extremely difficult to express and purify from bacterial overexpression systems. Therefore, I cloned a truncated version containing the active E3 ubiquitin ligase (HECT) domain (amino acids 2156-2612), which is required for

ubiquitylation of the target protein, plus an additional 389 amino acids immediately N-terminal to this domain (Figure 4.21). This would allow the protein of 96 kDa to be expressed and purified from *E coli* cells. Also, of note, murine HECTD1 protein displays very high homology (98.2 % homology by amino acid sequence) to the human protein.

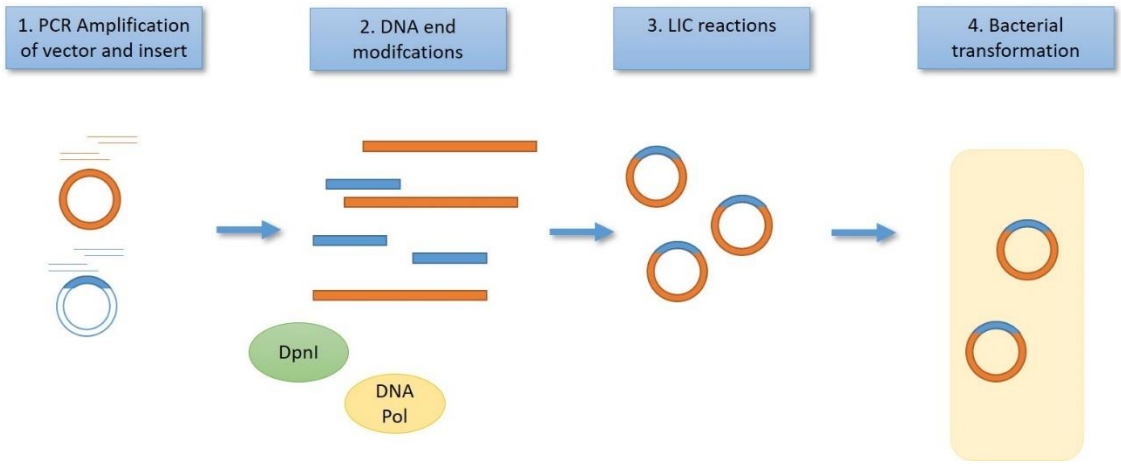


**Figure 4.18: Schematic diagram of the LIC strategy used to generate the pET28a-HECTD1-1761 plasmid**

1. Vector was linearised and along with the insert amplified by PCR. 2. Insert and vector DNA treated with DpnI and T4 DNA Polymerase to remove methylated DNA bases and create complimentary base overhangs between the vector and insert. 3. LIC (vector:insert) reactions were incubated at ratios of 1:0.5, 1:1 and 1:3 before 4. bacterial transformation of the insert containing plasmid into library efficient DH5α competent bacterial cells via heat shock.

Empty pET28a bacterial expression vector (Figure 4.19) and murine HECTD1 from the mammalian expression vector (kindly provided by Prof I. Zohn at the Childrens National Medical Center, USA) was first amplified by touchdown PCR using custom oligonucleotide primers flanked by LIC sequences (Table 3.3). The size of the pET28a DNA product (5369 bp) (Figure 4.22A) and ΔN-HECTD1 gene (2550 bp) (Figure 4.22B) was analysed and confirmed via agarose gel electrophoresis. Following PCR amplification, DpnI treatment for DNA methylation and purification of DNA products purified using the QIAquick PCR Purification Kit. The individual DNA products were treated with T4 DNA polymerase to generate the complementary LIC overhangs and the ΔN-HECTD1 insert incubated with the empty pET28a vector at vector:insert ratios of 1:0.5, 1:1 and 1:3 to anneal the insert into the bacterial expression vector. *E. coli* cells were transformed with pET28a: ΔN-HECTD1 LIC reactions and grown on selective media containing kanamycin. Successful colonies were inoculated into 5

ml of LB media with kanamycin and grown overnight at 37°C to amplify the pET28a-HECTD1-1761 plasmid DNA (Figure 4.20), which was then purified from bacterial contaminants using the QIAprep Spin Miniprep Kit (QIAGEN). Confirmation of successful cloning of the gene insert for ΔN-HECTD1 was achieved by DNA sequencing from the Sanger Sequencing Service (provided by Source Bioscience Sequencing, Nottingham, UK). This plasmid could now be used to overexpress and purify C-terminally His-tagged ΔN-HECTD1 from bacterial cells.

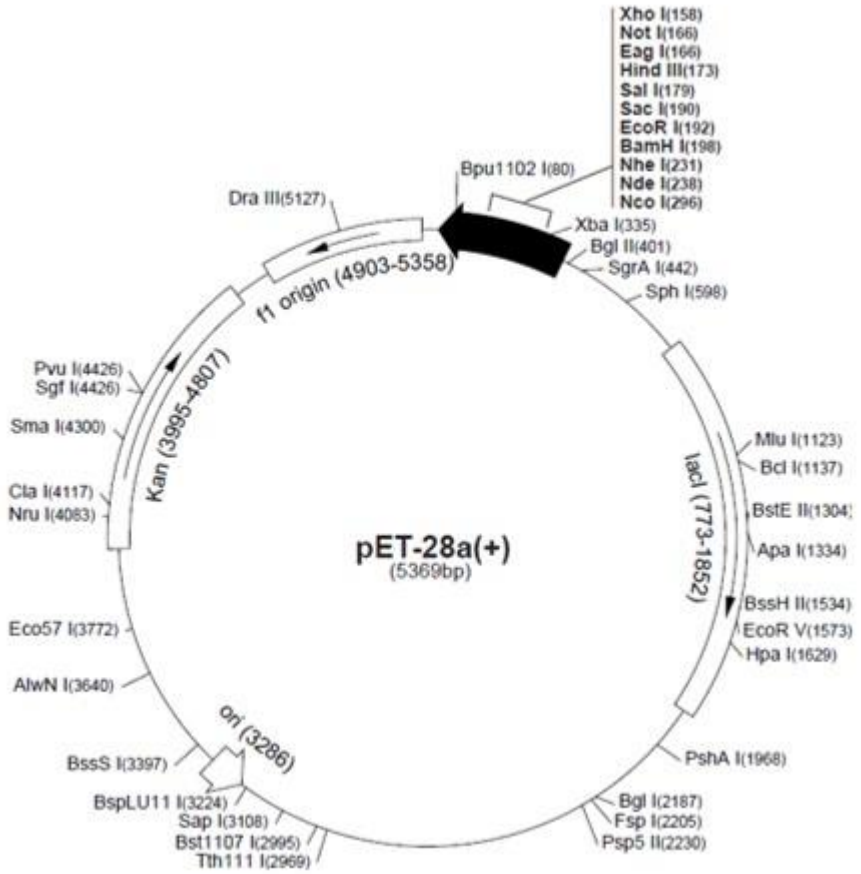


**Figure 4.19: Vector map for the empty pET28a bacterial expression plasmid**

Target genes were cloned into the empty pET28a vector and used for recombinant protein expression in bacteria. The target gene is transcribed by T7 bacteriophage RNA polymerase under control of the T7 promotor. The pETa28a vector carries kanamycin antibiotic resistance and the option for a 6x N-terminal or C-terminal poly-histidine tag. Adapted from the Novagen pET-28a-c(+) vector map.

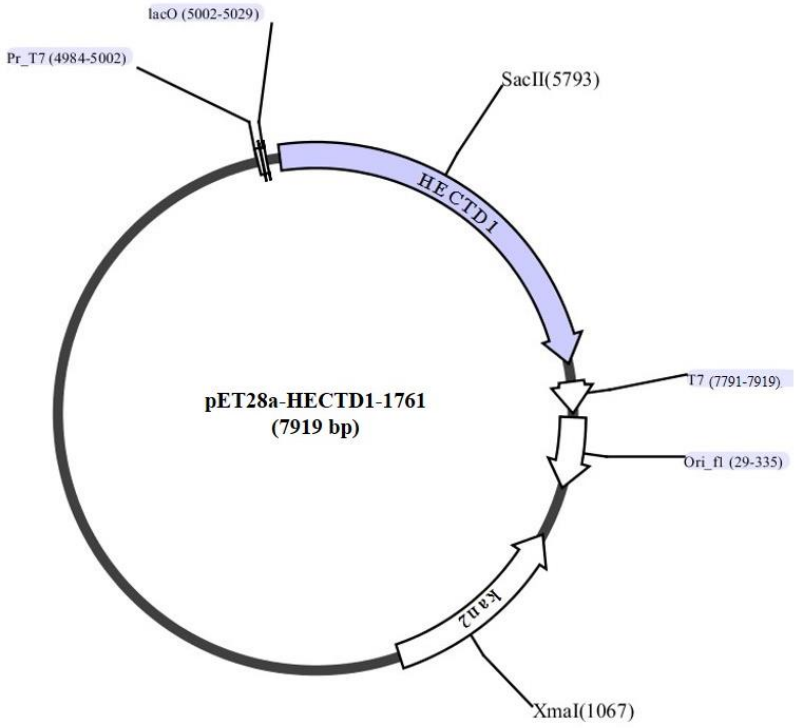


**Figure 4.20: Vector map for the empty pET28a-HECTD1-1761 bacterial expression plasmid**

The gene for murine HECTD1 truncated at aa 1761 was cloned from the mammalian expression plasmid for full length murine HECTD1 (pCMV-HA-HECTD1) into empty pET28a vector for expression of ΔN-HECTD1 in a bacterial system. The pETa28a vector carries kanamycin antibiotic resistance and adds a C-terminal poly-histidine tag.

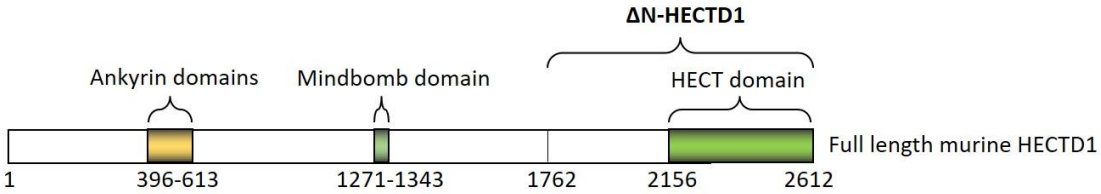


**Figure 4.21: Representative diagram of murine HECTD1**

Diagrammatic representation of the full length murine HECTD1 protein, including location of functional domains. Ankyrin domains (amino acids 396-613), Mindbomb domain (amino acids 1271-1343) and HECT domain (amino acids 2156-2612). The ΔN-HECTD1 truncated version of the protein is also indicated.

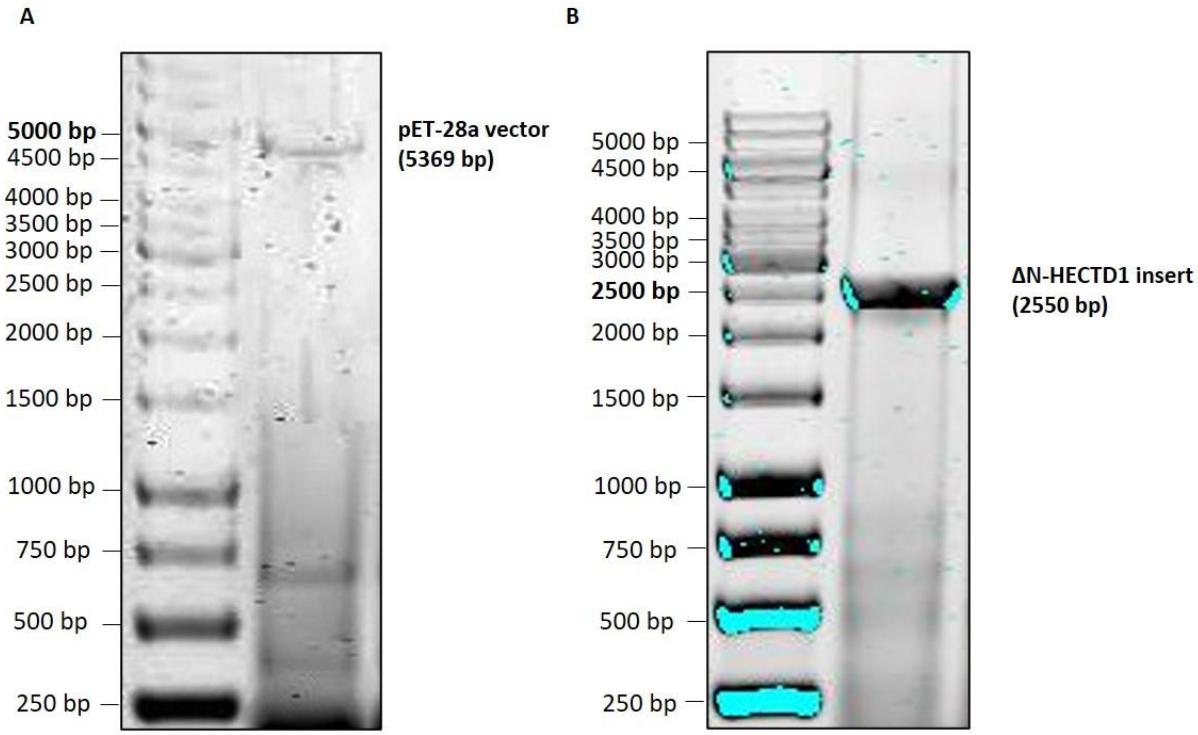


**Figure 4.22: PCR amplification of a pET28a vector and gene inserts for ΔN-HECTD1**

**A** PCR product of amplification of the empty pET28a vector using complementary oligonucleotide primers flanked by relevant LIC sequences **B** PCR product of amplification of the insert for ΔN-HECTD1 from pCMV-HA-HECTD1, separated by electrophoresis on a 1 % agarose gel at 100 V for 1 hour, imaged using the Li-Cor Odyssey Infrared Imaging Analysis System. A 1 kb GeneRuler DNA ladder was utilised to identify the size of the PCR product**.**

### 4.5.2 Affinity chromatography purification of HECTD1

Rosetta2(DE3)pLysS bacterial cells, transformed via heat shock with His-tagged pET28a-HECTD1-1761, were grown until an OD600nm of 0.6 in a 400 ml culture. Protein expression of C-terminally His-tagged ΔN-HECTD1 was induced via IPTG (1 mM) addition for 3-16 hours to determine test expression of the protein. SDS-PAGE protein separation, followed by Instant Blue protein staining and immunoblotting using anti-His-tag antibodies, revealed that the 96 kDa ΔN-HECTD1 was expressed and stable with a 3 hour IPTG induction (Figure 4.23A-B, lane 2), but not with overnight induction (Figure 4.23A-B, lane 3). From this test expression, protein inductions were routinely performed for 3 hours with IPTG and the bacterial cell lysate from a scaled up 1.2 L culture was purified using a 1 ml HisTrap HP affinity chromatography column and AKTA FPLC. Fractions were collected following a linear imidazole elution (0-250 mM) and the UV trace obtained from the FPLC with fraction number

(Figure 4.24A) is shown in addition to the separation of proteins by SDS-PAGE and analysis by Instant Blue protein staining to detect total protein (Figure 4.24B), and by immunoblotting with anti-His-tag antibodies to detect His-tagged ΔN-HECTD1 (Figure 4.24C). The first protein peak correlated with fractions 5-10 on the UV trace (Figure 4.24A) was associated with contaminating bacterial proteins. However, the shoulder on the UV trace from fraction 10 onwards, contained isolated and purified recombinant ΔN-HECTD1. Confirmation by SDS-PAGE protein staining (Figure 4.24B) and immunoblotting (Figure 4.24C), revealed the presence of ΔN-HECTD1 in fractions 10-32, but the full length protein (96 kDa) was found to undergo degradation to that of a slightly smaller molecular weight (85 kDa). Attempts were made to further isolate the intact ΔN-HECTD1 via ion exchange and size exclusion chromatography. In the first instance, the pooled ΔN-HECTD1 containing fractions from the initial HisTrap HP affinity column chromatography step were further purified by ion exchange chromatography using a Mono-Q column and a FPLC. Fractions were collected following a salt gradient elution (50-1000 mM KCl) and the UV trace obtained from the FPLC with fraction number (Figure 4.25A) is shown in addition to the separation of proteins by SDS-PAGE and analysis by Instant Blue protein staining to detect total protein (Figure 4.25B), and by immunoblotting with anti-His-tag antibodies to detect His-tagged ΔN-HECTD1 (Figure 4.25C). Although two peaks can be visualised on the UV trace between fractions 4 and 22 (Figure 4.25A), when the fractions were analysed by Instant Blue protein staining (Figure 4.25B) and immunoblotting with anti-His-tag antibodies (Figure 4.25C), His-tagged ΔN-HECTD1 was not detected, indicating that the protein was heavily degraded or lost. Following this, the second chromatography to further isolate the intact ΔN-HECTD1 was modified and the pooled ΔN-HECTD1 containing fractions from the initial HisTrap HP affinity column chromatography step were further purified by size exclusion chromatography using a Superdex 200 column and a FPLC using a 150 mM KCl gradient elution. The UV trace obtained from the FPLC with fraction number (Figure 4.26A) is shown in addition to the separation of proteins by SDS-PAGE and analysis by Instant Blue protein staining to detect total protein (Figure 4.26B), and by immunoblotting with anti-His-tag antibodies to detect His-tagged ΔN-HECTD1 (Figure 4.26C). The UV trace does not indicate any significant protein elution (Figure 4.26A) and when the fractions were analysed by Instant Blue protein staining (Figure 4.26B) and immunoblotting with anti-His-tag antibodies (Figure 4.26C), His-tagged ΔN-HECTD1 was not detected, indicating that the protein was heavily degraded or lost. Therefore, a single chromatography approach, using HisTrap HP affinity chromatography was adopted, as crucially this protein cross-reacts with the His-tagged antibodies, suggesting that the protein is being degraded

from the N terminus (as the protein is C-terminally tagged) and includes the fully intact E3 ligase HECT domain required for its enzymatic activity. Therefore, these fractions were pooled, buffer exchanged (50 mM Tris-HCl pH 8, 50 mM KCl, 1 mM EDTA, 10 % glycerol) to remove imidazole, the protein concentrated, and the concentration measured using a Nanodrop ND-1000 spectrometer at a wavelength of OD 280 nm with molecular weights and extinction coefficients (ε), before aliquoting and storage at -80°C.

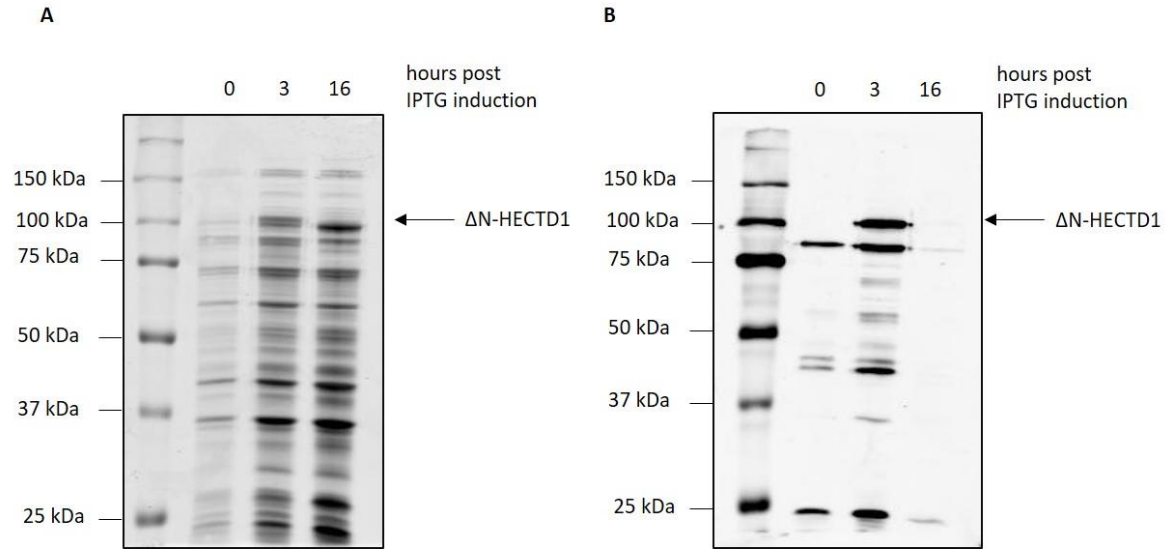


**Figure 4.23: Test expression via IPTG induction of recombinant His-tagged ΔN-HECTD1**

Following protein overexpression in *E-coli* of ΔN-HECTD1, cell lysate samples were taken pre IPTG (lane 2), 3 hours (lane 3) and 16 hours (lane 4) post IPTG induction. Bacterial cell lysates separated by 10 % SDS-PAGE and analysed by **A** Instant Blue protein stain and **B** immunoblotting using His-tag specific antibodies. Recombinant His-tagged ΔN-HECTD1 indicated, with protein marker (10-250 kDa). All gels were electrophoresed at 175 V for 110 minutes and imaged using the Li-Cor Odyssey Infrared Imaging Analysis System.

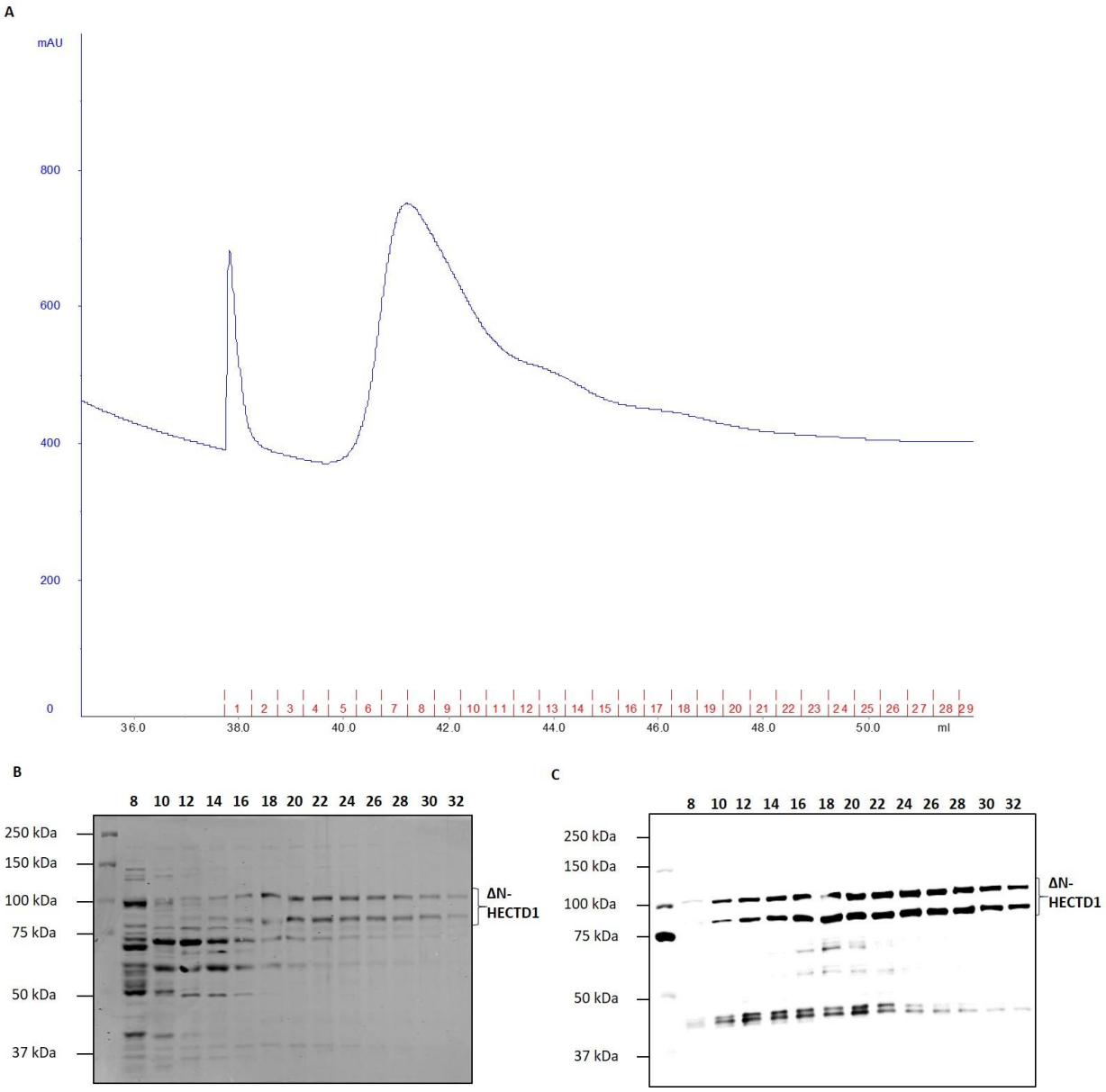


**Figure 4.24: HisTrap HP affinity column chromatography purification of recombinant His-tagged ΔN-HECTD1**

Following protein overexpression in *E-coli*, ΔN-HECTD1 was purified from the bacterial cell lysate by a HisTrap HP affinity chromatography column and AKTA FPLC using a linear 0-250 mM imidazole gradient elution. **A** UV trace (blue) from the FPLC is shown with the fraction number below in red. Corresponding analysis of the fractions by **B** 10 % SDS-PAGE gel stained with Instant Blue protein stain and **C** immunoblotting using His-tag specific antibodies. Fraction number and recombinant His-tagged ΔN-HECTD1 indicated, with protein marker (10-250 kDa). All gels were electrophoresed at 175 V for 110 minutes and imaged using the Li-Cor Odyssey Infrared Imaging Analysis System.

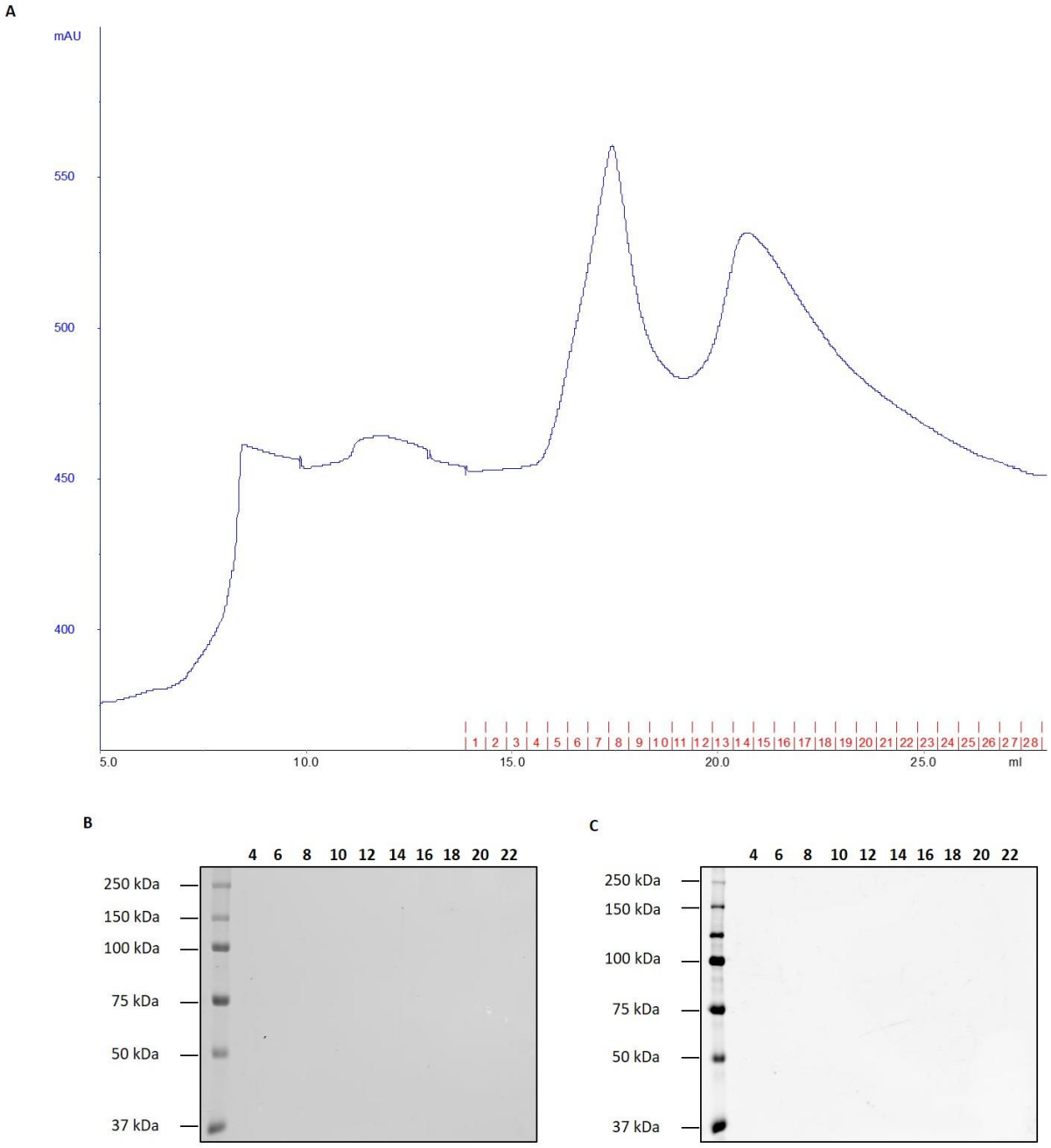


**Figure 4.25: Ion exchange chromatography purification of recombinant His-tagged ΔN-HECTD1**

Pooled ΔN-HECTD1 containing fractions from the initial HisTrap HP affinity column chromatography step were further purified using a Mono-Q column and a FPLC using a linear 50-1000 mM KCl gradient elution. **A** UV trace (blue) from the FPLC is shown with the fraction number below in red. Corresponding analysis of the fractions by **B** 10 % SDS-PAGE gel stained with Instant Blue protein stain and **C** immunoblotting using His-tag specific antibodies. Fraction number indicated, with protein marker (10-250 kDa). All gels were electrophoresed

at 175 V for 110 minutes and imaged using the Li-Cor Odyssey Infrared Imaging Analysis System.

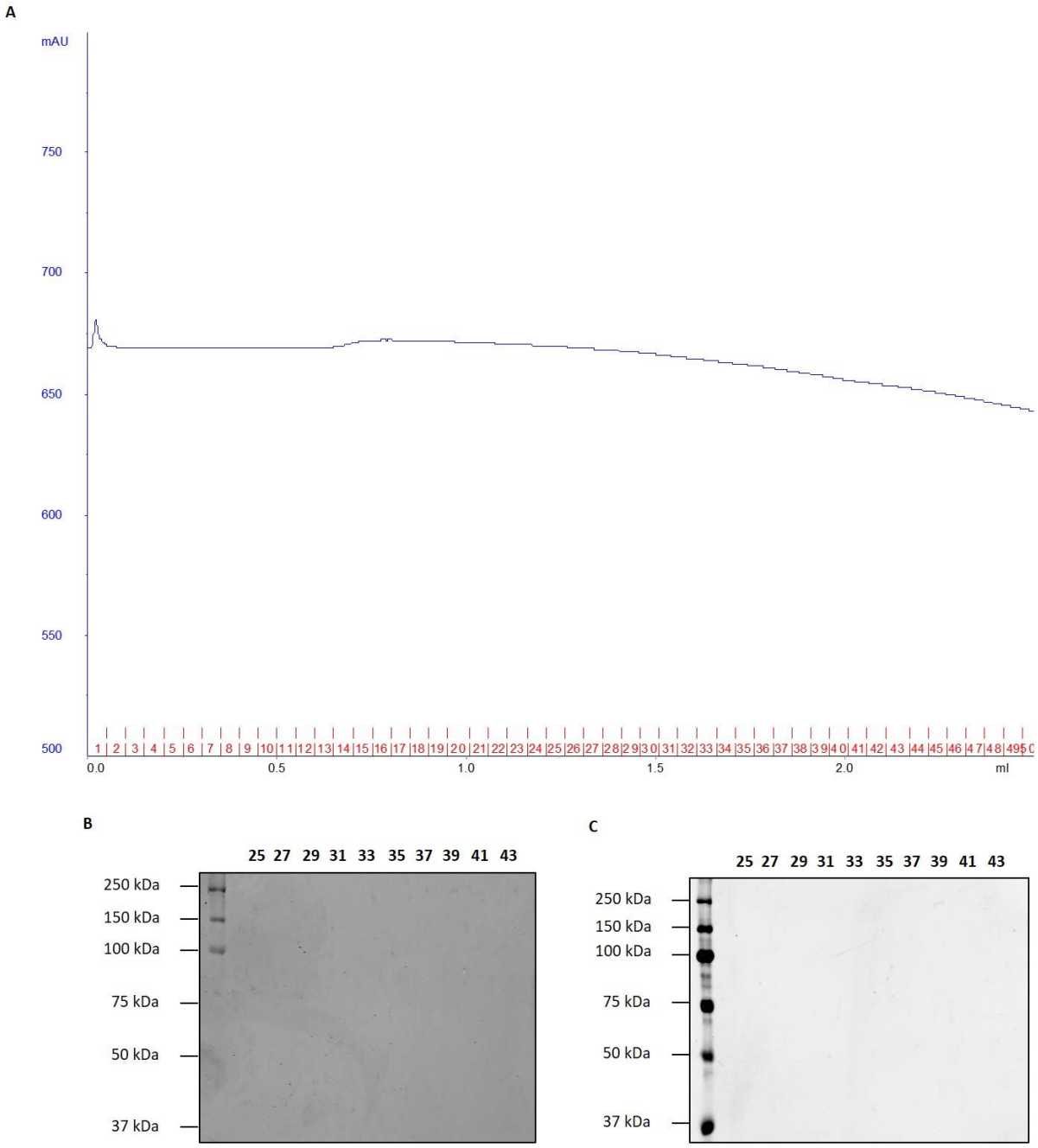


**Figure 4.26: Size exclusion chromatography purification of recombinant His-tagged ΔN-HECTD1**

Pooled ΔN-HECTD1 containing fractions from the initial HisTrap HP affinity column chromatography step were further purified by size exclusion chromatography using a Superdex 200 column and a FPLC using a 150 mM KCl gradient elution. **A** UV trace (blue) from the FPLC is shown with the fraction number below in red. Corresponding analysis of the

fractions by **B** 10 % SDS-PAGE gel stained with Instant Blue protein stain and **C** immunoblotting using His-tag specific antibodies. Fraction number indicated, with protein marker (10-250 kDa). All gels were electrophoresed at 175 V for 110 minutes and imaged using the Li-Cor Odyssey Infrared Imaging Analysis System.

## 4.6 *In vitro* BER activity of APE1 on THF-IN mononucleosome substrate

In the first instance, THF-IN site incision within a mononucleosome substrate (prepared as described in section 4.4.) by recombinant APE1 was examined. The percentage incision from two independent BER assays using a titration of APE1 was performed for the THF-IN mononucleosome substrate. As expected, this confirmed previous work within the group, that the THF-IN mononucleosome substrate (50 fmol) is poorly processed by recombinant APE1, with cleavage reaching a maximum of 35-40 % with 200 fmol (a four fold-excess) of APE1 (Figure 4.27). This is unsurprising due to the inability of APE1 to access the THF site when the DNA backbone is facing inwards towards the histone octamer. This APE1 titration was then used to establish reaction conditions for a ΔN-HECTD1 titration, where it was decided that 50 fmol APE1 (generating ∼20 % incision) was sufficient for future *in vitro* investigations to allow for any increases in incision to be observed.

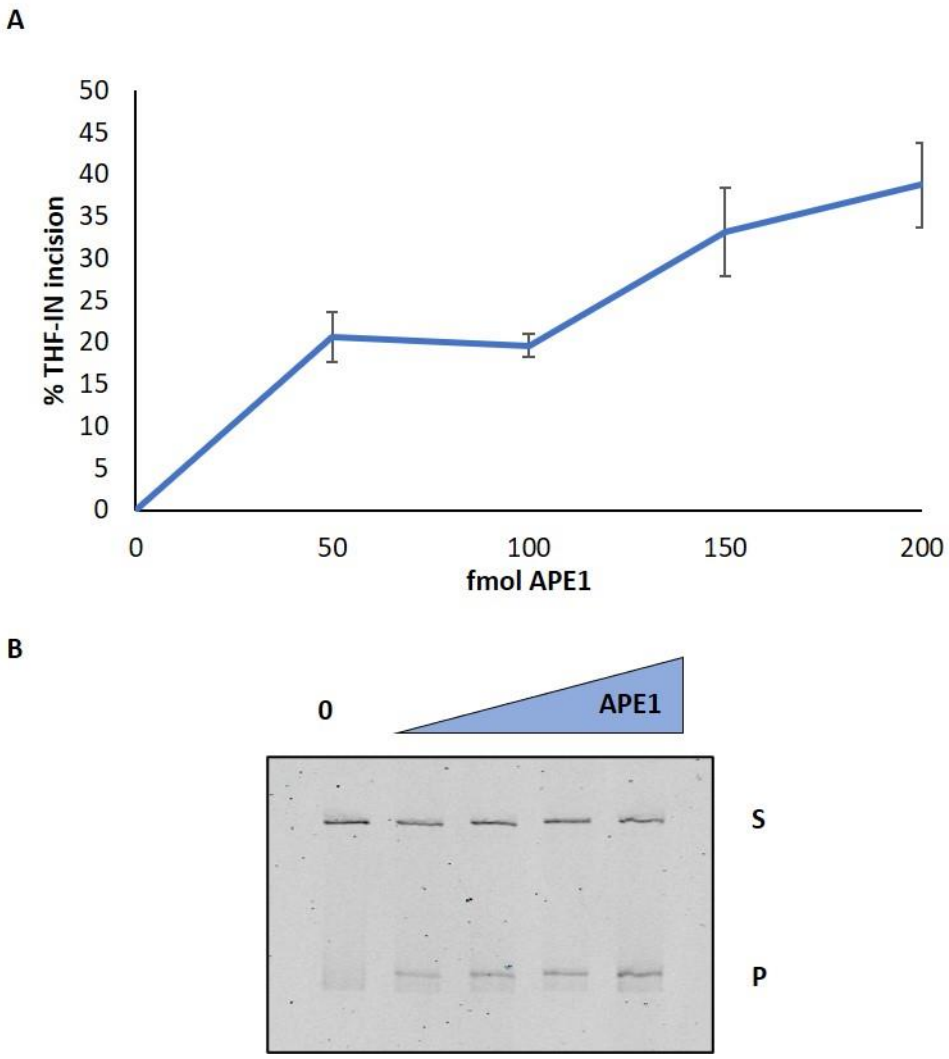


**Figure 4.27: APE1 *In vitro* BER assay titration on THF-IN mononucleosome substrates**

**A** Purified recombinant APE1 concentration titration (0-200 fmol) using THF-IN (blue) mononucleosome substrate (50 fmol) and **B** representative gel with full length 256 bp DNA (S) and cleaved 116 bp THF-IN DNA (P) indicated. PAGE gels contained 8 % polyacrylamide, 7 M Urea and 1x TBE and were run at 300 V, 20 W for 1.75 hours, gels were imaged and percentage incision quantified using the Li-Cor Odyssey Infrared Imaging Analysis System. Shown is the mean percent substrate incision ± S.E. from two independent experiments.

## 4.7 *In vitro* BER activity of APE1 and HECTD1 on THF-IN mononucleosome substrate

The ability of ΔN-HECTD1 to stimulate APE1 activity on THF-IN mononucleosome substrates was examined, from three independent BER assays using a titration of recombinant ΔN-HECTD1. I determined that ΔN-HECTD1 (0-15 pmol) was able to significantly stimulate the

activity of recombinant APE1 against the THF-IN mononucleosome substrate from 20 to 57 % THF-incision (Figure 4.28B, lanes 3-6 and Figure 4.28A (blue)), as determined by the proportion of cleaved 116 bp THF-IN DNA (P) relative to full length 256 bp DNA (S) (Figure 4.28B). When examining the effect of HECTD1 on THF site excision by APE1 within the mononucleosome substrate an initial titration of 2 pmol ΔN-HECTD1 resulted in a moderate increase in percentage THF-incision, from the observed control levels (20 %) to 26 % THF-incision. A further increase in the concentration of ΔN-HECTD1 in the reaction to 5 pmol resulted in a similar degree of increase in percentage THF-incision from 28 % THF-incision achieved with 2 pmol ΔN-HECTD1 to 34 % THF-incision. The following incubation with 10 pmol ΔN-HECTD1 resulted in a significant shift in APE1 incision of the THF-IN mononucleosome, reaching 50 % THF-incision, with the final titration step, an incubation of 15 pmol ΔN-HECTD1 reaching the observed maximum of 57 % THF-incision of the THF-IN mononucleosome by APE1.

It was also important to verify that ΔN-HECTD1 alone had no impact on the incision of the THF-IN mononucleosome. Therefore, except for the absence of APE1, in the same reaction conditions the THF-IN substrate was incubated with a titration of recombinant ΔN-HECTD1 (0-15 pmol) alone in the *in vitro* BER assay. In the absence of APE1 I observed no significant incision of the THF site, with percentage THF-incision, as determined by the proportion of cleaved 116 bp THF-IN DNA (P) relative to full length 256 bp DNA (S) (Figure 4.28B), remaining at control levels at all ΔN-HECTD1 titration points (Figure 4.28A (orange)). Therefore, I can conclude that there was no impact of ΔN-HECTD1 alone on incision of the THF-IN substrate (Figure 4.28B, lanes 7-10 and Figure 4.28A (orange)). This data confirmed HECTD1 as a chromatin remodelling enzyme candidate to take forward in this project.

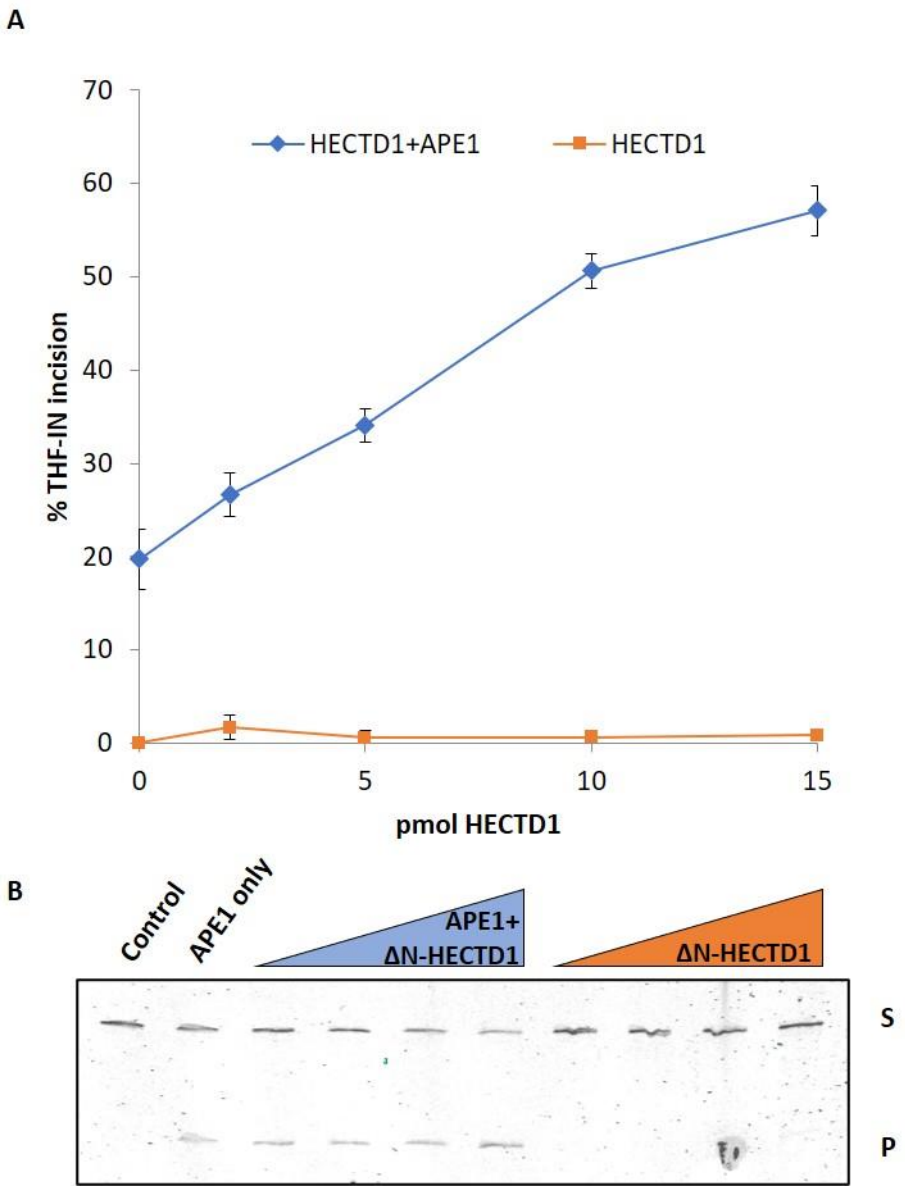


**Figure 4.28: HECTD1 promotes incision of THF-IN mononucleosome substrate by recombinant APE1 *in vitro***

Stimulation of APE1-dependent incision of the THF-IN mononucleosome substrate by ΔN-HECTD1. **A** Purified recombinant ΔN-HECTD1 concentration titration (0-15 pmol) using THF-IN mononucleosome substrate in the presence (blue) and absence (orange) of APE1 (50 fmol) and **B** representative gel with full length 256 bp DNA (S) and cleaved 116 bp THF-IN DNA (P) indicated. PAGE gels contained 8 % polyacrylamide, 7 M Urea and 1x TBE and were run at 300 V, 20 W for 1.75 hours, gels were imaged and percentage incision quantified using the Li-Cor Odyssey Infrared Imaging Analysis System. Shown is the mean percent substrate incision ± S.E. from three independent experiments.

## 4.8 Analysis of the E3 ubiquitin ligase dependency of HECTD1

In order to determine if the E3 ubiquitin ligase activity of HECTD1 is key for it to function as a chromatin remodelling enzyme, as we presume, a site directed mutagenesis (SDM) approach was chosen to mutate the active site cysteine (C) residue to a glycine (G) residue (Figure 4.29). This substitution was selected as both amino acids have similar biochemical properties, minimising the impact on the overall structure and folding of ΔN-HECTD1.

D D D Y V L K R Q F S A L V P A F D P R P G R
T N V Q Q T T D L E I P P P G T P H S E L L E
E V E C T P S P R L A L T L K V T G L G T T R
E V E L P L T N F R S T I F Y Y V Q K L L Q L
S C N G N V K S D K L R R I W E P T Y T I M Y
R E M K D S D K E K E N G K M G C W S I E H V
E Q Y L G T D E L P K N D L I T Y L Q K N A D
A A F L R H W K L T G T N K S I R K N R N C S
Q L I A A Y K D F C E H G T K S G L N Q G A I
S S L Q S S D I L N L T K E Q P Q A K A G N G
Q S P C G V E D V L Q L L R I L Y I V A S D P
Y S R I S Q E D G D E Q P Q F T F P P D E F T
S K K I T T K I L Q Q I E E P L A L A S G A L
P D W C E Q L T S K C P F L I P F E T R Q L Y
F T C T A F G A S R A I V W L Q N R R E A T V
E R T R T T S S V R R D D P G E F R V G R L K
H E R V K V P R G E S L M E W A E N V M Q I H
A D R K S V L E V E F L G E E G T G L G P T L
E F Y A L V A A E F Q R T D L G T W L C D D N
F P D D E S R H V D L G G G L K P P G Y Y V Q
R S C G L F T A P F P Q D S D E L E R I T K L
F H F L G I F L A K C I Q D N R L V D L P I S
K P F F K L M C M G D I K S N M S K L I Y E S
R G D R D L H C T E S Q S E A S T E E G H D S
L S V G S F E E D S K S E F I L D P P K P K P
P A W F N G I L T W E D F E L V N P H R A R F
L K E I K D L A I K R R Q I L G N K S L S E D
E K N T K L Q E L V L R N P S G S G P P L S I
E D L G L N F Q F C P S S R I Y G F T A V D L
K P S G E D E M I T M D N A E E Y V D L M F D
F C M H T G I Q K Q M E A F R D G F N K V F P
M E K L S S F S H E E V Q M I L C G N Q S P S
W A A E D I I N Y T E P K L G Y T R D S P G F
L R F V R V L C G M S S D E R K A F L Q F T T
G C S T L P P G G L A N L H P R L T V V R K V
D A T D A S Y P S V N T C V H Y L K L P E Y S
S E E I M R E R L L A A T M E K G F H L N –

**Figure 4.29: The amino acid sequence of ΔN-HECTD1**

Shown is the amino acid sequence of ΔN-HECTD1 (murine HECTD1 truncated at amino acid 1761). This sequence of ΔN-HECTD1 is 850 amino acids in length and contains to full HECT domain, amino acid 2151-2610 (highlighted in blue) and the active site, a cysteine residue at amino acid 2587 (C, in red, highlighted in yellow.

### 4.8.1 Site directed mutagenesis (SDM) of ΔN-HECTD1

Custom oligonucleotide primers were designed to generate a single point mutation in the active site of the HECT domain in ΔN-HECTD1 (Table 3.4). The bacterial expression plasmid, pET28a-HECTD1-1761, generated via LIC earlier in the chapter (section 4.5.2), was incubated with the relevant custom oligonucleotide primers and amplified by PCR. The expected size of the pET28a-mutHECTD1-1761 plasmid was 7919 bp, this was confirmed by analysis of the PCR DNA products by agarose gel electrophoresis (Figure 4.30). Although additional bands were present in the reaction, this would not be expected to interfere with the bacterial transformation. However, this analysis could not confirm whether the relevant mutation was present within the HECTD1 gene or not. Therefore, following PCR amplification, mutant DNA products were DpnI treated to remove DNA methylation and the DNA products purified using the QIAquick PCR Purification Kit. Following this, *E. coli* cells were transformed with the pET28a-mutHECTD1-1761 plasmid and grown on selective media containing kanamycin. Successful colonies were inoculated into 5 ml of LB media with kanamycin and grown overnight at 37°C to amplify the plasmid DNA, which was then purified from bacterial contaminants using the QIAprep Spin Miniprep Kit. Confirmation of a successful single point mutation, C to G at amino acid 2587, of ΔN-HECTD1 was achieved by DNA sequencing from the Sanger Sequencing Service (provided by Source Bioscience Sequencing, Nottingham, UK). This plasmid could now be used to overexpress and purify ΔN-mutHECTD1 from bacterial cells.

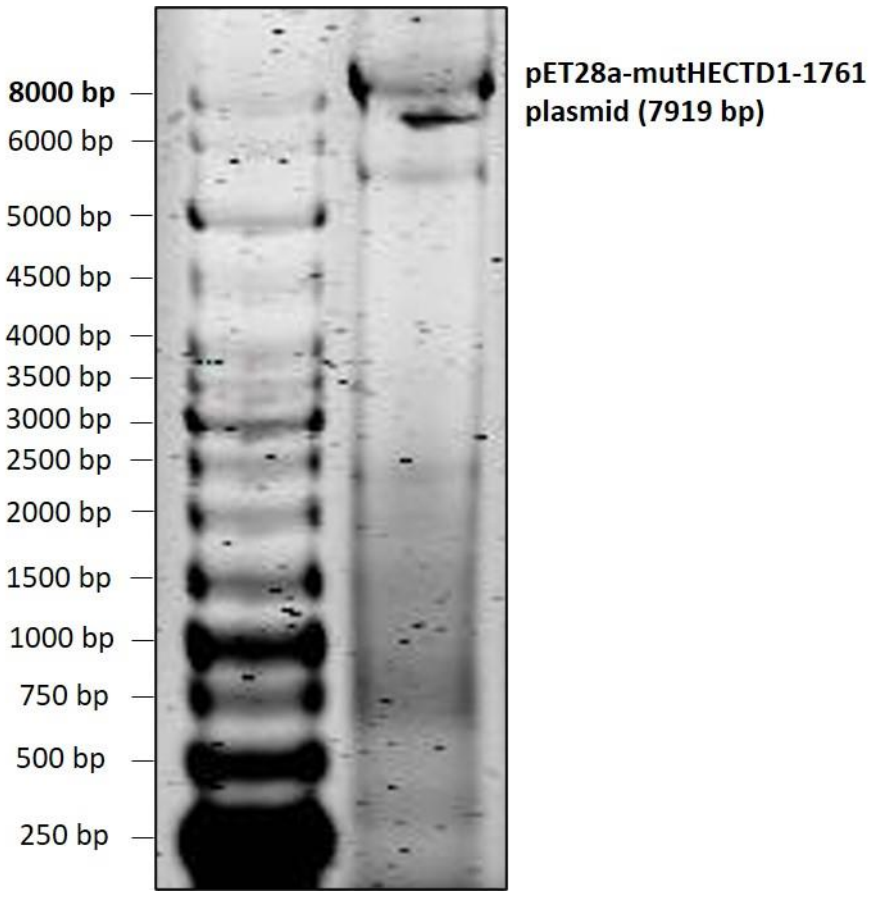


**Figure 4.30: PCR reaction product following site directed mutagenesis of pET28a-HECTD1-1761**

PCR product of amplification of the pET28a-HECTD1-1761 vector using custom oligonucleotide primers designed to generate a single point mutation in the active site of the HECT domain in ΔN-HECTD1. PCR reaction product separated by electrophoresis on a 1 % agarose gel at 100 V for 1 hour, imaged using the Li-Cor Odyssey Infrared Imaging Analysis System. A 1 kb GeneRuler DNA ladder was utilised to identify the size of the PCR product**.**

### 4.8.2 Affinity chromatography purification of ΔN-mutHECTD1

Rosetta2(DE3)pLysS bacterial cells, transformed via heat shock with His-tagged pET28a-mutHECTD1-1761 were grown until an OD600nm of 0.6 in a 400 ml culture. Protein expression of C-terminally His-tagged ΔN-HECTD1 was induced via IPTG addition for 3 hours, as previously determined by test expression (section 4.5.2) The bacterial cell lysate was purified using a 1 ml HisTrap HP affinity chromatography column and AKTA FPLC. Fractions were collected following a linear imidazole elution (5-250 mM) and the UV trace obtained from the FPLC with fraction number (Figure 4.31A) is shown in addition to the separation of

proteins by SDS-PAGE and analysis by Instant Blue protein staining to detect total protein (Figure 4.31B), and by immunoblotting with anti-histidine antibodies to detect His-tagged ΔN-mutHECTD1 (Figure 4.31C). The first peak is indicative of an injection peak and second protein peak correlated with fractions 1-2 on the UV trace (Figure 5.31A) was associated with contaminating bacterial proteins. However, the shoulder on the UV trace from fraction 7 onwards, contained isolated and purified recombinant ΔN-mutHECTD1. Confirmation by SDS-PAGE protein staining (Figure 4.31B) and immunoblotting (Figure 4.31C), revealed the presence of ΔN-mutHECTD1 in largely in fractions 7-16, but the protein, as did the wildtype, was found to undergo partial degradation to that of a slightly small molecular weight (85 kDa). Nevertheless, this protein crucially cross-reacts with the His-tagged antibodies, suggesting that the protein is being degraded from the N-terminus (as the protein is C-terminally tagged) and includes the fully intact mutant E3 ligase HECT domain required for my investigations. Therefore, relatively pure protein fractions (7-12) were pooled, buffer exchanged (50 mM Tris-HCl pH 8, 50 mM KCl, 1 mM EDTA, 10 % glycerol) to remove imidazole, the protein concentrated this measured using a Nanodrop ND-1000 spectrometer at a wavelength of OD 280 nm with molecular weights and extinction coefficients (ε). The protein was aliquoted before storage at -80°C.

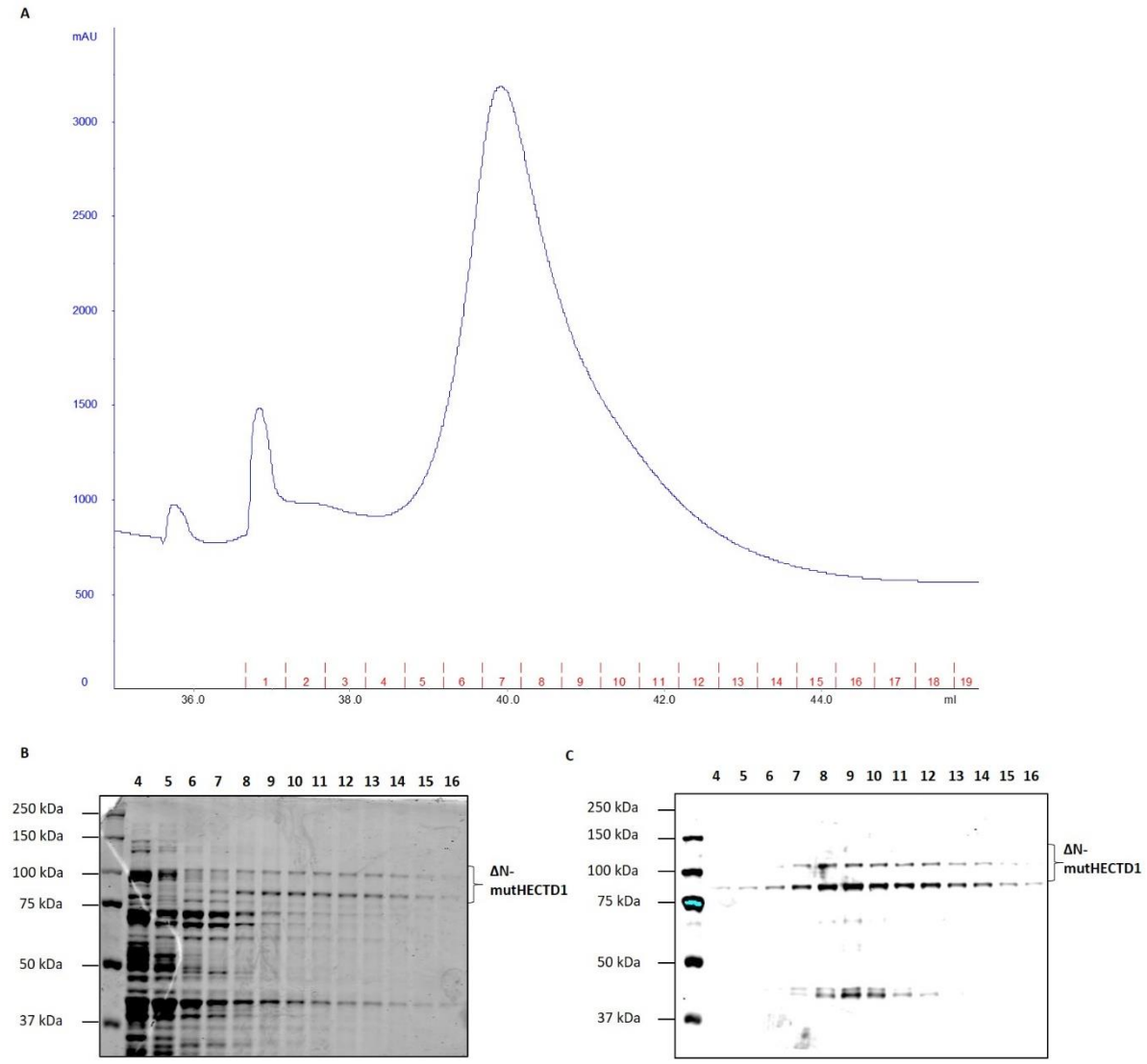


**Figure 4.31: HisTrap HP affinity column chromatography purification of recombinant His-tagged ΔN-mutHECTD1**

Following protein overexpression in *E-coli*, ΔN-mutHECTD1 was purified from the bacterial cell lysate by a HisTrap HP affinity chromatography column and AKTA FPLC using a linear 5-250 mM imidazole gradient elution. **A** UV trace (blue) from the FPLC is shown with the fraction number below in red. Corresponding analysis of the fractions by **B** 10 % SDS-PAGE gel stained with Instant blue protein stain and **C** immunoblotting using His-tag specific antibodies. Fraction number and recombinant His-tagged ΔN-HECTD1 indicated, with protein marker (10-250 kDa). All gels were electrophoresed at 175 V for 110 minutes and imaged using the Li-Cor Odyssey Infrared Imaging Analysis System.

### 4.8.3 *In vitro* BER activity of APE1 and ΔN-mutHECTD1 on the THF-IN mononucleosome substrate

To determine if it is indeed the E3 ubiquitin ligase activity of HECTD1 that is essential for its role in stimulating BER in chromatin. I assessed the ability of ΔN-mutHECTD1 to stimulate APE1 activity on THF-IN mononucleosome substrates. This was examined, from three independent BER assays, using a titration of ΔN-mutHECTD1, with percentage THF-incision calculated by the proportion of cleaved 116 bp THF-IN DNA (P) relative to full length 256 bp DNA (S). As when examining the effect of HECTD1 on THF site excision by APE1 within the mononucleosome substrate, as a control the incision of the THF site by APE1 alone was examined, upon examination of the cleavage product (S) it was determined that 20 % THF-incision was achieved (Figure 4.32A (blue)), comparable to THF-incision seen in previous *in vitro* BER experiments (section 4.7). Using a titration (0-15 pmol) of the inactive E3 ubiquitin ligase HECTD1, ΔN-mutHECTD1, I determined that ΔN-mutHECTD1 was not able to significantly stimulate the activity of recombinant APE1 against the THF-IN mononucleosome substrate (Figure 4.32B, lanes 3-6 and Figure 4.32A (blue)). Utilising an initial titration of 2 pmol ΔN-mutHECTD1 no increase in percentage THF-incision was observed, in fact a small decrease of 16 % THF-incision was seen at this titration step. Further increases in the concentration of ΔN-mutHECTD1 within the BER reactions also failed to stimulate APE1 activity of the THF-IN mononucleosome, with percentage THF-IN only reaching a maximum of 20 % at 5, 10 and 15 pmol ΔN-mutHECTD1 (Figure 4.32B, lanes 3-6 and Figure 4.32A (blue)).

It was also important to verify that ΔN-mutHECTD1 alone had no impact on the incision of the THF-IN mononucleosome. Therefore, except for the absence of APE1, in the same reaction conditions the THF-IN substrate was incubated with a titration of recombinant ΔN-mutHECTD1 (0-15 pmol) alone in the *in vitro* BER assay. In the absence of APE1 I observed no significant incision of the THF site, with percentage THF-incision, as determined by the proportion of cleaved 116 bp THF-IN DNA (P) relative to full length 256 bp DNA (S) (Figure 4.32B). Furthermore, percentage THF-incision largely remained at control levels at all ΔN-mutHECTD1 titration points, although small variations are seen with 2 % THF-incision seen with incubation of 2 pmol ΔN-mutHECTD1 and 3 % THF-incision at 5 and 10 pmol ΔN-mutHECTD1 incubation, it can be assumed that this variation is due to background signals from the Li-Cor Odyssey Infrared Imaging Analysis System and not true 116 bp THF-IN DNA cleavage product (Figure 4.32A (orange)). Therefore, I can conclude that there was no impact of ΔN-mutHECTD1 alone on incision of the THF-IN substrate (Figure 4.32B, lanes 7-10 and

Figure 4.32A (orange)). Thus, providing evidence that the E3 ubiquitin ligase activity of HECTD1 is essential for promoting THF-IN incision within mononucleosomes by APE1.

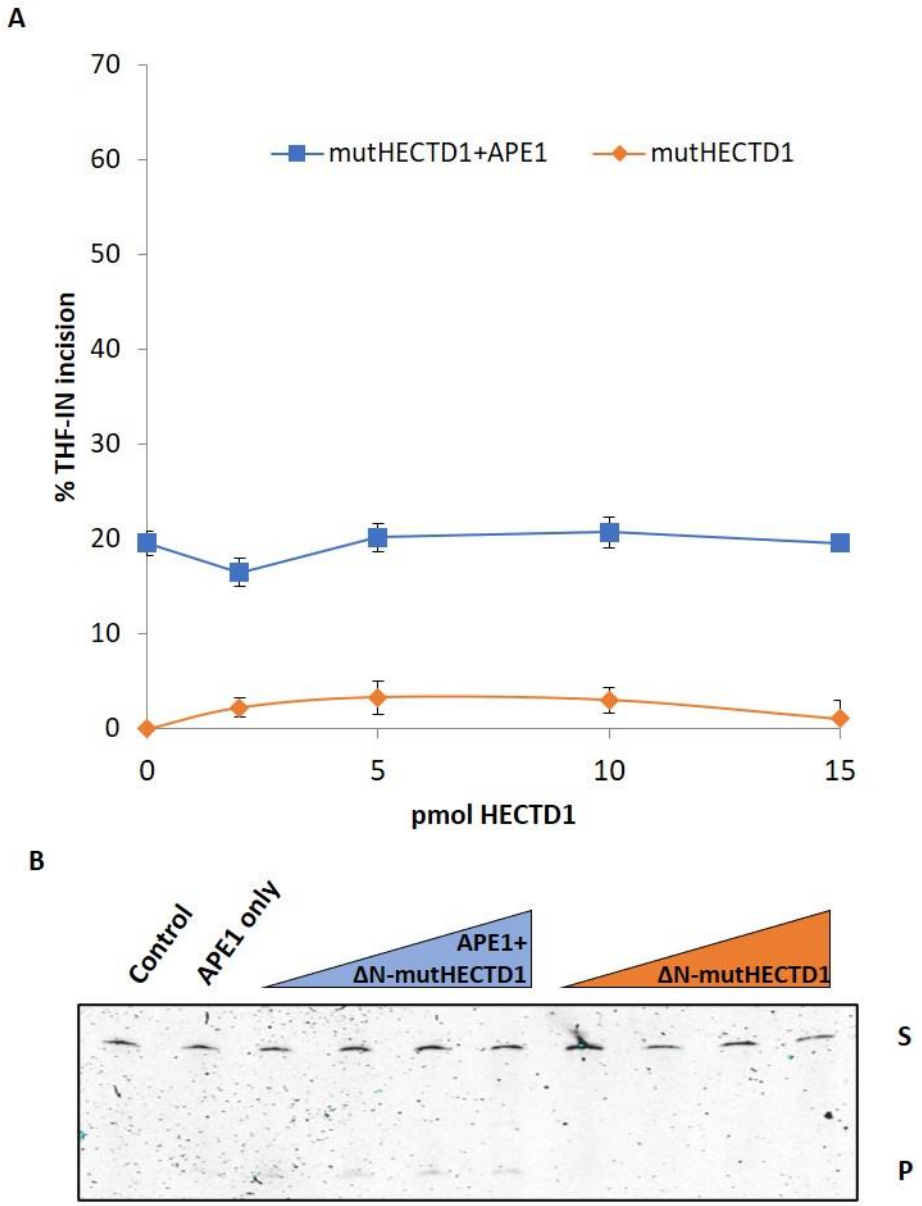


**Figure 4.32: mutant HECTD1 cannot promote incision of THF-IN mononucleosome substrate by recombinant APE1 *in vitro***

Stimulation of APE1-dependent incision of the THF-IN mononucleosome substrate by ΔN-mutHECTD1. **A** Purified recombinant ΔN-mutHECTD1 concentration titration (0-15 pmol) using THF-IN mononucleosome substrate in the presence (blue) and absence (orange) of APE1 (50 fmol) and **B** representative gel with full length 256 bp DNA (S) and cleaved 116 bp THF-IN DNA (P) indicated. PAGE gels contained 8 % polyacrylamide, 7 M Urea and 1x TBE and were run at 300 V, 20 W for 1.75 hours, gels were imaged and percentage incision quantified using the Li-Cor Odyssey Infrared Imaging Analysis System. Shown is the mean percent substrate incision ± S.E. from three independent experiments.

## 4.9 Summary

To investigate the role of HECTD1 as a potential histone modifier or ATP chromatin remodeller on BER in chromatin, it was first necessary to generate a THF-IN mononucleosome substrate. This substrate was designed to contain a THF site in an occluded position within the nucleosome, positioned so that the DNA backbone was facing towards the histone octamer, therefore making the site inaccessible to APE1 (Figure 4.1). Previous data within the Parsons' group established *in vitro* that this THF site was poorly cleaved by APE1. However, APE1 present in WCE generated from HeLa cells was found to efficiently cleave this THF site due to the presence of histone modifiers or ATP chromatin remodellers within the WCE. Following an unbiased purification scheme and mass spectrometry analysis, HECTD1 was identified as a strong chromatin remodeller candidate. In this chapter, I have demonstrated the generation of a THF-IN mononucleosome substrate, utilised LIC cloning and a bacterial expression system to produce recombinant ΔN-HECTD1 and clearly established an *in vitro* role of HECTD1 in BER where it acts to promote APE1 activity at occluded THF sites within mononucleosomes.

The Widom 601 sequence, selected due to its strong nucleosome positioning affinity, was amplified from the pGEM-3Z-601 plasmid using 5'-fluorescently labelled primers. Therefore, DNA could be quantitatively analysed using the Li-Cor Odyssey Image Analysis System, crucial not only for ensuring accurate generation of THF-IN containing DNA substrates, but also for ease of visualisation and accurate quantification of incision by APE1. The central 17 bp of the 601 nucleosome positioning sequence was removed using Van91I and BglI restriction enzymes to produce, once purified, two DNA sequence fragments. These were sequentially ligated to a pre-prepared 17 bp duplex oligonucleotide containing a THF site on the lower strand, resulting in the production of a site specific THF-IN DNA substrate, which when complexed with a histone octamer would produce a mononucleosome substrate. The histone octamer was successfully prepared, as previously reported [325]. *Xenopus Laevis* recombinant histones were overexpressed in *E.coli* and purified from inclusion bodies by gel filtration and ion-exchange chromatography under denaturing conditions, before unfolding and refolding in equimolar ratios to form the histone octamer. The THF-IN mononucleosome substrate was reconstituted by incubating THF-IN DNA with the histone octamer in a 1:1 ratio with a salt gradient dialysis, consistent with previous reports [325].

HECTD1 was cloned utilising a LIC strategy (Figure 4.18), this method does not require restriction enzymes or DNA ligases used in traditional cloning, rather employs the

polymerase/exonuclease activity of T4 DNA polymerase to generate complimentary long overhangs between the vector and insert to form stable associations [323]. The murine HECTD1 gene, truncated at amino acid 1761, to enable utilisation of a bacterial overexpression system, was cloned from the mammalian expression vector and into the pET28a bacterial expression vector. Recombinant ΔN-HECTD1 overexpression was optimised for 3 hours in *E-coli*, as determined by test expression, key for generation of the stable protein, and purified using affinity chromatography.

Following successful generation of the THF-IN mononuclesome substrate and ΔN-HECTD1 protein, I first confirmed the inefficiency of APE1 to access the THF site when the DNA backbone is facing inwards towards the histone octamer. I also used this to establish reaction conditions for a ΔN-HECTD1 titration, where I decided that 50 fmol APE1 (generating ∼20 % substrate incision) was sufficient for future *in vitro* investigations. Furthermore, I investigated the ability of ΔN-HECTD1 to stimulate APE1 activity on THF-IN mononucleosome substrates and concluded that ΔN-HECTD1 was able to significantly stimulate, in a dose-dependent manner, the activity of recombinant APE1 against the THF-IN mononucleosome substrate from 20 to 57 %. To confirm the requirement of ΔN-HECTD1 to stimulate APE1 activity on THF-IN mononucleosome substrates, I adopted a SDM approach to mutate the active site cysteine (C) residue to a glycine (G) residue within the HECT domain, generating ΔN-mutHECTD1, an E3 inactive ligase mutant of ΔN-HECTD1. Following bacterial overexpression and affinity purification, a ΔN-mutHECTD1 titration into the *in vitro* BER assay was able demonstrate that ΔN-mutHECTD1 was unable to stimulate APE1 activity against the THF-IN mononucleosome, providing evidence that via its E3 ligase activity ΔN-HECTD1 was able to stimulate APE1 activity at occluded THF sites. Therefore, confirming HECTD1 as a chromatin remodelling enzyme candidate to take forward into future chapters.

The findings in this chapter, corroborates previously published *in vitro* studies which found that the detection of AP sites by APE1 was dependent on damage orientation within mononucleosomes constructed using 150 bp TG motif containing DNA or with 147 bp 601 DNA. Here, at least a 2-fold (TG sequence) and 3-fold (601 sequence) reduction in cleavage of a natural AP site or tetrahydrofluran (THF) by APE1 was observed with inwardly facing lesions in comparison to outwardly facing sites [248]. Interestingly, the reduced substrate cleavage was demonstrated through gel shift mobility assays to be as a consequence of reduced binding of APE1 to the inwardly facing substrate, rather than reduced activity. This study was followed by demonstration that two naturally occurring variants of APE1, R237C

and G241R, have reduced activity on both inwardly and outwardly facing AP site containing 147 bp 601 DNA within mononucleosome substrates, but not on naked DNA [249]. This was despite the variants not demonstrating any dramatic differences in mononucleosome binding. Furthermore, the importance of epigenetics in this stage of BER has been shown *in vitro* with a 15-fold reduction in mononucleosome AP site reactivity with histone proteins observed following mutation of five lysine residues (to arginines) in the amino tail region of histone H4, predicting the involvement of histone tails and PTMs in DNA strand cleavage [250]. Therefore, this data suggests that APE1 itself may not be the target of any PTM or ACR involved in chromatin remodelling within BER. Also, of note, is that studies identifying ACRs targeting APE1 or AP site incision within BER are limited. An early *in vitro* study using 227 bp 601 DNA and recombinant *X. laevis* histones to generate mononucleosomes containing an 8-oxoguanine residue, identified yeast SWI/SNF as a factor increasing the efficiency of excision of the lesion by OGG1 and APE1 by ~8-fold, which improved processing efficiency similar to that of naked DNA alone [241]. Thus, the data presented in this chapter, highlighting a novel role of HECTD1 in promoting AP site incision within chromatin, is vital to accelerate our understanding of chromatin remodelling in BER.

All together this suggests that the action of any ACR or PTM, such as ubiquitylation, may not be targeting APE1 itself and altering enzyme activity but somehow improving APE1 accessibility via altering chromatin structure. Furthermore, this may also suggest that HECTD1, similarly to SWI/SNF, may play a more general role within BER beyond AP site incision. Therefore, when assessing potential mechanistic modes of action of HECTD1 it was vital to focus my attentions on assessing multiple targets, including the core histone proteins, as well as the specificity of HECTD1 to APE1 via investigations of further BER activities.

# CHAPTER 5: RESULTS II

## Investigation of the E3 ubiquitin ligase activity and targets of HECTD1

### 5.1 Introduction

A key way in which cells regulate normal cell physiology is through ubiquitylation which can modulate protein-protein or protein-DNA interactions as well as protein stability and activity. Ubiquitylation consists of three steps, ubiquitin activation by an E1 ubiquitin-activating enzyme, ubiquitin transfer from the E1 enzyme to the E2 active site by a E2 ubiquitin conjugating enzyme, before an E3 ubiquitin ligase enzyme catalyses the transfer of ubiquitin onto a lysine residue of the substrate protein.

With over 600 E3 ubiquitin ligases identified in the human proteome, it is assumed that this PTM is implicated in every cellular function. This includes the DDR, in particular, a number of E3 ubiquitin ligases have been identified to target BER proteins, particularly for ubiquitylation-dependent degradation. Multiple DNA glycosylases have been shown to be substrates for E3 ubiquitin ligases, for example, CRL4(Cdt2) targets TDG for degradation via the proteasomal pathway, during S phase of the cell cycle [328], [329]. Additionally, Mule and TRIM26 has been shown to regulate the steady state levels of the DNA glycosylase NEIL1 [246]. However, TRIM26 has also been shown to polyubiquitylate NTH1, yet this has no impact on steady state levels of the protein, instead regulating DNA damage inducible levels of NTH1 following oxidative DNA damage [247]. Furthermore, ubiquitylation of MUTYH by Mule has been shown to regulate the protein's cellular steady state levels [330], and the same E3 ubiquitin ligase is known to monoubiquitylate Pol β and to control its degradation by the proteasome [331]. It is important to highlight the range of biological effects that one E3 ligase can have. Furthermore, it has been suggested that steady state levels of BER proteins can be modulated by differing cellular states and E3 ligases. For example, UBR3 has been shown to ubiquitylate APE1 to regulate the cellular steady state levels [332]. Additionally Parkin, which is activated under cellular stress, has been shown to ubiquitylate APE1 under mitochondrial or oxidative stress in cells [333]. This further demonstrates the complexity and breadth of this PTM particularly in regulating BER.

The HECT domain containing E3 ubiquitin ligase, HECTD1 is a 289 kDa protein which was first characterised to target heat shock protein 90 (HSP90) for ubiquitylation and control the cellular localisation and secretion of the protein necessary for regulation of the behaviour of cranial mesenchyme cells [303]. HECTD1 has also been shown to function as a negative regulator of the Wnt pathway through catalysing the polyubiquitylation of the adenomatous polyposis coli (APC) protein in HEK293 cells, required for its interaction with Axin [308] . This is supported by a report observing, via a USP15 stabilisation of HECTD1, downregulation of Wnt pathway activity in LN-229 and LN-428 glioblastoma cells associated with HECTD1 overexpression [318]. Furthermore, it has been demonstrated that HECTD1 negatively impacts endothelial-mesenchymal transition in response to silicon dioxide in MML1 mouse lung cells, inhibiting cell proliferation and migration [314]. Additionally, in T47D breast cancer cells, HECTD1 depletion has been shown to enhance epithelial-mesenchymal transition and promotes tumour growth, survival and metastasis due to decreased HECTD1 mediated ubiquitylation-dependent degradation of ACF7 [312].

In addition to these reports demonstrating roles for HECTD1 in controlling cell signalling, proliferation and migration, in the previous chapter I provided new evidence that HECTD1 is required to promote efficient repair of synthetic AP sites (THF) by APE1 within mononucleosomes, as a model of the chromatin environment. In this chapter, I aimed to elucidate the mechanism via which HECTD1 is acting in this novel role. Initially, utilising DNase footprinting assays, I examined the ability of HECTD1 to act as a chromatin remodelling enzyme via nucleosome sliding. Furthermore, utilising *in vitro* ubiquitylation assays I aimed to identify targets of ubiquitylation by HECTD1. Additionally, in this chapter I aimed to examine the specificity of HECTD1 in stimulating BER in chromatin, and specifically to assess its ability to also stimulate NTH1 activity on TG mononucleosome substrates.

## 5.2 Nucleosome sliding by HECTD1

One theory of the mechanism by which HECTD1 was promoting APE1 activity within mononucleosomes, was via altering the accessibility of the occluded synthetic AP site to APE1 via nucleosome sliding. This is one mode of chromatin remodelling whereby ATP-chromatin remodelling enzymes utilise ATP-hydrolysis to relocate histone octamers to adjacent DNA segments (‘sliding’) [334]–[336]. In the case of HECTD1, an E3 ubiquitin ligase, I theorised that via a ubiquitylation event HECTD1 may be causing sliding or displacement of the histones. To examine this, DNase footprinting, where differences in DNA cleavage

patterns between free DNA and protein-bound DNA aid in the identification of DNA-protein interactions, was utilised here with the aim of identifying whether sliding of the nucleosome led to the increased substrate cleavage following incubation of the nucleosome with HECTD1.

### 5.2.1 DNase footprinting of the free DNA substrate

Initially, it was important to establish reaction conditions for the DNase footprinting assay on free DNA. Therefore, 50 fmol free THF-IN DNA was incubated for 2 minutes with increasing concentrations of DNase (0-0.5 units), reactions were stopped with the addition of formamide loading dye and denatured at 95°C for 5 minutes. Samples were run on a pre-warmed 8 % denaturing acrylamide sequencing gel in 0.5x TBE at 1800 V and 42 W for 80 minutes and gels imaged using the Li-Cor Odyssey Infrared Imaging Analysis System. As can be seen in Figure 5.1, incubation with 0.05 units DNase (lane 2) yielded no visible cleavage, with the observed pattern identical to that observed in control conditions (lane 1). With the increasing DNase titrations, cleavage patterns of the free THF-IN DNA was observed at 0.1-0.5 units DNase, which indicated that a 2 minute incubation period was sufficient for cleavage of the substrate. When optimising DNase dosing, although evidence of the free DNA cleavage pattern was visible following incubation with 0.1 units (lane 3), the full banding was not evident until incubation with 0.2 units (lane 4). However, as shown in lane 5, an optimised clear free THF-IN DNA cleavage pattern is observed with incubation of free DNA with 0.5 units DNase. Therefore, 0.5 units per 50 fmol free THF-IN DNA was accepted for future investigations. Also, of note, as can be seen in Figure 5.1, a DNA marker was not used in these preliminary investigations. This was deemed acceptable as the purpose of these experiments was to determine a cleavage pattern of the THF-IN free DNA for use in future experiments with the THF-IN mononucleosome substrate, where the free DNA cleavage pattern would be used as a DNA marker.

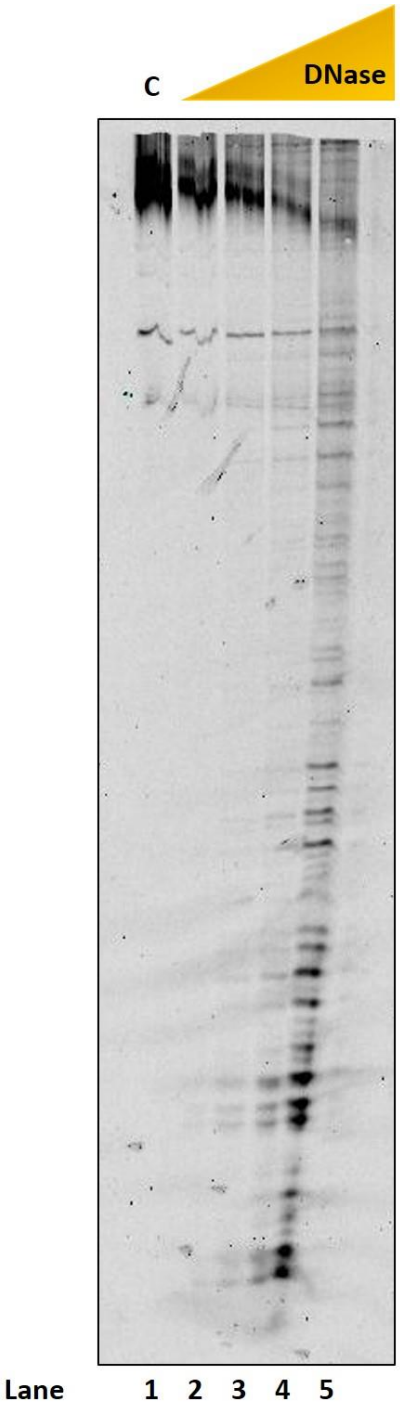


**Figure 5.1: DNase titration on THF-IN free DNA**

DNase footprinting assay of THF-IN free DNA. THF-IN free (50 fmol) DNA incubated with increasing doses of DNase (0 (lane 1), 0.05 (lane 2), 0.1 (lane 3), 0.2 (lane 4), 0.5 (lane 5) units) for 2 minutes at room temperature in DNase buffer. Samples were separated by a 8 % denaturing acrylamide sequencing gel in 0.5x TBE at 1800 V and 42 W for 80 minutes and gels imaged using the Li-Cor Odyssey Infrared Imaging Analysis System.

### 5.2.2 DNase footprinting of the THF-IN mononucleosome substrate

Following the titration of DNase on THF-IN free DNA, it was next essential to establish reaction conditions for the footprinting assay on mononucleosome DNA. In the first instance, 100 fmol of THF-IN mononucleosome substrate was used, where the increase in DNA concentration was to allow for loss during DNA extraction. The substrate was then incubated for 2 minutes with increasing concentrations of DNase (0-2 units). DNA was extracted initially via phenol:chloroform:isoamyl alcohol and Bio-Spin P-30 Gel Columns similar to the *in vitro* BER assay (section 3.18), however, this method resulted in too high a degree of DNA loss, as determined by comparison to the optimised THF-IN free DNA reactions (Figure 5.2A; lane 1) where the cleavage pattern was clearly visible. This resulted in the inability to quantify the THF-IN mononucleosome DNA via a sequencing gel following this DNA extraction technique (Figure 5.2A; lanes 2-6). Therefore, I adopted an ethanol precipitation technique to extract the THF-IN mononucleosome DNA following incubation of the substrate with increasing concentrations of DNase (0-2 units). In the same manner as the free DNA control, DNA samples following ethanol precipitation were denatured with the addition of formamide loading dye and boiling at 95°C for 5 minutes. Samples were run on a pre-warmed 8 % denaturing acrylamide sequencing gel in 0.5x TBE at 1800 V and 42 W for 80 minutes and gels imaged using the Li-Cor Odyssey Infrared Imaging Analysis System. This alternative DNA extraction method proved successful in retaining a sufficient DNA concentration for analysis via a sequencing gel, where a clearly different cleavage pattern can be seen between the protein bound DNA (Figure 5.2B lanes 2-6) and the free DNA (Figure 5.2B, lane 1). The predicted location of the histone octamer is indicated in Figure 5.2B, where a clear section of the cleavage pattern lacks DNA banding, indicative of DNA protection due to protein binding from the action of the DNase enzyme. Furthermore, inspection of the THF-IN mononucleosome cleavage patterns indicated that 1 unit of DNase (Figure 5.2B, lane 4) was optimal for qualitative analysis of DNA footprinting of this substrate.

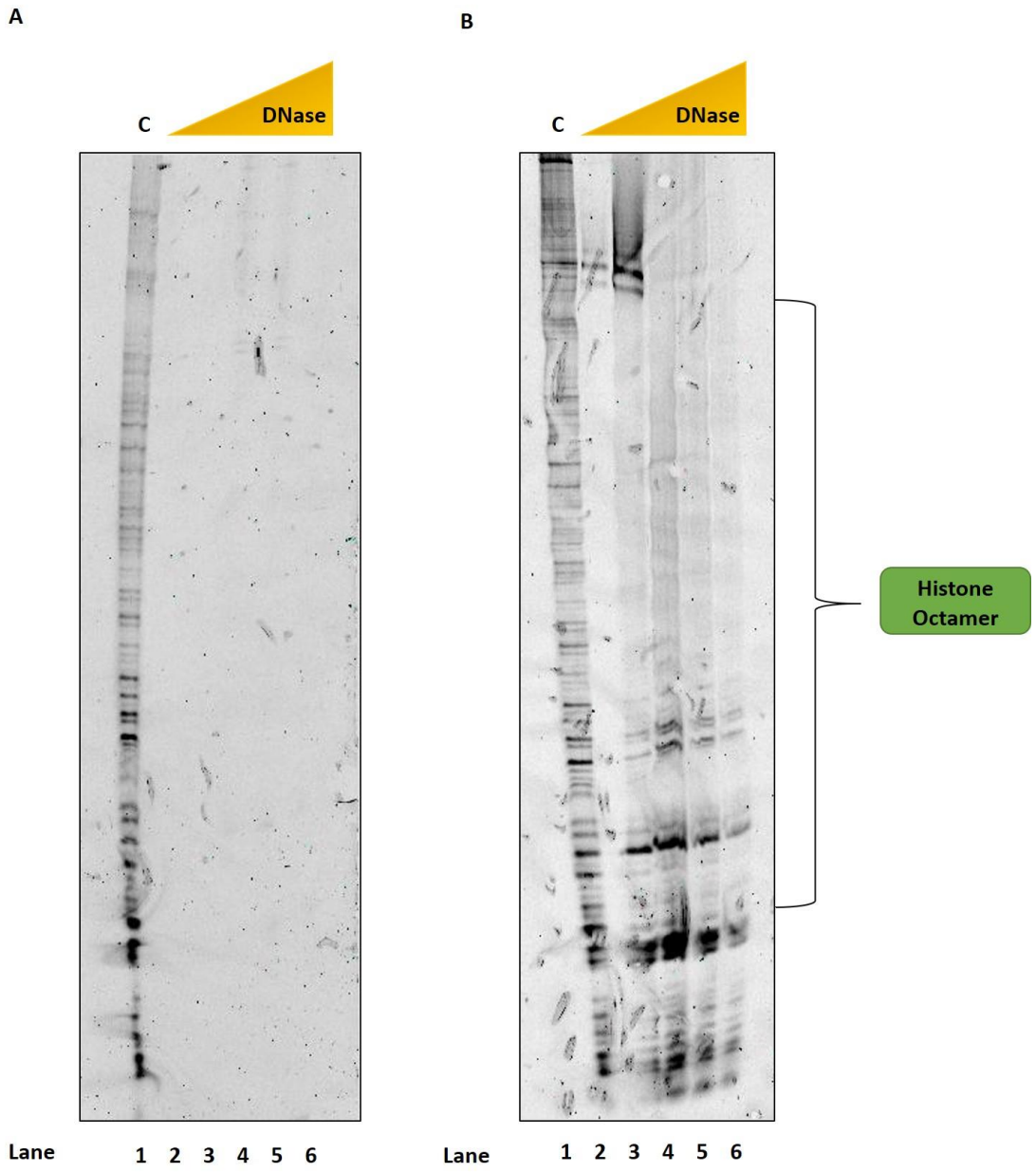


**Figure 5.2: DNase titration on THF-IN mononucleosome DNA**

DNase footprinting assay of THF-IN mononucleosomes. THF-IN mononucleosome (100 fmol) incubated with increasing doses of DNase (0 (lane 2), 0.5 (lane 3), 1.0 (lane 4), 1.5 (lane 5), 2.0 (lane 6) units) for 2 minutes at room temperature in DNase buffer. As a control, THF-IN free (50 fmol) DNA was incubated with 0.5 units DNase (lane 1). DNA was extracted via phenol:chloroform:isoamyl alcohol and purified via **A** Bio-Spin P-30 Gel Columns or **B** ethanol precipitation. Samples were separated by a 8 % denaturing acrylamide sequencing gel in 0.5x TBE at 1800 V and 42 W for 80 minutes and gels imaged using the Li-Cor Odyssey Infrared Imaging Analysis System.

### 5.2.3 DNase footprinting of the THF-IN mononucleosome substrate following HECTD1 incubation

Once reaction conditions for both THF-IN free and mononucleosome DNA had been established, the aim was to analyse any differences in the cleavage pattern of the THF-IN mononucleosome in the absence versus the presence of incubation with HECTD1 in the *in vitro* BER assay. Therefore, the THF-IN mononucleosome substrate (100 fmol) was incubated with either 0 pmol or 10 pmol ΔN-HECTD1 in the *in vitro* BER assay, reactions were fully complemented with one E1 activating enzyme (0.7 pmol), nine combined E2 conjugating enzymes (2.5 pmol), and ubiquitin (0.6 nmol). DNA extraction was performed with ethanol precipitation before undergoing DNase cleavage in the DNase footprinting assay via incubation with 1 unit DNase for 2 minutes. Similarly, THF-IN free DNA (50 fmol) was incubated with 0.5 units DNase for 2 minutes as a control. Samples were denatured with the addition of formamide loading dye and boiling at 95°C for 5 minutes and run on a pre-warmed 8 % denaturing acrylamide sequencing gel in 0.5x TBE at 1800 V and 42 W for 80 minutes. Gels imaged using the Li-Cor Odyssey Infrared Imaging Analysis System. Unfortunately following the *in vitro* BER assay, THF-IN mononucleosomal DNA was not successfully visualised on sequencing gels despite multiple attempts. This could be a result of unsuccessful ethanol precipitation of DNA or inefficient DNA extraction using phenol:chloroform, which is not unexpected given the complexity of this approach. I was not able to mitigate this by increasing the concentration of the THF-IN mononucleosome to 200 fmol (Figure 5.3). Here, samples in both the presence and absence of ΔN-HECTD1, in which the DNA had undergone the *in vitro* BER assay and DNA extraction prior to DNase footprinting, I was unable to visualise any DNA cleavage pattern (Figure 5.3 lanes 2 and 3). However, the cleavage pattern of the optimised THF-IN free DNA reactions was clearly visible (Figure 5.3; lane 1), demonstrating that the electrophoresis of samples was successful. Therefore, I am unable to conclude that HECTD1 is or is not altering accessibility of the AP site via nucleosome sliding. However, in the following work, I aimed to investigate the ubiquitylation activity of HECTD1 against both APE1 and the histone proteins to elucidate the mechanism by which HECTD1 promotes APE1 activity on occluded THF sites.

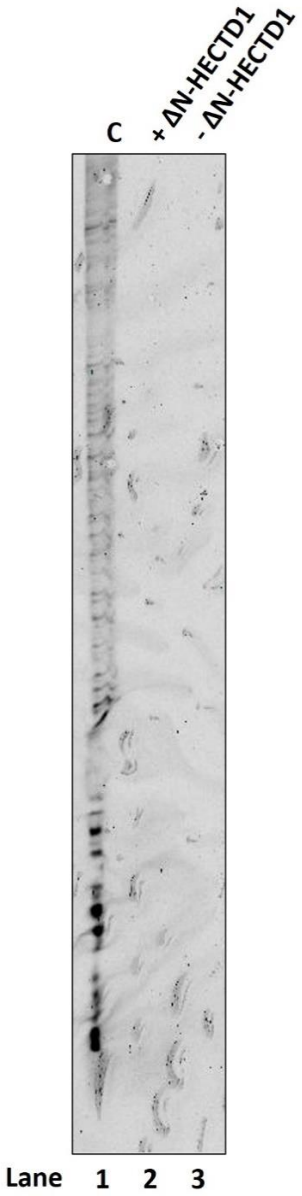


**Figure 5.3: DNase footprinting on THF-IN mononucleosome following HECTD1 chromatin remodelling**

DNase footprinting assay of THF-IN mononucleosomes following *in vitro* BER assay. THF-IN mononucleosome (200 fmol) incubated with 0.7 pmol GST-E1 activating enzyme, 2.5 pmol E2 conjugating enzyme (combination of 9 different E2s), 0.6 nmol ubiquitin, 1 µg acetylated BSA, 50 fmol APE1 with (lane 2) or without (lane 3) 10 pmol ΔN-HECTD1 for 1 hour at 30°C with 800 rpm. DNA was extracted via phenol:chloroform:isoamyl alcohol and ethanol precipitation. Following the *in vitro* BER assay, DNA was incubated with 1 unit DNase for 2 minutes at room temperature in DNase buffer. As a control, THF-IN free (50 fmol) DNA was incubated with 0.5 units DNase (lane 1). Samples were separated by a 8 % denaturing

acrylamide sequencing gel in 0.5x TBE at 1800 V and 42 W for 80 minutes and gels imaged using the Li-Cor Odyssey Infrared Imaging Analysis System.

## 5.3 *In vitro* ubiquitylation of APE1 by HECTD1

Whilst in the previous section I was unsuccessful in confirming the ability of HECTD1 to cause changes to the mononucleosome via altering histone-DNA contact and nucleosome sliding, I moved on to investigate the specific targets for HECTD1 ubiquitylation activity. In the first instance, I utilised the *in vitro* ubiquitylation assay with recombinant APE1 and increasing concentrations of ΔN-HECTD1 (2.8-14.1 pmol) in the presence of one E1 activating enzyme, nine separate E2 conjugating enzymes, and ubiquitin. This was to examine whether APE1 itself was being ubiquitylated by HECTD1, potentially increasing AP endonuclease enzymatic activity. Whilst evidence from the *in vitro* ubiquitylation assay did suggest E2-dependent monoubiquitylation of APE1 in the absence of HECTD1 (Figure 5.4, lane 1), which has previously been observed [332], an increasing presence of ΔN-HECTD1 (Figure 5.4, lanes 2-4) did not stimulate APE1 ubiquitylation. In fact, addition of ΔN-HECTD1 actually supressed E2-dependent monoubiquitylation at the highest protein concentration (Figure 5.4, lanes 2-4). This however confirmed that APE1 protein is not a direct target for HECTD1 ubiquitylation.

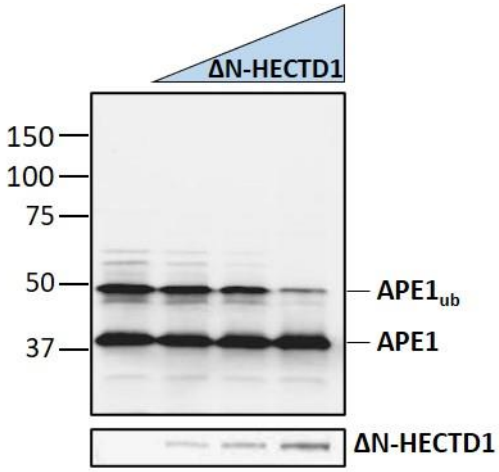


**Figure 5.4: In vitro ubiquitylation activity of APE1 by HECTD1**

*In vitro* ubiquitylation assays contained recombinant APE1 (5.9 pmol) in the presence of increasing amounts of ΔN-HECTD1 (2.8–14.1 pmol), one E1 activating enzyme (0.7 pmol), nine separate E2 conjugating enzymes (2.5 pmol), and ubiquitin (0.6 nmol) (Ub). Reactions were incubated at 30°C for 1 hour with shaking. Samples were separated by 10 % SDS-PAGE, analysed by immunoblotting using APE1 antibodies, or with antibodies targeting HECTD1 (lower panel) and imaged using the Li-Cor Odyssey Infrared Imaging Analysis System.

## 5.4 *In vitro* ubiquitylation of the histone proteins by HECTD1

As there was no evidence of APE1 ubiquitylation, as predicted, I went onto examine *in vitro* ubiquitylation of histone proteins within the octamer. Again, I utilised the *in vitro* ubiquitylation assay but with the histone octamer and increasing concentrations of ΔN-HECTD1 (2.8-14.1 pmol) in the presence of one E1 activating enzyme, nine separate E2 conjugating enzymes, and ubiquitin. I investigated whether HECTD1 could ubiquitylate the individual histone proteins within the histone octamer, *in vitro*. On examination of histone H2A ubiquitylation, it does not appear, at least *in vitro*, to be a target for ubiquitylation by ΔN-HECTD1. In control conditions (Figure 5.5A, lane 1), where just the histone octamer, the E1 enzyme, E2 enzymes and ubiquitin (no ΔN-HECTD1) are present, as expected the 14 kDa histone H2A is visible, however given the multiple bands detected, especially at higher molecular weights (25-50 kDa), any statements drawn from this data cannot be considered a definitive conclusion. Yet, with increasing concentrations of ΔN-HECTD1 (Figure 5.5A, lanes 2-4), there was no difference in the detection of histone H2A (14 kDa) as a slower migrating species which would be expected if the protein was being ubiquitylated by ΔN-HECTD1 due to the addition of 8 kDa ubiquitin moieties. This indicated that ΔN-HECTD1 does not ubiquitylate histone H2A. Again, the poor quality of this antibody is evidenced by the cross-reactivity seen in control conditions (Figure 5.5A, lanes 5-8), where only the E1 enzyme, E2 enzymes, ubiquitin and increasing concentrations of ΔN-HECTD1 are present in reactions. Therefore, no histone H2A should be detected due to the absence of the histone octamer. However, given the visible banding in reactions (Figure 5.5A, lanes 5-8), both off-target and at ~14 kDa the apparent evidence that histone H2A is not a target for HECTD1 can not be accepted as fully conclusive. Similarly, it does not appear, at least *in vitro*, that histone H4 is a target for ubiquitylation by ΔN-HECTD1. In control conditions (Figure 5.5D, lane 1), where just the histone octamer, the E1 enzyme, E2 enzymes and ubiquitin (no ΔN-HECTD1) are present, as expected the 11 kDa histone H4 is visible. With increasing concentrations of ΔN-HECTD1 (Figure 5.5D, lanes 2-4), there is no difference in the detection of histone H4 (11 kDa) as a slower migrating species which would be expected if the protein was being ubiquitylated by ΔN-HECTD1 due to the addition of 8 kDa ubiquitin moieties. Furthermore, as histone H4 was not detected in duplicate control reactions (Figure 5.5D, lanes 5-8), where only the E1 enzyme, E2 enzymes, ubiquitin and increasing concentrations of ΔN-HECTD1 are present, it can be concluded that ΔN-HECTD1 does not ubiquitylate histone H4.

When examining histone H2B ubiquitylation by ΔN-HECTD1, again in control conditions (Figure 5.5B, lane 1), where just the histone octamer, the E1 enzyme, E2 enzymes and

ubiquitin (no ΔN-HECTD1) are present, histone H2B (17 kDa) was successfully detected. Furthermore, with increasing concentrations of ΔN-HECTD1 (Figure 5.5B, lanes 2-4), a gradual increase in a slower migrating species is visible, due to the addition of 8 kDa ubiquitin moieties and providing evidence of modest mono/diubiquitylation of histone H2B, this is particularly apparent in lanes 3 and 4 (Figure 5.5B, lanes 3-4). Furthermore, as histone H2B was not detected in duplicate control reactions (Figure 5.5B, lanes 5-8), where only the E1 enzyme, E2 enzymes, ubiquitin and increasing concentrations of ΔN-HECTD1 are present. Here, evidence of ΔN-HECTD1 mediated in mono/diubiquitylation of histone H2B is revealed. In addition, I also present more convincing evidence that ΔN-HECTD1 promotes histone H3 polyubiquitylation (Figure 5.5C, lanes 2-4). Again, in control conditions (Figure 5.5C, lane 1), where just the histone octamer, the E1 enzyme, E2 enzymes and ubiquitin (no ΔN-HECTD1) are present, histone H3 (17 kDa) was successfully detected. Also, with increasing concentrations of ΔN-HECTD1 (Figure 5.5C, lanes 2-4), a gradual but prominent increase in a slower migrating species of 25-35 kDa is visible, due to the addition of 8 kDa ubiquitin moieties. Importantly, no significant cross-reactivity in duplicate control reactions (Figure 5.5C, lanes 5-8), where only the E1 enzyme, E2 enzymes, ubiquitin and increasing concentrations of ΔN-HECTD1 are present was observed. Thus, providing evidence of polyubiquitylation of histone H3. Therefore, this data suggests that HECTD1 is promoting histone H2B/H3 ubiquitylation, and predictably that this is increasing accessibility of APE1 to the THF-IN mononucleosome substrate.

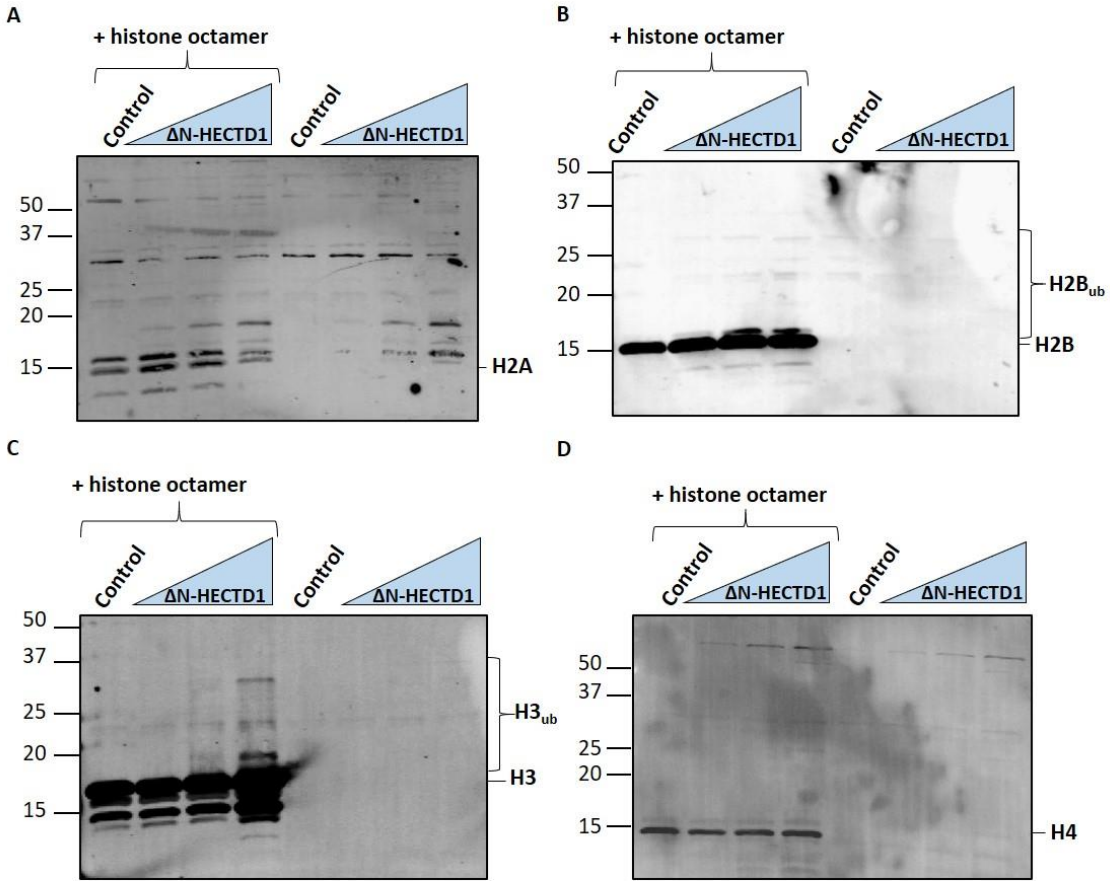


**Figure 5.5: In vitro ubiquitylation activity of the histone proteins by HECTD1**

*In vitro* ubiquitylation assays contained histone octamer (2 pmol) in the presence of increasing amounts of ΔN-HECTD1 (2.8–14.1 pmol), one E1 activating enzyme (0.7 pmol), nine separate E2 conjugating enzymes (2.5 pmol), and ubiquitin (0.6 nmol) (Ub). Reactions were incubated at 30°C for 1 hour with shaking. Samples were separated by 16 % SDS-PAGE, analysed by immunoblotting using **A** histone H2A, **B** histone H2B, **C** histone H3, **D** histone H4 antibodies and imaged using the Li-Cor Odyssey Infrared Imaging Analysis System. The respective control reactions (Control) were performed in the absence of any HECTD1.

## 5.5 *In vivo* ubiquitylation of the histone H2B and H3 by HECTD1

Given the promising *in vitro* evidence that ΔN-HECTD1 appears to ubiquitylate histones H2B and H3 in *in vitro* ubiquitylation assays, I went on to investigate if HECTD1 dependent ubiquitylation of histones H2B and H3 could be seen in a cellular environment. Therefore, I adopted an siRNA-mediated approach to effectively deplete the cellular levels of HECTD1. Thus, WI-38 cells were grown until 30-50 % confluent before being transfected with HECTD1 siRNA or Qiagen AllStars non-targeting control siRNA using Lipofectamine RNAiMax

transfection reagent. Cells were then incubated at 37°C and 5 % $CO_2$ in a humidified cell culture incubator for 48 hours. Following effective knockdown (section 6.2, Figure 6.1), cells were incubated on ice for 5 minutes to limit DNA repair activity and irradiated with 10 Gy IR. IR was selected as a DNA damaging agent as it is well known to generate a large proportion (>95 %) of DNA damage, including DNA base oxidation, AP sites and SSBs, processed by the BER pathway and is commonly used to assess the efficiency of BER in cultured cells as well overall cell sensitivity [246][337]. Following induction of DNA damage, cells were washed and returned to a humidified cell culture incubator set at 37°C and 5 % $CO_2$ for repair along a set time course. Repair was stopped at 0- 60-minutes post irradiation via cell harvesting. Histones were prepared using acid extraction and analysed via SDS-PAGE and immunoblotting.

On examination of histone H2B ubiquitylation, it does not appear, at least in WI-38 cells, to be a target for ubiquitylation by HECTD1. In control conditions (Figure 5.6A, lane 1), where WI-38 cells were treated with Qiagen AllStars non-targeting control siRNA, as expected the 17 kDa histone H2B is visible. Furthermore, in control conditions, immediately following induction of DNA damage (Figure 5.6A, lane 2), there appears to be no difference in the detection of histone H2B antibody cross-reactivity, perhaps to be expected, due to a lack of time available for repair to be initiated. However, along the time course, (Figure 5.6A, lanes 3-5), at 15- 60-minutes post irradiation, there too appears to be no difference in the detection of histone H2B as a slower migrating species which would be expected if the protein was being ubiquitylated by HECTD1 due to the addition of 8 kDa ubiquitin moieties. A similar profile is detected for histone H2B in conditions where the cellular levels of HECTD1 had been depleted (Figure 5.6A, lanes 7-11). This data suggests that histone H2B is not a target for HECTD1, at least in WI-38 cells. In addition, upon examination of the presence of ubiquitin in each sample, this further validates that histone H2B appears to not be a target for ubiquitylation by HECTD1. In conditions containing HECTD1, (Figure 6.6B, lanes 1-5), it appears that histone H2B is ubiquitylated, however, given that this is detected at 17 kDa, the expected molecular weight of unmodified histone H2B, not at 25 kDa, which would be expected given the addition of an 8 kDa ubiquitin moiety. This may be indicative of cross-reactivity of the antibody instead. Additionally, given that there is no increasing shifting of ubiquitin to higher molecular weight species across any control conditions post IR (Figure 6.6B, lanes 2-5), and that a similar detection of ubiquitin is observed in duplicate experiments where the cellular levels of HECTD1 had been depleted (Figure 5.6B, lanes 7-11). The

conclusion that histone H2B is not ubiquitylated by HECTD1 in WI-38 cells is seemingly confirmed.

However, upon examination of histone H3 ubiquitylation, it does appear, at least in WI-38 cells, that HECTD1 polyubiquitylates histone H3 (Figure 5.6C, lanes 2-5). In control conditions (Figure 5.6C, lane 1), where WI-38 cells were treated with Qiagen AllStars non-targeting control siRNA, as expected the 17 kDa histone H3 is visible. In addition to this, background levels of histone H3 polyubiquitylation is observed, evidenced by an apparent smearing above the unmodified histone H3 band, indicative of slower migrating species, due to the addition of 8 kDa ubiquitin moieties. In conditions immediately following induction of DNA damage (Figure 5.6C, lane 2), there appears to be a marked induction of histone H3 polyubiquitylation, above that of background levels (Figure 5.6C, lane 1). Additionally, histone H3 polyubiquitylation is sustained at all time points post IR (Figure 5.6C, lanes 3-5). Interestingly, although still present at 15-30-minutes post IR, there is a visible gradual decrease in the levels of histone H3 ubiquitylation (Figure 5.6C, lanes 3-4). Yet, at 60 minutes post IR, an induction of histone H3 polyubiquitylation (Figure 5.6C, lane 5), greater than levels seen at 0 minutes post IR (Figure 5.6C, lane 2), is observed. In unirradiated conditions where cellular HECTD1 levels are depleted, as expected the 17 kDa histone H3 is visible, and as in conditions containing HECTD1 (Figure 5.6C, lane 1), background levels of histone H3 polyubiquitylation are observed (Figure 5.6C, lane 7). However, immediately following IR exposure (Figure 5.6C, lane 8), there is no apparent induction above the background level (Figure 5.6C, lane 7) observed in control conditions of histone H3 ubiquitylation in the absence of HECTD1. Additionally, across the time course, (Figure 5.6C, lanes 9-11), there is no apparent induction of histone H3 ubiquitylation, particularly at 60 min post-IR. This suggests that the induction of histone H3 polyubiquitylation (seen in Figure 5.6C, lanes 2-5) is HECTD1 dependent. This is supported by evidence from probing with ubiquitin antibodies (Figure 5.6D). In conditions in the presence of HECTD1, it also appears that histone H3 is polyubiquitylated, and this polyubiquitylation is induced following IR treatment (particularly at time 0 and 60 min), given the detection of slower migrating ubiquitin species, which is expected when detecting ubiquitylated protein, due to the addition of 8 kDa ubiquitin moieties (Figure 5.6D, lanes 1-5). Additionally, in un-irradiated conditions where cellular HECTD1 levels are depleted, evidence of protein ubiquitylation is visible (Figure 5.6D, lane 7). However, immediately following IR exposure (Figure 5.6D, lane 8-11), there is no apparent induction of histone H3 ubiquitylation above the background level (Figure 5.6D, lane 7). Given that this detection of ubiquitin appears to mirror that seen when probing for histone

H3 in both control (Figure 5.6C, lanes 1-5) and HECTD1 depleted conditions (Figure 5.6C, lanes 7-11), it strengthens the evidence of HECTD1 dependent histone H3 polyubiquitylation presented. Thus, in combination with evidence from *in vitro* ubiquitylation assays, I provide strong evidence for HECTD1 targeting histone H3 for ubiquitylation in WI-38 cells.

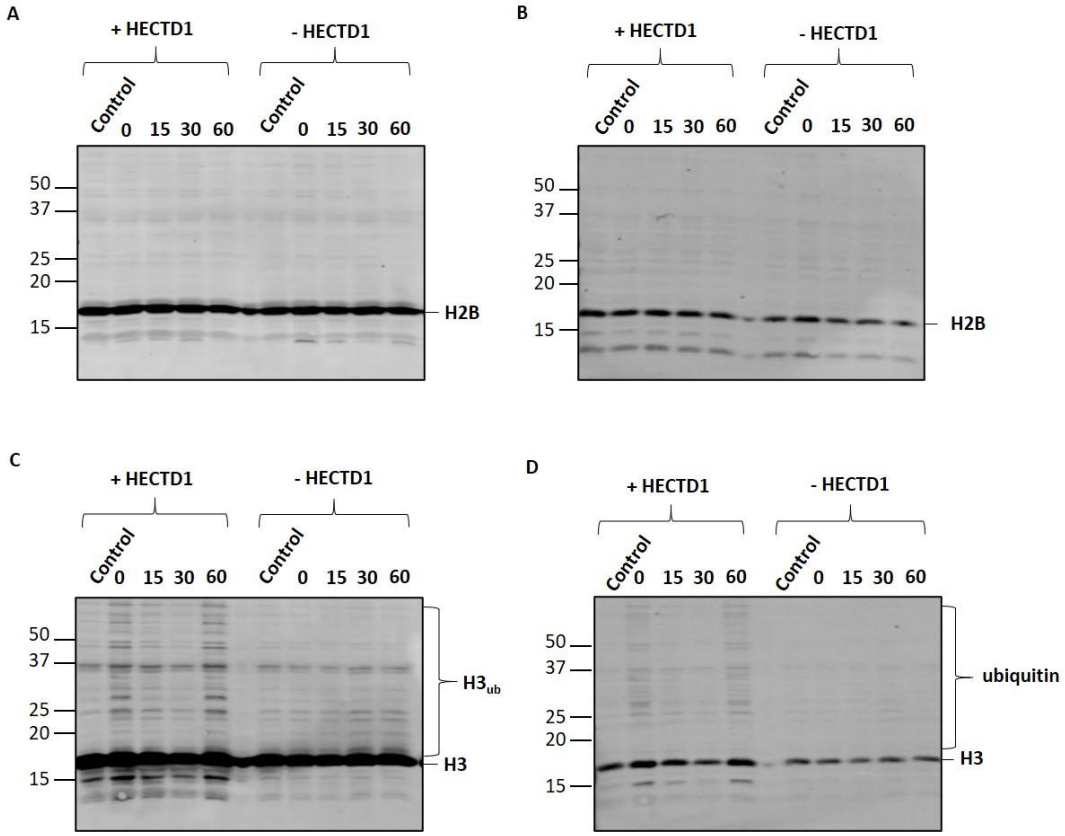


**Figure 5.6: *In vivo* ubiquitylation activity of histone H2B and H3 by HECTD1**

WI-38 cells were treated with 40 nM Qiagen AllStars non-targeting control (NT) siRNA (+ HECTD1) or HECTD1 siRNA (- HECTD1) for 48 hours. Cells were then unirradiated (control) or irradiated with 10 Gy IR and incubated at 37°C and 5 % $CO_2$ in a humidified cell culture incubator for zero (0), 15 (15), 30 (30) or 60 (60) minutes before cells were harvested, WCE prepared and analysed via 16 % SDS-PAGE and immunoblotting immunoblotting using **A** histone H2B, **B** ubiquitin, **C** histone H3, **D** ubiquitin antibodies and imaged using the Li-Cor Odyssey Infrared Imaging Analysis System.

## 5.6 Preparation of TG-IN site containing DNA

To elucidate the specificity of HECTD1 to either APE1 or as playing a more general role within BER, I aimed to investigate further stages of BER. To examine the role of HECTD1 within BER initiation by DNA glycosylases, in the first instance I generated DNA substrate containing a

site specific thymine glycol (TG), which would then be utilised for generating the lesion where the DNA backbone is inwardly facing within the nucleosome and therefore resistant to DNA glycosylase activity. Adopting the same protocol established in chapter 4, the Widom 601 nucleosome positioning sequence was amplified from the pGEM-3Z-601 plasmid using PCR and the central 17 bp removed using Van91l and BgII restriction enzymes to produce, once purified, two DNA sequence fragments. These were sequentially ligated to a pre-prepared 17 bp duplex oligonucleotide containing a TG site on the lower strand, resulting in the production of a site specific TG-IN DNA substrate, which when complexed with a histone octamer, generated a TG-IN mononucleosome substrate where the DNA backbone of the TG site faced inwards towards the histone octamer and was therefore occluded from excision by endonuclease III homologue (NTH1).

### 5.6.1 Amplification of the 601 nucleosome positioning sequence

The Widom 601 wild- type strong nucleosome positioning sequence was amplified from the pGEM-3Z-601 plasmid using PCR with 5'-fluroescent labelled primers (Section 4.2, Figure 4.2, stage 1). For production of TG-IN DNA, the forward primer was labelled with IRDye800 (green label) and the reverse with IRDye700 (red label), due to the increased signal intensity of the IRDye700 tag so TG incision could be more strongly visualised using the Odyssey Image Analysis system. As the DNA marker was not visible due to the use of fluorescently tagged primers, successful generation of the 256 bp 601 nucleosome positioning sequence PCR product was visualised as yellow, as the product contained both IRDye700 and IRDye800 5'-labelled ends, and the excess fluorescent primers were also clearly visible underneath each of the PCR products (Figure 5.7). The verified 256 bp DNA was subsequently purified using a PCR purification kit and the yield was found to be ~135 μg for 15 pooled PCR reactions.

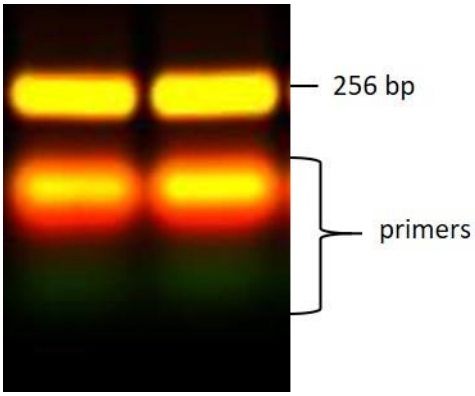


**Figure 5.7: Amplification of the 256 bp 601 nucleosome positioning sequence for production of TG-IN DNA**

PCR product of the 601 wild-type strong nucleosome positioning sequence containing both the IRDye800 and IRDye700 florescent tags and the IRDye800 forward primer IRDye700 reverse primer separated by electrophoresis on a 1.5 % agarose gel at 100 V for 1 hour, imaged using the Li-Cor Odyssey Infrared Imaging Analysis System.

### 5.6.2 Double restriction digest of the 601 nucleosome positioning sequence

Following purification of the 256 bp 601 nucleosome positioning sequence, the central 17 bp region was removed using Van91I and BglI restriction enzymes (region shown in section 3.1.1, Figure 3.1). These enzymes produced a IRDye800 tagged 127 bp DNA fragment and a IRDye700 tagged 106 bp DNA fragment, both with sticky ends to facilitate subsequent ligation (section 4.2, Figure 4.2, stage 2). Completion of the restriction digest was confirmed by comparison to the original purified 256 bp PCR product (Figure 5.8A, lane 1), where the Van91I and BglI digestion product (Figure 5.8A, lane 2) is absent of the 256 bp PCR product and only the 127 bp and 106 bp DNA fragments are present. The 127 bp and 106 bp DNA fragments were then purified from each other using PAGE separation and gel extraction. To assure efficiency in the production and purification of these digest products, the 106 bp (Figure 5.8B, lane 2) and 127 bp (Figure 5.8B, lane 3) DNA products were compared to the original PCR product (Figure 5.8B, lane 1). Again, as the DNA is fluorescently labelled, use of a DNA marker was not applicable here.

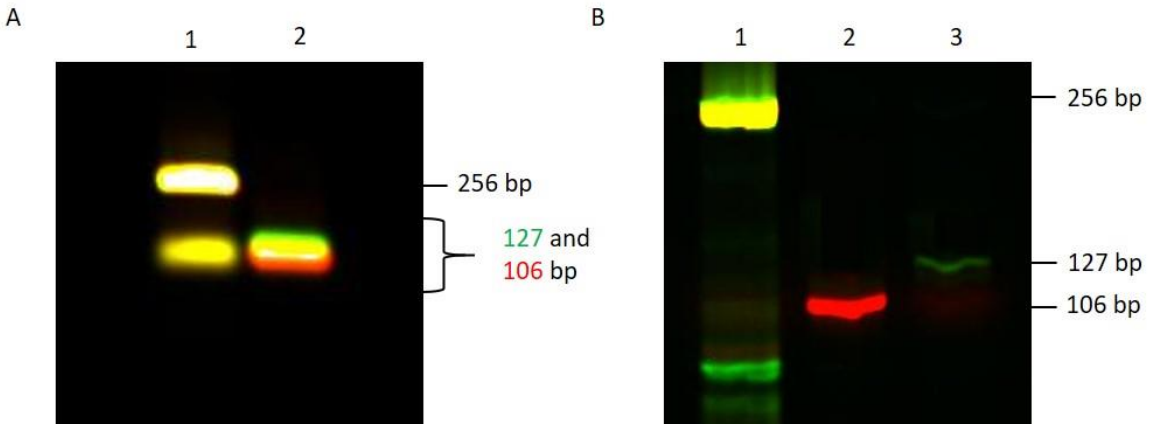


**Figure 5.8: 127bp and 106 bp Van91I/Bg11 restriction digest products**

**A.** Original 256 bp PCR product (lane 1) against the Van91l and BgII digestion product (lane 2) following separation by electrophoresis on a 1.5 % agarose gel at 100 V for 1 hour. **B.** Original 256 bp PCR product (lane 1) against the IRDye700 tagged 106 bp DNA digest product (lane 2) and IRDye800 tagged 127 bp DNA digest product (lane 3) following PAGE separation on an 8 % polyacrylamide gel in 0.5x TBE run at 175 V, 20 W for 3 hours, gel extraction and DNA purification. Gels were imaged using the Li-Cor Odyssey Infrared Imaging Analysis System.

### 5.6.3 Sequential ligations to incorporate the TG-IN site

To maximise ligation efficiency, the 127 bp and 106 bp DNA digest products were ligated sequentially to a 17 bp TG-IN containing duplex oligonucleotide with complimentary sticky ends (section 3.1.2.1, Table 3.2) (section 4.2, Figure 4.2, stage 3). In the first instance, the 127 bp segment was ligated to the TG-IN containing duplex oligonucleotide. This was successfully observed as a ligated 147 bp DNA ligation product (Figure 5.9A, lane 3) in comparison to the original 5'-IRDye800 labelled 127 bp DNA (Figure 5.9A, lane 2). This product was purified using the MinElute reaction clean up kit and then ligated to the 106 bp DNA digest product. Successful ligation was evidenced by the formation of the full 256 bp substrate DNA (Figure 5.9B, lane 3), in comparison to the unligated second ligation mix (Figure 5.9B, lane 2). This was purified using PAGE separation and gel extraction, and the successful purification of the final 256 bp substrate containing a site specific TG-IN site (Figure 5.9C, lane 2) was confirmed via comparison to the original purified PCR product (Figure 5.9C, lane 1). As before, the use of a DNA marker was not applicable here, due to the DNA being fluorescently labelled. This 256 bp substrate containing a site specific TG-IN site now could be used in the nucleosome reconstitution with the prepared histone octamer.

This demonstrates that I had successfully transferred this technique to generate a DNA substrate containing a site specific TG-IN site, which I could use to examine the effect of HECTD1 on NTH1 incision activity rates at occluded TG sites in mononucleosomes. For ease of quantification, the DNA substrates were labelled so the IRDye700, the most intense signal when imaging with the Li-Cor Odyssey Infrared Imaging Analysis System, was on the lower DNA strand, which would be incised by NTH1, therefore the incision rate by NTH1 could be better visualised and accurately quantified.

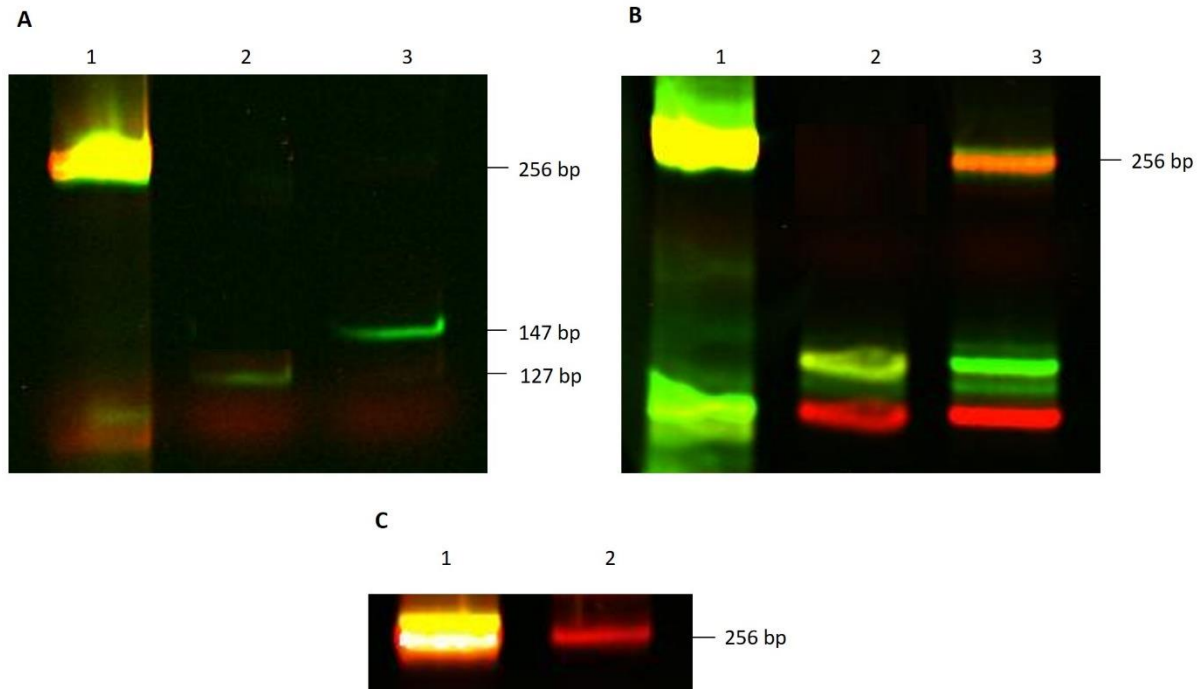


**Figure 5.9: Sequential Ligations to generate a 256 bp DNA substrate containing a TG-IN site** **A**. Ligation Reaction 1. Original 256 bp PCR product (lane 1), before (lane 2) and after ligation (lane 3) of the IRDye800 tagged 127 bp DNA with the 17 bp duplex TG-IN oligonucleotide. **B**. Ligation Reaction 2. Original 256 bp PCR product (lane 1), before (lane 2) and after the second ligation (lane 3) using the IRDye800 tagged 147 bp and IRDye700 tagged 106 bp DNA, producing a 256 bp product containing a TG-IN site. **C.** Original 256 bp PCR product (lane 1), final 256 bp substrate containing a site specific TG-IN site following purification by PAGE separation and gel extraction (lane 2). All PAGE gels contained 8 % polyacrylamide and 0.5x TBE, and were run at 175 V, 20 W for 3 hours, gels were imaged using the Li-Cor Odyssey Infrared Imaging Analysis System.

## 5.7 Generation of the TG-IN mononucleosome substrate

TG-IN mononucleosomes were reconstituted by incubation of the purified histone octamer with the site specific TG-IN DNA substrate, in a 1:1 ratio in a high salt (2 M NaCl) containing buffer. The reconstitution was then dialysed using a salt gradient to promote mononucleosome formation. This was confirmed by agarose gel electrophoresis, where a shift from the lower molecular weight of 256 bp free DNA to a higher molecular weight of approximately 750 kDa was observed (Figure 5.10), indicating successful nucleosome formation. Near full nucleosome reconstitution was observed (Figure 5.10, lane 3), with a reconstitution efficiency of 95 % deemed as acceptable for use of the mononucleosome substrate in *in vitro* BER repair assays to measure NTH1 activity.

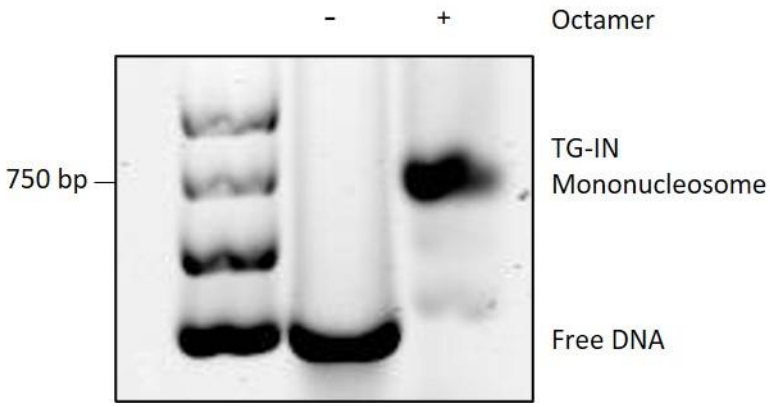


**Figure 5.10: Generation of a TG-IN Mononucleosome**

Nucleosome reconstitution was compared to free DNA (lane 2), whereby a shift from the 256 bp free DNA control, to a high molecular weight species (lane 3), approximately 700 bp, was observed when the TG-IN nucleosome was successfully formed. A 1:1 DNA: histone octamer ratio was used. DNA was separated using a 0.7 % agarose gel and electrophoresed in 0.2x TAE at 75 V for 1.5 hours. A 1 kb GeneRuler DNA ladder (lane 1) was utilised to identify the size of the DNA**.**

## 5.8 *In vitro* BER activity of NTH1 on the TG-IN mononucleosome substrate

In the first instance, TG-IN site incision within a mononucleosome substrate by increasing concentrations of recombinant NTH1 was examined. The percentage incision from an *in vitro* BER assay using a titration of NTH1 (0-270 pmol) was performed on the TG-IN mononucleosome substrate. Surprisingly, the TG-IN mononucleosome substrate (50 fmol)

was processed efficiently with 70 % cleavage achieved with 27 pmol NTH1 (a 540-fold excess) (Figure 5.11). Therefore, to achieve a comparable baseline incision to that of the THF-IN mononucleosome by APE1 of ~20 %, I decided to extrapolate from this titration curve and scale down the NTH1 concentration to 1.35 pmol (a 27-fold excess), to establish reaction conditions for a ΔN-HECTD1 titration.

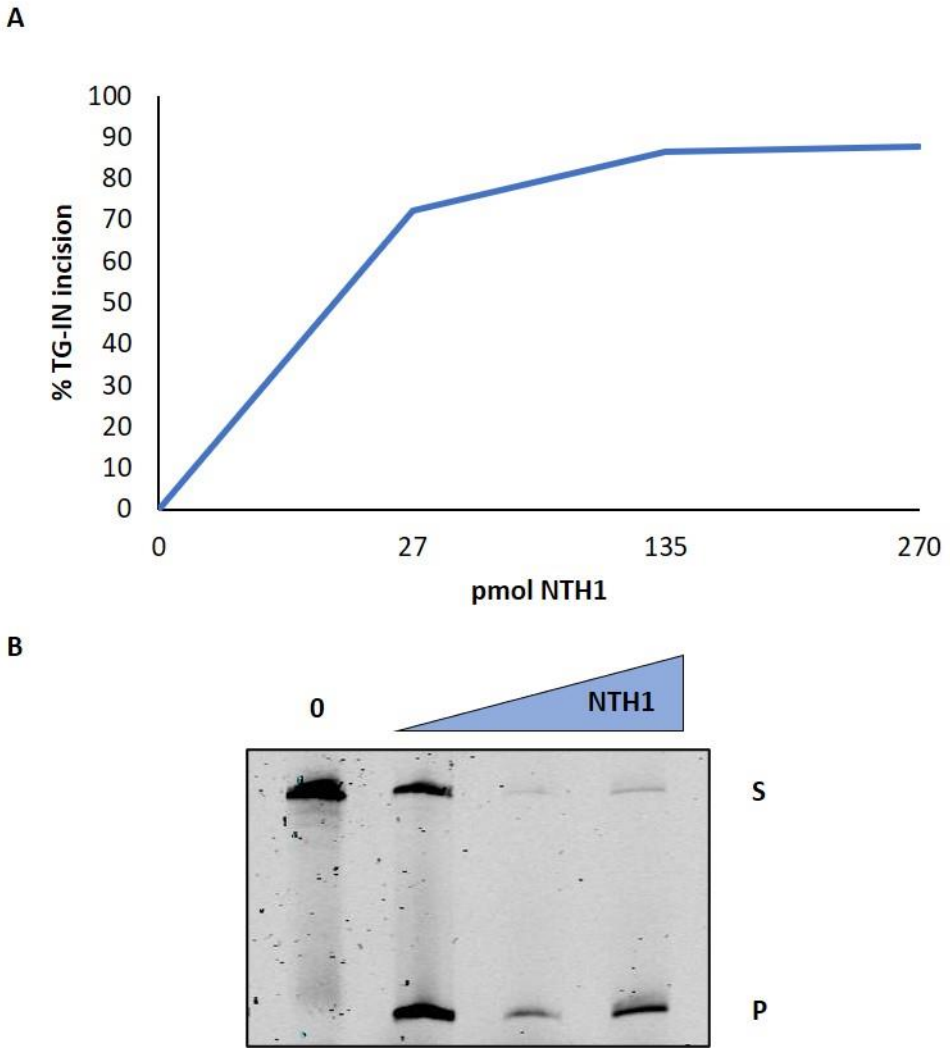


**Figure 5.11: NTH1 *In vitro* BER assay titration on TG-IN mononucleosome substrates**

**A** Purified recombinant NTH1 concentration titration (0-270 pmol) using TG-IN (blue) mononucleosome substrate and **B** representative gel with full length 256 bp DNA (S) and cleaved 116 bp TG-IN DNA (P) indicated. PAGE gels contained 8 % polyacrylamide, 7 M Urea and 1x TBE and were run at 300 V, 20 W for 1.75 hours, gels were imaged and percentage incision quantified using the Li-Cor Odyssey Infrared Imaging Analysis System. Shown is the percent substrate incision from one experiment.

## 5.9 *In vitro* BER activity of NTH1 and HECTD1 on TG-IN mononucleosome substrate

The ability of ΔN-HECTD1 to stimulate NTH1 activity on a TG-IN mononucleosome substrate was examined, from three independent *in vitro* BER assays using a titration of recombinant ΔN-HECTD1. I determined that ΔN-HECTD1 (0-15 pmol) was able to significantly stimulate the activity of recombinant NTH1 (1.35 pmol) against the TG-IN mononucleosome (50 fmol) substrate (in a substrate to enzyme ratio of 1:27) from 24 to 60 % TG-incision (Figure 5.12B, lanes 3-6 and Figure 5.12A (blue)), as determined by the proportion of cleaved 116 bp TG-IN DNA (P) relative to full length 256 bp DNA (S) (Figure 5.12B). When examining the effect of HECTD1 on TG site excision by NTH1 within the mononucleosome substrate an initial titration of 2 pmol ΔN-HECTD1 (a 40-fold excess in comparison to the substrate) resulted in a moderate increase in percentage TG-incision, from the observed control levels (24 %) to 33 % TG-incision. A further increase in the concentration of ΔN-HECTD1 in the reaction to 5 pmol (a 100-fold excess in comparison to the substrate), resulted in a similar degree of increase in percentage TG-incision from 33 % TG-incision achieved with 2 pmol ΔN-HECTD1 to 40 % TG-incision. The following incubation with 10 pmol ΔN-HECTD1 (a 200-fold excess in comparison to the substrate), resulted in a significant shift in NTH1 incision of the TG-IN mononucleosome, reaching 54 % TG-incision, with the final titration step, an incubation of 15 pmol ΔN-HECTD1 (a 300-fold excess in comparison to the substrate), reaching the observed maximum of 60 % TG-incision of the TG-IN mononucleosome by NTH1.

It was also important to verify that ΔN-HECTD1 alone had no impact on the incision of the TG-IN mononucleosome. Therefore, except for the absence of NTH1, in the same reaction conditions the TG-IN substrate was incubated with a titration of recombinant ΔN-HECTD1 (0-15 pmol) alone in the *in vitro* BER assay. In the absence of NTH1, I observed no significant incision of the TG site, with percentage TG-incision, as determined by the proportion of cleaved 116 bp TG-IN DNA (P) relative to full length 256 bp DNA (S) (Figure 5.12B), remaining at control levels at all ΔN-HECTD1 titration points (Figure 5.12A (orange)). Therefore, I can conclude that there was no impact of ΔN-HECTD1 alone on incision of the TG-IN substrate (Figure 5.12B, lanes 7-10 and Figure 5.12A (orange)). These data provide evidence that HECTD1 appears to promote both BER initiation by DNA glycosylases and AP site incision.

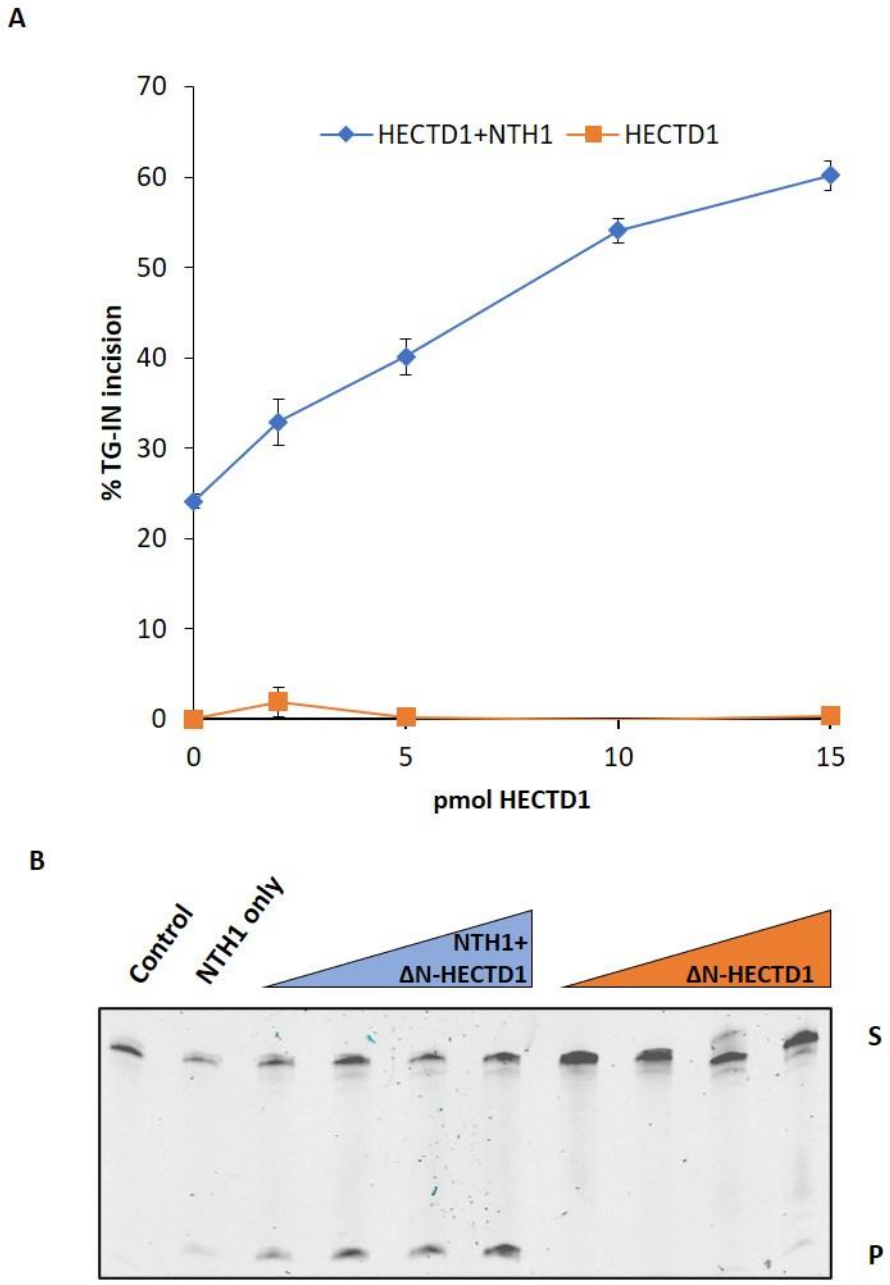


**Figure 5.12: HECTD1 promotes incision of TG-IN mononucleosome substrate by recombinant NTH1 *in vitro***

Stimulation of NTH1-dependent incision of the TG-IN mononucleosome substrate by ΔN-HECTD1. **A** Purified recombinant ΔN-HECTD1 concentration titration (0-15 pmol) using TG-IN mononucleosome substrate in the presence (blue) and absence (orange) of NTH1 (1.35 pmol) and **B** representative gel with full length 256 bp DNA (S) and cleaved 116 bp TG-IN DNA (P) indicated. PAGE gels contained 8 % polyacrylamide, 7 M Urea and 1x TBE and were run at 300 V, 20 W for 1.75 hours, gels were imaged and percentage incision quantified using the Li-Cor Odyssey Infrared Imaging Analysis System. Shown is the mean percent substrate incision ± S.E. from three independent experiments.

## 5.10 Summary

In the previous chapter, I established an *in vitro* role of HECTD1 in BER where it acts to promote APE1 activity at occluded THF sites. To investigate the mechanism behind this role, I initially aimed to examine whether HECTD1 was acting via nucleosome sliding to relocate histone octamers to adjacent DNA segments, therefore, altering the accessibility of the occluded THF site to APE1. Unfortunately, I was unable to optimise the DNase footprinting assay for my needs, despite optimisation on the free DNA substrate using DNase, I was unable to examine the *in vitro* BER reactions. This could be a result of unsuccessful ethanol precipitation of DNA or inefficient DNA extraction using phenol:chloroform thus leading to a loss of DNA, which is not unexpected given the complexity of this approach. Furthermore, I was unable to mitigate this with increasing concentrations of the THF-IN mononucleosome. Therefore, I am unable to conclude whether HECTD1 does or does not act via a DNA sliding or eviction mechanism.

Another aim in this chapter was to establish the target/s of ubiquitylation. Firstly, I show utilising *in vitro* ubiquitylation assays that ΔN-HECTD1 does not stimulate APE1 ubiquitylation, therefore is not increasing AP endonuclease enzymatic activity. This finding is corroborated by previously published gel shift mobility assays which observed reduced substrate cleavage with inwardly facing lesions, that was as a consequence of reduced binding of APE1 to the inwardly facing substrate, rather than reduced APE1 activity [248]. Additionally, a further study demonstrated that two naturally occurring variants of APE1, R237C and G241R, have reduced activity on both inwardly and outwardly facing AP sites containing 147 bp 601 DNA within mononucleosome substrates, but not on naked DNA, despite the variants not demonstrating any dramatic differences in mononucleosome binding [249]. Furthermore, a 15-fold reduction in mononucleosome AP site reactivity with histone proteins was observed with incorporation of mutant histone H4. Of note, these mutations (five lysine residues to arginines) were in the amino tail region of histone H4, predicting the involvement of histone tails and PTMs in DNA strand cleavage [250]. Therefore, this evidence, in support of my own findings, suggests that APE1 itself may not be the target of any PTM or ACR involved in chromatin remodelling within BER.

As there was no evidence of APE1 and HECTD1 interaction, I moved to examine *in vitro* ubiquitylation of histone proteins within the octamer. This revealed evidence that ΔN-HECTD1 appears to cause a modest increase in mono/diubiquitylation of histone H2B, but more convincingly promotes histone H3 polyubiquitylation. Furthermore, I also provide

preliminary evidence of HECTD1 dependent histone H3 ubiquitylation in WI-38 cells. Interestingly, a biphasic induction of histone H3 ubiquitylation was observed and could be indicative of the repair of DNA damage in less compact regions at the induction of DNA damage, seen at 0 minutes post IR. Followed by repair of DNA damage in heterochromatin, where there is a requirement for DNA unwinding, and particularly at 60 minutes post IR I observed histone H3 ubiquitylation, suggestive of alternative chromatin remodelling events. Although preliminary in nature, these findings are exciting given that our general understanding of ubiquitylation events that can affect chromatin structure, particularly during BER, is unfortunately not well characterised. Currently, the most extensive evidence of histone ubiquitylation is histone H2B monoubiquitylation at K120, associated with active chromatin and found on 1-1.5 % of total H2B in mammals [338]. My evidence *in vitro* of ΔN-HECTD1 dependent mono/diubiquitylation of histone H2B could be indicative of this monoubiquitylation event in promoting BER. Utilising a more extensive approach with antibodies specific for H2BK120 ubiquitylation and indeed other less well characterised histone H2B ubiquitin docking sites (K34, K46, K108, K116, and K125) [339], [340] would provide further validation to this claim. However, given the more convincing evidence of histone H3 ubiquitylation I present, any future attentions to elucidate the mechanism via which HECTD1 is acting should primarily focus on histone H3 ubiquitylation, which appears the strongest target. Previous reports have shown an involvement of histone H3 ubiquitylation in DNA repair, namely, the implication of CUL4–DDB–ROC1 mediated ubiquitylation of histone H3 and H4 in NER [341] and the role of NEDD4-mediated ubiquitylation of histone H3 at K23/K36/K37 in transcription activation via stimulation of the histone acetyltransferase GCN5 [340]. Also, as histone H3 ubiquitylation has only been found to occur globally on 0.3 % of H3 histones [340]–[342], this may be suggestive of a specific role for histone H3 ubiquitylation in the DDR, therefore a focus on histone H3 ubiquitylation may further elucidate a mode of action for HECTD1 in BER.

A final aim of this chapter was to begin to elucidate the specificity of HECTD1 to either APE1 or as playing a more general role within BER. Previous studies have established in *in vitro* mononucleosome studies that DNA glycosylase recognition of the DNA base lesion is dependent on lesion orientation. Examples, using chicken erythrocyte histones and TG nucleosome positioning sequence DNA to generate mononucleosomes, demonstrated a 2-3-fold increase in excision by UDG and APE1 of the outwardly facing versus the inwardly facing mononucleosome substrate [238]. Similarly, an assessment of the activity of UDG and APE1 against mononucleosomes containing the 601 DNA sequence present a 3-5-fold more

effective excision of the out substrate in comparison to IN mononucleosome substrates [239]. Furthermore, compromised incision of inwardly facing TG substrates by NTH1 alone, seen by a 2-fold reduction in NTH1 activity against mononucleosomes containing inwardly facing TG site in a 184 bp DNA fragment containing the *L. variegatus* 5S ribosomal DNA nucleosome positioning sequence constructed with recombinant *X. laevis* histones, has also previously been presented [244]. This is supported by a comparative study utilising similar substrates assessing the activity of NTH1, where only 10 % of the inwardly facing TG sites from mononucleosomes were processed [245]. In this chapter, I examined the role of HECTD1 within BER initiation by generating a site specific TG-IN DNA substrate, in the same manner as established in the previous chapter for THF-IN. I determined that ΔN-HECTD1 was able to significantly stimulate the activity of recombinant NTH1 against the TG-IN mononucleosome substrate from 24 to 60 %. Although this is a key finding in establishing the specificity of HECTD1 in stimulating BER, this needs to be confirmed using multiple different DNA lesion-containing mononucleosome substrates reflecting the alternative steps of BER and including the appropriate BER enzymes *in vitro*. Primarily this would involve investigations with GAP and NICK mononucleosome substrates, incorporating the end processing mechanisms of BER. In the first instance, an assessment of GAP-IN vs OUT mononucleosome processing by Pol β would be of interest. Of note, it would be vital to incorporate THF, uracil and TG substrates and the respective enzymes (APE1, UDG and NTH1) to generate a natural SSB flanked by 5'-dRP ends to more fully assess the action of Pol β which necessitates both dRPase and DNA polymerase activity. Similarly, the impact of chromatin on DNA ligation, particularly XRCC1-Lig IIIα complex, should be assessed using the appropriate nick-containing substrates. Furthermore, in addition to measuring the impact of chromatin on the individual enzymes, and of HECTD1 in stimulating these, it is also vital to consider the efficiency of the complete repair process. Therefore, for example, examining processing of TG substrates in different locations and/or orientations when supplemented with NTH1, APE1, Pol β and XRCC1-LigIIIα and analysing the final product is of significant interest. Thus, further elucidation of HECTD1's mode of action may be gained through these more expansive *in vitro* studies.

In summary, I have provided evidence that HECTD1 is promoting THF-IN incision within mononucleosomes by APE1, via histone H2B/H3 ubiquitylation. Additionally, I have also acquired evidence that HECTD1 is able to stimulate the excision of a TG-IN containing mononucleosome substrate by NTH1, suggesting that HECTD1 may be able to promote multiple stages of BER. Given this *in vitro* data, demonstrating that HECTD1 is able to

promote both NTH1 and APE1 during DNA base excision and strand incision, it would be prudent to examine the requirement for HECTD1 *in vivo.* In the following chapter, I will assess the role of HECTD1 in the survival and DNA damage repair kinetics of normal lung fibroblasts in response to a variety of DNA damaging agents; x-ray irradiation, $H_2O_2$ and MMS, to elucidate how specific or indeed general the role HECTD1 plays in BER in normal cell physiology.

# CHAPTER 6: RESULTS III

## Dependence of HECTD1 in a cellular environment

### 6.1 Introduction

Cellular DNA is subject to constant attack by ROS, generating an estimated 10 000 DNA base lesions and SSBs per cell per day due to DNA hydrolysis, cellular oxidative metabolism and exposure to exogenous sources such as IR, which, if left unrepaired compromise genomic integrity [7]. Maintaining genome integrity is essential to ensure competent biochemical functions, cellular survival and ultimately the error-free passage of the genome to future progeny. BER, a sophisticated cellular mechanism, plays a vital role in repairing DNA base damage and SSBs, thus reducing the frequency of cellular mutations threatening genomic integrity [167]. Unsurprisingly, it is of the upmost importance to tightly regulate the DNA repair proteins involved in BER, ensuring an effective and coordinated response. One such mode of regulation is the action of ubiquitylation on BER [177], [343].

Ubiquitylation mediated regulation of BER has clearly been demonstrated to have wide ranging effects on the proteins involved in the repair pathway and, thus impacts the DDR. Furthermore, through investigating how E3 ubiquitin ligases alter their target proteins, in a multitude of ways, including the steady state levels of the protein, function or enzymatic activity and cellular localisation *in vivo*, we can improve our understanding of BER and the DDR within a cellular context. This knowledge can aid with the understanding of misregulation of the BER pathway, which can lead to the accumulation of SSBs, AP sites and oxidised DNA bases, all of which compromise genomic integrity. This been implicated in human disease development including premature ageing, neurodegenerative diseases and several cancers. This could form the basis of the development of novel therapeutics, such as small molecular inhibitors, to improve current treatment of these diseases (for example, radiotherapy) targeting E3 ubiquitin ligases involved in the regulation of BER proteins.

It must also be highlighted that HECTD1 is known to be mutated, deleted and amplified in a variety of cancers, including but not limited to, breast, brain and lung (small lung cell carcinoma and lung adenocarcinoma) cancers). Therefore, in addition to reports

demonstrating roles of HECTD1 in controlling cell signalling, proliferation and migration [303], [308], [312], [314], [318], it is important to examine the role of HECTD1 in the promotion of efficient repair of DNA base damage and investigate its function within normal cell physiology.

In previous chapters, I have highlighted the role of HECTD1 in promoting BER *in vitro,* demonstrating the ubiquitylation dependent promotion of APE1 and NTH1 activity on occluded THF and TG sites, respectively, via H2B/H3 ubiquitylation. Logically, I also aimed to establish this role of HECTD1 in cultured cells *in vivo* and in the forthcoming chapter will investigate the requirement of HECTD1 in normal cell physiology. Utilising siRNA targeting HECTD1 to effectively deplete the protein levels in normal lung fibroblasts, I used the clonogenic survival assay and the single cell gel electrophoresis (comet) assays to examine the requirement of HECTD1 in promoting cell survival and effective DNA repair kinetics to elucidate the role of HECTD1 in a cellular context.

## 6.2 Effect of siRNA knockdown of HECTD1 on steady state levels of HECTD1

To investigate HECTD1 in a cellular environment, it was essential to firstly test, and if necessary optimise, HECTD1 knockdown efficiency. A pool of four siRNA sequences, to increase knockdown efficiency, was used to test transfection and HECTD1 knockdown in three normal lung fibroblast cell lines; AG06173, AG16409 and WI-38. These cell lines were used in future experiments as my aim was to understand the role of HECTD1 in normal cell physiology. In particular, the WI-38 cell line was adopted for use in clonogenic survival assays, where the AG06173 and AG16409 were not appropriate due to their lack of colony forming ability.

AG06173, AG16409 and WI-38 cells were grown until 30-50 % confluent before being transfected with 40 nM HECTD1 siRNA pool using Lipofectamine RNAiMax transfection reagent. As a control, duplicate cells were transfected with Qiagen AllStars non-targeting control siRNA. Cells were then incubated at 37$^{o}$C and 5 % $CO_2$ in a humidified cell culture incubator for 48 hours. Following this, cells were harvested and WCE generated. Protein extracts were then separated by 4-12 % gradient SDS-PAGE and analysed via immunoblotting using HECTD1 and tubulin specific antibodies. From the immunoblot analysis, in comparison to the Qiagen AllStars non-targeting control, it is clear that the levels of HECTD1 protein has been effectively knocked down in all three cell lines. Additionally, equal loading is

demonstrated by the equivalent protein levels of tubulin in comparative samples (Figure 6.1). To confirm this qualitative assessment of HECTD1 knockdown, the HECTD1 and tubulin protein bands were quantified using the Li-Cor Odyssey Infrared Imaging Analysis System. Levels of HECTD1 relative to tubulin quantified and shown in Figure 6.1D is the HECTD1/tubulin ratio normalised to the Qiagen AllStars non-targeting control transfected control cells, which was set to 1.0. All three cell lines exhibited sufficient HECTD1 knockdown following HECTD1 siRNA treatment, with a relative knockdown efficiency of 84 % in the AG06173's, 86 % in the AG16409's and 88 % in the WI-38's (Figure 6.1D).

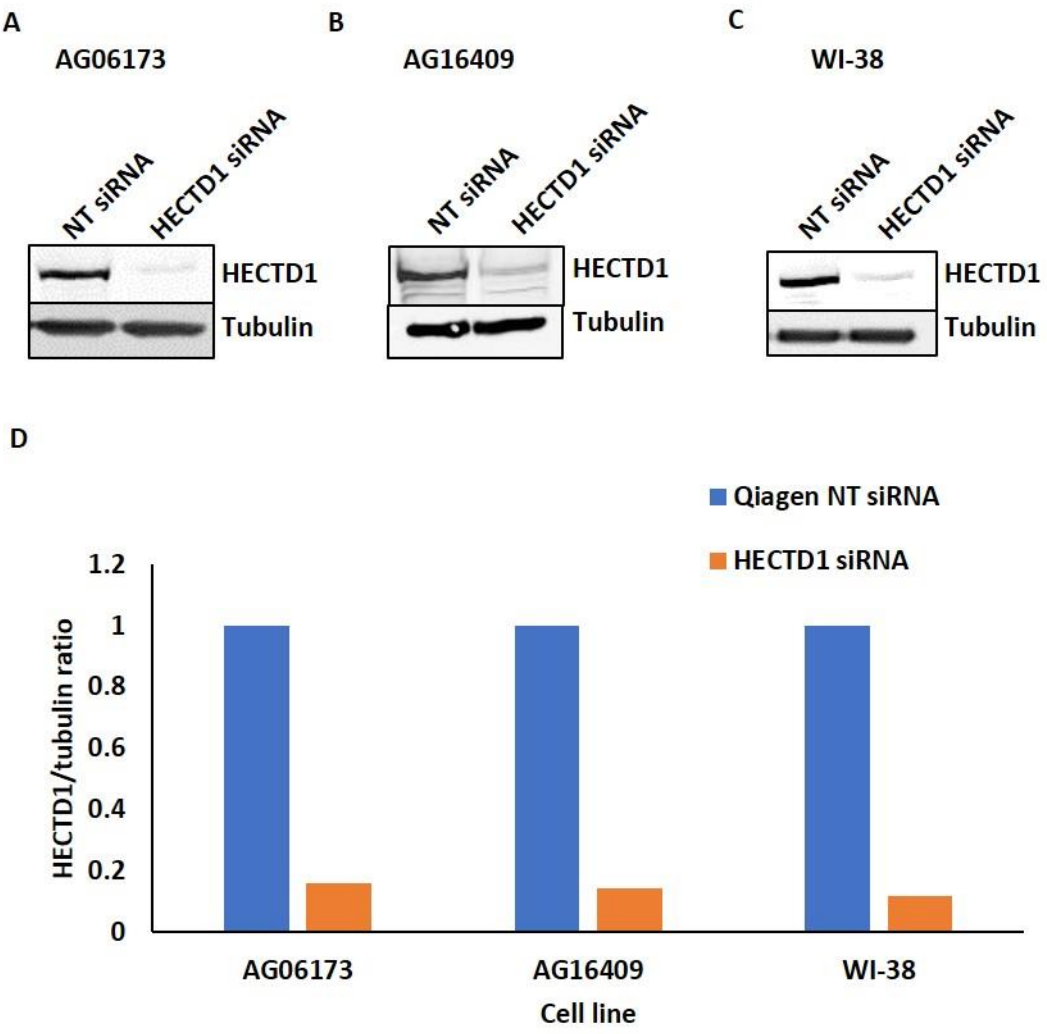


**Figure 6.1: Knockdown of HECTD1 using siRNA pool in normal lung fibroblast cell lines**

**A** AG06173, **B** AG16409, **C** WI-38 cells grown until 30-50 % confluent and then treated with Lipofectamine RNAiMax transfection reagent in the presence of Dharmacon HECTD1 siRNA or Qiagen AllStars non-targeting control (40 nM) for 48 hours. Cells were harvested and WCE prepared and analysed via 4-12 % gradient SDS-PAGE and immunoblotting using HECTD1 and tubulin specific antibodies. Membranes were imaged and quantified using the Li-Cor Odyssey Infrared Imaging Analysis System. **D** Levels of HECTD1 relative to tubulin, from one experiment, was quantified and shown as the HECTD1/tubulin ratio normalised to the Qiagen AllStars non-targeting control transfected control cells, which was set to 1.0.

## 6.3 Analysis of cell survival following HECTD1 siRNA knockdown

After demonstrating the involvement of HECTD1 in promoting efficient BER *in vitro* (Chapter 4 and 5), I hypothesised that this had an impact on overall cell survival. This was investigated

in the normal lung fibroblast cell line, WI-38, due to its colony forming ability, using the clonogenic survival assay, which assesses a cells ability to grow and form a colony of >50 cells, following induction of DNA damage. To induce DNA damage, cells were treated with increasing doses of either IR, $H_2O_2$ or MMS to investigate the full range of DNA base lesions and SSBs repaired by the BER pathway. Relative colony forming units (surviving fraction) were expressed as colonies per treatment relative to colonies observed in the untreated control for each treatment. Statistical analysis was performed by the CFAssay for R package [326].

### 6.3.1 Clonogenic cell survival following IR

WI-38 cells were grown until 30-50 % confluent before being transfected with HECTD1 siRNA or Qiagen AllStars non-targeting control siRNA using Lipofectamine RNAiMax transfection reagent. Cells were then incubated at 37$^{o}$C and 5 % $CO_2$ in a humidified cell culture incubator for 48 hours. Following effective knockdown (Figure 6.1), cells were incubated on ice for 5 minutes to limit DNA repair activity and irradiated with increasing doses of IR (0-4 Gy). IR was selected as a DNA damaging agent as it is well known to generate a large proportion (>95 %) of DNA damage, including DNA base oxidation, AP sites and SSBs, processed by the BER pathway and is commonly used to assess the efficiency of BER in cultured cells as well overall cell sensitivity [246][337]. After induction of DNA damage, the cells were trypsinised and counted. A defined number of cells (Table 3.9) were then seeded into six-well plates and incubated for 7 days at 37$^{o}$C and 5 % $CO_2$ in a humidified cell culture incubator to allow colony growth (Figure 6.2B). As a control, unirradiated WI-38 cells treated with either HECTD1 siRNA or Qiagen AllStars non-targeting control siRNA was used. The colonies were fixed with 6 % glutaraldehyde, stained with 0.5 % crystal violet and counted using the GelCount colony counter from Oxford Optronix (Oxford, UK). From three independent experiments, colonies were calculated and normalised to that of the untreated control, which was set to 1.0 (Figure 6.2).

From the analysis of the clonogenic assay I was able to show significantly decreased survival, at 4 Gy IR of HECTD1 depleted WI38 cells (16.7-fold reduction versus unirradiated cells) compared to NT siRNA treated cells (10-fold reduction in survival) in response to x-ray irradiation (Figure 6.2A). The decrease in survival associated with HECTD1 depletion is most apparent at an IR dose of 1 Gy where a 2.2-fold decrease in survival is observed in HECTD1 depleted WI38 cells compared to a 1.1-fold decrease in survival of NT siRNA treated cells.

The decrease in survival associated with increasing IR dose to 2 Gy, again was more apparent in HECTD1 depleted WI38 cells, where a further 2.3-fold reduction is survival was observed in comparison to a 1.7-fold decrease in survival of NT siRNA treated cells. A further 3.3-fold reduction in survival was seen with increased IR dose from 2 Gy to 4 Gy is HECTD1 siRNA treated cells. However, a 5.4-fold reduction in survival was observed with increased IR dose from 2 Gy to 4 Gy in NT siRNA control cells. However, this greater dose effect at 4 Gy is most likely indicative of the cytotoxicity associated with higher doses of X-ray IR and not an effect of the Qiagen NT siRNA on the WI-38 cells. Furthermore, as the overall decrease in cell survival was greater in HECTD1 depleted cells (16.7-fold) than NT control cells (10-fold), I concluded that HECTD1 knockdown resulted in reduced survival following X-ray IR exposure. This is verified by statistical analysis of the surviving fraction following irradiation, which revealed that a HECTD1 knockdown caused a statistically significant ($p<0.001$) increase in sensitivity to radiation-induced cell killing, when compared to the control NT siRNA treated cells.

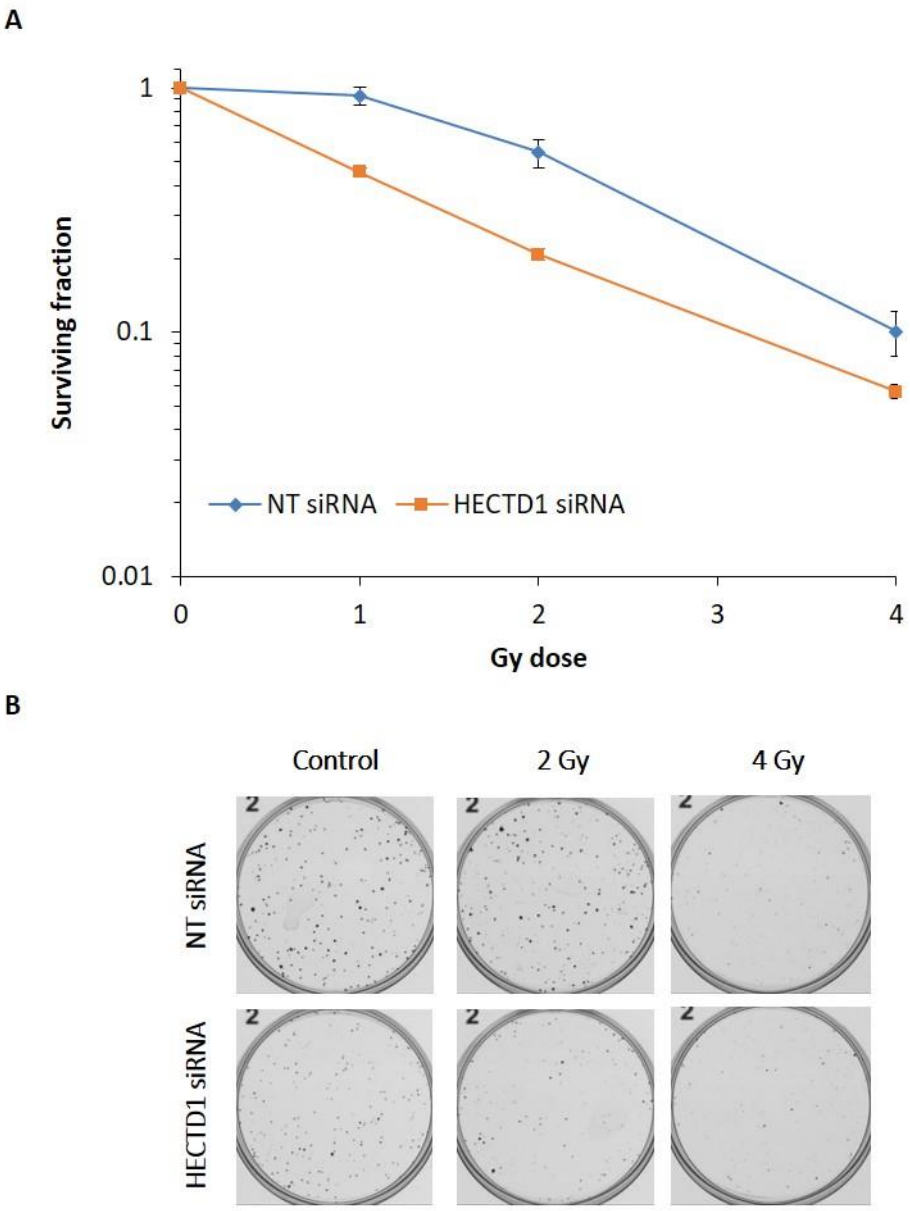


**Figure 6.2: HECTD1 depletion enhances cellular radiosensitivity to ionising radiation**

**A** Clonogenic survival of WI-38 cells treated with 40 nM Qiagen AllStars non-targeting control (NT) siRNA (blue) or HECTD1 siRNA (orange) for 48 hours. Cells were then unirradiated (control) or irradiated with increasing doses of x-ray irradiation (0-4 Gy), trypsinised, counted and a defined number plated into 6 well plates. Increasing cell numbers were used for increasing doses of x-ray irradiation to account for cellular plating efficiencies. Colonies were allowed to grow for 7 days prior to staining. Colonies were counted using the GelCount colony counter (Oxford Optronix, Oxford, UK). Shown are the mean surviving fractions with standard error from at least three independent experiments. $p<0.001$ as analysed by the CFAssay for R package. **B** Representative clonogenic plate images of cells treated with NT siRNA or HECTD1 siRNA following irradiation treatment (control, 2 or 4 Gy).

### 6.3.2 Clonogenic cell survival following $H_2O_2$

WI-38 cells were grown until 30-50 % confluent before being transfected with HECTD1 siRNA or Qiagen AllStars non-targeting control siRNA using Lipofectamine RNAiMax transfection reagent. Cells were then incubated at 37°C and 5 % $CO_2$ in a humidified cell culture incubator for 48 hours. Following effective knockdown (Figure 6.1), cells were incubated with increasing does of $H_2O_2$ (0-300 µM) at 37°C and 5 % $CO_2$ in a humidified cell culture incubator. $H_2O_2$ was selected as a DNA damaging agent as it is well known to generate oxidative DNA damage processed by BER. After induction of DNA damage, the cells were trypsinised and counted. A defined number of cells (Table 3.9) were then seeded into six-well plates and incubated for 7 days at 37°C and 5 % $CO_2$ in a humidified cell culture incubator to allow colony growth (Figure 6.3B). As a control, WI-38 cells treated with either HECTD1 siRNA or Qiagen AllStars non-targeting control siRNA but untreated with $H_2O_2$ was used. The colonies were fixed with 6 % glutaraldehyde, stained with 0.5 % crystal violet and counted using the GelCount colony counter from Oxford Optronix (Oxford, UK). From three independent experiments, colonies were calculated and normalised to that of the untreated control, which was set to 1.0 (Figure 6.3).

From the analysis of the clonogenic assay I was able to also show HECTD1 depleted WI38 cells compared to NT siRNA treated cells were more sensitive to the cell killing effects of $H_2O_2$ (Figure 6.3A). Overall, in comparison to control conditions, I observed a 50-fold reduction in survival associated with a HECTD1 depletion, compared to a 9-fold decrease in NT siRNA treated cells following exposure to 300 µM $H_2O_2$. At all $H_2O_2$ doses investigated, the fold decrease in survival was greater in HECTD1 siRNA treated cells with the cell killing effects of $H_2O_2$ increasing with dose. Fold decrease in survival between control and 50 µM $H_2O_2$ treated HECTD1 depleted cells was 1.5-fold, with a 2.2-fold, 3-fold and 5-fold decrease in survival at 100, 200 and 300 µM $H_2O_2$, respectively. This trend was not seen in NT siRNA treated cells, with a fold decrease in survival of ~2-fold between each dose increase. Furthermore, statistical analysis shows a significant ($p<0.001$) decrease in the surviving fraction of a HECTD1 knockdown cells following $H_2O_2$ exposure compared to that of NT siRNA treated cells, demonstrating an increase in sensitivity to $H_2O_2$-induced cell killing associated with HECTD1 depletion.

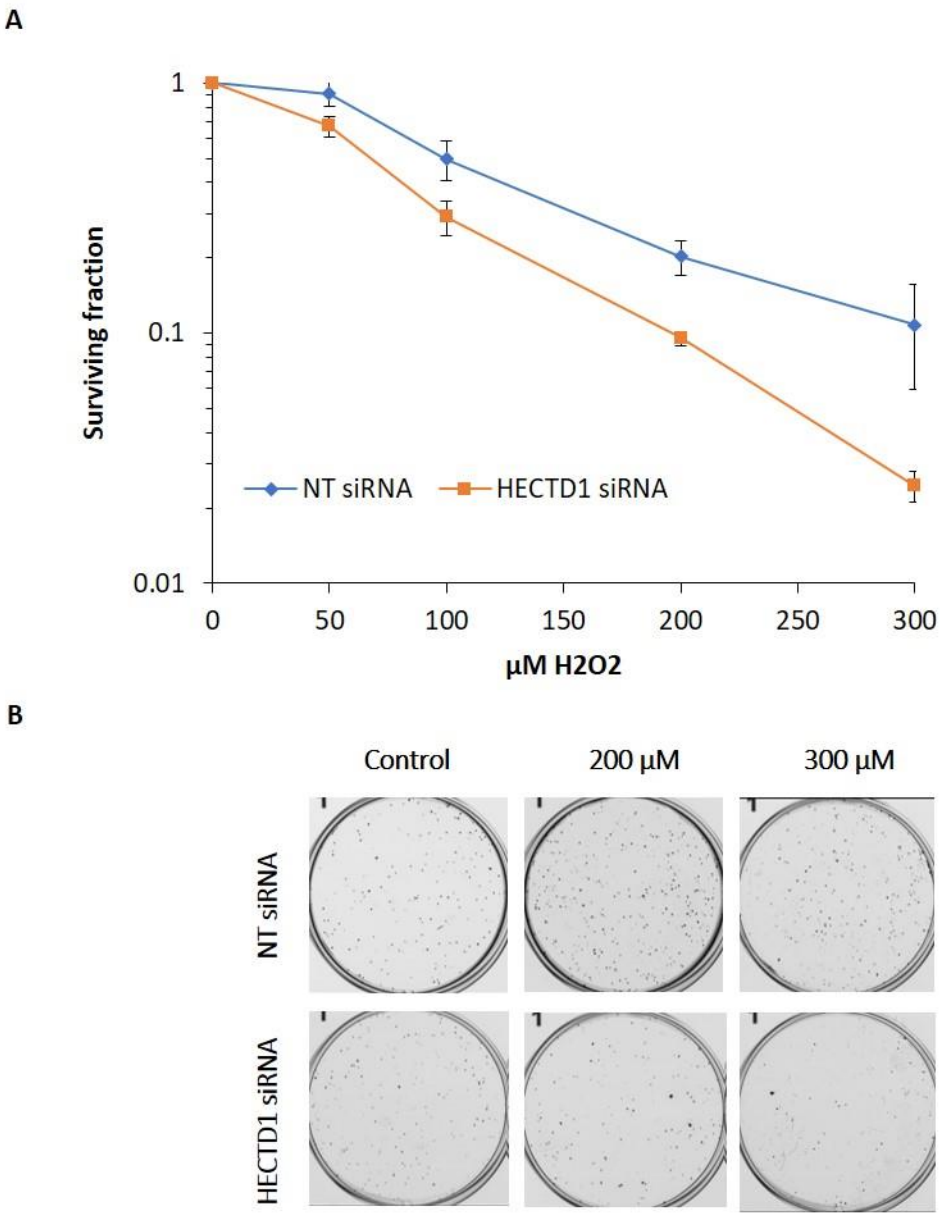


**Figure 6.3: HECTD1 depletion enhances cellular radiosensitivity to hydrogen peroxide**

**A** Clonogenic survival of WI-38 cells treated with 40 nM Qiagen AllStars non-targeting control (NT) siRNA (blue) or HECTD1 siRNA (orange) for 48 hours. Cells were then untreated (control) or incubated with increasing doses of $H_2O_2$ (0-300 µM) at 37°C and 5 % $CO_2$ in a humidified cell culture incubator, trypsinised, counted and a defined number plated into 6 well plates. Increasing cell numbers were used for increasing doses of $H_2O_2$ to account for cellular plating efficiencies. Colonies were allowed to grow for 7 days prior to staining. Colonies were counted using the GelCount colony counter (Oxford Optronix, Oxford, UK). Shown are the mean surviving fractions with standard error from at least three independent experiments. P <0.001 as analysed by the CFAssay for R package[326]. **B** Representative clonogenic plate

images of cells treated with NT siRNA or HECTD1 siRNA following $H_2O_2$ treatment (control, 200 or 300 μM).

### 6.3.3 Clonogenic cell survival following MMS

WI-38 cells were grown until 30-50 % confluent before being transfected with HECTD1 siRNA or Qiagen AllStars non-targeting control siRNA using Lipofectamine RNAiMax transfection reagent. Cells were then incubated at 37°C and 5 % $CO_2$ in a humidified cell culture incubator for 48 hours. Following effective knockdown (Figure 6.1), cells were incubated with increasing doses of MMS (0-1.5 mM) at 37°C and 5 % $CO_2$ in a humidified cell culture incubator. MMS was selected as a DNA damaging agent as it is well known to generate DNA base alkylation, which is processed by BER. After induction of DNA damage, the cells were trypsinised and counted. A defined number of cells (Table 3.9) were then seeded into six-well plates and incubated for 7 days at 37°C and 5 % $CO_2$ in a humidified cell culture incubator to allow colony growth (Figure 6.4B). As a control, WI-38 cells treated with either HECTD1 siRNA or Qiagen AllStars non-targeting control siRNA but untreated with MMS was used. The colonies were fixed with 6 % glutaraldehyde, stained with 0.5 % crystal violet and counted using the GelCount colony counter from Oxford Optronix (Oxford, UK). From three independent experiments, colonies were calculated and normalised to that of the untreated control, which was set to 1.0 (Figure 6.4).

From the analysis of the clonogenic assay I was able to also show HECTD1 depleted WI38 cells compared to NT siRNA treated cells were more sensitive to the cell killing effects of MMS (Figure 6.4A). Overall, in comparison to untreated conditions, I observed a 50-fold reduction in survival associated with a HECTD1 depletion, compared to a 20-fold decrease in NT siRNA treated cells following exposure to 1.5 mM MMS. Although, initially at 0.25 mM MMS a greater reduction in survival is seen in NT siRNA treated cells (1.5-fold) versus HECTD1 siRNA treated cells (1.1-fold), at all other dose increments the fold decrease in survival is greater in HECTD1 depleted cells; 2.3-fold (0.5 mM MMS), 2.7-fold (0.75 mM MMS), 1.7-fold (1 mM MMS) and 4.5-fold (1.5 mM MMS), in comparison to NT siRNA control conditions; 1.5-fold (0.5 mM MMS), 1.6-fold (0.75 mM MMS), 1.8-fold (1 mM MMS) and 3-fold (1.5 mM MMS). Furthermore, statistical analysis shows a significant ($p<0.001$) decrease in the surviving fraction of a HECTD1 knockdown cells following MMS exposure compared to that of NT siRNA treated cells, demonstrating an increase in sensitivity to MMS-induced cell killing associated with HECTD1 depletion.

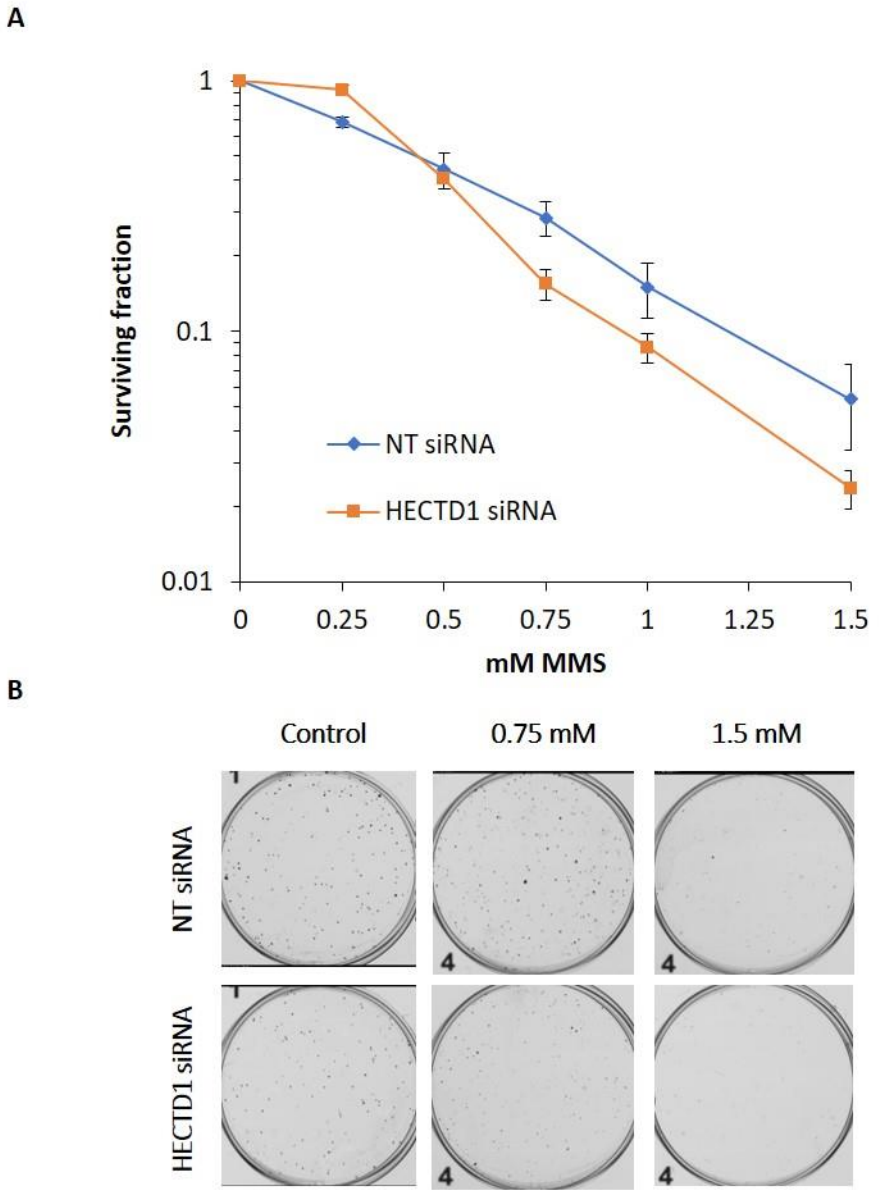


**Figure 6.4: HECTD1 depletion enhances cellular radiosensitivity to MMS**

**A** Clonogenic survival of WI-38 cells treated with 40 nM Qiagen AllStars non-targeting control (NT) siRNA (blue) or HECTD1 siRNA (orange) for 48 hours. Cells were then untreated (control) or incubated with increasing doses of MMS (0-1.5 mM) at 37°C and 5 % $CO_2$ in a humidified cell culture incubator, trypsinised, counted and a defined number plated into 6 well plates. Increasing cell numbers were used for increasing doses of MMS to account for cellular plating efficiencies. Colonies were allowed to grow for 7 days prior to staining. Colonies were counted using the GelCount colony counter (Oxford Optronix, Oxford, UK). Shown are the mean surviving fractions with standard error from at least three independent experiments.

p<0.001 as analysed by the CFAssay for R package[326]. **B** Representative clonogenic plate images of cells treated with NT siRNA or HECTD1 siRNA following MMS treatment (control, 0.75 or 1.5 mM).

## 6.4 Analysis of SSB repair kinetics following HECTD1 siRNA knockdown

As the results in previous chapters 4 and 5 show, HECTD1 plays a role within BER, promoting access to occluded AP and TG sites via histone H2B/H3 ubiquitylation. It can therefore be assumed that HECTD1 is also required within cultured cells to promote efficient DNA repair. Furthermore, as HECTD1 appears to be required for normal lung fibroblast cell survival following IR, $H_2O_2$ and MMS exposure (Section 6.3), I aimed to examine whether this is caused by changes to the DNA damage repair kinetics in three normal lung fibroblast cell lines; AG01673, AG16409 and WI-38, by utilising the alkaline comet assay, following IR, $H_2O_2$ and MMS exposure. The alkaline comet assay measures collectively alkali-labile sites and DNA SSBs.

### 6.4.1 Cell dose titrations for the alkaline comet assay

In the first instance, it was important to establish the correct doses of IR, $H_2O_2$ and MMS required to generate an appropriate level of initial DNA damage (~40 % tail DNA) for use in studying cell repair kinetics, and which doesn't exceed the cellular DNA repair capacity. Therefore, WI-38 cells were individually grown until 30-50 % confluent before being transfected with HECTD1 siRNA or Qiagen AllStars non-targeting control siRNA using Lipofectamine RNAiMax transfection reagent. Cells were then incubated at 37$^{o}$C and 5 % $CO_2$ in a humidified cell culture incubator for 48 hours. Following effective knockdown (Figure 6.1), DNA damage was induced with increasing doses of either IR (0-4 Gy), $H_2O_2$ (0-30 μM) or MMS (0-1 mM). After induction of DNA damage, cells were embedded in agarose on microscope slides, immediately lysed for 1 hour, and the DNA electrophoresed in alkaline conditions. SYBR gold stained cells were imaged using the BX61 Olympus microscope and 10x magnification. Images were analysed using Komet 6.0 software and % tail DNA values calculated.

Following induction of DNA damage in WI-38 cells via IR (Figure 6.5A), $H_2O_2$ (Figure 6.5B) and MMS (Figure 6.5C), in both HECTD1 depleted and control cells, I demonstrated a clear dose response, with the amount of DNA damage increasing linearly in HECTD1 siRNA and NT siRNA

treated cells following exposure to all three DNA damaging agents. Also, of note, the levels of DNA damage are comparable in HECTD1 siRNA and NT siRNA treated cells, which is of importance to confirm prior to DNA repair kinetics analysis. Furthermore, these cell dose titrations also verify dosage for repair kinetic studies. Within Jason Parsons' laboratory, and as indicated above, it has been well established that 40 % tail DNA is required as an initial level of DNA damage to effectively assess the cellular repair of alkali-labile sites and DNA SSBs using the alkaline comet assay, and which limits cells going into apoptosis. Upon examination of DNA damage induced by IR, it was shown that 1 Gy IR generated ~35 % tail DNA whereas 2 Gy produced ~55 % tail DNA (Figure 6.5A), therefore 1.5 Gy IR was decided upon as the dose for use in DNA repair studies to ensure 40 % tail DNA was achieved as an initial level of DNA damage. Assessment of $H_2O_2$ induced DNA damage demonstrates that 10 μM $H_2O_2$ generated 45 % and 41 % tail DNA in Qiagen NT control and HECTD1 siRNA cells, respectively (Figure 6.5B), therefore this $H_2O_2$ dose was accepted for use in further work. Finally, MMS induced DNA damage was shown to generate approximately 45 % tail DNA in both conditions when WI-38 cells were incubated with 0.5 mM MMS (Figure 6.5C), thus, this was agreed upon for use in DNA damage repair kinetic studies. These cell doses; 1.5 Gy IR, 10 μM $H_2O_2$ and 0.5 mM MMS were established in the WI-38 cell line, however as all three cell lines used in future work are normal lung fibroblasts, these doses were deemed generally appropriate for use in alkaline comets assays using AG06173 and AG16409 cells.

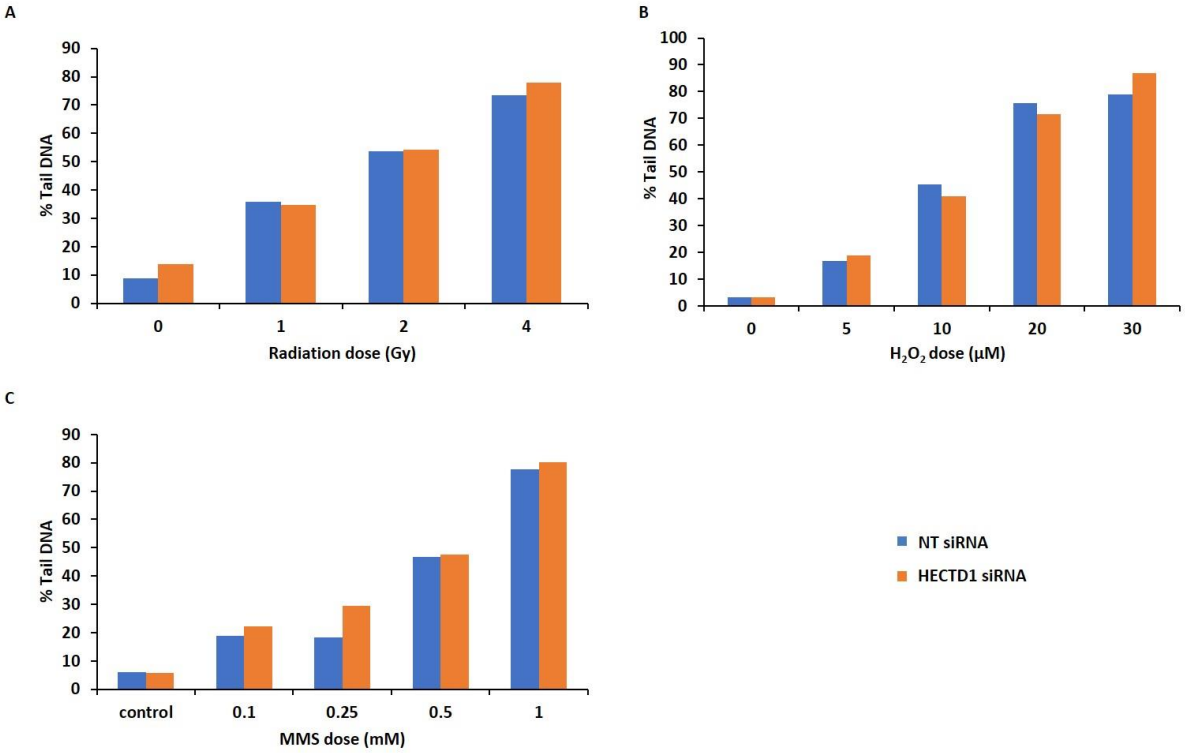


**Figure 6.5: Establishing IR, $H_2O_2$ and MMS alkaline comet assay doses for induction of DNA damage following siRNA knockdown of HECTD1 in WI-38 cells**

Alkaline comet assay cell dose titration of **A** IR **B** $H_2O_2$ and **C** MMS in WI-38 cells treated with 40 nM Qiagen AllStars non-targeting control (NT) siRNA (blue) or HECTD1 siRNA (orange) for 48 hours. DNA damage was induced with increasing doses of **A** IR (0-4 Gy) **B** $H_2O_2$ (0-30 µM) or **C** MMS (0-1 mM) and the resulting alkali labile sites and DNA SSBs measured by the alkaline comet assay. Cells were stained with SYBR gold, imaged using the BX61 Olympus microscope and 10x magnification and analysed using Komet 6.0 software. Shown is % tail DNA values from one experiment.

### 6.4.2 Alkaline comet assay following IR

AG06173, AG16409 or WI-38 cells were individually grown until 30-50 % confluent before being transfected with HECTD1 siRNA or Qiagen AllStars non-targeting control siRNA using Lipofectamine RNAiMax transfection reagent. Cells were then incubated at 37°C and 5 % $CO_2$ in a humidified cell culture incubator for 48 hours. Following effective knockdown (Figure 6.1), cells were trypsinised, incubated on ice for 5 minutes to prevent DNA repair and irradiated in a cell suspension with 1.5 Gy IR, as determined by cell dose titrations (Figure 6.5A). After induction of DNA damage, cells were embedded in agarose on a microscope

slide, and then allowed to repair for a defined time point (0-60 minutes) at 37$^{o}$C in a humidified chamber. Following repair, the cells were lysed and the DNA electrophoresed in alkaline conditions. As a control, unirradiated cells treated with either HECTD1 siRNA or Qiagen AllStars non-targeting control siRNA was used. SYBR gold stained cells were imaged using the BX61 Olympus microscope and 10x magnification. Images were analysed using Komet 6.0 software, % tail DNA values calculated and normalised to that of the irradiated unrepaired timepoint, which was set to 100 %.

From at least three independent experiments, and for all cell lines, NT siRNA control treated cells (blue) repaired IR-induced DNA damage by 60 minutes. The majority of repair events occurred from 10-60 minutes post-irradiation in AG06173's (Figure 6.6A) and WI-38's (Figure 6.6C) and from 20-60 minutes post-irradiation in the AG16409's (Figure 6.6B). Furthermore, in all three cell lines, depletion of HECTD1 caused a significant delay in the repair of SSBs and alkali-labile sites versus NT siRNA treated cells. This is evidenced by significantly higher levels of DNA damage, as analysed by a two sample *t*-test, in the AG06173 cells (Figure 6.6A) at all time points post-irradiation and a 4.7-fold difference in DNA damage levels at 60 minutes post-irradiation. Significantly higher levels (two sample *t*-test) of DNA damage are also seen in the WI-38 cells (Figure 6.6C) at all time points post-irradiation, with a 3.2-fold increase in DNA damage levels at 60 minutes post-irradiation. Additionally, significantly higher levels (two sample *t*-test) of DNA damage are seen at 20-, 30- and 60-minutes post-irradiation in the AG16409 cells (Figure 6.6B), and at 60-minutes post-irradiation a 2.9-fold difference in the levels of DNA damage is observed.

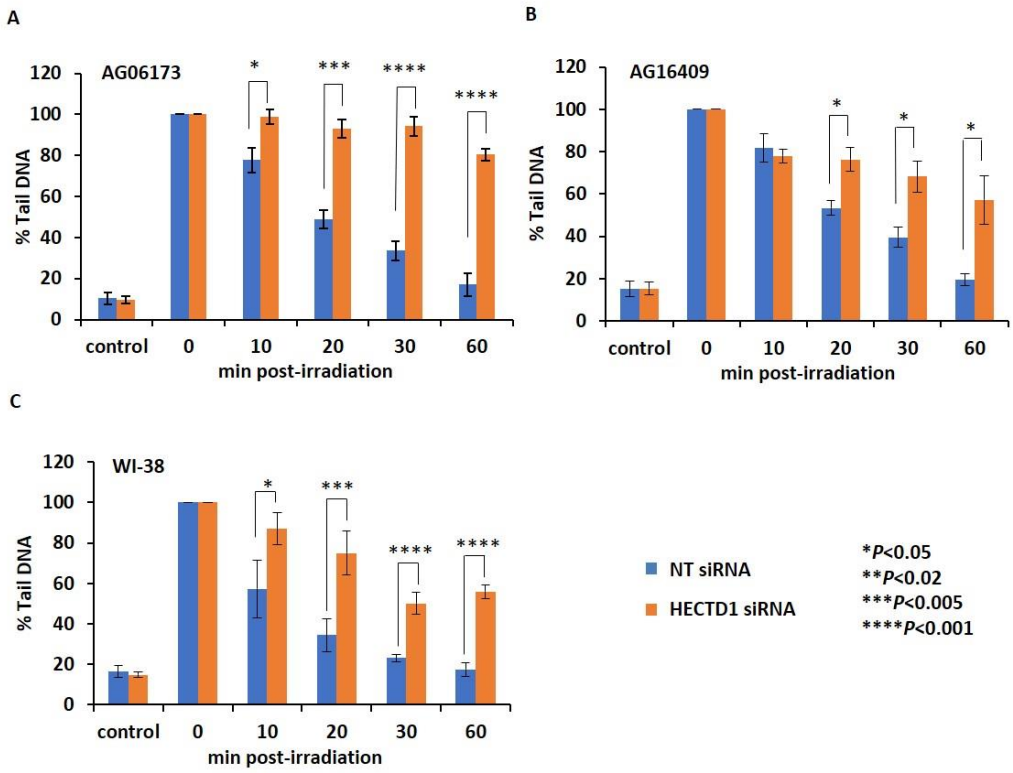


**Figure 6.6: Analysing IR-induced DNA damage repair kinetics following siRNA knockdown of HECTD1 in normal lung fibroblasts**

Alkaline comet assay of **A** AG06173 **B** AG16409 and **C** WI-38 cells treated with 40 nM Qiagen AllStars non-targeting control (NT) siRNA (blue) or HECTD1 siRNA (orange) for 48 hours. Cells were then unirradiated (control) or irradiated (1.5 Gy) and alkali labile sites and DNA SSBs measured at various time points post-irradiation (0-60 min) by the alkaline comet assay. Cells were stained with SYBR gold, imaged using the BX61 Olympus microscope and 10x magnification and analysed using Komet 6.0 software. Shown is % tail DNA values normalised to that of the 0 minutes timepoint, which was set to 100 % with standard errors from at least three independent experiments. *p<0.05, **p<0.02, ***p<0.005, ****p<0.001 as analysed by a two sample *t*-test.

### 6.4.3 Alkaline comet assay following $H_2O_2$

AG06173, AG16409 or WI-38 cells were individually grown until 30-50 % confluent before being transfected with HECTD1 siRNA or Qiagen AllStars non-targeting control siRNA using

Lipofectamine RNAiMax transfection reagent. Cells were then incubated at 37°C and 5 % $CO_2$ in a humidified cell culture incubator for 48 hours. Following effective knockdown (Figure 6.1), cells were trypsinised, incubated on ice for 5 minutes to prevent DNA repair and incubated on ice in a cell suspension with 10 µM $H_2O_2$ for 5 minutes, as determined by cell dose titrations (Figure 6.5B). After induction of DNA damage, cells were embedded in agarose on a microscope slide, and then allowed to repair for a defined timepoint (0-60 minutes) at 37°C in a humidified chamber. Following repair, the cells were lysed and the DNA electrophoresed in alkaline conditions. As a control, untreated cells treated with either HECTD1 siRNA or Qiagen AllStars non-targeting control siRNA was used. SYBR gold stained cells were imaged using the BX61 Olympus microscope and 10x magnification. Images were analysed using Komet 6.0 software, % tail DNA values calculated and normalised to that of the $H_2O_2$ treated unrepaired timepoint, which was set to 100 %.

From at least three independent experiments, and for all cell lines, NT siRNA cells (blue) repaired almost all $H_2O_2$-induced DNA damage by 60 minutes post-treatment. Repair was most proficient from 10-60 minutes post $H_2O_2$ incubation observed in WI-38's (Figure 6.7C) and from 20-60 minutes post $H_2O_2$ incubation in the AG06173's (Figure 6.7A) and AG16409's (Figure 6.7B). Furthermore, in all three cell lines, depletion of HECTD1 caused a significant delay in the repair of SSBs and alkali-labile sites versus NT siRNA treated cells. This is demonstrated by significantly higher levels of DNA damage in the AG06173's (Figure 6.7A) at 20-60 minutes post treatment, with a 3.9-fold difference in DNA damage levels at 60 minutes post treatment. This is less evident in the AG16409's, nevertheless significant differences between the HECTD1 depleted and NT control cells is observed at 30 and 60 minutes post treatment, and a 1.9-fold difference in DNA damage levels is evident 60 minutes post treatment (Figure 6.7B). The greatest significantly delayed repair of oxidative DNA base damage associated with HECTD1 depletion is seen WI-38 cells (Figure 6.7C), where significance, as determined by a two sample *t*-test, is seen at all time points post-$H_2O_2$ incubation, and at 60-minutes post treatment a 4.5-fold difference in the levels of DNA damage is observed.

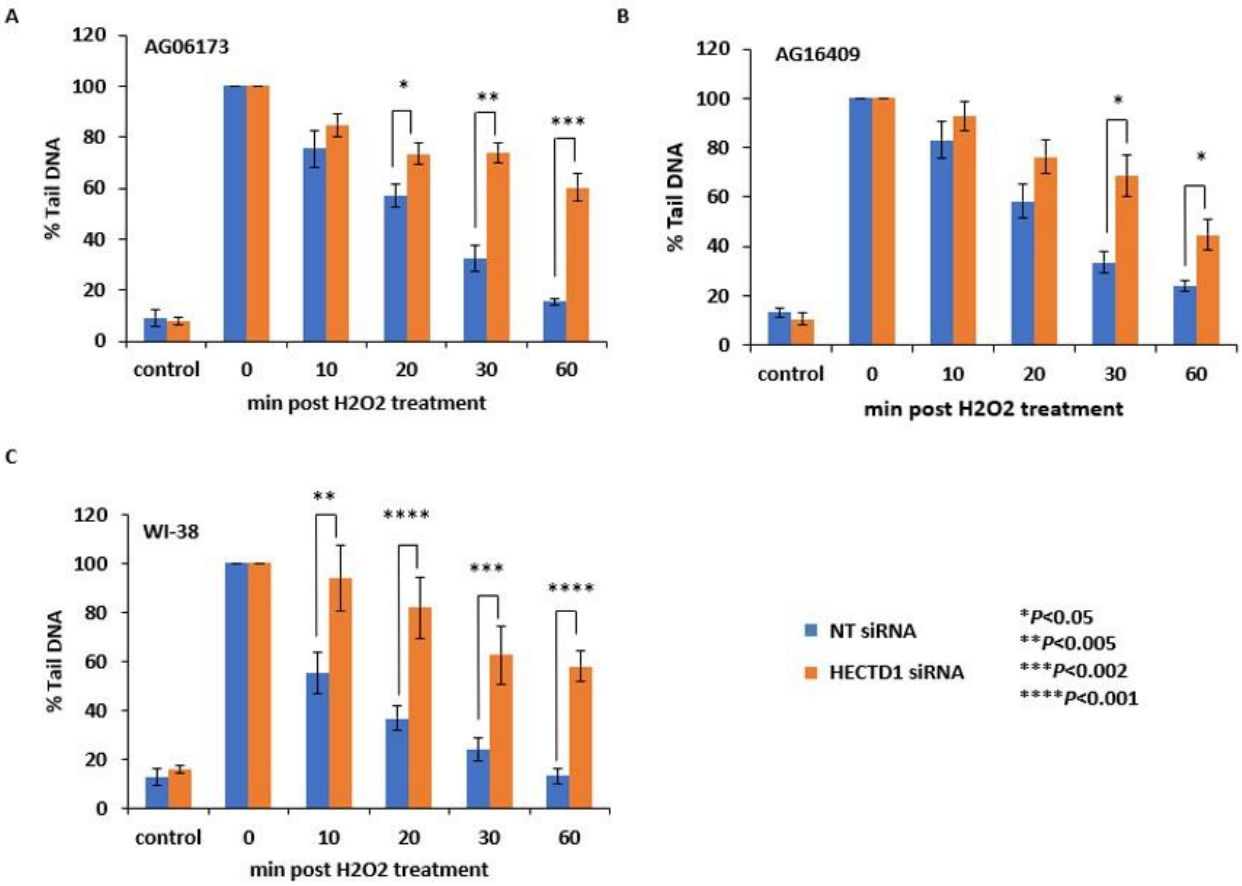


**Figure 6.7: Analysing $H_2O_2$-induced oxidative DNA damage repair kinetics following siRNA knockdown of HECTD1 in normal lung fibroblasts**

Alkaline comet assay of **A** AG06173 **B** AG16409 and **C** WI-38 cells treated with 40 nM Qiagen AllStars non-targeting control (NT) siRNA (blue) or HECTD1 siRNA (orange) for 48 hours. Cells were then untreated (control) or incubated with $H_2O_2$ (10 µM) and oxidative DNA damage measured at various time points post-treatment (0-60 min) by the alkaline comet assay. Cells were stained with SYBR gold, imaged using the BX61 Olympus microscope and 10x magnification and analysed using Komet 6.0 software. Shown is % tail DNA values normalised to that of the 0 minutes timepoint, which was set to 100 % with standard errors from at least three independent experiments. *p<0.05, **p<0.005, ***p<0.002, ****p<0.001 as analysed by a two sample *t*-test.

### 6.4.4 Alkaline comet assay following MMS

AG06173, AG16409 or WI-38 cells were individually grown until 30-50 % confluent before being transfected with HECTD1 siRNA or Qiagen AllStars non-targeting control siRNA using

Lipofectamine RNAiMax transfection reagent. Cells were then incubated at 37°C and 5 % $CO_2$ in a humidified cell culture incubator for 48 hours. Following effective knockdown (Figure 6.1), cells in a monolayer were incubated at 37°C and 5 % $CO_2$ in a humidified cell culture incubator with 0.5 mM MMS for 1 hour, as determined by cell dose titrations (Figure 6.5C). After induction of DNA damage, cells were trypsinised, embedded in agarose on a microscope slide, and then allowed to repair for a defined timepoint (0-60 minutes) at 37°C in a humidified chamber. Following repair, the cells were lysed and the DNA was electrophoresed in alkaline conditions. As a control, untreated cells treated with either HECTD1 siRNA or Qiagen AllStars non-targeting control siRNA was used. SYBR gold stained cells were imaged using the BX61 Olympus microscope and 10x magnification. Images were analysed using Komet 6.0 software, % tail DNA values calculated and normalised to that of the MMS treated unrepaired timepoint, which was set to 100 %.

From at least three independent experiments, and for all cell lines, NT siRNA cells (blue) repaired the majority of MMS-induced DNA damage by 60 minutes post-treatment. This was most evident in the AG16409's where repair was seen from 10-60 minutes post MMS incubation (Figure 6.8B). Repair from 10-60 minutes was also observed in the WI-38's (Figure 6.8C) and from 20-60 minutes in the AG06173's (Figure 6.8A). Furthermore, in all three cell lines, depletion of HECTD1 caused a significant delay in the repair of MMS-induced DNA base damage in comparison to NT siRNA treated cells. This is demonstrated by significantly higher levels, as determined by a two sample *t*-test, of DNA damage in the AG06173's 20-60 minutes post treatment, where at 60 minutes post treatment a 2.5-fold difference in the levels of DNA damage is observed (Figure 6.8A). Again, in AG16409's at 20-60 minutes post treatment, significantly higher levels (two sample *t*-test) of DNA damage are observed, with a 2.2-fold difference in the levels of DNA damage at 60-minutes post treatment (Figure 6.8B). In the WI-38's this difference between the HECTD1 depleted and NT control cells is only observed at 30 (1.8-fold) and 60 (2.2-fold) minutes post treatment (Figure 6.8C). However, this displays the greatest significantly delayed repair of MMS-induced DNA damage associated.

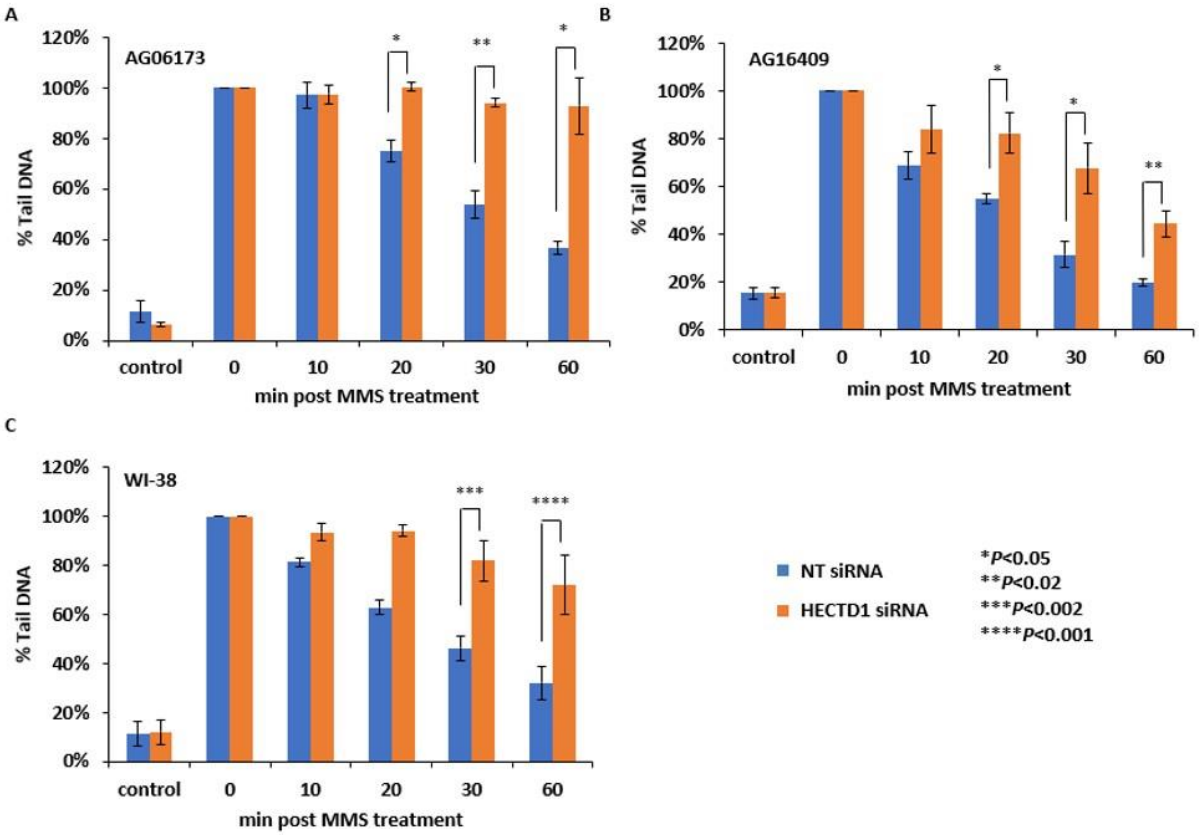


**Figure 6.8: Analysing MMS-induced DNA damage repair kinetics following siRNA knockdown of HECTD1 in normal lung fibroblasts**

Alkaline comet assay of **A** AG06173 **B** AG16409 and **C** WI-38 cells treated with 40 nM Qiagen AllStars non-targeting control (NT) siRNA (blue) or HECTD1 siRNA (orange) for 48 hours. Cells were then untreated (control) or incubated with MMS (0.5 mM) and alkylated DNA base damage measured at various time points post-treatment (0-60 min) by the alkaline comet assay. Cells were stained with SYBR gold, imaged using the BX61 Olympus microscope and 10x magnification and analysed using Komet 6.0 software. Shown is % tail DNA values normalised to that of the 0 minutes timepoint, which was set to 100 % with standard errors from at least three independent experiments. *p<0.05, **p<0.02, ***p<0.002, ****p<0.001 as analysed by a two sample *t*-test.

Cumulatively, this data demonstrates the importance of HECTD1 in the efficient processing of DNA base damage and single strand breaks through the BER pathway, which is required for maintaining cell survival in response to exogenous DNA damaging agents.

## 6.5 Analysis of DSB repair kinetics following HECTD1 siRNA knockdown

Following successful investigations into the observed delayed SSB repair kinetics of HECTD1 depleted normal lung fibroblast cells, which demonstrate a requirement of HECTD1 in promoting efficient DNA repair following induction of DNA damage via IR, $H_2O_2$ and MMS, the next step was to begin to assess the specificity of HECTD1 within DNA repair. Therefore, DSB repair kinetics of HECTD1 depleted normal lung fibroblast cells were elucidated. Utilising the neutral comet assay, which detects DNA DSB breaks repaired by the HR and NHEJ pathways, I aimed to determine if HECTD1 plays a role within these DNA repair pathways. Similarly to alkaline comet assay experiments, the three normal lung fibroblast cell lines; AG06173, AG16409 and WI-38 were used and DNA damage induced via IR and $H_2O_2$, which both have been characterised to induce DNA DSBs, albeit at higher doses than those required for induction of DNA SSBs.

### 6.5.1 Cell dose titrations for the neutral comet assay

As for examining the repair of alkali-labile sites and DNA SSBs, when assessing DSB repair kinetics it was firstly essential to establish the correct doses of IR and $H_2O_2$ required to generate an appropriate level of initial DNA damage for use in neutral comet assays. Therefore, WI-38 cells were individually grown until 30-50 % confluent before being transfected with HECTD1 siRNA or Qiagen AllStars non-targeting control siRNA using Lipofectamine RNAiMax transfection reagent. Cells were then incubated at 37$^{o}$C and 5 % $CO_2$ in a humidified cell culture incubator for 48 hours. Following effective knockdown (Figure 6.1), DNA damage was induced with increasing doses of either IR (0-8 Gy) or $H_2O_2$ (0-40 μM). After induction of DNA damage, cells were embedded in agarose on microscope slides, immediately lysed for 1 hour, and DNA electrophoresed in neutral conditions. SYBR gold stained cells were imaged using the BX61 Olympus microscope and 10x magnification. Images were analysed using Komet 6.0 software and % tail DNA values calculated. Within Jason Parsons' laboratory, it has been well established that approximately 30 % tail DNA is required as an initial level of DNA damage to effectively assess the repair of DNA DSBs using the neutral comet assay, and which doesn't exceed the cellular capacity for repair. Following induction of DNA damage in WI-38 cells via IR in both HECTD1 depleted and control cells, 4 Gy IR generated approximately 30 % tail DNA (Figure 6.9A) and was therefore agreed upon for use in DNA damage repair kinetic studies. Assessing induction of DNA damage via $H_2O_2$ indicated that 30 μM $H_2O_2$ generated approximately 30 % tail DNA (Figure 6.9B) in both

conditions and was accepted as the $H_2O_2$ dose for use in further work. These cell doses; 4 Gy IR and 30 μM $H_2O_2$ were established in the WI-38 cell line, however as all three cell lines used in future work are normal lung fibroblasts, these doses were deemed generally appropriate for use in neutral comet assays using AG06173 and AG16409 cells.

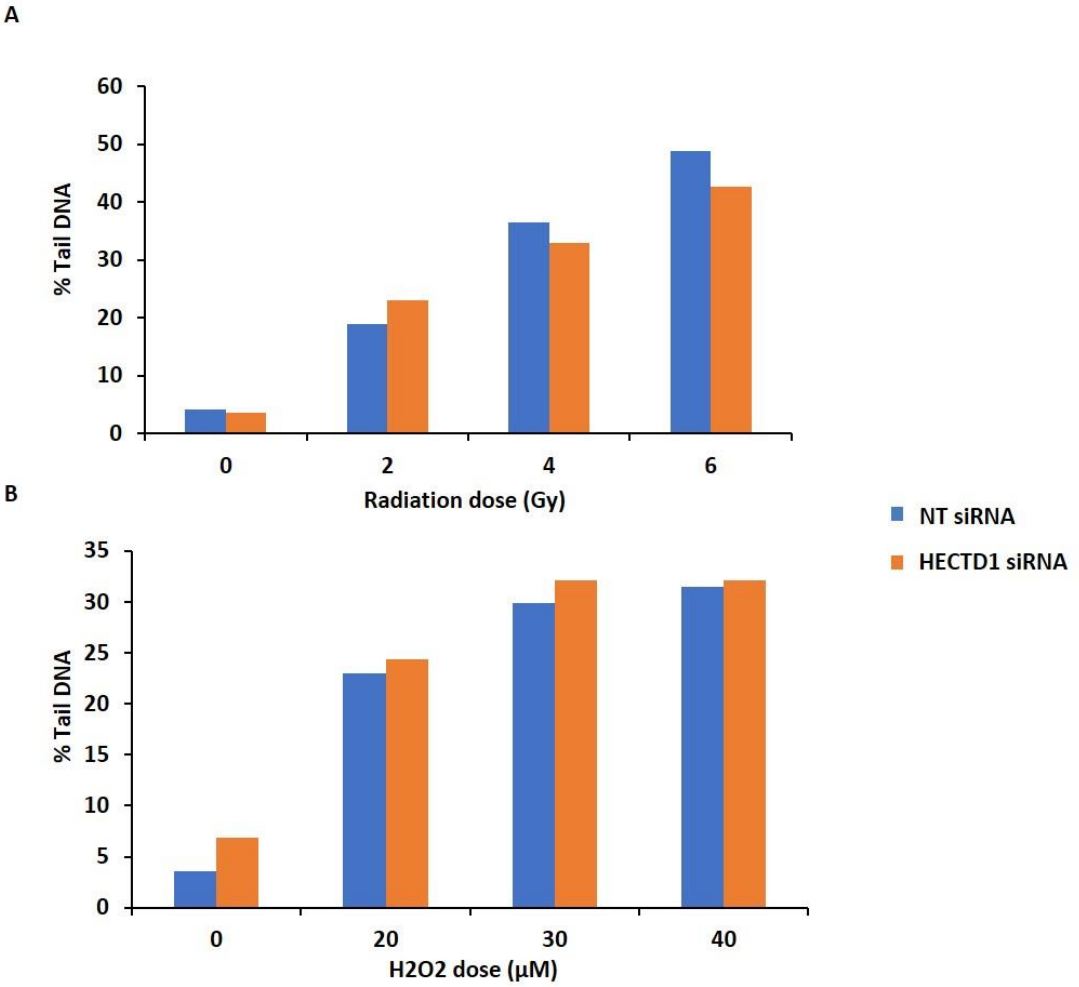


**Figure 6.9: Establishing IR and $H_2O_2$ neutral comet assay doses for induction of DNA damage following siRNA knockdown of HECTD1 in WI-38 cells**

Neutral comet assay cell dose titration of **A** IR and **B** $H_2O_2$ in WI-38 cells treated with 40 nM Qiagen AllStars non-targeting control (NT) siRNA (blue) or HECTD1 siRNA (orange) for 48 hours. DNA damage was induced with increasing doses of **A** IR (0-8 Gy) or **B** $H_2O_2$ (0-40 μM) and the resulting DNA DSBs measured by the neutral comet assay. Cells were stained with SYBR gold, imaged using the BX61 Olympus microscope and 10x magnification and analysed using Komet 6.0 software. Shown is % tail DNA values from one experiment.

### 6.5.2 Neutral comet assay following IR

AG06173, AG16409 or WI-38 cells were individually grown until 30-50 % confluent before being transfected with HECTD1 siRNA or Qiagen AllStars non-targeting control siRNA using Lipofectamine RNAiMax transfection reagent. Cells were then incubated at 37°C and 5 % $CO_2$ in a humidified cell culture incubator for 48 hours. Following effective knockdown (Figure 6.1), cells were trypsinised, incubated on ice for 5 minutes to prevent DNA repair and irradiated in a cell suspension with 4 Gy IR, as determined by cell dose titrations (Figure 6.9A). After induction of DNA damage, cells were embedded in agarose on a microscope slide, and allowed to repair for a defined timepoint (0-120 minutes) at 37°C in a humidified chamber. Following repair, the cells were lysed and the DNA electrophoresed in neutral conditions. As a control, unirradiated cells treated with either HECTD1 siRNA or Qiagen AllStars non-targeting control siRNA was used. SYBR gold stained cells were imaged using the BX61 Olympus microscope and 10x magnification. Images were analysed using Komet 6.0 software, % tail DNA values calculated and normalised to that of the irradiated unrepaired timepoint, which was set to 100 %.

From at least three independent experiments, and for all cell lines, both HECTD1 (orange) and NT (blue) siRNA cells repaired IR-induced DSBs gradually from 30-120 minutes, and by 120 minutes post-irradiation all the damage had been repaired and was similar to that observed in control, unirradiated cells (Figure 6.10). Furthermore, and again in all three cell lines, the kinetics of repair of DNA DSBs was comparable between HECTD1 depleted and non-targeting control cells with no statistical difference, as analysed by a two sample *t*-test in the % tail DNA at any time point.

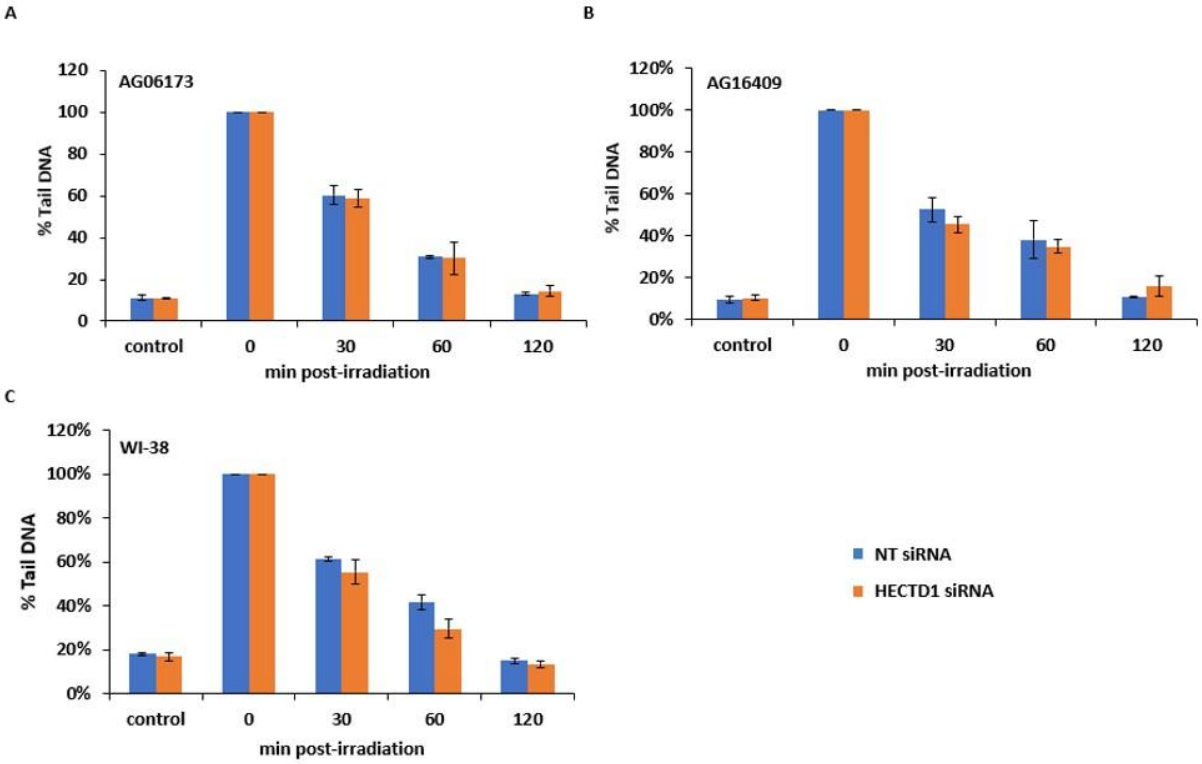


**Figure 6.10: Analysing IR-induced DSB DNA damage repair kinetics following siRNA knockdown of HECTD1 in normal lung fibroblasts**

Neutral comet assay of **A** AG06173 **B** AG16409 and **C** WI-38 cells treated with 40 nM Qiagen AllStars non-targeting control (NT) siRNA (blue) or HECTD1 siRNA (orange) for 48 hours. Cells were then unirradiated (control) or irradiated (4 Gy) and DNA DSBs measured at various time points post-irradiation (0-120 min) by the neutral comet assay. Cells were stained with SYBR gold, imaged using the BX61 Olympus microscope and 10x magnification and analysed using Komet 6.0 software. Shown is % tail DNA values normalised to that of the 0 minutes timepoint, which was set to 100 % with standard errors from at least three independent experiments. No statistical significance as analysed by a two sample *t*-test.

### 6.5.3 Neutral comet assay following $H_2O_2$

AG06173, AG16409 or WI-38 cells were individually grown until 30-50 % confluent before being transfected with HECTD1 siRNA or Qiagen AllStars non-targeting control siRNA using Lipofectamine RNAiMax transfection reagent. Cells were then incubated at 37°C and 5 % $CO_2$ in a humidified cell culture incubator for 48 hours. Following effective knockdown (Figure 6.1), cells were trypsinised, incubated on ice for 5 minutes to prevent DNA repair and

incubated on ice in a cell suspension with 30 µM $H_2O_2$ for 5 minutes, as determined by cell dose titrations (Figure 6.9B). After induction of DNA damage, cells were embedded in agarose on a microscope slide, and allowed to repair for a defined timepoint (0-120 minutes) at 37$^{o}$C in a humidified chamber. Following repair, the cells were lysed and the DNA electrophoresed in neutral conditions. As a control, untreated cells treated with either HECTD1 siRNA or Qiagen AllStars non-targeting control siRNA was used. SYBR gold stained cells were imaged using the BX61 Olympus microscope and 10x magnification. Images were analysed using Komet 6.0 software, % tail DNA values calculated and normalised to that of the $H_2O_2$ treated unrepaired timepoint, which was set to 100 %.

From at least three independent experiments, and for all cell lines, both HECTD1 (orange) and NT (blue) siRNA cells repaired $H_2O_2$-induced DNA damage gradually from 30-120 minutes, and by 120 minutes post-treatment all the damage had been repaired and was similar to that observed in control, untreated cells (Figure 6.11). Furthermore, in all three cell lines, depletion of HECTD1 caused no significant delay in the repair of $H_2O_2$-induced DNA DSBs. This is evidenced by comparable levels of DNA damage at all time points between HECTD1 depleted and NT control cells, where significance, as determined by a two sample *t*-test was not seen in any cell line at any time point.

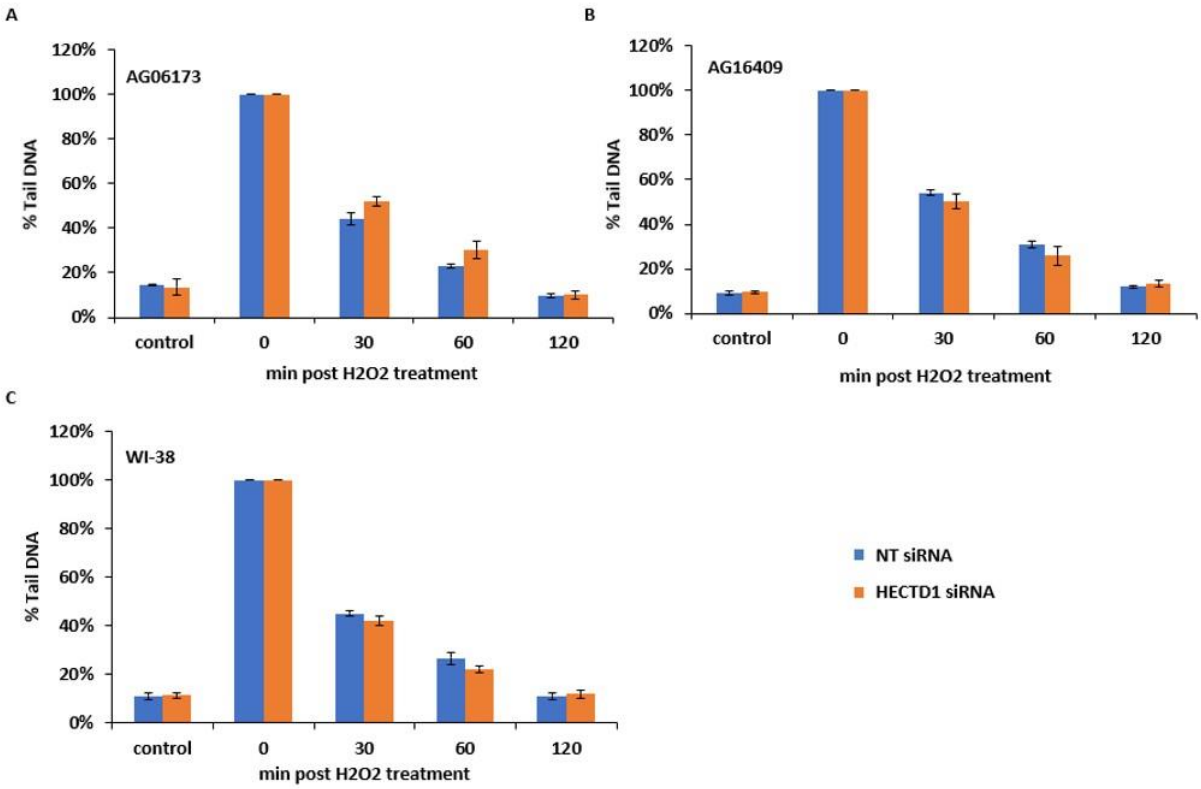


**Figure 6.11: Analysing $H_2O_2$-induced DSB DNA damage repair kinetics following siRNA knockdown of HECTD1 in normal lung fibroblasts**

Neutral comet assay of **A** AG06173 **B** AG16409 and **C** WI-38 cells treated with 40 nM Qiagen AllStars non-targeting control (NT) siRNA (blue) or HECTD1 siRNA (orange) for 48 hours. Cells were then untreated (control) or incubated with $H_2O_2$ (30 µM) and DNA DSBs measured at various time points post-irradiation (0-120 min) by the neutral comet assay. Cells were stained with SYBR gold, imaged using the BX61 Olympus microscope and 10x magnification and analysed using Komet 6.0 software. Shown is % tail DNA values normalised to that of the 0 minutes timepoint, which was set to 100 % with standard errors from at least three independent experiments. No statistical significance as analysed by a two sample *t*-test.

This data on the DSB repair kinetics of normal lung fibroblasts following exposure to x-ray irradiation and $H_2O_2$, suggests that HECTD1 does not play a key role in the processing of DNA DSBs. This implies that the protein is not directly involved in promoting the efficiency of the DSB repair, but rather, suggests a specificity of HECTD1 to the BER pathway within DNA repair.

## 6.6 Summary

In previous chapters 4 and 5, I established an *in vitro* role of HECTD1 in BER where it acts to promote accessibility of occluded sites of DNA damage to BER repair proteins in a ubiquitylation dependent manner via H2B/H3 ubiquitylation. The next logical step in the development of this project was to examine the requirement for HECTD1 in cultured cells *in vivo*. Therefore, I aimed to determine the impact of HECTD1 knockdown on overall cell survival and the DNA repair kinetics within normal cell physiology. As my aim was to understand the role of HECTD1 in normal cell physiology, I used the normal lung fibroblast cell lines; AG06173, AG16409 and WI-38 for these investigations.

In the first instance to examine the requirement of HECTD1 in a cellular context, it was essential to develop a method to knockdown HECTD1 efficiently. I adopted a siRNA mediated approach and transfected the three normal lung fibroblast cell lines with a pool of four siRNA sequences, to increase knockdown efficiency, using Lipofectamine RNAiMax as a transfection reagent. Following a 48 hour incubation, I analysed HECTD1 protein levels via immunoblotting and achieved a depletion of at least 80 % in the cellular levels of the proteins in all the cell lines, an acceptable level of depletion for analysing the impact of HECTD1 loss on survival and DNA damage repair.

Following this, I utilised the clonogenic survival assay to investigate the contribution of HECTD1 to overall cell survival, which HECTD1 was hypothesised to impact due to its involvement in promoting efficient BER *in vitro*. Analysis of the clonogenic assays in WI38 cells, used as these were the only normal lung fibroblast cell line which could be optimised for this technique, showed that HECTD1 depleted WI38 cells compared to NT siRNA treated cells were more sensitive to the cell killing effects of IR, $H_2O_2$ and MMS. This clearly demonstrated that HECTD1 is vital for the effective processing of DNA damage (particularly DNA base damage, AP sites and SSBs) repaired by the BER pathway and which promotes cell survival.

As HECTD1 appears to be required for cell survival following IR, $H_2O_2$ and MMS exposure, I aimed to examine whether this is predictably caused by changes to the DNA damage repair kinetics in three normal lung fibroblast cell lines; AG01673, AG16409 and WI-38. This was based on the assumption that HECTD1 is required to promote BER within a cellular context, as well as *in vitro,* improving accessibility of APE1 and NTH1 to occluded AP and TG sites via histone H2B/H3 ubiquitylation (shown in chapter 4). A key approach in examining DNA repair kinetics in a cellular environment is via the comet assay, which assesses directly the levels of

DNA strand breaks. Indeed, this technique has been previously adopted when establishing the role of Mdm2/USP7 in chromatin remodelling via H2B ubiquitylation [253], and to define a role for the chromatin remodeller, ALC1, in BER in chicken DT40 and human TK6 cell lines [263], [264], [344]. Similarly in this project I utilised the alkaline comet assay, and investigated the effects of HECTD1 depletion on the repair of alkali-labile sites and DNA SSBs. I demonstrated a significant delay in the repair of alkali-labile sites and DNA SSBs associated with a HECTD1 depletion in all three cell lines, following induction of DNA damage by IR, $H_2O_2$ and MMS. Cumulatively, this demonstrates the importance of HECTD1 in the efficient processing of a variety of DNA damage processed by the BER pathway including; DNA base oxidation, AP sites and SSBs generated by IR, oxidative DNA damage and SSBs produced by exposure to $H_2O_2$ and DNA base alkylation, a product of MMS exposure. This complements previous *in vitro* data showing a promotion of both APE1 and NTH1 on THF-IN and TG-IN mononucleosome substrates by HECTD1 via histone H2B/H3 ubiquitylation (chapter 5). The data in this chapter further suggests that HECTD1 may not be recruited to specific DNA damage intermediates, given the range of DNA damage types HECTD1 appears to be essential for the efficient processing of. Instead, this data supports the theory of HECTD1 being actively recruited and associating with the chromatin itself.

In addition to this evidence, it was also prudent to begin to examine the requirement of HECTD1 within other repair pathways. As a first step towards this, I examined DSB repair pathways (NHEJ and HR) by assessing the repair kinetics of DNA DSBs following HECTD1 depletion in the normal lung fibroblast cell lines; AG01673, AG16409 and WI-38 using the neutral comet assay. When assessing DSB repair, DNA damage was induced via IR and $H_2O_2$, which have been characterised to induce DNA DSBs, albeit at higher doses than required for induction of DNA SSBs. In this assessment, in all three cells lines I observed no significant difference in the repair kinetics of DSB induced by IR or $H_2O_2$ between HECTD1 depleted and control cells. This indicated that HECTD1 does not play a significant role in the NHEJ pathway, given that cells are largely in resting phase ($G_0/G_1$), this technique will mainly examine NHEJ efficiency and not HR, which is S-phase specific. However, this data does provide some evidence of the specificity of HECTD1 in promoting BER. Yet, although promising, this is preliminary data and gathering further evidence as to whether HECTD1 is responsive to other types of DNA damage, such as UV-induced bulky DNA lesions processed by nucleotide excision repair, DNA crosslinks induced by crosslinking agents such as cisplatin, or DNA DSBs is essential. Furthermore, it would be interesting to extend the comet assay based studies in the project by adopting a similar approach as recently used in the Parsons laboratory, which

examined unrepaired OGG1-dependent sites using enzyme modification in alkaline comet assays [345]. Utilising this technique to assess NTH1 and OGG1-dependent unrepaired DNA base damage, would be of particular relevance, and predictably, in the absence of HECTD1, there would be delayed or unrepaired oxidised pyrimidines processed by NTH1 (and possibly 8-oxoguanine residues recognised by OGG1), whereas overexpression of HECTD1 should stimulate repair.

In this chapter, I have provided evidence that HECTD1 is required to promote efficient repair of DNA base damage in cultured cells. Also, of note, this is the first reporting of a role of HECTD1 within DNA repair. Previously, reports have demonstrated roles of HECTD1 in controlling cell signalling, proliferation and migration, implicating the protein in several biological processes [303], [308], [312], [314], [318]. These include, targeting HSP90 for K63-linked polyubiquitylation [301], [303], ubiquitylation of PIPKIγ90 at K97 [304]–[306] and K63 linked polyubiquitylation of APC [308]–[311]. Furthermore, HECTD1 has also been well characterised to have a role within EMT, through a ubiquitylation triggered degradation of the EMT transcription factor SNAIL [299] and by regulation of K48 polyubiquitylation of ACF7 [312]. More recently, the DUB TRABID has been shown to target HECTD1, controlling the substrate's stability [346], which provides an interesting avenue for future investigations into whether TRABID is involved in controlling HECTD1 stability, required for promoting DNA repair. However, currently, I highlight a novel essential role for HECTD1 in the cellular DNA damage response. This data cumulatively supports the vital function that HECTD1 plays in normal cell physiology.

# CHAPTER 7: Discussion

## 7.1 Overview

DNA is under constant attack both endogenously, including ROS generated from normal cellular metabolism, and from exogenous sources, such as UV radiation. By design, the double helical structure of DNA provides a degree of protection, but DNA is still susceptible to damage from spontaneous chemical reactions [6]. In fact, it has been estimated that over 10,000 DNA base lesions and SSBs are generated per cell per day due to the instability of the DNA molecule. This is largely a result of DNA hydrolysis, cellular oxidation and environmental factors, such as ionising radiation. BER, a sophisticated cellular mechanism first reported in the 1970s by Thomas Lindahl, detects small, non-helical distorting lesions, and is essential for the repair of the majority of endogenously generated DNA base damages, and thus in maintaining genomic stability [167]. If left unrepaired, accumulation of DNA damage can lead to mutations, blocked transcription and translation, incomplete DNA replication or segregation of chromosomes leading to chromosomal abnormalities and cell cycle delay, arrest or even apoptosis [6]. This resulting genomic instability is well established to be a hallmark of all forms of cancer [2] and has been implicated in the development of neurodegenerative diseases including Huntington's and Alzheimer's disease [9], as well as premature ageing [10]. This further highlights the importance of our understanding of the global BER process, including the mechanism of action within the complex chromatin structure. This would provide an increasingly complete view of the repair of DNA lesions by BER, vital, especially as proteins associated with DNA repair have previously been utilised as targets for novel therapies for diseases, such as cancer. Perhaps the most well-known example being the use of PARP-1 inhibitors for treating BRCA-deficient breast and ovarian tumours in a synthetic lethal context [347]–[349]. Therefore, it is of specific interest to determine the mode of action of BER within chromatin and to discover novel ACR complexes and their role within BER.

Within the cell, DNA is condensed and packaged into a highly ordered structure, called chromatin, which consists of a number of loops and coils, organised by histones and non-histone chromosomal proteins which bind to DNA and structure chromosomes. At its most basic level, chromatin is arranged in nucleosomes, a histone-DNA complex, which link to form nucleosome arrays [200]. The nucleosome consists of ~145-147 base pairs of DNA wrapped ~1.7 times around a histone octamer, composed of two copies of the four core

histone proteins, H2A, H2B, H3 and H4 [201]. Nucleosomal arrays are further folded on top of one another to condense DNA to form chromatin fibres, which are coiled and condensed to form chromosomes. This compaction into chromatin allows DNA to be packaged into small regions, but also serves to protect it from damage, control gene expression and strengthen DNA to allow for mitosis or meiosis when entering anaphase. Via multiple mechanisms, DNA within compacted regions is made accessible to the complex machinery of essential biological processes, including gene transcription, DNA replication, and importantly for this work, DNA repair.

This dynamic nature of chromatin is facilitated by the nature of histones, which can be regulated to either repress or stimulate biological functions via PTMs. These PTMs, which include phosphorylation, ubiquitylation, acetylation, methylation, SUMOylation and PARylation, target the N-terminal tails of the histones, which protrude out from the nucleosomes. The histone tails present lysine residues to be targeted for the addition, but also removal, of chemical moieties that alter chromatin composition and function [204], [205]. In particular, these function to promote DNA accessibility either through direct destabilisation of the chromatin structure, or via stimulation of the recruitment of ACR enzymes. Increasing evidence, at least acquired *in vitro*, suggests that histone PTMs and/or recruitment of ACR factors may be integral in the processing of DNA damage through the BER pathway.

The dominating view on how BER operates within chromatin is that chromatin remodelling events are required to facilitate accessibility of BER enzymes to sites of DNA base damage and SSBs, particularly in occluded regions within the DNA. Indeed, *in vitro* studies utilising mononucleosome substrates containing site-specific DNA damage sites have clearly demonstrated that individual stages of the BER process can be inhibited to a significant degree depending on orientation of the damage relative to the histone core, but also relative to its proximity to the histone dyad [236]–[241], [243]–[245], [251]. Yet despite this evidence, how BER functions within a chromatin environment *in vivo* still remains elusive. Some promising progress has been made with identifying potential ACRs which facilitate BER from *in vitro* studies (e.g. RSC [242]) and from those conducted in cultured cells (e.g. ALC1 [344]). However, there are still clear gaps in knowledge as to how these, or other potential ACR complexes, mechanistically orchestrate chromatin remodelling during BER *in vivo*.

The study presented in this thesis builds upon previous work in the Parsons laboratory, where using mononucleosome substrates, it was demonstrated that a sterically occluded

THF-IN site was more efficiently processed by APE1 present in HeLa WCE in a largely ubiquitylation-dependent manner, than by recombinant APE1 protein alone. The factor promoting THF-IN incision was therefore predicted to be a E3 ubiquitin ligase, and a sequential chromatography approach of proteins purified from HeLa WCE identified the E3 ubiquitin ligase HECTD1 as a candidate enzyme facilitating BER via chromatin remodelling events [293], [294]. Here, I have successfully demonstrated that the E3 ubiquitin ligase activity of a recombinant truncated form of HECTD1 can stimulate incision of THF-IN and TG-IN by APE1 *in vitro* by promoting histone H2B/H3 ubiquitylation. Furthermore, depletion of HECTD1 in normal lung fibroblasts lead to significant deficiencies in SSB DNA damage repair, and decreased cell survival following x-ray IR, $H_2O_2$ and MMS treatment. Thus, I have now identified and characterised HECTD1 as a novel and important factor in promoting BER in chromatin.

## 7.2 Role of HECTD1 in BER where it acts to promote enzyme activity at occluded DNA lesions *in vitro*

Nucleosomal studies are the current major focus for investigating chromatin remodelling events occurring in BER, as they are relatively straightforward to perform. Several *in vitro* studies have utilised mononucleosome substrates with site specific DNA lesions as a representation of the chromatin environment. These studies have provided strong evidence for altered BER efficiency in chromatin, in particular, they have highlighted proximity to the dyad axis and orientation relative to the histone core as major factors effecting BER efficacy [236]–[241], [243]–[245], [251]. However, relatively little attention has been given to the assessment of the efficiency of repair of these substrates by BER proteins present within cell extracts, which contain stimulatory histone modifiers and chromatin remodellers. Although an approach utilising size exclusion chromatography to isolate factors promoting chromatin remodelling within WCE has been previously attempted, this only isolated the proteins into four size pools. Therefore, this study could only conclude that the NTH1 enhancing activity co-fractionates in pool three, with proteins of 6.5-45 kDa, and failed to provide sufficient information to isolate individual ACR candidates [350]. Further efforts into the isolation of candidates, via more extensive fractionation of proteins within this protein pool by chromatography, and MS analysis of the most active fractions is essential to identify candidates with any confidence. Therefore, utilising a more extensive approach, a previous PhD student (Laura Bennett) in the Parsons laboratory performed an unbiased purification scheme involving the separation of proteins in HeLa cell extracts by different ion-exchange

and size exclusion chromatography columns, and following MS analysis identified HECTD1 as a candidate enzyme involved in chromatin remodelling within BER [293], [294]. In this Thesis, I present data characterising a previously unpublished role for HECTD1 in DNA repair, expanding the breadth of current mononucleosomal studies.

THF-IN and TG-IN mononucleosomal substrates were prepared using the Widom 601 sequence, chosen due to its strong nucleosome positioning affinity. The DNA sequence was amplified using 5'-fluorescently labelled primers, to allow for DNA to be quantitatively analysed using the Odyssey Image Analysis System. This was crucial for accurate quantification of incision by APE1 or NTH1, but also to ensure successful generation of THF-IN or TG-IN containing DNA substrates. Here, the Widom 601 positioning sequence was modified via restriction enzyme digestion, then sequential DNA ligation employed using a pre-prepared duplex oligonucleotide containing either a THF or TG site on the lower strand, resulting in the production of a site specific THF-IN or TG-IN DNA substrate. A THF site was chosen as an alternative to a natural AP-site, as it is significantly more stable and exhibits virtually no difference in being recognised and cleaved by the activity of APE1, compared to AP-sites generated directly by DNA glycosylases [248]. The histone octamer was successfully prepared using *Xenopus Laevis* recombinant histones, and the THF-IN and TG-IN mononucleosome substrates produced by incubating the THF-IN or TG-IN DNA with the histone octamer in a 1:1 ratio with a salt gradient dialysis, consistent with previous reports [325]. Mononucleosome substrates were chosen over free DNA as it is a commonly used *in vitro* representation of chromatin, as previously stated, and the system has been utilised in many studies as it provides an insight into nucleosome dynamics during DNA repair. However, there are draw backs to this single nucleosome system, as they lack the full chromatin structure found in a cellular environment which may provide different chromatin remodelling events and histone dynamics. There are reports of more complex chromatin structures being developed, including dinucleosomes and nucleosome arrays [242], [351]. However, at present, the most common and popular model for investigating chromatin dynamics during BER continues to be the mononucleosome substrate.

Previously in the Parsons laboratory, immunoprecipitation of HECTD1 from the chromatography fraction purified from HeLa WCE displaying potential ACR activity, was attempted to confirm that HECTD1 was indeed responsible for stimulating APE1 activity against the THF-IN mononucleosome. However, most probably due to the size of the protein (289 kDa), it was not possible to optimise this strategy. Promisingly though, a partial

depletion of the protein was achieved and corresponded to a small decrease in the promotion of THF-IN mononucleosome repair by recombinant APE1 [293], [294]. Therefore, I adopted a LIC strategy to clone HECTD1, as this method does not require restriction enzymes or DNA ligases used in traditional cloning, but rather employs the polymerase/exonuclease activity of T4 DNA polymerase to generate complimentary long overhangs between the vector and insert to form stable associations [323]. Using this method, I opted to use the murine HECTD1 protein (mHECTD1), as this had already been cloned and was kindly provided by Prof Irene Zohn (Center for Neuroscience Research, Children's Research Institute, Washington, DC, USA). Using the murine protein was also deemed acceptable, as it displays very high homology (98.2 % by amino acid sequence) to the human HECTD1 protein. Also, this enabled the use of a bacterial overexpression system to purify the protein, which would be extremely difficult for the full length protein given that the full length mHECTD1 consists of 2612 amino acids and is 289 kDa in size. I choose to clone a truncated version containing the active E3 ubiquitin ligase (HECT) domain (amino acids 2156-2612), which is required for ubiquitylation of the target protein, plus an additional 389 amino acids immediately N-terminal to this domain (diagrammatic representation shown in Figure 4.21). This allowed for the protein to be expressed and purified from *E coli* cells.

I first utilised the *in* vitro BER assay, to confirm the inefficiency of APE1 to access the THF site when the DNA backbone is facing inwards towards the histone octamer. These preliminary investigations also established conditions (50 fmol APE1 generated ~20 % THF-IN substrate incision) for the *in* vitro BER assay in which to assess the ability of ΔN-HECTD1 in promoting APE1 activity against the THF-IN mononucleosome. I concluded that ΔN-HECTD1 was able to significantly stimulate, in a dose-dependent manner, the activity of recombinant APE1 against the THF-IN mononucleosome substrate. In a similar fashion, I also utilised the *in* vitro BER assay in which to assess the ability of ΔN-HECTD1 in promoting NTH1 activity against the TG-IN mononucleosome. Again, I demonstrated that ΔN-HECTD1 was able to significantly stimulate, in a dose-dependent manner, the activity of recombinant NTH1 against the TG-IN mononucleosome substrate. This provided evidence that HECTD1, at least *in vitro,* was functioning actively within the first two stages of BER. Validation of this conclusion was achieved by adopting a SDM approach to mutate the active site cysteine (C) residue to a glycine (G) residue within the HECT domain, generating ΔN-mutHECTD1, an E3 inactive ligase mutant of ΔN-HECTD1. Comparison of ΔN-mutHECTD1 and ΔN-HECTD1 supplemented *in vitro* BER assays measuring APE1 activity against the THF-IN mononucleosome, demonstrated that ΔN-mutHECTD1 was unable to stimulate APE1 activity. Firstly, this

strengthened my conclusion that HECTD1 is a candidate chromatin remodelling enzyme functioning to promote BER, but also provided evidence that the stimulatory activity of ΔN-HECTD1 was dependent on its E3 ligase activity.

These findings corroborate with previous studies, where it is well established using *in vitro* mononucleosome substrates that DNA glycosylase recognition of the DNA base lesion is efficient when the sugar phosphate backbone is outwardly facing away from the histone octamer, as this positioning is optimal for the enzyme to utilise its "base-flipping" mechanism. In contrast where the sugar phosphate backbone is inwardly facing, it is predicted that sufficient DNA glycosylase access is enabled by the action of ACRs or histone PTMS, to dissociate DNA from histones. For example, studies using chicken erythrocyte histones and TG nucleosome positioning sequence DNA to generate mononucleosomes, a 2-3-fold increase in excision by UDG and APE1 of the outwardly facing versus the inwardly facing mononucleosome substrate was observed [238]. Similarly, an assessment of the activity of UDG and APE1 against mononucleosomes containing the 601 DNA sequence present a 3-5-fold more effective excision of the out substrate in comparison to IN mononucleosome substrates [239]. These approaches compliment the reactions with APE1, as APE1 is essential for quantification of UDG activity given its monofunctional activity. However, other studies, in support of the data presented in this Thesis, have demonstrated compromised incision of inwardly facing TG substrates by NTH1 alone, seen by a 2-fold reduction in NTH1 activity against mononucleosomes containing inwardly facing TG site in a 184 bp DNA fragment containing the *L. variegatus* 5S ribosomal DNA nucleosome positioning sequence constructed with recombinant *X. laevis* histones [244]. This is supported by a comparative study utilising similar substrates assessing the activity of NTH1, where only 10 % of the inwardly facing TG sites from mononucleosomes were processed [245]. Yet, these approaches, and the one used for this project only assessed the activity of NTH1 alone against TG mononucleosome substrates. Therefore, a more stringent approach going forward would be to also assess NTH1 activity when reactions are supplemented with APE1. As in a cellular environment, due the cellular abundance of APE1 and relatively low activities of bifunctional glycosylases, it is generally thought, that although NTH1 possesses the ability to cleave the DNA backbone, APE1 circumvents this step and directly cleaves the AP site itself [175]. This would provide a more accurate assessment of NTH1 activity against TG mononucleosomes, reducing the limitations of *in vitro* studies.

Similarly, in support of the findings presented here, previously published data concludes that AP site detection by APE1 is dependent on damage orientation within both a natural AP site,

and a THF-containing mononucleosome. At least a 2-fold (AP site) and 3-fold (THF) reduction in cleavage by APE1 was observed with inwardly facing lesions in comparison to outwardly facing sites [248]. Interestingly, this study chose to investigate incision of both a natural AP and artificial THF site. Using a THF site as an alternative to a natural AP-site is often chosen, as in this project, it is significantly more stable and exhibits virtually no difference in being recognised and cleaved by APE1. However, this may place further limitations on an *in vitro* system and a more realistic option may be to use natural AP sites despite them being less stable than the THF alternative. Also of interest, gel shift mobility assays demonstrated that reduced substrate cleavage, observed with inwardly facing lesions, was as a consequence of reduced binding of APE1 to the inwardly facing substrate, rather than reduced APE1 activity [248]. Following on from this study, it was demonstrated that two naturally occurring variants of APE1, R237C and G241R, have reduced activity on both inwardly and outwardly facing AP sites containing 147 bp 601 DNA within mononucleosome substrates, but not on naked DNA, despite the variants not demonstrating any dramatic differences in mononucleosome binding [249]. Furthermore, the importance of mononucleosome composition has been highlighted within *in vitro* studies, where a 15-fold reduction in mononucleosome AP site reactivity with histone proteins was observed with incorporation of mutant histone H4. Of note, these mutations (five lysine residues to arginines) were in the amino tail region of histone H4, predicting the involvement of histone tails and PTMs in DNA strand cleavage [250]. Therefore, this evidence suggests that APE1 itself may not be the target of any PTM or ACR involved in chromatin remodelling within BER. Indeed, my own *in vitro* ubiquitylation investigations demonstrated that HECTD1 did not appear to directly ubiquitylate APE1.

Also, of importance to note is the lack of previous studies identifying ACRs or PTMs promoting APE1 or AP site incision within BER. Data is limited to an early *in vitro* study using 227 bp 601 DNA and recombinant *X. laevis* histones to generate mononucleosomes containing an 8-oxoguanine residue, which identified yeast SWI/SNF as a factor increasing the efficiency of excision of the lesion by OGG1 and APE1 by ~8-fold, which improved processing efficiency similar to that of naked DNA alone [241]. More extensive evidence both *in vitro* using WCE containing SWI/SNF, or the purified SWI-SNF complex itself, in combination with recombinant OGG1 and APE1, as used previously in the Parsons laboratory [293], [294] is necessary to see the impact on mononucleosome activity. These data should also be supplemented with investigations in cells. Adopting an siRNA screening approach to assess the impact of individual SWI/SNF ACRs on cellular survival post-DNA damaging

treatment would initially aid in the identification of whether SWI/SNF plays an active role in the cellular DDR, which could then be more thoroughly characterised. Of importance would be to examine the effect of protein depletion, either through an siRNA or CRISPR/Cas9 approach and protein overexpression with a mammalian plasmid delivery technique, on the DNA damage repair kinetics of cells in response to specific treatments (e.g. IR, MMS and $H_2O_2$). However currently, the data presented in this thesis, highlighting a novel role of HECTD1 in promoting TG and AP site incision within chromatin, is unique in characterisation of a specific enzyme acting to remodel chromatin within BER and is vital to accelerate our understanding of chromatin remodelling in BER.

An exciting extension of this would be to further characterise HECTD1 within BER, namely through investigating DNA end processing and ligation. This would be of particular interest for further study as reports on the constraints of Pol β activity within chromatin are varied. One study investigating the individual steps co-ordinated by Pol β in the form of gap filling and 5'-dRP lyase activity, found that removal of the 5'dRP residue within the mononucleosome at positions 35 (outward facing) and 49 (inward facing) were cleaved with the same efficiency as free DNA. When assessing DNA synthesis activity though, there was strong inhibition (~2600-fold) when the gap was close to the dyad (position 10) in comparison to free DNA. At positions 49 (inward facing) and 35 (outward facing), the difference in kinetics was 277-fold and 4-fold, respectively versus the free DNA [251]. This suggests that of the two enzymatic steps that Pol β catalyses, the DNA synthesis stage is most greatly impacted by the presence of histone proteins within the mononucleosome. Other reports conclude a complete inhibition of Pol β DNA synthesis activity caused by the presence of the histone octamer in natural GAP mononucleosomes, generated from processing of both a uracil and 8-oxoG site [238] [241]. This data indicates that irrespective of rotational setting, this stage of the pathway is a major restriction on BER in chromatin, demonstrating nucleosome remodelling as an essential step for promoting Pol β activity. In contrast, a study utilising 184 bp DNA fragment containing the *L. variegatus* 5S ribosomal DNA nucleosome positioning sequence and mononucleosomes constructed with recombinant *X. laevis* histones, demonstrated that Pol β was ~3-fold more active on a gap where the DNA backbone was outwardly facing versus inwardly facing. It was hypothesised that this difference observed with rotational positioning was a result of the inherent bending of the outward substrate, facilitating the 90 degree bend required for Pol β activity [244]. Furthermore, translational positioning has been suggested to have a greater impact of efficiency of Pol β [244]. In mononucleosomes constructed utilising chicken erythrocyte

histone octamers and a 146 bp DNA fragment containing the *L. variegatus* 5S rRNA gene sequence, Pol β was able to extend at greater efficiency the 3'-hydroxyl terminus generated by UDG and APE1 incision of uracil (in position 22) than the uracil placed (in position 51) closer to the dyad axis [236]. Again, this apparent difference was theorised to be linked to kink formation required for Pol β activity, the result of increased energetic cost associated with introducing a 90 degree kink into the DNA at these locations. The mixed reports on the efficiency of Pol β on mononucleosome substrates again could be a result of the limitations of *in vitro* reactions and supplementing either with WCE for a full complement of the pathway, or at least with XRCC1-Lig IIIα which is known to stabilise and form a complex on DNA with Pol β is required for efficient BER [352], would help mitigate this. This issue could also be rectified via conducting a full pathway reconstitution in mononucleosomes, for example, TG substrates in different locations/orientations could be supplemented with NTH1, APE1, Pol β and XRCC1-LigIIIα and the final product analysed. However, as Lig IIIα is not the only ligase to function within BER (Lig I is predominantly employed in LP-BER), the effect of ligase competition will be missed when only using XRCC1-LigIIIα in reactions. As is the case in current studies investigating DNA ligation within BER, only ligation of the nick substrate by XRCC1-LigIIIα has been examined [244] [252]. Consequently, fully complemented reactions with WCE would also be vital in these investigations, as current evidence suggests that occluded nicked DNA mononucleosomes can only be ligated by XRCC1-LigIIIα, when it is exposed by periodic, spontaneous partial unwrapping of the DNA from the histone octamer [252]. More complex reactions involving mononucleosome substrates that promote SP-BER (XRCC1-LigIIIα-dependent) versus LP-BER (Lig I-dependent) would also be of significant interest for future studies.

## 7.3 HECTD1 acts via a H2B/H3 ubiquitylation mechanism to promote BER

A major form of cellular regulation is achieved via ubiquitylation, which can modulate protein-protein or protein-DNA interactions, as well as being more commonly involved in protein stability and activity. Ubiquitylation occurs in a three step ATP-dependent process by an enzyme cascade involving ubiquitin activation by an E1 ubiquitin-activating enzyme, ubiquitin transfer from the E1 enzyme to the E2 active site by a E2 ubiquitin conjugating enzyme, before an E3 ubiquitin ligase enzyme catalyses the transfer of ubiquitin onto a lysine residue of the substrate protein [266]. Ubiquitylation and the UPP has been demonstrated to mediate protein-protein interactions, play a regulatory role in protein localisation,

conformation and activity as well as have an involvement in signalling networks and transcriptional regulation of a range of pathways including the cellular DDR, the cell cycle and apoptosis [265].

Our general understanding of ubiquitylation events that can affect chromatin structure, particularly required for enhancing BER efficiency, is unfortunately not well characterised. The strongest evidence for such events is through histone H2B monoubiquitylation at K120, associated with active chromatin and found on 1-1.5 % of total H2B in mammals [338]. The data reported here could be indicative of this monoubiquitylation event in promoting BER, given the evidence that ΔN-HECTD1 appeared to cause a modest increase in mono/di-ubiquitylation of histone H2B *in vitro*. However, as I could not reveal preliminary evidence of a HECTD1 dependence of histone H2B ubiquitylation in WI-38 cells, the strength of this argument could be reduced. Yet, a more extensive approach utilising antibodies specific for H2BK120 ubiquitylation and indeed other less well characterised histone H2B ubiquitin docking sites (K34, K46, K108, K116, and K125) is worthwhile, given the preliminary nature of my data from WI-38 cells, for these accurate conclusions to be definitively drawn [339], [340]. Furthermore, given my evidence presented in this thesis, it appears at least *in vitro,* that HECTD1 does not act on histone H2A or H4. In fact, histone H2A ubiquitylation at K119 appears to play a primarily chromatin repressive role, in X inactivation, stabilisation of histone H1 and inhibition of histone H3 methylation. In addition to this, it is the most abundant site of ubiquitylation on histone H2A (5-15 % total H2A in higher eukaryotes) [338], [340]. It therefore appears unlikely that HECTD1 would target histone H2A for ubiquitylation as this at least in theory, this would be counterintuitive to the promotion of DNA repair I have seen in this research project. However, less common H2A ubiquitylation sites, including K13/15 and K127/129 have been reported to be involved in DNA damage signalling and homologous DNA pairing [339], and therefore perhaps histone H2A ubiquitylation cannot fully be dismissed as a HECTD1-dependent mechanism.

In the first instance though, any future attentions to elucidate the mechanism via which HECTD1 is acting should primarily focus on histone H3 ubiquitylation, which appears the strongest target as evidenced in this research project. Indeed, I provide evidence that ΔN-HECTD1 causes polyubiquitylation of histone H3 *in vitro,* as well as a HECTD1 dependent histone H3 polyubiquitylation event in WI-38 cells. Also, of interest, is that NEDD4-mediated ubiquitylation of histone H3 at K23/K36/K37 reportedly has a role in transcription activation, stimulating the histone acetyltransferase GCN5. Furthermore, CUL4–DDB–ROC1 mediated ubiquitylation of both histone H3 and H4 has been implicated to have a role in NER. More

recently, UbiCRES, Ub-AQUA proteomics and *in vitro* autoubiquitylation assays have demonstrated that HECTD1 preferentially assembled K29 and K48 linked ubiquitin chains and that branching at K29/K48 was essential for the protein's full ubiquitin ligase activity [346]. Therefore, given that none of the published cellular functions of HECTD1 have been attributed to K29 linked polyubiquitylation and for validation of this study, it is essential that chain dependence of HECTD1 substrates be defined. A key way in which histone H3 polyubiquitylation by HECTD1 be validated is via identification of the type of ubiquitin chains modifying histone H3. For example, MS analysis of the HECTD1 dependent ubiquitylation sites of histone H3 may identify chain dependence which could then be validated by a SDM approach once a site is identified. Furthermore, if this ubiquitylation event was found to be K29 linked, exploring the regulatory role of TRABID, a DUB which cleaves K29 linked chains and HECTD1 is a known substrate of [346], may be a good next step to reveal the mechanism of opening chromatin to promote BER. Also, as histone H3 ubiquitylation has only been found to occur globally on 0.3 % of H3 histones [340]–[342], this may be suggestive of a specific role for histone H3 ubiquitylation in the DDR. Therefore, at least initially, the most productive use of time going forward may indeed be to focus attention on histone H3 ubiquitylation as a mode of action for HECTD1 in BER, and particularly in accumulating more data from cultured cell experiments supporting this process, as well as characterising the specific site within histone H3 that is targeted by HECTD1 for ACR activity.

## 7.4 HECTD1 is required for efficient repair of DNA base damage and SSBs

Following clear evidence that HECTD1 functions within BER *in vitro*, logically this role was further explored in cultured cells. Although HECTD1 was previously identified following purification from HeLa WCE, the focus of this project was to establish the role of HECTD1 in normal cell physiology, therefore normal lung fibroblast cell lines, namely AG06173, AG16409 and WI-38 were utilised for this purpose. A key approach in examining DNA repair kinetics in a cellular environment is via the comet assay, which assesses directly the levels of DNA strand breaks. Indeed, this technique has been previously adopted when establishing the role of Mdm2/USP7 in chromatin remodelling via H2B ubiquitylation. Using siRNA mediated depletion of USP7 in HeLa cells, it was demonstrated using alkaline comet assays that DNA damage induced by $H_2O_2$ resulted in a 2-fold delay of repair up to one hour post treatment. Furthermore, when HeLa cells overexpressed USP7, a 2-fold increase in the rate of repair of $H_2O_2$ induced DNA damage was observed. These key findings aided development

of the proposed model, whereby the stabilised Mdm2/USP7 complex allows for ubiquitylation of histone H2B by Mdm2 when DNA damage is detected, promoting open chromatin and therefore repair [253]. More recently, ALC1, a member of the SNF2 superfamily, was defined to play a role in BER in chicken DT40 and human TK6 cell lines. ALC1 knockout DT40 and TK6 cells were found to be sensitive to both $H_2O_2$ and MMS, displaying deficient SSB repair through alkaline comet assay analysis [264]. This comet assay data, coupled with alkaline-elusion assays, demonstrated that ALC1 promotes BER after SSB formation in both chicken DT40 and human TK6 cells, consistent with previously suggested roles of ALC1 in DNA repair [263], [344].

Similarly, in this project I also utilised alkaline comet assays coupled with an siRNA mediated depletion of the cellular levels of the HECTD1 protein to determine the contribution of HECTD1 in DNA repair in normal lung fibroblasts. Specifically, I investigated the repair of DNA damage known to be processed by BER, including IR and $H_2O_2$ that generate alkali-labile sites, SSBs and oxidative DNA damage, and MMS that mediates DNA base alkylation. The data presented in this thesis clearly demonstrates a significant delay in the repair in DNA damage induced by these DNA damaging agents, as analysed by the alkaline comet assay, in HECTD1 depleted cells. Cumulatively, this shows the importance of HECTD1 in normal cells in the efficient processing of a variety of DNA damage processed by the BER pathway. Furthermore, as I have shown that HECTD1 promotes BER in chromatin by targeting histones for ubiquitylation *in vitro*, it is possible that this role of HECTD1 does not only have functionality within BER. However, assessing the DNA DSB repair kinetics through neutral comet assay analysis, I observed that there was no significant delay in the repair of DNA DSBs induced via IR and $H_2O_2$ associated with HECTD1 deficiency. This suggests that HECTD1 does not appear to have a major role within DSB repair pathways, however, this is a preliminary conclusion and further evidence would be essential to confirm this observation.

Investigations have utilised the enzyme-modified neutral comet assay, previously described here [353] and successfully used in the Parsons laboratory [80], where treatment of the DNA with recombinant DNA repair enzymes post cell lysis incises residual DNA damage, therefore revealing additional strand breaks which can be analysed following electrophoresis. This technique has been used to assess the repair kinetics of complex DNA damage (also referred to as clustered/complex DNA damage), which is defined as two or more lesions induced within one to two DNA helical turns. Alternatively, and of particular relevance, would be adopting a similar approach as recently used in the Parsons laboratory, which examined unrepaired OGG1-dependent sites using enzyme modification in alkaline comet assays [345].

A natural extension of the comet assay studies conducted as part of this research project would therefore be to assess NTH1 and OGG1-dependent unrepaired DNA base damage. Predictably, and in the absence of HECTD1, there would be delayed or unrepaired oxidised pyrimidines processed by NTH1 (and possibly 8-oxoguanine residues recognised by OGG1), whereas overexpression of HECTD1 should stimulate repair. In addition to comet assays, further extensions of these experiments could include examination by immunofluorescence microscopy as to whether HECTD1 co-localises with either γH2A.X or XRCC1 foci, commonly used as markers of DSB and SSB, respectively. This technique has similarly been used to assess the effect of cellular localisation on HSP90, a known ubiquitylation target of HECTD1. However, cellular localisation of HECTD1 was not reported, leading to queries as to the suitability of HECTD1 antibodies for immunofluorescence [303]. Additionally, further *in vitro* mononucleosome studies described earlier in this chapter would too be vital in designing other experiments to be performed in cultured cells and therefore to generate more concrete conclusions on HECTD1's precise role in DNA repair, which may be beyond the roles in BER described in this thesis.

Also of interest, is that this is the first reporting of a role of HECTD1 within DNA repair. Previously, HECTD1 has been shown to target a range of distinct signalling pathways, implicating HECTD1 in several biological processes [301], [302]. In relation to cellular localisation and secretion, HECTD1 has been characterised to target HSP90 for K63-linked polyubiquitylation [301], [303] and ubiquitylation of PIPKIγ90 at K97 [304]–[306]. In the context of Wnt/β-catenin signalling, HECTD1 has been identified as a negative regulator of the pathway, via K63 linked polyubiquitylation of APC [308]–[311]. HECTD1 has also been well characterised to have a role within EMT, implicated in the mediation of a range of target proteins. For example, through a ubiquitylation triggered degradation of the EMT transcription factor SNAIL [299] and by regulation of K48 polyubiquitylation of ACF7 [312]. Of interest, these previously defined roles of HECTD1 have identified the ability of the protein to modify K48 and K63 linked chains, the most extensively studied form of polyubiquitylation modification. However, more recently, HECTD1 has been identified as a substrate of the DUB TRABID, which recognises and cleaves K29 and K33 linked chains. Through analysis of this interaction, it was shown that upon cellular depletion of TRABID, HECTD1 is readily degraded, suggesting that TRABID controls HECTD1 stability [346]. As stated previously, it would be of interest to identify the specific chain linkage of the histone H3 polyubiquitylation event reported here, as none of the previously published cellular functions of HECTD1 have been attributed to K29 linked polyubiquitylation. Therefore, if indeed HECTD1 is assembling K29

linked ubiquitin chains on histone H3, further investigations into whether TRABID is involved in controlling HECTD1 stability, required for promoting DNA repair, would be of significant interest.

## 7.5 Future directions

The data presented in this thesis provides strong evidence that HECTD1 is a histone modifier which functions within BER at occluded sites of base damage. This has been characterised in mononucleosome substrates with occluded THF and TG sites. However, a more extensive validation of this general role of HECTD1 within BER, which I have proposed, is essential. Primarily this would involve extending current *in vitro* investigations to include GAP and NICK mononucleosome substrates incorporating the end processing mechanisms of BER. In the first instance, an assessment of GAP-IN vs OUT mononucleosome processing by Pol β would be of interest, perhaps providing more clarity as to the ability of Pol β to function as a DNA polymerase through single nucleotide insertion in a chromatin environment. However, I believe it to also be essential to expand into translational positioning variants for a more extensive assessment, using for example THF, uracil and TG substrates and the respective enzymes (APE1, UDG and NTH1) which will generate a more natural SSB flanked by 5'-dRP ends which also require Pol β end processing. This would naturally follow with an assessment of the ability of HECTD1 to promote Pol β polymerase and dRP lyase activity where either rotational or translational positioning is potentially limiting repair. Of course, the impact of chromatin on DNA ligation would similarly be assessed, realistically in parallel to investigations with GAP mononucleosome substrates. Furthermore, in addition to measuring the impact of chromatin on the individual enzymes, and of HECTD1 in stimulating these, it is also vital to consider the efficiency of the complete repair process. Therefore, for example, examining processing of TG substrates in different locations and/or orientations when supplemented with NTH1, APE1, Pol β and XRCC1-LigIIIα and analysing the final product. Thus, further elucidation of HECTD1's mode of action may be gained through these *in vitro* studies. Further avenues to extend *in vitro* studies could also incorporate dinucleosomes, incorporating linker DNA and histones (H1), or nucleosomal arrays into the *in vitro* BER investigations [242], [351], providing a more accurate representation of the chromatin environment which should be taken into consideration for future work. In addition to this, it would also be useful to validate these *in vitro* mononucleosome studies with human HECTD1.

Therefore, efforts should be taken to clone and purify human HECTD1 and confirm the data generated using the mouse protein described here.

This thesis also provides evidence that HECTD1 acts via histone H2B/H3 ubiquitylation at least *in vitro.* However, a precise site-specific target of ubiquitylation is still lacking. Attentions might be best spent on histone H3 given the *in vitro* evidence and that HECTD1 dependent ubiquitylation of histone H3 is preliminarily observed in WI-38 cells. Furthermore, although ubiquitylation of the core histones is common (10-15 %), only <0.3 % of histone H3 are found to be ubiquitylated, therefore this may be indicative of histone H3 ubiquitylation playing a precise and specific role in the DDR [340]. Therefore, this may be worth further attention, assessing *in vitro* ubiquitylation using antibodies against the histone H3 ubiquitylation sites (K14, K23, K36 and K37 [340], [354]). Beyond this, an examination of ubiquitylation sites of histone H3 by MS analysis following *in vitro* incubation of histone octamer, or histone H3 alone, in combination with HECTD1 would also aid identification. This could be confirmed using a SDM approach to mutate the predicted ubiquitylation site and use the mutant histone in mononucleosome reconstitutions and subsequent *in vitro* assays to verify the specific target of HECTD1. Predictably, mutation of the histone ubiquitylation site targeted by HECTD1 would prevent chromatin remodelling and therefore DNA damage accessibility, leading to deficient BER of the DNA damage site. These *in vitro* studies could be complemented by MS analysis of histones extracted from cells following HECTD1 overexpression and induction of DNA damage by IR, $H_2O_2$ and MMS. Although to maximise the utility of this approach, the histone proteins and HECTD1 may need to be overexpressed in cells to provide optimal ubiquitylation. Consequently, rather than analysing the endogenous histones, the exogenously expressed histone H3 could be purified using pull-downs before analysis by MS. A further approach, although not currently within the reach of this laboratory, would be to utilise a structural biology approach, using nuclear magnetic resonance (NMR) spectroscopy to analyse the interactions between the histones and HECTD1. However, given this size of the protein (289 kDa) and that currently the crystal structure of HECTD1 has not been defined, this may not be feasible in the near future.

In addition to the expansion of *in vitro* investigations, more extensive work in cells would be a logical continuation of this project. One area to highlight would be to extend the examination of sensitivity to DNA damaging agents, incorporating agents known to induce DSB, such as bleomycin/phelomycin or crosslinking agents such as cisplatin, to define whether HECTD1 is specific to BER, or also functional in other DNA repair pathways. A more detailed characterisation of HECTD1 would also be aided by the generation of a CRISPR

HECTD1 knock out cell line, to complement experiments conducted using an siRNA mediated and transient depletion of HECTD1. HECTD1, via regulation of its known target proteins, has been implicated in cancer development, for example, dysregulation of HECTD1 has been linked to ER-α-negative breast cancer cell invasion [304] and aberrant gene expression, triggered by elevated HECTD1 expression, possibly underlies human cancer development [316]. Indeed, HECTD1 has also been implicated in fibroblast migration/proliferation expression of breast cancer patients [317]. Furthermore, the reported links between HECTD1 and reduced survival in multiple cancer types, including breast, lung and brain [312], [319]–[321] heavily suggest that investigations in cancer cell models to examine tumour-specific expression and roles of HECTD1, particularly related to regulation of the cellular DDR identified in this thesis, would be a vital extension of the work given the current focus on normal lung fibroblasts.

## 7.6 Concluding remarks

The findings presented in this thesis have clearly demonstrated:

- HECTD1 promotes DNA glycosylase and AP endonuclease stages of BER in chromatin *in vitro*
- HECTD1 ubiquitylates histones H2B and H3 *in vitro*
- HECTD1 is essential for efficient SSB DNA repair and the promotion of cellular survival following exposure to X-ray IR, $H_2O_2$ and MMS in normal lung fibroblasts
- A novel role for HECTD1 within DNA repair where it acts to promote BER in occluded regions of chromatin

The work described in this research project is important as it has elucidated a novel role for the E3 ubiquitin ligase HECTD1 within DNA repair. Furthermore, this research project has focused on a relatively understudied area within the DNA repair field, strengthening evidence for chromatin remodelling events in BER, and having identified HECTD1 that functions in this capacity. This has increased our knowledge and understanding of the cellular response to DNA damage and further validation of the underlying regulatory mechanism of HECTD1 within BER will undoubtedly aid in our understanding of how defects in DNA repair leads to genomic instability and pathogenesis. This solid foundation provides hope for the long-term goal of potentially utilising HECTD1 as a novel therapeutic target

given that HECTD1 is frequently mutated in breast, brain and lung cancers, and therefore improving current cancer treatment strategies, in particular sensitivity to radiotherapy.

# References


[1] S. P. Jackson and J. Bartek, “Europe PMC Funders Group The DNA-damage response in human biology and disease,” *Nature*, vol. 461, no. 7267, pp. 1071–1078, 2010, doi: 10.1038/nature08467.The.

[2] D. Hanahan and R. A. Weinberg, “Hallmarks of cancer: The next generation,” *Cell*, vol. 144, no. 5, pp. 646–674, 2011, doi: 10.1016/j.cell.2011.02.013.

[3] Watson JD & Crick FH, “Molecular structure of nucleic acids; a structure for deoxyribose nucleic acid.,” *Nature*, vol. 1, no. 7, pp. 737–738, 1953.

[4] O. Avery, C. MacLeod, and M. Mccarty, “( STUDIES ON THE CHEMICAL NATURE OF THE SUBSTANCE INDUCING TRANSFORMATION OF PNEUMOCOCCAL TYPES ),” no. 6, 1944.

[5] E. Chargraff, R. Lipshitz, C. Green, and M. E. Hodes, “THE COMPOSITION OF THE DESOXYRIBONUCLEIC ACID OF SALMON SPERM*,” *J. Biol. Chem.*, vol. 192, pp. 223–230, 1951.

[6] J. H. J. Hoeijmakers, “DNA Damage, Aging, and Cancer,” pp. 1475–1485, 2009.

[7] T. Lindahl, “Instability and decay of the primary structure of DNA,” *Nature*, vol. 362, no. 6422, pp. 709–715, 1993, doi: 10.1038/362709a0.

[8] M. Sander *et al.*, “Proceedings of a workshop on DNA adducts: Biological significance and applications to risk assessment Washington, DC, April 13-14, 2004,” *Toxicol. Appl. Pharmacol.*, vol. 208, no. 1, pp. 1–20, 2005, doi: 10.1016/j.taap.2004.12.012.

[9] K. S. Rao, “Mechanisms of disease: DNA repair defects and neurological disease,” *Nat. Clin. Pract. Neurol.*, vol. 3, no. 3, pp. 162–172, 2007, doi: 10.1038/ncpneuro0448.

[10] L. J. Niedernhofer, A. U. Gurkar, Y. Wang, J. Vijg, J. H. J. Hoeijmakers, and P. D. Robbins, “Nuclear Genomic Instability and Aging,” *Annu. Rev. Biochem.*, vol. 87, no. 1, pp. 295–322, 2018, doi: 10.1146/annurev-biochem-062917-012239.

[11] A. L. Jackson and L. A. Loeb, “The contribution of endogenous sources of DNA damage to the multiple mutations in cancer,” *Mutat. Res. - Fundam. Mol. Mech. Mutagen.*, vol. 477, no. 1–2, pp. 7–21, 2001, doi: 10.1016/S0027-5107(01)00091-4.

[12] R. De Bont and N. van Larebeke, “Endogenous DNA damage in humans: A review of quantitative data,” *Mutagenesis*, vol. 19, no. 3, pp. 169–185, 2004, doi: 10.1093/mutage/geh025.

[13] T. Lindahl, “DNA Repair Enzymes,” *Annu. Rev. Biochem.*, vol. 51, no. 1, pp. 61–87, 1982, doi: 10.1146/annurev.biochem.57.1.29.

[14] Y. Yu, P. Wang, Y. Cui, and Y. Wang, “Chemical Analysis of DNA Damage,” vol. 90, no. 1, pp. 556–576, 2018, doi: 10.1021/acs.analchem.7b04247.Chemical.

[15] M. S. Cooke, M. D. Evans, M. Dizdaroglu, and J. Lunec, “Oxidative DNA damage: mechanisms, mutation, and disease,” *FASEB J.*, vol. 17, no. 10, pp. 1195–1214, 2003, doi: 10.1096/fj.02-0752rev.

[16] P. A. Ward, J. S. Warren, and K. J. Johnson, “Oxygen radicals, inflammation, and tissue injury,” *Free Radic. Biol. Med.*, vol. 5, no. 5–6, pp. 403–408, 1988, doi: 10.1016/0891-5849(88)90114-1.

[17] K. P. Arjunan, V. K. Sharma, and S. Ptasinska, “Effects of atmospheric pressure plasmas on isolated and cellular DNA—a review,” *Int. J. Mol. Sci.*, vol. 16, no. 2, pp. 2971–3016, 2015, doi: 10.3390/ijms16022971.

[18] T. Tabatabaie and A. Floyd, Robert, “Susceptibility of glutathione peroxidase and glutathione reductase to oxidative damage and the protective effect of spin trapping agent.” 1994.

[19] Y. Kono and I. Fridovich, “Superoxide radical inhibits catalase.,” *J. Biol. Chem.*, vol. 257, no. 10, pp. 5751–5754, 1982.

[20] R. A. Floyd, “Measurement of Oxidative Stress in vivo,” *Free Radic. Biol. Med.*, vol. 15, no. 5, p. 479, 1993.

[21] S. Maynard, S. H. Schurman, C. Harboe, N. C. de Souza-Pinto, and V. A. Bohr, “Base excision repair of oxidative DNA damage and association with cancer and aging,” *Carcinogenesis*, vol. 30, no. 1, pp. 2–10, 2009, doi: 10.1093/carcin/bgn250.

[22] B. Chance, H. Sies, and A. Boveris, “Hydroperoxide metabolism in mammalian organs,” *Physiol. Rev.*, vol. 59, no. 3, pp. 527–605, 1979, doi: 10.1152/physrev.1979.59.3.527.

[23] A. R. Cross and O. T. G. Jones, “Enzymic mechanisms of superoxide production,” *BBA - Bioenerg.*, vol. 1057, no. 3, pp. 281–298, 1991, doi: 10.1016/S0005-2728(05)80140-9.

[24] H. Kamata and H. Hirata, “Redox regulation of cellular signalling,” *Cell. Signal.*, vol. 11, no. 1, pp. 1–14, 1999, doi: 10.1016/S0898-6568(98)00037-0.

[25] W. a Pryor, “OXY-RADICALS AND RELATED and Reactions,” *Annu. Rev. Physiol.*, vol. 48, pp. 657–667, 1986.

[26] L. J. Marnett, “Oxyradicals and DNA damage,” *Carcinogenesis*, vol. 21, no. 3, pp. 361–370, 2000, doi: 10.1093/carcin/21.3.361.

[27] N. R. Jena and P. C. Mishra, “Formation of ring-opened and rearranged products of guanine: Mechanisms and biological significance,” *Free Radic. Biol. Med.*, vol. 53, no. 1, pp. 81–94, 2012, doi: 10.1016/j.freeradbiomed.2012.04.008.

[28] S. Steenken and S. V. Jovanovic, “How easily oxidizable is DNA? One-electron reduction potentials of adenosine and guanosine radicals in aqueous solution,” *J. Am. Chem. Soc.*, vol. 119, no. 3, pp. 617–618, 1997, doi: 10.1021/ja962255b.

[29] J. E. Klaunig *et al.*, “The role of oxidative stress in chemical carcinogenesis,” *Environ. Health Perspect.*, vol. 106, no. SUPPL. 1, pp. 289–295, 1998, doi: 10.2307/3433929.

[30] B. van Loon, E. Markkanen, and U. Hübscher, “Oxygen as a friend and enemy: How to combat the mutational potential of 8-oxo-guanine,” *DNA Repair (Amst).*, vol. 9, no. 6, pp. 604–616, 2010, doi: 10.1016/j.dnarep.2010.03.004.

[31] S. Shibutani, M. Takeshita, and A. P. Grollman, “Insertion of specific bases during DNA synthesis past the oxidationdamaged base 8-oxodG,” *J J al. Proc. natn. Acad. Sci. USA*, vol. 349, no. 2, pp. 139–149, 1991.

[32] C. Greenman *et al.*, “Patterns of somatic mutation in human cancer genomes,” vol. 446, no. 7132, pp. 153–158, 2009, doi: 10.1038/nature05610.Patterns.

[33] J. C. Niles, J. S. Wishnok, and S. R. Tannenbaum, “Spiroiminodihydantoin Is the Major Product of the 8-Oxo-7,8-dihydroguanosine Reaction with Peroxynitrite in the Presence of Thiols and Guanosine Photooxidation by Methylene Blue,” *Org. Lett.*, vol. 3, no. 7, pp. 963–966, 2001, doi: 10.1021/ol006993n.

[34] V. Duarte *et al.*, “Oxaluric acid as the major product of singlet oxygen-mediated oxidation of 8-oxo-7,8-dihydroguanine in DNA,” *J. Am. Chem. Soc.*, vol. 122, no. 51, pp. 12622–12628, 2000, doi: 10.1021/ja002218r.

[35] G. Slupphaug, B. Kavli, and H. E. Krokan, “The interacting pathways for prevention and repair of oxidative DNA damage,” *Mutat. Res. - Fundam. Mol. Mech. Mutagen.*, vol. 531, no. 1–2, pp. 231–251, 2003, doi: 10.1016/j.mrfmmm.2003.06.002.

[36] N. G. Dolinnaya, E. A. Kubareva, E. A. Romanova, R. M. Trikin, and T. S. Oretskaya, “Thymidine glycol: The effect on DNA molecular structure and enzymatic processing,” *Biochimie*, vol. 95, no. 2, pp. 134–147, 2013, doi: 10.1016/j.biochi.2012.09.008.

[37] A. K. Basu, E. L. Loechler, S. A. Leadon, and J. M. Essigmann, “Genetic effects of thymine glycol: Site-specific mutagenesis and molecular modeling studies,” *Proc. Natl. Acad. Sci. United States Am.*, vol. 86, no. October, pp. 7677–7681, 1989.

[38] R. Hayes and J. E. LeClerc, “Sequence dependence for bypass of thymine glycols in DNA by DNA polymerase I,” *Nucleic Acids Res.*, vol. 14, no. 2, pp. 1045–1061, 1986.

[39] J. M. Clark and G. P. Beardsley, “Template Length, Sequence Context, and 3’-5’ Exonuclease Activity Modulate Replicative Bypass of Thymine Glycol Lesions in Vitro,” *Biochemistry*, vol. 28, no. 2, pp. 775–779, 1989, doi: 10.1021/bi00428a054.

[40] R. Cathcart, E. Schwiers, R. L. Saul, and B. N. Ames, “Thymine glycol and thymidine glycol in human and rat urine: A possible assay for oxidative DNA damage,” *Proc. Natl. Acad. Sci. U. S. A.*, vol. 81, no. 18 I, pp. 5633–5637, 1984, doi: 10.1073/pnas.81.18.5633.

[41] R. Adelman, R. L. Saul, and B. N. Ames, “Oxidative damage to DNA: relation to species metabolic rate and life span.,” *Proc. Natl. Acad. Sci. U. S. A.*, vol. 85, no. 8, pp. 2706–2708, 1988, doi: 10.1073/pnas.85.8.2706.

[42] R. Saul and B. Ames, “BACKGROUND LEVELS OF DNA DAMAGE IN THE POPULATION,” in *Mechanisms of DNA Damage and Repair.*, vol. 189, 1986, pp. 529–535.

[43] J. Nakamura, D. K. La, and J. A. Swenberg, “5’-Nicked apurinic/apyrimidinic sites are resistant to β-elimination by β-polymerase and are persistent in human cultured cells after oxidative stress,” *J. Biol. Chem.*, vol. 275, no. 8, pp. 5323–5328, 2000, doi: 10.1074/jbc.275.8.5323.

[44] F. Drabløs *et al.*, “Alkylation damage in DNA and RNA - Repair mechanisms and medical significance,” *DNA Repair (Amst).*, vol. 3, no. 11, pp. 1389–1407, 2004, doi: 10.1016/j.dnarep.2004.05.004.

[45] T. Lindahl and O. Karlström, “Heat-Induced Depyrimidination of Deoxyribonucleic Acid in Neutral Solution,” *Biochemistry*, vol. 12, no. 25, pp. 5151–5154, 1973, doi: 10.1021/bi00749a020.

[46] J. Nakamura and J. A. Swenberg, “Endogenous apurinic/apyrimidinic sites in genomic DNA of mammalian tissues,” *Cancer Res.*, vol. 59, no. 11, pp. 2522–2526, 1999.

[47] S. P. Hussain and C. C. Harris, “Molecular epidemiology of human cancer: Contribution of mutation spectra studies of tumor suppressor genes,” *Cancer Res.*, vol. 58, no. 18, pp. 4023–4037, 1998.

[48] S. Boiteux and M. Guillet, “Abasic sites in DNA: Repair and biological consequences in Saccharomyces cerevisiae,” *DNA Repair (Amst).*, vol. 3, no. 1, pp. 1–12, 2004, doi: 10.1016/j.dnarep.2003.10.002.

[49] T. Lindahl and B. Nyberg, “Heat-induced deamination of cytosine residues in deoxyribonucleic acid,” *Biochemistry*, vol. 13, no. 16, pp. 3405–3410, 1974, doi: 10.1021/bi00713a035.

[50] D. N. Cooper and H. Youssoufian, “The CpG dinucleotide and human genetic disease,” *Hum. Genet.*, vol. 78, no. 2, pp. 151–155, 1988, doi: 10.1007/BF00278187.

[51] J. X. Chen, Y. Zheng, M. West, and M. S. Tang, “Carcinogens preferentially bind at methylated CpG in the p53 mutational hot spots,” *Cancer Res.*, vol. 58, no. 10, pp. 2070–2075, 1998.

[52] W. M. Rideout, G. A. Coetzee, A. F. Olumi, C. H. Spruck, and P. A. Jones, “5-Methylcytosine as an endogenous mutagen in the p53 tumor suppressor gene.,” *Princess Takamatsu Symp.*, vol. 22, no. 13, pp. 207–219, 1991.

[53] S. L. Washington *et al.*, “A genetic system to identify DNA polymerase β mutator mutants,” *Proc. Natl. Acad. Sci. U. S. A.*, vol. 94, no. 4, pp. 1321–1326, 1997, doi: 10.1073/pnas.94.4.1321.

[54] R. Hindges and U. Hübscher, “Production of active mouse DNA polymerase β in bacteria,” *Gene*, vol. 158, no. 2, pp. 241–246, 1995, doi: 10.1016/0378-1119(95)00065-E.

[55] A. Umar and T. A. Kunkel, “DNA-replication fidelity, mismatch repair and genome instability in cancer cells,” *Eur. J. Biochem.*, vol. 238, no. 2, pp. 297–307, 1996, doi: 10.1111/j.1432-1033.1996.0297z.x.

[56] J. Syvaoja *et al.*, “DNA polymerases α, δ, and ε: Three distinct enzymes from HeLa cells,” *Proc. Natl. Acad. Sci. U. S. A.*, vol. 87, no. 17, pp. 6664–6668, 1990, doi: 10.1073/pnas.87.17.6664.

[57] P. Modrich, “Mismatch Repair in Replication Fidelity, Genetic Recombination, and Cancer Biology,” *Annu. Rev. Biochem.*, vol. 65, no. 1, pp. 101–133, 1996, doi: 10.1146/annurev.biochem.65.1.101.

[58] M. Fry and L. A. Loeb, “The fragile X syndrome d(CGG)(n) nucleotide repeats form a stable tetrahelical structure,” *Proc. Natl. Acad. Sci. U. S. A.*, vol. 91, no. 11, pp. 4950–4954, 1994, doi: 10.1073/pnas.91.11.4950.

[59] O. V. Iarovaia, M. Rubtsov, E. Ioudinkova, T. Tsfasman, S. V. Razin, and Y. S. Vassetzky, “Dynamics of double strand breaks and chromosomal translocations,” *Mol. Cancer*, vol. 13, no. 1, pp. 1–10, 2014, doi: 10.1186/1476-4598-13-249.

[60] K. Rodgers and M. McVey, “Error-prone repair of DNA double-strand breaks,” *J Cell Physiol*, vol. 231, no. 1, pp. 15–24, 2016, doi: 10.1016/j.physbeh.2017.03.040.

[61] H. Ghezraoui *et al.*, “Chromosomal Translocations in Human Cells Are Generated by Canonical Nonhomologous End-Joining,” *Mol. Cell*, vol. 55, no. 6, pp. 829–842, 2014, doi: 10.1016/j.molcel.2014.08.002.

[62] P. J. Stephens *et al.*, “Massive genomic rearrangement acquired in a single catastrophic event during cancer development,” *Cell*, vol. 144, no. 1, pp. 27–40, 2011, doi: 10.1016/j.cell.2010.11.055.

[63] H. Cai, N. Kumar, H. C. Bagheri, C. von Mering, M. D. Robinson, and M. Baudis, “Chromothripsis-like patterns are recurring but heterogeneously distributed features in a survey of 22,347 cancer genome screens,” *BMC Genomics*, vol. 15, no. 1, 2014, doi: 10.1186/1471-2164-15-82.

[64] G. P. Margison, M. F. Santiba, and A. C. Povey, “Mechanisms of carcinogenicity / chemotherapy by O 6 -methylguanine ´ n,” *Mutagenesis*, vol. 17, no. 6, pp. 483–487, 2002.

[65] M. Christmann, M. T. Tomicic, W. P. Roos, and B. Kaina, “Mechanisms of human DNA repair: An update,” *Toxicology*, vol. 193, no. 1–2, pp. 3–34, 2003, doi: 10.1016/S0300-483X(03)00287-7.

[66] H. E. Krokan, R. Standal, and G. Slupphaug, “DNA glycosylases in the base excision repair of DNA,” *Biochem. J.*, vol. 325, no. 1, pp. 1–16, 1997, doi: 10.1042/bj3250001.

[67] D. Mielecki, M. Wrzesiński, and E. Grzesiuk, “Inducible repair of alkylated DNA in microorganisms,” *Mutat. Res. - Rev. Mutat. Res.*, vol. 763, pp. 294–305, 2015, doi: 10.1016/j.mrrev.2014.12.001.

[68] D. T. Beranek, “Distribution of methyl and ethyl adducts following alkylation with monofunctional alkylating agents,” *Mutat. Res. - Fundam. Mol. Mech. Mutagen.*, vol. 231, no. 1, pp. 11–30, 1990, doi: 10.1016/0027-5107(90)90173-2.

[69] N. Shrivastav, D. Li, and J. M. Essigmann, “Chemical biology of mutagenesis and DNA repair: Cellular responses to DNA alkylation,” *Carcinogenesis*, vol. 31, no. 1, pp. 59–70, 2009, doi: 10.1093/carcin/bgp262.

[70] B. Rydberg and T. Lindahl, “Nonenzymatic methylation of DNA by the intracellular methyl group donor S-adenosyl-L-methionine is a potentially mutagenic reaction.,” *EMBO J.*, vol. 1, no. 2, pp. 211–216, 1982, doi: 10.1002/j.1460-2075.1982.tb01149.x.

[71] S. S. Hecht, “DNA adduct formation from tobacco-specific N-nitrosamines,” *Mutat. Res. - Fundam. Mol. Mech. Mutagen.*, vol. 424, no. 1–2, pp. 127–142, 1999, doi: 10.1016/S0027-5107(99)00014-7.

[72] N. Kondo, A. Takahashi, K. Ono, and T. Ohnishi, “DNA damage induced by alkylating agents and repair pathways,” *J. Nucleic Acids*, vol. 2010, 2010, doi: 10.4061/2010/543531.

[73] J. M. Soll, R. W. Sobol, and N. Mosammaparast, “Regulation of DNA Alkylation Damage Repair: Lessons and Therapeutic Opportunities,” *Trends Biochem Sci*, vol. 42, no. 3, pp. 206–218, 2017, doi: 10.1016/j.physbeh.2017.03.040.

[74] D. L. Bordin *et al.*, “DNA alkylation damage and autophagy induction,” *Mutat. Res. - Rev. Mutat. Res.*, vol. 753, no. 2, pp. 91–99, 2013, doi: 10.1016/j.mrrev.2013.07.001.

[75] J. Cadet, T. Douki, D. Gasparutto, and J. L. Ravanat, “Oxidative damage to DNA: Formation, measurement and biochemical features,” *Mutat. Res. - Fundam. Mol.*

*Mech. Mutagen.*, vol. 531, no. 1–2, pp. 5–23, 2003, doi: 10.1016/j.mrfmmm.2003.09.001.

[76] E. T. Vitti and J. L. Parsons, "The radiobiological effects of proton beam therapy: Impact on DNA damage and repair," *Cancers (Basel).*, vol. 11, no. 7, pp. 1–15, 2019, doi: 10.3390/cancers11070946.

[77] M. E. Lomax, L. K. Folkes, and P. O'Neill, "Biological consequences of radiation-induced DNA damage: Relevance to radiotherapy," *Clin. Oncol.*, vol. 25, no. 10, pp. 578–585, 2013, doi: 10.1016/j.clon.2013.06.007.

[78] J. Cadet, T. Douki, and J. L. Ravanat, "Oxidatively generated damage to the guanine moiety of DNA: Mechanistic aspects and formation in cells," *Acc. Chem. Res.*, vol. 41, no. 8, pp. 1075–1083, 2008, doi: 10.1021/ar700245e.

[79] R. Hanai, M. Yazu, and K. Hieda, "On the experimental distinction between ssbs and dsbs in circular DNA," *Int. J. Radiat. Biol.*, vol. 73, no. 5, pp. 475–479, 1998, doi: 10.1080/095530098142013.

[80] R. J. Carter, C. M. Nickson, J. M. Thompson, A. Kacperek, M. A. Hill, and J. L. Parsons, "Complex DNA Damage Induced by High Linear Energy Transfer Alpha-Particles and Protons Triggers a Specific Cellular DNA Damage Response," *Int. J. Radiat. Oncol. Biol. Phys.*, vol. 100, no. 3, pp. 776–784, 2018, doi: 10.1016/j.ijrobp.2017.11.012.

[81] R. D. Stewart, V. K. Yu, A. G. Georgakilas, C. Koumenis, J. H. Park, and D. J. Carlson, "Effects of Radiation Quality and Oxygen on Clustered DNA Lesions and Cell Death," *Radiat. Res.*, vol. 176, no. 5, pp. 587–602, 2011, doi: 10.1667/rr2663.1.

[82] H. Nikjoo, P. O'Neill, W. E. Wilson, and D. T. Goodhead, "Computational Approach for Determining the Spectrum of DNA Damage Induced by Ionizing Radiation," *Radiat. Res.*, vol. 156, no. 5, pp. 577–583, 2001, doi: 10.1667/0033-7587(2001)156[0577:cafdts]2.0.co;2.

[83] H. Nikjoo *et al.*, "Modelling of DNA damage induced by energetic electrons (100 eV to 100 keV)," *Radiat. Prot. Dosimetry*, vol. 99, no. 1–4, pp. 77–80, 2002, doi: 10.1093/oxfordjournals.rpd.a006843.

[84] R. Watanabe, S. Rahmanian, and H. Nikjoo, "Spectrum of Radiation-Induced Clustered Non-DSB Damage – A Monte Carlo Track Structure Modeling and Calculations," *Radiat. Res.*, vol. 183, no. 5, pp. 525–540, 2015, doi: 10.1667/rr13902.1.

[85] L. J. Eccles, P. O'Neill, and M. E. Lomax, "Delayed repair of radiation induced clustered DNA damage: Friend or foe?," *Mutat. Res. - Fundam. Mol. Mech. Mutagen.*, vol. 711, no. 1–2, pp. 134–141, 2011, doi: 10.1016/j.mrfmmm.2010.11.003.

[86] E. Gollapalle *et al.*, "Detection of Oxidative Clustered DNA Lesions in X-Irradiated Mouse Skin Tissues and Human MCF-7 Breast Cancer Cells," vol. 167, no. 2, pp. 207–216, 2007.

[87] K. Magnander, R. Hultborn, K. Claesson, and K. Elmroth, "Clustered DNA Damage in Irradiated Human Diploid Fibroblasts: Influence of Chromatin Organization," *Radiat. Res.*, vol. 173, no. 3, pp. 272–282, 2010, doi: 10.1667/rr1891.1.

[88] R. P. Gallagher and T. K. Lee, "Adverse effects of ultraviolet radiation: A brief review," *Prog. Biophys. Mol. Biol.*, vol. 92, no. 1, pp. 119–131, 2006, doi:

10.1016/j.pbiomolbio.2006.02.011.

[89] J. Dahle and E. Kvam, “Induction of delayed mutations and chromosomal instability in fibroblasts after UVA-, UVB-, and X-radiation,” *Cancer Res.*, vol. 63, no. 7, pp. 1464–1469, 2003.

[90] F. El Ghissassi *et al.*, “A review of human carcinogens--part D: radiation.,” *Lancet Oncol.*, vol. 10, no. 8, pp. 751–752, 2009, doi: 10.1016/s1470-2045(09)70213-x.

[91] G. P. Pfeifer, “Formation and Processing of UV Photoproducts: Effetcs of DNA Sequence and Chromatin Environment,” *Photochem. Photobiol.*, vol. 65, no. 2, pp. 270–283, 1997, doi: 10.1111/j.1751-1097.1997.tb08560.x.

[92] D. L. Mitchell and R. S. Nairn, “THE BIOLOGY OF THE (6-4) PHOTOPRODUCT Introduction,” *Photochem. Photobiol.*, vol. 49, no. 6, pp. 805–819, 1989.

[93] R. P. Sinha and D. P. Häder, “UV-induced DNA damage and repair: A review,” *Photochem. Photobiol. Sci.*, vol. 1, no. 4, pp. 225–236, 2002, doi: 10.1039/b201230h.

[94] S. L. Yu and S. K. Lee, “Ultraviolet radiation: DNA damage, repair, and human disorders,” *Mol. Cell. Toxicol.*, vol. 13, no. 1, pp. 21–28, 2017, doi: 10.1007/s13273-017-0002-0.

[95] R. P. Rastogi, Richa, A. Kumar, M. B. Tyagi, and R. P. Sinha, “Molecular mechanisms of ultraviolet radiation-induced DNA damage and repair,” *J. Nucleic Acids*, vol. 2010, 2010, doi: 10.4061/2010/592980.

[96] E. Sage, B. Lamolet, E. Brulay, E. Moustacchi, A. Châteauneuf, and E. A. Drobetsky, “Mutagenic specificity of solar UV light in nucleotide excision repair-deficient rodent cells,” *Proc. Natl. Acad. Sci. U. S. A.*, vol. 93, no. 1, pp. 176–180, 1996, doi: 10.1073/pnas.93.1.176.

[97] M. Y. Kim, H. J. Park, S. C. Baek, D. G. Byun, and D. Houh, “Mutations of the p53 and PTCH gene in basal cell carcinomas: UV mutation signature and strand bias,” *J. Dermatol. Sci.*, vol. 29, no. 1, pp. 1–9, 2002, doi: 10.1016/S0923-1811(01)00170-0.

[98] J. Cadet, T. Douki, J. L. Ravanat, and P. Di Masico, “Sensitized formation of oxidatively generated damge to cellular DNA by UVA radiation.” pp. 903–911, 2009.

[99] J. Cadet and T. Douki, “Oxidatively generated damage to DNA by UVA radiation in cells and human skin,” *J. Invest. Dermatol.*, vol. 131, no. 5, pp. 1005–1007, 2011, doi: 10.1038/jid.2011.51.

[100] A. Banyasz, I. Vayá, P. Changenet-Barret, T. Gustavsson, T. Douki, and D. Markovitsi, “Base pairing enhances fluorescence and favors cyclobutane dimer formation induced upon absorption of UVA radiation by DNA,” *J. Am. Chem. Soc.*, vol. 133, no. 14, pp. 5163–5165, 2011, doi: 10.1021/ja110879m.

[101] L. H. Pearl, A. C. Schierz, S. E. Ward, B. Al-Lazikani, and F. M. G. Pearl, “Therapeutic opportunities within the DNA damage response,” *Nat. Rev. Cancer*, vol. 15, no. 3, pp. 166–180, 2015, doi: 10.1038/nrc3891.

[102] N. Pannunzio, G. Watanabe, and M. R. Lieber, “Nonhomologous DNA end-joining for repair of DNA double-strand breaks,” vol. 293, no. 27, pp. 10512–10523, 2018, doi: 10.1074/jbc.TM117.000374.

[103] M. R. Lieber, “Mechanisms of Human Lmphoid Chromosomal Translocations,” *Nat. Rev. Cancer*, vol. 16, no. 6, pp. 387–398, 2016, doi:

10.1038/nrc.2016.40.Mechanisms.

[104] K. P. Kohl and J. Sekelsky, “Meiotic and mitotic recombination in meiosis,” *Genetics*, vol. 194, no. 2, pp. 327–334, 2013, doi: 10.1534/genetics.113.150581.

[105] A. Beucher *et al.*, “ATM and Artemis promote homologous recombination of radiation-induced DNA double-strand breaks in G2,” *EMBO J.*, vol. 28, no. 21, pp. 3413–3427, 2009, doi: 10.1038/emboj.2009.276.

[106] J. R. Walker, R. A. Corpina, and J. Goldberg, “Structure of the Ku heterodimer bound to dna and its implications for double-strand break repair,” *Nature*, vol. 412, no. 6847, pp. 607–614, 2001, doi: 10.1038/35088000.

[107] K. Meek, P. Douglas, X. Cui, Q. Ding, and S. P. Lees-Miller, “trans Autophosphorylation at DNA-Dependent Protein Kinase’s Two Major Autophosphorylation Site Clusters Facilitates End Processing but Not End Joining,” *Mol. Cell. Biol.*, vol. 27, no. 10, pp. 3881–3890, 2007, doi: 10.1128/mcb.02366-06.

[108] Y. Ma *et al.*, “A biochemically defined system for mammalian nonhomologous DNA end joining,” *Mol. Cell*, vol. 16, no. 5, pp. 701–713, 2004, doi: 10.1016/j.molcel.2004.11.017.

[109] H. Lu *et al.*, “A Biochemically Defined System for Coding Joint Formation in V(D)J Recombination,” *Mol. Cell*, vol. 31, no. 4, pp. 485–497, 2008, doi: 10.1016/j.molcel.2008.05.029.

[110] C. Chappell, L. A. Hanakahi, F. Karimi-Busheri, M. Weinfeld, and S. C. West, “Involvement of human polynucleotide kinase in double-strand break repair by non-homologous end joining,” *EMBO J.*, vol. 21, no. 11, pp. 2827–2832, 2002, doi: 10.1093/emboj/21.11.2827.

[111] J. Della-Maria *et al.*, “Human Mre11/human Rad50/Nbs1 and DNA ligase IIIα/XRCC1 protein complexes act together in an alternative nonhomologous end joining pathway,” *J. Biol. Chem.*, vol. 286, no. 39, pp. 33845–33853, 2011, doi: 10.1074/jbc.M111.274159.

[112] V. Gomez and A. Hergovich, *Cell-Cycle Control and DNA-Damage Signaling in Mammals*, vol. 1. Elsevier Inc., 2016.

[113] S. P. Jackson, “Sensing and repairing DNA double-strand breaks,” *Carcinogenesis*, vol. 23, no. 5, pp. 687–696, 2002, doi: 10.1093/carcin/23.5.687.

[114] G. Borrego-Soto, R. Ortiz-López, and A. Rojas-Martínez, “Ionizing radiation-induced DNA injury and damage detection in patients with breast cancer,” *Genet. Mol. Biol.*, vol. 38, no. 4, pp. 420–432, 2015, doi: 10.1590/S1415-475738420150019.

[115] S. C. Kowalczykowski, “An overview of the molecular mechanismsof recombinational DNA repair,” *Cold Spring Harb. Perspect. Biol.*, vol. 7, no. 11, pp. 1–36, 2015, doi: 10.1101/cshperspect.a016410.

[116] A. Orthwein *et al.*, “A mechanism for the suppression of homologous recombination in G1 cells,” *Nature*, vol. 528, no. 7582, pp. 422–426, 2015, doi: 10.1038/nature16142.

[117] A. Shibata *et al.*, “DNA Double Strand Break Repair Pathway Choice Is Directed by Distinct MRE11 Nuclease Activities,” *Mol. Cell*, vol. 53, no. 1, pp. 7–18, 2014, doi: 10.1016/j.molcel.2013.11.003.DNA.

[118] R. Anand, L. Ranjha, E. Cannavo, and P. Cejka, “Phosphorylated CtIP Functions as a Co-factor of the MRE11-RAD50-NBS1 Endonuclease in DNA End Resection,” *Mol. Cell*, vol. 64, no. 5, pp. 940–950, 2016, doi: 10.1016/j.molcel.2016.10.017.

[119] V. Garcia, S. E. L. Phelps, S. Gray, and M. J. Neale, “Bidirectional resection of DNA double-strand breaks by Mre11 and Exo1,” *Nature*, vol. 479, no. 7372, pp. 241–244, 2011, doi: 10.1038/nature10515.

[120] Z. Zhu, W.-H. Chung, E. Y. Shim, S. E. Lee, and G. Ira, “Sgs1 helicase and two nucleases Dna2 and Exo1 resect DNA double strand break ends,” *Cell*, vol. 134, no. 6, pp. 981–994, 2008, doi: 10.1016/j.cell.2008.08.037.Sgs1.

[121] F. E. Benson, A. Stasiak, and S. C. West, “Purification and characterization of the human Rad51 protein, an analogue of E.coli RecA,” *EMBO J.*, vol. 13, no. 23, pp. 5764–5771, 1994, doi: 10.1002/j.1460-2075.1994.tb06914.x.

[122] W. Zhao *et al.*, “Promotion of RAD51-mediated homologous DNA pairing by BRCA1-BARD1,” *Nature.*, vol. 47, no. 3, pp. 549–562, 2017, doi: 10.1038/nature24060.Promotion.

[123] R. B. Jensen, A. Carreira, and S. C. Kowalczykowski, “Purified human BRCA2 stimulates RAD51-mediated recombination Ryan,” *Nature*, vol. 467, no. 7316, pp. 678–683, 2010, doi: 10.1016/j.physbeh.2017.03.040.

[124] J. Y. Masson *et al.*, “Identification and purification of two distinct complexes containing the five RAD51 paralogs,” *Genes Dev.*, vol. 15, no. 24, pp. 3296–3307, 2001, doi: 10.1101/gad.947001.

[125] J. Renkawitz, C. A. Lademann, and S. Jentsch, “Mechanisms and principles of homology search during recombination,” *Nat. Rev. Mol. Cell Biol.*, vol. 15, no. 6, pp. 369–383, 2014, doi: 10.1038/nrm3805.

[126] Z. Qi *et al.*, “DNA sequence alignment by microhomology sampling during homologous recombination,” *Cell*, vol. 160, no. 5, pp. 856–869, 2015, doi: 10.1016/j.cell.2015.01.029.DNA.

[127] L. Ranjha, S. M. Howard, and P. Cejka, “Main steps in DNA double-strand break repair: an introduction to homologous recombination and related processes,” *Chromosoma*, vol. 127, no. 2, pp. 187–214, 2018, doi: 10.1007/s00412-017-0658-1.

[128] X. Li, C. M. Stith, P. M. Burgers, and W. D. Heyer, “PCNA Is Required for Initiation of Recombination-Associated DNA Synthesis by DNA Polymerase δ,” *Mol. Cell*, vol. 36, no. 4, pp. 704–713, 2009, doi: 10.1016/j.molcel.2009.09.036.

[129] W. M. Hicks, M. Kim, and J. E. Haber, “Increased mutagenesis and unique mutation signature associated with mitotic gene conversion Wade,” *Science (80-. ).*, vol. 329, no. 5687, pp. 82–85, 2010, doi: 10.1126/science.1191125.Increased.

[130] M. A. Wilson *et al.*, “Pif1 helicase and Polδ promote recombination-coupled DNA synthesis via bubble migration,” *Nature*, vol. 502, no. 7471, pp. 393–396, 2013, doi: 10.1038/nature12585.Pif1.

[131] T. Kawamoto *et al.*, “Dual roles for DNA polymerase η in homologous DNA recombination and translesion DNA synthesis,” *Mol. Cell*, vol. 20, no. 5, pp. 793–799, 2005, doi: 10.1016/j.molcel.2005.10.016.

[132] M. J. Mcllwraith, A. Vaisman, Y. Liu, E. Fanning, R. Woodgate, and S. C. West,

"Human DNA polymerase η promotes DNA synthesis from strand invasion intermediates of homologous recombination," *Mol. Cell*, vol. 20, no. 5, pp. 783–792, 2005, doi: 10.1016/j.molcel.2005.10.001.

[133] J. W. Szostak, T. L. Orr-Weaver, R. J. Rothstein, and F. W. Stahl, "The double-strand-break repair model for recombination," *Cell*, vol. 33, no. 1, pp. 25–35, 1983, doi: 10.1016/0092-8674(83)90331-8.

[134] P. Sung and H. Klein, "Mechanism of homologous recombination: Mediators and helicases take on regulatory functions," *Nat. Rev. Mol. Cell Biol.*, vol. 7, no. 10, pp. 739–750, 2006, doi: 10.1038/nrm2008.

[135] K. Kaniecki, L. De Tullio, and E. C. Greene, "A change of view: Homologous recombination at single-molecule resolution," *Nat. Rev. Genet.*, vol. 19, no. 4, pp. 191–207, 2018, doi: 10.1038/nrg.2017.92.

[136] L. C. J. Gillet and O. D. Schärer, "Molecular mechanisms of mammalian global genome nucleotide excision repair," *Chem. Rev.*, vol. 106, no. 2, pp. 253–276, 2006, doi: 10.1021/cr040483f.

[137] F. von Hebra and M. Kaposi, *On Diseases of the Skin, Including the Exanthemata*, vol. 3. 1874.

[138] E. A. Cockayne, "Dwarfism With Retinal Atrophy," *Arch. Dis. Child.*, vol. 11, no. 61, pp. 1–8, 1935.

[139] J. A. Marteijn, H. Lans, W. Vermeulen, and J. H. J. Hoeijmakers, "Understanding nucleotide excision repair and its roles in cancer and ageing," *Nat. Rev. Mol. Cell Biol.*, vol. 15, no. 7, pp. 465–481, 2014, doi: 10.1038/nrm3822.

[140] C. Masutani *et al.*, "Purification and cloning of a nucleotide excision repair complex involving the xeroderma pigmentosum group C protein and a human homologue of yeast RAD23," *EMBO J.*, vol. 13, no. 8, pp. 1831–1843, 1994, doi: 10.1002/j.1460-2075.1994.tb06452.x.

[141] R. Nishi *et al.*, "Centrin 2 Stimulates Nucleotide Excision Repair by Interacting with Xeroderma Pigmentosum Group C Protein," *Mol. Cell. Biol.*, vol. 25, no. 13, pp. 5664–5674, 2005, doi: 10.1128/mcb.25.13.5664-5674.2005.

[142] J. H. Min and N. P. Pavletich, "Recognition of DNA damage by the Rad4 nucleotide excision repair protein," *Nature*, vol. 449, no. 7162, pp. 570–575, 2007, doi: 10.1038/nature06155.

[143] D. Hoogstraten *et al.*, "Versatile DNA damage detection by the global genome nucleotide excision repair protein XPC," *J. Cell Sci.*, vol. 121, no. 23, p. 3991, 2008, doi: 10.1242/jcs.03503.

[144] K. Sugasawa, T. Okamoto, Y. Shimizu, C. Masutani, S. Iwai, and F. Hanaoka, "A multistep damage recognition mechanism for global genomic nucleotide excision repair," *Genes Dev.*, vol. 15, no. 5, pp. 507–521, 2001, doi: 10.1101/gad.866301.

[145] J. T. Reardon and A. Sancar, "Recognition and repair of the cyclobutane thymine dimer, a major cause of skin cancers, by the human excision nuclease," *Genes Dev.*, vol. 17, no. 20, pp. 2539–2551, 2003, doi: 10.1101/gad.1131003.

[146] M. Wakasugi *et al.*, "DDB accumulates at DNA damage sites immediately after UV irradiation and directly stimulates nucleotide excision repair," *J. Biol. Chem.*, vol.

277, no. 3, pp. 1637–1640, 2002, doi: 10.1074/jbc.C100610200.

[147] A. Scrima *et al.*, “Structural Basis of UV DNA-Damage Recognition by the DDB1-DDB2 Complex,” *Cell*, vol. 135, no. 7, pp. 1213–1223, 2008, doi: 10.1016/j.cell.2008.10.045.

[148] R. Groisman *et al.*, “The ubiquitin ligase activity in the DDB2 and CSA complexes is differentially regulated by the COP9 signalosome in response to DNA damage,” *Cell*, vol. 113, no. 3, pp. 357–367, 2003, doi: 10.1016/S0092-8674(03)00316-7.

[149] M. Yokoi, C. Masutani, T. Maekawa, K. Sugasawa, Y. Ohkuma, and F. Hanaoka, “The xeroderma pigmentosum group C protein complex XPC-HR23B plays an important role in the recruitment of transcription factor IIH to damaged DNA,” *J. Biol. Chem.*, vol. 275, no. 13, pp. 9870–9875, 2000, doi: 10.1074/jbc.275.13.9870.

[150] A. Tapias *et al.*, “Ordered Conformational Changes in Damaged DNA Induced by Nucleotide Excision Repair Factors,” *J. Biol. Chem.*, vol. 279, no. 18, pp. 19074–19083, 2004, doi: 10.1074/jbc.M312611200.

[151] A. F. Fagbemi, B. Orelli, and O. D. Schärer, “Regulation of endonuclease activity in human nucleotide excision,” *DNA Repair (Amst).*, vol. 10, no. 7, pp. 722–729, 2011, doi: 10.1016/j.dnarep.2011.04.022.Regulation.

[152] T. Ogi *et al.*, “Three DNA Polymerases, Recruited by Different Mechanisms, Carry Out NER Repair Synthesis in Human Cells,” *Mol. Cell*, vol. 37, no. 5, pp. 714–727, 2010, doi: 10.1016/j.molcel.2010.02.009.

[153] J. Moser, H. Kool, I. Giakzidis, K. Caldecott, L. H. F. Mullenders, and M. I. Fousteri, “Sealing of Chromosomal DNA Nicks during Nucleotide Excision Repair Requires XRCC1 and DNA Ligase IIIα in a Cell-Cycle-Specific Manner,” *Mol. Cell*, vol. 27, no. 2, pp. 311–323, 2007, doi: 10.1016/j.molcel.2007.06.014.

[154] M. Ljungman and F. Zhang, “Blockage of RNA polymerase as a possible trigger for UV light-induced apoptosis,” *Oncogene*, vol. 13, pp. 823–831, 1996.

[155] P. C. Hanawalt and G. Spivak, “Transcription-coupled DNA repair: Two decades of progress and surprises,” *Nat. Rev. Mol. Cell Biol.*, vol. 9, no. 12, pp. 958–970, 2008, doi: 10.1038/nrm2549.

[156] M. Fousteri, W. Vermeulen, A. A. van Zeeland, and L. H. F. Mullenders, “Cockayne Syndrome A and B Proteins Differentially Regulate Recruitment of Chromatin Remodeling and Repair Factors to Stalled RNA Polymerase II In Vivo,” *Mol. Cell*, vol. 23, no. 4, pp. 471–482, 2006, doi: 10.1016/j.molcel.2006.06.029.

[157] P. Schwertman *et al.*, “UV-sensitive syndrome protein UVSSA recruits USP7 to regulate transcription-coupled repair,” *Nat. Genet.*, vol. 44, no. 5, pp. 598–602, 2012, doi: 10.1038/ng.2230.

[158] D. E. Barnes and T. Lindahl, “Repair and genetic consequences of endogenous DNA base damage in mammalian cells,” *Annu. Rev. Genet.*, vol. 38, pp. 445–476, 2004, doi: 10.1146/annurev.genet.38.072902.092448.

[159] H. Echols and M. F. Goodman, “Mutation induced by DNA damage: a many protein affair,” *Mutat. Res. Repair*, vol. 236, no. 2–3, pp. 301–311, 1990, doi: 10.1016/0921-8777(90)90013-U.

[160] G. Levinson and G. A. Gutman, “Slipped-strand mispairing: A major mechanism for

DNA sequence evolution," *Mol. Biol. Evol.*, vol. 4, no. 3, pp. 203–221, 1987, doi: 10.1093/oxfordjournals.molbev.a040442.

[161] T. Q. Trinh and R. R. Sinden, "Preferential DNA secondary structure mutagenesis in the lagging strand of replication in E. coli," *Nature*, vol. 352, no. 6335, pp. 544–547, 1991, doi: 10.1038/352544a0.

[162] M. J. Schofield and P. Hsieh, "Dna Mismatch Repair: Molecular Mechanisms and Biological Function," *Annu. Rev. Microbiol.*, vol. 57, pp. 579–608, 2003, doi: 10.1146/annurev.micro.57.030502.090847.

[163] A. De La Chapelle, "Genetic predisposition to colorectal cancer," *Nat. Rev. Cancer*, vol. 4, no. 10, pp. 769–780, 2004, doi: 10.1038/nrc1453.

[164] H. T. Lynch and A. De la Chapelle, "Genetic susceptibility to non-polyposis colorectal cancer," *J. Med. Genet.*, vol. 36, no. 11, pp. 801–818, 1999, doi: 10.1136/jmg.36.11.801.

[165] R. R. Lyer, A. Pluciennik, V. Burdett, and P. L. Modrich, "DNA mismatch repair: Functions and mechanisms," *Chem. Rev.*, vol. 106, no. 2, pp. 302–323, 2006, doi: 10.1021/cr0404794.

[166] P. Hsieh and Y. Zhang, "The Devil is in the details for DNA mismatch repair," *Proc. Natl. Acad. Sci. U. S. A.*, vol. 114, no. 14, pp. 3552–3554, 2017, doi: 10.1073/pnas.1702747114.

[167] T. Lindahl, "An N glycosidase from Escherichia coli that releases free uracil from DNA containing deaminated cytosine residues," *Proc. Natl. Acad. Sci. U. S. A.*, vol. 71, no. 9, pp. 3649–3653, 1974, doi: 10.1073/pnas.71.9.3649.

[168] S. Boiteux, F. Coste, and B. Castaing, "Repair of 8-oxo-7,8-dihydroguanine in prokaryotic and eukaryotic cells: Properties and biological roles of the Fpg and OGG1 DNA N-glycosylases," *Free Radic. Biol. Med.*, vol. 107, no. November 2016, pp. 179–201, 2017, doi: 10.1016/j.freeradbiomed.2016.11.042.

[169] J. L. Parsons and G. L. Dianov, "Co-ordination of base excision repair and genome stability," *DNA Repair (Amst).*, vol. 12, no. 5, pp. 326–333, 2013, doi: 10.1016/j.dnarep.2013.02.001.

[170] E. C. E. T. Madders and J. L. Parsons, "Base Excision Repair in Chromatin and the Requirement for Chromatin Remodelling," in *Advances in Experimental Medicine and Biology*, vol. 1241, 2020, pp. 59–75.

[171] S. S. Wallace, "DNA glycosylases search for and remove oxidized DNA bases," *Environ. Mol. Mutagen.*, vol. 54, no. 9, pp. 691–704, 2013, doi: 10.1002/em.21820.

[172] A. L. Jacobs and P. Schär, "DNA glycosylases: In DNA repair and beyond," *Chromosoma*, vol. 121, no. 1, pp. 1–20, 2012, doi: 10.1007/s00412-011-0347-4.

[173] C. N. Robson and I. D. Hickson, "Isolation of cDNA clones encoding a human apurini/apyrimidinic endonuclease that corects DNA repair and mutagenisis defects in E.coli xth (exonuclease III) mutants," *Nucleic Acids Res.*, vol. 19, no. 20, pp. 5519–5523, 1991, doi: 10.1093/nar/19.20.5519.

[174] B. Demple, T. Herman, and D. S. Chen, "Cloning and expression of APE, the cDNA encoding the major human apurinic endonuclease: Definition of a family of DNA repair enzymes," *Proc. Natl. Acad. Sci. U. S. A.*, vol. 88, no. 24, pp. 11450–11454,

1991, doi: 10.1073/pnas.88.24.11450.

[175] A. E. Vidal, S. Boiteux, I. D. Hickson, and J. P. Radicella, “XRCC1 coordinates the initial and late stages of DNA abasic site repair through protein-protein interactions,” *EMBO J.*, vol. 20, no. 22, pp. 6530–6539, 2001, doi: 10.1093/emboj/20.22.6530.

[176] L. Wiederhold *et al.*, “AP endonuclease-independent DNA base excision repair in human cells,” *Mol. Cell*, vol. 15, no. 2, pp. 209–220, 2004, doi: 10.1016/j.molcel.2004.06.003.

[177] M. J. Edmonds and J. L. Parsons, “Regulation of base excision repair proteins by ubiquitylation,” *Exp. Cell Res.*, vol. 329, no. 1, pp. 132–138, 2014, doi: 10.1016/j.yexcr.2014.07.031.

[178] A. M. Whitaker and B. D. Freudenthal, “APE1 : A skilled nucleic acid surgeon,” *DNA Repair (Amst).*, vol. 71, pp. 93–100, 2018.

[179] B. D. Freudenthal, W. A. Beard, M. J. Cuneo, N. S. Dyrkheeva, and S. H. Wilson, “Capturing Snapshots of APE1 Processing DNA Damage,” *Nat Struct Mol Biol*, vol. 22, no. 11, pp. 924–931, 2015, doi: 10.1016/j.physbeh.2017.03.040.

[180] C. D. Mol, T. Izumi, S. Mitra, and J. A. Tainer, “DNA-bound structures and mutants reveal abasic DNA binding by APE1 and DNA repair coordination,” *Nature*, vol. 404, no. 6777, p. 525, 2000, doi: 10.1038/35006693.

[181] P. R. Strauss, W. A. Beardt, T. A. Patterson, and S. H. Wilson, “Substrate binding by human apurinic/apyrimidinic endonuclease indicates a Briggs-Haldane mechanism,” *J. Biol. Chem.*, vol. 272, no. 2, pp. 1302–1307, 1997, doi: 10.1074/jbc.272.2.1302.

[182] J. P. Erzberger and D. M. Wilson, “The role of Mg2+ and specific amino acid residues in the catalytic reaction of the major human abasic endonuclease: New insights from EDTA-resistant incision of acyclic abasic site analogs and site-directed mutagenesis,” *J. Mol. Biol.*, vol. 290, no. 2, pp. 447–457, 1999, doi: 10.1006/jmbi.1999.2888.

[183] S. N. Khodyreva *et al.*, “Apurinic/apyrimidinic (AP) site recognition by the 5’-dRP/AP lyase in poly(ADP-ribose) polymerase-1 (PARP-1),” *Proc. Natl. Acad. Sci. U. S. A.*, vol. 107, no. 51, pp. 22090–22095, 2010, doi: 10.1073/pnas.1009182107.

[184] K. M. Chou and Y. C. Cheng, “An exonucleolytic activity of human apurinic/apyrimidinic endonuclease on 3’ mispaired DNA,” *Nature*, vol. 415, no. 6872, pp. 655–659, 2002, doi: 10.1038/415655a.

[185] L. Lirussi, G. Antoniali, C. D’Ambrosio, A. Scaloni, H. Nilsen, and G. Tell, “APE1 polymorphic variants cause persistent genomic stress and affect cancer cell proliferation,” *Oncotarget*, vol. 7, no. 18, pp. 26293–26306, 2016, doi: 10.18632/oncotarget.8477.

[186] J. L. Illuzzi *et al.*, “Functional Assessment of Population and Tumor-Associated APE1 Protein Variants,” *PLoS One*, vol. 8, no. 6, 2013, doi: 10.1371/journal.pone.0065922.

[187] A. M. Whitaker, T. S. Flynn, and B. D. Freudenthal, “Molecular snapshots of APE1 proofreading mismatches and removing DNA damage,” *Nat. Commun.*, vol. 9, no. 1, 2018, doi: 10.1038/s41467-017-02175-y.

[188] M. Stucki *et al.*, “Mammalian base excision repair by DNA polymerases δ and ε,” *Oncogene*, vol. 17, no. 7, pp. 835–843, 1998, doi: 10.1038/sj.onc.1202001.

[189] E. K. Braithwaite, R. Prasad, D. D. Shock, E. W. Hou, W. A. Beard, and S. H. Wilson, "DNA polymerase λ mediates a back-up base excision repair activity in extracts of mouse embryonic fibroblasts," *J. Biol. Chem.*, vol. 280, no. 18, pp. 18469–18475, 2005, doi: 10.1074/jbc.M411864200.

[190] R. W. Sobol *et al.*, "Requirement of mammalian DNA polymerase-β in base-excision repair," *Nature*, vol. 379, no. 6561, pp. 183–186, 1996, doi: 10.1038/379183a0.

[191] H. Pelletier, M. R. Sawaya, W. Wolfle, S. H. Wilson, and J. Kraut, "Crystal structures of human DNA polymerase β complexed with DNA: Implications for catalytic mechanism, processivity, and fidelity," *Biochemistry*, vol. 35, no. 39, pp. 12742–12761, 1996, doi: 10.1021/bi952955d.

[192] M. R. Sawaya, H. Pelletier, A. Kumar, S. H. Wilson, and J. Kraut, "Crystal structure of rat DNA polymerase β: Evidence for a common polymerase mechanism," *Science (80-. ).*, vol. 264, no. 5167, pp. 1930–1935, 1994, doi: 10.1126/science.7516581.

[193] Y. Matsumoto and K. Kim, "Excision of deoxyribose phosphate residues by DNA polymerase β during DNA repair," *Science (80-. ).*, vol. 269, no. 5224, pp. 699–702, 1995, doi: 10.1126/science.7624801.

[194] G. Frosina *et al.*, "Two pathways for base excision repair in mammalian cells," *J. Biol. Chem.*, vol. 271, no. 16, pp. 9573–9578, 1996, doi: 10.1074/jbc.271.16.9573.

[195] A. J. Podlutsky, I. I. Dianova, V. N. Podust, V. A. Bohr, and G. L. Dianov, "Human DNA polymerase β initiates DNA synthesis during long-patch repair of reduced AP sites in DNA," *EMBO J.*, vol. 20, no. 6, pp. 1477–1482, 2001, doi: 10.1093/emboj/20.6.1477.

[196] M. García-Díaz *et al.*, "DNA polymerase lambda (Pol λ), a novel eukaryotic DNA polymerase with a potential role in meiosis," *J. Mol. Biol.*, vol. 301, no. 4, pp. 851–867, 2000, doi: 10.1006/jmbi.2000.4005.

[197] M. Masson, C. Niedergang, V. Schreiber, S. Muller, J. Menissier-de Murcia, and G. de Murcia, "XRCC1 Is Specifically Associated with Poly(ADP-Ribose) Polymerase and Negatively Regulates Its Activity following DNA Damage," *Mol. Cell. Biol.*, vol. 18, no. 6, pp. 3563–3571, 1998, doi: 10.1128/mcb.18.6.3563.

[198] E. Cappelli, R. Taylor, M. Cevasco, A. Abbondandolo, K. Caldecott, and G. Frosina, "Involvement of XRCC1 and DNA ligase III gene products in DNA base excision repair," *J. Biol. Chem.*, vol. 272, no. 38, pp. 23970–23975, 1997, doi: 10.1074/jbc.272.38.23970.

[199] R. A. Nash, K. W. Caldecott, D. E. Barnes, and T. Lindahl, "XRCC1 protein interacts with one of two distinct forms of DNA ligase III," *Biochemistry*, vol. 36, no. 17, pp. 5207–5211, 1997, doi: 10.1021/bi962281m.

[200] R. Kornberg, "Chromatin Structure : A Repeating Unit of Histones and DNA Chromatin structure is based on a repeating unit of eight," *Science (80-. ).*, vol. 184, pp. 868–871, 1974.

[201] K. Luger, A. W. Mäder, R. K. Richmond, D. F. Sargent, and T. J. Richmond, "Crystal structure of the nucleosome core particle at 2.8 Å resolution," *Nature*, vol. 389, no. 6648, pp. 251–260, 1997, doi: 10.1038/38444.

[202] C. A. Davey, D. F. Sargent, K. Luger, A. W. Maeder, and T. J. Richmond, "Solvent mediated interactions in the structure of the nucleosome core particle at 1.9 Å resolution," *J. Mol. Biol.*, vol. 319, no. 5, pp. 1097–1113, 2002, doi: 10.1016/S0022-

2836(02)00386-8.

[203] D. J. Tremethick, “Higher-Order Structures of Chromatin: The Elusive 30 nm Fiber,” *Cell*, vol. 128, no. 4, pp. 651–654, 2007, doi: 10.1016/j.cell.2007.02.008.

[204] B. D. Strahl and C. D. Allis, “The language of covalent histone modifications,” *Nature*, vol. 403, no. 6765, pp. 41–45, 2000, doi: 10.1038/47412.

[205] B. M. Turner, “Histone acetylation and an epigenetic code,” *BioEssays*, vol. 22, no. 9, pp. 836–845, 2000, doi: 10.1002/1521-1878(200009)22:9<836::AID-BIES9>3.0.CO;2-X.

[206] A. Flaus, K. Luger, S. Tan, and T. J. Richmond, “Mapping nucleosome position at single base-pair resolution by using site-directed hydroxyl radicals,” *Proc. Natl. Acad. Sci. U. S. A.*, vol. 93, no. 4, pp. 1370–1375, 1996, doi: 10.1073/pnas.93.4.1370.

[207] G. Arents, R. W. Burlingame, B. I. C. Wang, W. E. Love, and E. N. Moudrianakis, “The nucleosomal core histone octamer at 3.1 Å resolution: A tripartite protein assembly and a left-handed superhelix,” *Proc. Natl. Acad. Sci. U. S. A.*, vol. 88, no. 22, pp. 10148–10152, 1991, doi: 10.1073/pnas.88.22.10148.

[208] G. Arents and E. N. Moudrianakis, “The histone fold: A ubiquitous architectural motif utilized in DNA compaction and protein dimerization,” *Proc. Natl. Acad. Sci. U. S. A.*, vol. 92, no. 24, pp. 11170–11174, 1995, doi: 10.1073/pnas.92.24.11170.

[209] R. K. McGinty and S. Tan, “Nucleosome structure and function,” *Chem. Rev.*, vol. 115, no. 6, pp. 2255–2273, 2015, doi: 10.1021/cr500373h.

[210] J. L. Workman and S. M. Abmayr, *Fundamentals of chromatin*. 2014.

[211] M. P. F. Marsden and U. K. Laemmli, “Metaphase chromosome structure: Evidence for a radial loop model,” *Cell*, vol. 17, no. 4, pp. 849–858, 1979, doi: 10.1016/0092-8674(79)90325-8.

[212] J. P. Langmore and C. Schutt, “The higher order structure of chicken erythrocyte chromosomes in vivo,” *Nature*, vol. 288, no. 5791, pp. 620–2, 1980.

[213] J. T. Finch and A. Klug, “Solenoidal model for superstructure in chromatin,” *Proc. Natl. Acad. Sci. U. S. A.*, vol. 73, no. 6, pp. 1897–1901, 1976, doi: 10.1073/pnas.73.6.1897.

[214] F. Thoma, T. Koller, and A. Klug, “Involvement of histone H1 in the organization of t... [J Cell Biol. 1979] - PubMed result,” *J. Cell Biol.*, vol. 83, no. 2 Pt 1, pp. 403–27, 1979.

[215] J. D. McGhee, J. M. Nickol, G. Felsenfeld, and D. C. Rau, “Higher order structure of chromatin: Orientation of nucleosomes within the 30 nm chromatin solenoid is independent of species and spacer length,” *Cell*, vol. 33, no. 3, pp. 831–841, 1983, doi: 10.1016/0092-8674(83)90025-9.

[216] J. Widom and A. Klug, “Structure of the 3000Å chromatin filament: X-ray diffraction from oriented samples,” *Cell*, vol. 43, no. 1, pp. 207–213, 1985, doi: 10.1016/0092-8674(85)90025-X.

[217] S. P. Williams, B. D. Athey, L. J. Muglia, R. S. Schappe, A. H. Gough, and J. P. Langmore, “Chromatin fibers are left-handed double helices with diameter and mass per unit length that depend on linker length,” *Biophys. J.*, vol. 49, no. 1, pp. 233–248, 1986, doi: 10.1016/S0006-3495(86)83637-2.

[218] C. L. F. Woodcock, L. L. Y. Frado, and J. B. Rattner, “The higher-order structure of chromatin: Evidence for a helical ribbon arrangement,” *J. Cell Biol.*, vol. 99, no. 1 I, pp. 42–52, 1984, doi: 10.1083/jcb.99.1.42.

[219] A. Worcel, S. Strogatz, and D. Riley, “Structure of chromatin and the linking number of DNA.,” *Proc. Natl. Acad. Sci. U. S. A.*, vol. 78, no. 3, pp. 1461–1465, 1981, doi: 10.1073/pnas.78.3.1461.

[220] J. R. Paulson and U. K. Laemmli, “The structure of histone-depleted metaphase chromosomes,” *Cell*, vol. 12, no. 3, pp. 817–828, 1977, doi: 10.1016/0092-8674(77)90280-X.

[221] K. Luger, M. L. Dechassa, and D. J. Tremethick, “New insights into nucleosome and chromatin structure: An ordered state or a disordered affair?,” *Nat. Rev. Mol. Cell Biol.*, vol. 13, no. 7, pp. 436–447, 2012, doi: 10.1038/nrm3382.

[222] W. G. Müller, D. Rieder, G. Kreth, C. Cremer, Z. Trajanoski, and J. G. McNally, “Generic Features of Tertiary Chromatin Structure as Detected in Natural Chromosomes,” *Mol. Cell. Biol.*, vol. 24, no. 21, pp. 9359–9370, 2004, doi: 10.1128/mcb.24.21.9359-9370.2004.

[223] E. Fussner, R. W. Ching, and D. P. Bazett-Jones, “Living without 30nm chromatin fibers,” *Trends Biochem. Sci.*, vol. 36, no. 1, pp. 1–6, 2011, doi: 10.1016/j.tibs.2010.09.002.

[224] M. Eltsov, K. M. MacLellan, K. Maeshima, A. S. Frangakis, and J. Dubochet, “Analysis of cryo-electron microscopy images does not support the existence of 30-nm chromatin fibers in mitotic chromosomes in situ,” *Proc. Natl. Acad. Sci. U. S. A.*, vol. 105, no. 50, pp. 19732–19737, 2008, doi: 10.1073/pnas.0810057105.

[225] M. S. Cosgrove, J. D. Boeke, and C. Wolberger, “Regulated nucleosome mobility and the histone code,” *Nat. Struct. Mol. Biol.*, vol. 11, no. 11, pp. 1037–1043, 2004, doi: 10.1038/nsmb851.

[226] Y. Zhao and B. A. Garcia, “Comprehensive catalog of currently documented histone modifications,” *Cold Spring Harb. Perspect. Biol.*, vol. 7, no. 9, pp. 1–21, 2015, doi: 10.1101/cshperspect.a025064.

[227] J. C. Chan and I. Maze, “Nothing Is Yet Set in (Hi)stone: Novel Post-Translational Modifications Regulating Chromatin Function,” *Trends Biochem. Sci.*, vol. 45, no. 10, pp. 829–844, 2020, doi: 10.1016/j.tibs.2020.05.009.

[228] S. B. Rothbart and B. D. Strahl, “Interpreting the language of histone and DNA modifications,” *Biochim. Biophys. Acta - Gene Regul. Mech.*, vol. 1839, no. 8, pp. 627–643, 2014, doi: 10.1016/j.bbagrm.2014.03.001.

[229] P. Tessarz and T. Kouzarides, “Histone core modifications regulating nucleosome structure and dynamics,” *Nat. Rev. Mol. Cell Biol.*, vol. 15, no. 11, pp. 703–708, 2014, doi: 10.1038/nrm3890.

[230] M. H. Hauer and S. M. Gasser, “Chromatin and nucleosome dynamics in DNA damage and repair,” *Genes Dev.*, vol. 31, no. 22, pp. 2204–2221, 2017, doi: 10.1101/gad.307702.117.

[231] C. R. Clapier, J. Iwasa, B. R. Cairns, and C. L. Peterson, “Mechanisms of action and regulation of ATP-dependent chromatin-remodelling complexes,” *Nat. Rev. Mol. Cell Biol.*, vol. 18, no. 7, pp. 407–422, 2017, doi: 10.1038/nrm.2017.26.

[232] H. Lans, J. A. Marteijn, and W. Vermeulen, “ATP-dependent chromatin remodeling in the DNA-damage response,” *Epigenetics and Chromatin*, vol. 5, no. 1, p. 4, 2012, doi: 10.1186/1756-8935-5-4.

[233] S. P. Jackson and D. Durocher, “Regulation of DNA Damage Responses by Ubiquitin and SUMO,” *Mol. Cell*, vol. 49, no. 5, pp. 795–807, 2013, doi: 10.1016/j.molcel.2013.01.017.

[234] P. C. Blainey, A. M. Van Oijen, A. Banerjee, G. L. Verdine, and X. S. Xie, “A base-excision DNA-repair protein finds intrahelical lesion bases by fast sliding in contact with DNA,” *Proc. Natl. Acad. Sci. U. S. A.*, vol. 103, no. 15, pp. 5752–5757, 2006, doi: 10.1073/pnas.0509723103.

[235] P. C. Blainey *et al.*, “Nonspecifically bound proteins spin while diffusing along DNA Bagchi2,” *Nat Struct Mol Biol*, vol. 16, no. 12, pp. 1224–1229, 2009, doi: 10.1038/nsmb.1716.Nonspecifically.

[236] H. Nilsen, T. Lindahl, and A. Verreault, “DNA base excision repair of uracil residues in reconstituted nucleosome core particles,” *EMBO J.*, vol. 21, no. 21, pp. 5943–5952, 2002, doi: 10.1093/emboj/cdf581.

[237] H. A. Cole, J. M. Tabor-Godwin, and J. J. Hayes, “Uracil DNA glycosylase activity on nucleosomal DNA depends on rotational orientation of targets,” *J. Biol. Chem.*, vol. 285, no. 4, pp. 2876–2885, 2010, doi: 10.1074/jbc.M109.073544.

[238] B. C. Beard, S. H. Wilson, and M. J. Smerdon, “Suppressed catalytic activity of base excision repair enzymes on rotationally positioned uracil in nucleosomes,” *Proc. Natl. Acad. Sci. U. S. A.*, vol. 100, no. 13, pp. 7465–7470, 2003, doi: 10.1073/pnas.1330328100.

[239] Y. Rodriguez and M. J. Smerdon, “The structural location of DNA lesions in nucleosome core particles determines accessibility by base excision repair enzymes,” *J. Biol. Chem.*, vol. 288, no. 19, pp. 13863–13875, 2013, doi: 10.1074/jbc.M112.441444.

[240] J. M. Hinz, Y. Rodriguez, and M. J. Smerdon, “Rotational dynamics of DNA on the nucleosome surface markedly impact accessibility to a DNA repair enzyme,” *Proc. Natl. Acad. Sci. U. S. A.*, vol. 107, no. 10, pp. 4646–4651, 2010, doi: 10.1073/pnas.0914443107.

[241] H. Menoni *et al.*, “ATP-Dependent Chromatin Remodeling Is Required for Base Excision Repair in Conventional but Not in Variant H2A.Bbd Nucleosomes,” *Mol. Cell. Biol.*, vol. 27, no. 17, pp. 5949–5956, 2007, doi: 10.1128/mcb.00376-07.

[242] H. Menoni, M. S. Shukla, V. Gerson, S. Dimitrov, and D. Angelov, “Base excision repair of 8-oxoG in dinucleosomes,” *Nucleic Acids Res.*, vol. 40, no. 2, pp. 692–700, 2012, doi: 10.1093/nar/gkr761.

[243] A. Prasad, S. S. Wallace, and D. S. Pederson, “Initiation of Base Excision Repair of Oxidative Lesions in Nucleosomes by the Human, Bifunctional DNA Glycosylase NTH1,” *Mol. Cell. Biol.*, vol. 27, no. 24, pp. 8442–8453, 2007, doi: 10.1128/mcb.00791-07.

[244] I. D. Odell *et al.*, “Nucleosome Disruption by DNA Ligase III-XRCC1 Promotes Efficient Base Excision Repair,” *Mol. Cell. Biol.*, vol. 31, no. 22, pp. 4623–4632, 2011, doi: 10.1128/mcb.05715-11.

[245] I. D. Odell, K. Newick, N. H. Heintz, S. S. Wallace, and D. S. Pederson, “Non-specific DNA binding interferes with the efficient excision of oxidative lesions from chromatin by the human DNA glycosylase, NEIL1,” *DNA Repair (Amst).*, vol. 9, no. 2, pp. 134–143, 2010, doi: 10.1016/j.dnarep.2009.11.005.

[246] M. J. Edmonds, R. J. Carter, C. M. Nickson, S. C. Williams, and J. L. Parsons, “Ubiquitylation-dependent regulation of NEIL1 by Mule and TRIM26 is required for the cellular DNA damage response,” *Nucleic Acids Res.*, vol. 45, no. 2, pp. 726–738, 2017, doi: 10.1093/nar/gkw959.

[247] S. C. Williams and J. L. Parsons, “NTH1 Is a New Target for Ubiquitylation-Dependent Regulation by TRIM26 Required for the Cellular Response to Oxidative Stress,” *Mol. Cell. Biol.*, vol. 38, no. 12, pp. 1–15, 2018, doi: 10.1128/mcb.00616-17.

[248] J. M. Hinz, “Impact of abasic site orientation within nucleosomes on human APE1 endonuclease activity,” *Mutat. Res. - Fundam. Mol. Mech. Mutagen.*, vol. 766–767, pp. 19–24, 2014, doi: 10.1016/j.mrfmmm.2014.05.008.

[249] J. M. Hinz, P. Mao, D. R. McNeill, and D. M. Wilson, “Reduced nuclease activity of apurinic/apyrimidinic endonuclease (APE1) variants on nucleosomes: Identification of access residues,” *J. Biol. Chem.*, vol. 290, no. 34, pp. 21067–21075, 2015, doi: 10.1074/jbc.M115.665547.

[250] J. T. Sczepanski, C. Zhou, and M. M. Greenberg, “Nucleosome core particle catalyzed strand scission at abasic sites,” *Biochemistry*, vol. 52, no. 12, pp. 1–21, 2013, doi: 10.1021/bi3010076.Nucleosome.

[251] Y. Rodriguez, M. J. Howard, M. J. Cuneo, R. Prasad, and S. H. Wilson, “Unencumbered pol β lyase activity in nucleosome core particles,” *Nucleic Acids Res.*, vol. 45, no. 15, pp. 8901–8915, 2017, doi: 10.1093/nar/gkx593.

[252] W. J. Cannan, I. Rashid, A. E. Tomkinson, S. S. Wallace, and D. S. Pederson, “The human ligase IIIα-XRCC1 protein complex performs DNA nick repair after transient unwrapping of nucleosomal DNA,” *J. Biol. Chem.*, vol. 292, no. 13, pp. 5227–5238, 2017, doi: 10.1074/jbc.M116.736728.

[253] S. V. Khoronenkova, I. I. Dianova, J. L. Parsons, and G. L. Dianov, “USP7/HAUSP stimulates repair of oxidative DNA lesions,” *Nucleic Acids Res.*, vol. 39, no. 7, pp. 2604–2609, 2011, doi: 10.1093/nar/gkq1210.

[254] K. Bilotti, E. E. Kennedy, C. Li, and S. Delaney, “Human OGG1 activity in nucleosomes is facilitated by transient unwrapping of DNA and is influenced by the local histone environment,” *DNA Repair (Amst).*, vol. 59, pp. 1–8, 2017, doi: 10.1016/j.dnarep.2017.08.010.Human.

[255] Y. Rodriguez, J. M. Hinz, M. F. Laughery, J. J. Wyrick, and M. J. Smerdon, “Site-specific acetylation of histone H3 decreases polymerase β activity on nucleosome core particles in vitro,” *J. Biol. Chem.*, vol. 291, no. 21, pp. 11434–11445, 2016, doi: 10.1074/jbc.M116.725788.

[256] H. Koyama, M. Itoh, K. Miyahara, and E. Tsuchiya, “Abundance of the RSC nucleosome-remodeling complex is important for the cells to tolerate DNA damage in Saccharomyces cerevisiae,” *FEBS Lett.*, vol. 531, no. 2, pp. 215–221, 2002, doi: 10.1016/S0014-5793(02)03504-4.

[257] W. Czaja, P. Mao, and M. J. Smerdon, “Chromatin remodelling complex RSC

promotes base excision repair in chromatin of Saccharomyces cerevisiae," *DNA Repair (Amst).*, vol. 16, no. 1, pp. 35–43, 2014, doi: 10.1016/j.dnarep.2014.01.002.

[258] J. L. Charles Richard *et al.*, "FACT Assists Base Excision Repair by Boosting the Remodeling Activity of RSC," *PLoS Genet.*, vol. 12, no. 7, pp. 1–21, 2016, doi: 10.1371/journal.pgen.1006221.

[259] S. Nakanishi, R. Prasad, S. H. Wilson, and M. Smerdon, "Different structural states in oligonucleosomes are required for early versus late steps of base excision repair," *Nucleic Acids Res.*, vol. 35, no. 13, pp. 4313–4321, 2007, doi: 10.1093/nar/gkm436.

[260] D. Yasui, M. Miyano, S. Cai, P. Varga-Weisz, and T. Kohwi-Shigematsu, "SATB1 targets chromatin remodelling to regulate genes over long distances," *Nature*, vol. 419, no. 6907, pp. 641–645, 2002, doi: 10.1038/nature01084.

[261] S. Kaur, Y. Coulombe, Z. M. Ramdzan, L. Leduy, J. Y. Masson, and A. Nepveu, "Special AT-rich sequence-binding protein 1 (SATB1) functions as an accessory factor in base excision repair," *J. Biol. Chem.*, vol. 291, no. 43, pp. 22769–22780, 2016, doi: 10.1074/jbc.M116.735696.

[262] D. Ahel *et al.*, "Poly(ADP-ribose)-dependent regulation of DNA repair by the chromatin remodelling enzyme ALC1," *Science (80-. ).*, vol. 325, no. 5945, pp. 1240–1243, 2012, doi: 10.1126/science.1177321.Poly(ADP-ribose)-dependent.

[263] H. Sellou *et al.*, "The poly(ADP-ribose)-dependent chromatin remodeler Alc1 induces local chromatin relaxation upon DNA damage," *Mol. Biol. Cell*, vol. 27, no. 24, pp. 3791–3799, 2016, doi: 10.1091/mbc.E16-05-0269.

[264] M. Tsuda *et al.*, "ALC1/CHD1L, a chromatin-remodeling enzyme, is required for efficient base excision repair," *PLoS One*, vol. 12, no. 11, pp. 1–17, 2017, doi: 10.1371/journal.pone.0188320.

[265] K. Haglund and I. Dikic, "Ubiquitylation and cell signaling," *EMBO J.*, vol. 24, no. 19, pp. 3353–3359, 2005, doi: 10.1038/sj.emboj.7600808.

[266] A. Hershko and A. Ciechanover, "The ubiquitin system," *Annu. Rev. Biochem.*, vol. 67, pp. 425–79, 1998, doi: 10.1038/458421a.

[267] L. Hicke and R. Dunn, "Regulation of Membrane Protein Transport by Ubiquitin and Ubiquitin-Binding Proteins," *Annu. Rev. Cell Dev. Biol.*, vol. 19, pp. 141–172, 2003, doi: 10.1146/annurev.cellbio.19.110701.154617.

[268] K. Haglund, P. P. Di Fiore, and I. Dikic, "Distinct monoubiquitin signals in receptor endocytosis," *Trends Biochem. Sci.*, vol. 28, no. 11, pp. 598–604, 2003, doi: 10.1016/j.tibs.2003.09.005.

[269] C. M. Pickart and D. Fushman, "Polyubiquitin chains: Polymeric protein signals," *Curr. Opin. Chem. Biol.*, vol. 8, no. 6, pp. 610–616, 2004, doi: 10.1016/j.cbpa.2004.09.009.

[270] L. Hicke, H. L. Schubert, and C. P. Hill, "Ubiquitin-binding domains," *Nat. Rev. Mol. Cell Biol.*, vol. 6, no. 8, pp. 610–621, 2005, doi: 10.1038/nrm1701.

[271] M. B. Metzger, J. N. Pruneda, R. E. Klevit, and A. M. Weissman, "RING-type E3 ligases: Master manipulators of E2 ubiquitin- conjugating enzymes and ubiquitination," *Biochem Biophys Acta*, vol. 1843, no. 1, pp. 47–60, 2014, doi: 10.1016/j.bbamcr.2013.05.026.RING-type.

[272] P. Roos-Mattjus and L. Sistonen, “The ubiquitin-proteasome pathway,” *Ann. Med.*, vol. 36, no. 4, pp. 285–295, 2004, doi: 10.1080/07853890310016324.

[273] P. Cohen and M. Tcherpakov, “Will the ubiquitin system furnish as many drug targets as protein kinases?,” *Cell*, vol. 143, no. 5, pp. 686–693, 2010, doi: 10.1016/j.cell.2010.11.016.

[274] J. Sluimer and B. Distel, “Regulating the human HECT E3 ligases,” *Cell. Mol. Life Sci.*, vol. 75, no. 17, pp. 3121–3141, 2018, doi: 10.1007/s00018-018-2848-2.

[275] K. K. Dove and R. E. Klevit, “RING-Between-RING E3 Ligases: Emerging Themes amid the Variations,” *J. Mol. Biol.*, vol. 429, no. 22, pp. 3363–3375, 2017, doi: 10.1016/j.jmb.2017.08.008.

[276] M. D. Ohi, C. W. Vander Kooi, J. A. Rosenberg, W. J. Chazin, and K. L. Gould, “Structural insights into the U-box, a domain associated with multi-ubiquitination,” *Nat. Struct. Biol.*, vol. 10, no. 4, pp. 250–255, 2003, doi: 10.1038/nsb906.

[277] M. D. Petroski and R. J. Deshaies, “Function and regulation of cullin-RING ubiquitin ligases,” *Nat. Rev. Mol. Cell Biol.*, vol. 6, no. 1, pp. 9–20, 2005, doi: 10.1038/nrm1547.

[278] A. Schreiber *et al.*, “Structural basis for the subunit assembly of the anaphase-promoting complex,” *Nature*, vol. 470, no. 7333, pp. 227–235, 2011, doi: 10.1038/nature09756.

[279] J. M. Huibregtse, M. Scheffner, S. Beaudenon, and P. M. Howley, “A family of proteins structurally and functionally related to the E6-AP ubiquitin-protein ligase,” *Proc. Natl. Acad. Sci. U. S. A.*, vol. 92, no. 7, pp. 2563–2567, 1995, doi: 10.1073/pnas.92.7.2563.

[280] J. M. Huibregtse, M. Scheffner, and P. M. Howley, “A cellular protein mediates association of p53 with the E6 oncoprotein of human papillomavirus types 16 or 18,” *EMBO J.*, vol. 10, no. 13, pp. 4129–4135, 1991, doi: 10.1002/j.1460-2075.1991.tb04990.x.

[281] M. Scheffner, U. Nuber, and J. M. Huibregtse, “Protein ubiquitination involving an E1–E2–E3 enzyme ubiquitin thioester cascade,” *Nature*, vol. 373, no. 6509, pp. 81–83, 1995, doi: 10.1038/373081a0.

[282] T. Kitada *et al.*, “Mutations in the parkin gene causeautosomal recessive juvenile parkinsonism,” *Nat. Lett.*, vol. 392, pp. 605–608, 1998.

[283] H. Matsumine *et al.*, “Localization of a gene for an autosomal recessive form of juvenile parkinsonism to chromosome 6q25.2-27,” *Am. J. Hum. Genet.*, vol. 60, no. 3, pp. 588–596, 1997.

[284] E. Morett and P. Bork, “A novel transactivation domain in parkin,” *Trends Biochem. Sci.*, vol. 24, no. 6, pp. 229–231, 1999, doi: 10.1016/S0968-0004(99)01381-X.

[285] B. A. Van Der Reijden, C. A. J. Erpelinck-Verschueren, BOB LÖWENBERG, and J. H. Jansen, “TRIADs: A new class of proteins with a novel cysteine-rich signature,” *Protein Sci.*, vol. 8, no. 7, pp. 1557–1561, 1999, doi: 10.1110/ps.8.7.1557.

[286] M. Akutsu, I. Dikic, and A. Bremm, “Ubiquitin chain diversity at a glance,” *J. Cell Sci.*, vol. 129, no. 5, pp. 875–880, 2016, doi: 10.1242/jcs.183954.

[287] D. Komander and M. Rape, “The ubiquitin code,” *Annu. Rev. Biochem.*, vol. 81, pp.

203–229, 2012, doi: 10.1146/annurev-biochem-060310-170328.

[288] K. Selvaraju, M. Mazurkiewicz, X. Wang, J. Gullbo, S. Linder, and P. D'Arcy, "Inhibition of proteasome deubiquitinase activity: A strategy to overcome resistance to conventional proteasome inhibitors?," *Drug Resist. Updat.*, vol. 21–22, pp. 20–29, 2015, doi: 10.1016/j.drup.2015.06.001.

[289] J. S. Thrower, L. Hoffman, M. Rechsteiner, and C. M. Pickart, "Recognition of the polyubiquitin proteolytic signal," *EMBO J.*, vol. 19, no. 1, pp. 94–102, 2000, doi: 10.1117/12.21634.

[290] E. Lafont, T. Hartwig, and H. Walczak, "Paving TRAIL's Path with Ubiquitin," *Trends Biochem. Sci.*, vol. 43, no. 1, pp. 44–60, 2018, doi: 10.1016/j.tibs.2017.11.002.

[291] J. E. Sale, A. R. Lehmann, and R. Woodgate, "Y-family DNA polymerases and their role in tolerance of cellular DNA damage," *Nat. Rev. Mol. Cell Biol.*, vol. 13, no. 3, pp. 141–152, 2012, doi: 10.1038/nrm3289.

[292] I. Unk, I. Hajdú, A. Blastyák, and L. Haracska, "Role of yeast Rad5 and its human orthologs, HLTF and SHPRH in DNA damage tolerance," *DNA Repair (Amst).*, vol. 9, no. 3, pp. 257–267, 2010, doi: 10.1016/j.dnarep.2009.12.013.

[293] L. G. Bennett, "Epigenetic mechanisms involved in the cellular response to DNA damage processed by Base Excision Repair," 2017.

[294] L. Bennett, E. C. E. T. Madders, and J. L. Parsons, "HECTD1 promotes base excision repair in nucleosomes through chromatin remodelling," *Nucleic Acids Res.*, vol. 48, no. 3, pp. 1301–1313, 2020, doi: 10.1093/nar/gkz1129.

[295] E. Conti, M. Uy, L. Leighton, G. Blobel, and J. Kuriyan, "Crystallographic analysis of the recognition of a nuclear localization signal by the nuclear import factor karyopherin α," *Cell*, vol. 94, no. 2, pp. 193–204, 1998, doi: 10.1016/S0092-8674(00)81419-1.

[296] C. C. Stempin, L. Chi, J. P. Giraldo-Vela, A. A. High, H. Häcker, and V. Redecke, "The E3 ubiquitin ligase mind bomb-2 (MIB2) protein controls B-cell CLL/lymphoma 10 (BCL10)-dependent NF-κB activation," *J. Biol. Chem.*, vol. 286, no. 43, pp. 37147–37157, 2011, doi: 10.1074/jbc.M111.263384.

[297] Y. B. Tzur, K. L. Wilson, and Y. Gruenbaum, "SUN-domain proteins: 'Velcro' that links the nucleoskeleton to the cytoskeleton," *Nat. Rev. Mol. Cell Biol.*, vol. 7, no. 10, pp. 782–788, 2006, doi: 10.1038/nrm2003.

[298] Y. Wang, D. Argiles-Castillo, E. I. Kane, A. Zhou, and D. E. Spratt, "HECT E3 ubiquitin ligases - Emerging insights into their biological roles and disease relevance," *J. Cell Sci.*, vol. 133, no. 7, 2020, doi: 10.1242/jcs.228072.

[299] X. Wang, C. De Geyter, Z. Jia, Y. Peng, and H. Zhang, "HECTD1 regulates the expression of SNAIL: Implications for epithelial–mesenchymal transition," *Int. J. Oncol.*, vol. 56, no. 5, pp. 1186–1198, 2020, doi: 10.3892/ijo.2020.5002.

[300] S. Hugel *et al.*, "Identification of importin α 7 specific transport cargoes using a proteomic screening approach," *Mol. Cell. Proteomics*, vol. 13, no. 5, pp. 1286–1298, 2014, doi: 10.1074/mcp.M112.026856.

[301] I. E. Zohn, K. V Anderson, and L. Niswander, "The Hectd1 Ubiquitin Ligase is Required for Development of the Head Mesenchyme and Neural Tube Closure," *Dev*

*Biol*, vol. 306, no. 1, pp. 208–221, 2007, doi: 10.1016/j.ydbio.2007.03.018.The.

[302] D. D'Alonzo, F. H. Emch, X. Shen, E. Bruder, C. De Geyter, and H. Zhang, "Hectd1 is essential for embryogenesis in mice," *Gene Expr. Patterns*, vol. 34, no. July, p. 119064, 2019, doi: 10.1016/j.gep.2019.119064.

[303] A. A. Sarkar and I. E. Zohn, "Hectd1 regulates intracellular localization and secretion of Hsp90 to control cellular behavior of the cranial mesenchyme," *J. Cell Biol.*, vol. 196, no. 6, pp. 789–800, 2012, doi: 10.1083/jcb.201105101.

[304] X. Li *et al.*, "Ubiquitylation of phosphatidylinositol 4-phosphate 5-kinase type I γ by HECTD1 regulates focal adhesion dynamics and cell migration," *J. Cell Sci.*, vol. 126, no. 12, pp. 2617–2628, 2013, doi: 10.1242/jcs.117044.

[305] S. Deng and C. Huang, "E3 ubiquitin ligases in regulating stress fiber, lamellipodium, and focal adhesion dynamics," *Cell Adhes. Migr.*, vol. 8, no. 1, pp. 49–54, 2014, doi: 10.4161/cam.27480.

[306] Q. Zheng1 *et al.*, "Leptin Up-Regulates HECTD1 to Promote Phosphoinositide Metabolism and Cell Migration and Invasion in Breast Cancer Cells," *Cent. J. Pharmacol. J Pharmacol Clin Toxicol*, vol. 1, no. 1, pp. 1–6, 2014.

[307] X. Shen *et al.*, "HECTD1 controls the protein level of IQGAP1 to regulate the dynamics of adhesive structures," *Cell Commun. Signal.*, vol. 15, no. 1, pp. 1–16, 2017, doi: 10.1186/s12964-016-0156-8.

[308] H. Tran *et al.*, "HectDI E3 ligase modifies adenomatous polyposis coli (APC) with polyubiquitin to promote the APC-axin interaction," *J. Biol. Chem.*, vol. 288, no. 6, pp. 3753–3767, 2013, doi: 10.1074/jbc.M112.415240.

[309] J. L. Riffell, C. J. Lord, and A. Ashworth, "Tankyrase-targeted therapeutics: Expanding opportunities in the PARP family," *Nat. Rev. Drug Discov.*, vol. 11, no. 12, pp. 923–936, 2012, doi: 10.1038/nrd3868.

[310] L. Lehtiö, N. W. Chi, and S. Krauss, "Tankyrases as drug targets," *FEBS J.*, vol. 280, no. 15, pp. 3576–3593, 2013, doi: 10.1111/febs.12320.

[311] A. Bhardwaj, Y. Yang, B. Ueberheide, and S. Smith, "Whole proteome analysis of human tankyrase knockout cells reveals targets of tankyrase-mediated degradation," *Nat. Commun.*, vol. 8, no. 1, 2017, doi: 10.1038/s41467-017-02363-w.

[312] S. Duhamel, M. A. Goyette, M. P. Thibault, D. Filion, L. Gaboury, and J. F. Côté, "The E3 Ubiquitin Ligase HectD1 Suppresses EMT and Metastasis by Targeting the +TIP ACF7 for Degradation," *Cell Rep.*, vol. 22, no. 4, pp. 1016–1030, 2018, doi: 10.1016/j.celrep.2017.12.096.

[313] Z. Zhou *et al.*, "circRNA mediates silica-induced macrophage activation via HECTD1/ZC3H12A-dependent ubiquitination," *Theranostics*, vol. 8, no. 2, pp. 575–592, 2018, doi: 10.7150/thno.21648.

[314] S. Fang *et al.*, "CircHECTD1 promotes the silica-induced pulmonary endothelial-mesenchymal transition via HECTD1," *Cell Death Dis.*, vol. 9, no. 3, pp. 1–16, 2018, doi: 10.1038/s41419-018-0432-1.

[315] N. Brunetti-Pierri *et al.*, "Duplications of FOXG1 in 14q12 are associated with developmental epilepsy, mental retardation, and severe speech impairment," *Eur. J. Hum. Genet.*, vol. 19, no. 1, pp. 102–107, 2011, doi: 10.1038/ejhg.2010.142.

[316] W. Li *et al.*, “Condensin I and II Complexes License Full Estrogen Receptor α-Dependent Enhancer Activation,” *Mol Cell*, vol. 59, no. 2, pp. 188–202, 2015, doi: 10.1016/j.molcel.2015.06.002.Condensin.

[317] P. R. Del Valle *et al.*, “Transcriptional profile of fibroblasts obtained from the primary site, lymph node and bone marrow of breast cancer patients,” *Genet. Mol. Biol.*, vol. 37, no. 3, pp. 480–489, 2014, doi: 10.1590/S1415-47572014000400002.

[318] M. Oikonomaki, P. Bady, and M. E. Hegi, “Ubiquitin Specific Peptidase 15 (USP15) suppresses glioblastoma cell growth via stabilization of HECTD1 E3 ligase attenuating WNT pathway activity,” *Oncotarget*, vol. 8, no. 66, pp. 110490–110502, 2017, doi: 10.18632/oncotarget.22798.

[319] E. M. Yousef, M. R. Tahir, Y. St-Pierre, and L. A. Gaboury, “MMP-9 expression varies according to molecular subtypes of breast cancer,” *BMC Cancer*, vol. 14, no. 1, pp. 1–12, 2014, doi: 10.1186/1471-2407-14-609.

[320] B. Győrffy *et al.*, “An online survival analysis tool to rapidly assess the effect of 22,277 genes on breast cancer prognosis using microarray data of 1,809 patients,” *Breast Cancer Res. Treat.*, vol. 123, no. 3, pp. 725–731, 2010, doi: 10.1007/s10549-009-0674-9.

[321] C. P. Goswami and H. Nakshatri, “PROGgene: gene expression based survival analysis web application for multiple cancers,” *J. Clin. Bioinforma.*, vol. 3, no. 22, 2013, doi: 10.1093/jnci/djj329.

[322] P. T. Lowary and J. Widom, “New DNA sequence rules for high affinity binding to histone octamer and sequence-directed nucleosome positioning,” *J. Mol. Biol.*, vol. 276, no. 1, pp. 19–42, 1998, doi: 10.1006/jmbi.1997.1494.

[323] C. Aslanidis and P. J. de Jong, “Ligation-independent cloning of PCR products (LIC-PCR),” *Nucleic Acids Res.*, vol. 18, no. 20, pp. 6069–6074, 1990, doi: 10.1093/nar/18.20.6069.

[324] R. W. J. Thuring, J. P. M. Sanders, and P. Borst, “A freeze-squeeze method for recovering long DNA from agarose gels,” *Anal. Biochem.*, vol. 66, no. 1, pp. 213–220, 1975, doi: 10.1016/0003-2697(75)90739-3.

[325] K. Luger, T. J. Rechsteiner, and T. J. Richmond, “[ 1 ] PREPARATION OF NCPs FROM RECOMBINANT HISTONES 3 [1] Preparation of Nucleosome Core Particle from Recombinant Histones,” 1999.

[326] H. Braselmann, A. Michna, J. Heß, and K. Unger, “CFAssay: Statistical analysis of the colony formation assay,” *Radiat. Oncol.*, vol. 10, no. 1, pp. 1–6, 2015, doi: 10.1186/s13014-015-0529-y.

[327] C. M. Nickson and J. L. Parsons, “Monitoring regulation of DNA repair activities of cultured cells in-gel using the comet assay,” *Front. Genet.*, vol. 5, no. JUL, pp. 1–11, 2014, doi: 10.3389/fgene.2014.00232.

[328] T. J. Slenn, B. Morris, C. G. Havens, R. M. Freeman, T. S. Takahashi, and J. C. Walter, “Thymine DNA glycosylase is a CRL4Cdt2 substrate,” *J. Biol. Chem.*, vol. 289, no. 33, pp. 23043–23055, 2014, doi: 10.1074/jbc.M114.574194.

[329] E. Shibata, A. Dar, and A. Dutta, “CRL4Cdt2 E3 ubiquitin ligase and Proliferating Cell Nuclear Antigen (PCNA) cooperate to degrade thymine DNA glycosylase in S phase,” *J. Biol. Chem.*, vol. 289, no. 33, pp. 23056–23064, 2014, doi:

10.1074/jbc.M114.574210.

[330] J. Dorn, E. Ferrari, R. Imhof, N. Ziegler, and U. Hübscher, “Regulation of human MutYH DNA glycosylase by the E3 ubiquitin ligase mule,” *J. Biol. Chem.*, vol. 289, no. 10, pp. 7049–7058, 2014, doi: 10.1074/jbc.M113.536094.

[331] J. L. Parsons *et al.*, “Ubiquitin ligase ARF-BP1/Mule modulates base excision repair,” *EMBO J.*, vol. 28, no. 20, pp. 3207–3215, 2009, doi: 10.1038/emboj.2009.243.

[332] C. Meisenberg *et al.*, “Ubiquitin ligase UBR3 regulates cellular levels of the essential DNA repair protein APE1 and is required for genome stability,” *Nucleic Acids Res.*, vol. 40, no. 2, pp. 701–711, 2012, doi: 10.1093/nar/gkr744.

[333] T. L. Scott *et al.*, “Polyubiquitination of apurinic/apyrimidinic endonuclease 1 by Parkin,” *Mol. Carcinog.*, vol. 56, no. 2, pp. 325–336, 2017, doi: 10.1002/mc.22495.

[334] P. D. Gregory, K. Wagner, and W. Hörz, “Histone acetylation and chromatin remodeling,” *Exp. Cell Res.*, vol. 265, no. 2, pp. 195–202, 2001, doi: 10.1006/excr.2001.5187.

[335] G. J. Narlikar, H. Fan, and R. E. Kingston, “Cooperation between Complexes that Regulate Chromatin Structure and Transcription Chromatin structure creates barriers for each step,” *Cell*, vol. 108, pp. 475–487, 2002.

[336] P. B. Becker and W. Hörz, “ATP-Dependent Nucleosome Remodeling,” *Annu. Rev. Biochem.*, vol. 71, no. 1, pp. 247–273, 2002, doi: 10.1146/annurev.biochem.71.110601.135400.

[337] C. M. Nickson, P. Moori, R. J. Carter, C. P. Rubbi, and J. L. Parsons, “Misregulation of DNA damage repair pathways in HPV-positive head and neck squamous cell carcinoma contributes to cellular radiosensitivity,” *Oncotarget*, vol. 8, no. 18, pp. 29963–29975, 2017, doi: 10.18632/oncotarget.16265.

[338] R. Meas and P. Mao, “Histone ubiquitylation and its roles in transcription and DNA damage response,” *DNA Repair (Amst).*, vol. 36, pp. 36–42, 2015, doi: 10.1016/j.dnarep.2015.09.016.

[339] C. Chatterjee, R. K. McGinty, B. Fierz, and T. W. Muir, “Disulfide-directed histone ubiquitylation reveals plasticity in hDot1L activation,” *Nat. Chem. Biol.*, vol. 6, no. 4, pp. 267–269, 2010, doi: 10.1038/nchembio.315.

[340] W. A. Krajewski, “Ubiquitylation: How Nucleosomes Use Histones to Evict Histones,” *Trends Cell Biol.*, vol. 29, no. 9, pp. 689–694, 2019, doi: 10.1016/j.tcb.2019.06.002.

[341] H. Wang *et al.*, “Histone H3 and H4 Ubiquitylation by the CUL4-DDB-ROC1 Ubiquitin Ligase Facilitates Cellular Response to DNA Damage,” *Mol. Cell*, vol. 22, no. 3, pp. 383–394, 2006, doi: 10.1016/j.molcel.2006.03.035.

[342] R. Y. Tweedie-Cullen, J. M. Reck, and I. M. Mansuy, “Comprehensive mapping of post-translational modifications on synaptic, nuclear, and histone proteins in the adult mouse brain,” *J. Proteome Res.*, vol. 8, no. 11, pp. 4966–4982, 2009, doi: 10.1021/pr9003739.

[343] R. J. Carter and J. L. Parsons, “Base Excision Repair, a Pathway Regulated by Posttranslational Modifications,” *Mol. Cell. Biol.*, vol. 36, no. 10, pp. 1426–1437, 2016, doi: 10.1128/mcb.00030-16.

[344] D. Ahel *et al.*, “Poly(ADP-ribose)-dependent regulation of DNA repair by the

chromatin remodeling enzyme ALC1," *Science (80-. ).*, vol. 325, no. 5945, pp. 1240–1243, 2009, doi: 10.1126/science.1177321.

[345] J. R. Hughes and J. L. Parsons, "The E3 Ubiquitin Ligase NEDD4L Targets OGG1 for Ubiquitylation and Modulates the Cellular DNA Damage Response," *Front. Cell Dev. Biol.*, vol. 8, no. November, pp. 1–13, 2020, doi: 10.3389/fcell.2020.607060.

[346] L. D. Harris *et al.*, "The deubiquitinase TRABID stabilises the K29/K48-specific E3 ubiquitin ligase HECTD1," *J. Biol. Chem.*, p. 100246, 2021, doi: 10.1074/jbc.ra120.015162.

[347] S. Benafif and M. Hall, "An update on PARP inhibitors for the treatment of cancer," *Onco. Targets. Ther.*, vol. 8, pp. 519–528, 2015, doi: 10.2147/OTT.S30793.

[348] H. E. Bryant *et al.*, "Specific killing of BRCA2-deficient tumours with inhibitors of poly(ADP-ribose) polymerase.[erratum appears in Nature. 2007 May 17;447(7142):346]," *Nature*, vol. 434, no. 7035, pp. 913–917, 2005.

[349] H. Farmer *et al.*, "Targeting the DNA repair defect in BRCA mutant cells as a therapeutic strategy," *Nature*, vol. 434, no. 7035, pp. 917–921, 2005, doi: 10.1038/nature03445.

[350] R. L. Maher, C. G. Marsden, A. M. Averill, S. S. Wallace, J. B. Sweasy, and D. S. Pederson, "Human cells contain a factor that facilitates the DNA glycosylase-mediated excision of oxidized bases from occluded sites in nucleosomes," *DNA Repair (Amst).*, vol. 57, no. April, pp. 91–97, 2017, doi: 10.1016/j.dnarep.2017.06.029.

[351] L. A. Cirillo and K. S. Zaret, "Preparation of Defined Mononucleosomes, Dinucleosomes, and Nucleosome Arrays In Vitro and Analysis of Transcription Factor Binding," in *Methods in Enzymology*, vol. 375, no. 1993, 2003, pp. 131–158.

[352] I. I. Dianova *et al.*, "XRCC1-DNA polymerase β interaction is required for efficient base excision repair," *Nucleic Acids Res.*, vol. 32, no. 8, pp. 2550–2555, 2004, doi: 10.1093/nar/gkh567.

[353] M. R. Fabbrizi, J. R. Hughes, and J. L. Parsons, "The enzyme-modified neutral comet (Emnc) assay for complex dna damage detection," *Methods Protoc.*, vol. 4, no. 1, pp. 1–12, 2021, doi: 10.3390/MPS4010014.

[354] E. Oya *et al.*, "H3K14 ubiquitylation promotes H3K9 methylation for heterochromatin assembly," *EMBO Rep.*, vol. 20, no. 10, pp. 1–15, 2019, doi: 10.15252/embr.201948111.